A DESIGN STUDY FOR THE USE OF A MULTIPLE
APERTURE DEPLOYABLE ANTENNA FOR SOIL MOISTURE
REMOTE SENSING SATELLITE APPLICATIONS

Peter Foldes

FOLDES INCORPORATED
Wayne, Pennsylvania

NASA

National Aeronautics and
Space Administration

Langley Research Center
Hampton, Virginia 23665

TABLE OF CONTENTS

LIST OF FIGURES

LIST OF TABLES

Acknowledgment

The author wishes to express his deep appreciation for the help of all those NASA Langley Research Center people, whose contribution made this report possible. Particular thanks are due to Mr. J. K. Johnston and Mr. L. A. Dillion-Townes, who worked on the configuration and thermal problems.

1. BACKGROUND

It was recognized quite early in the development of space technology, that a unique opportunity exists to make observations of the earth from space on a global scale. Since most physical phenomenon affects electromagnetic radiations it was expected that the most effective data collection might be implemented by space based instruments with properly controlled electromagnetic transmit and/or receive capabilities.

While radiations of materials from very low to optical frequencies can be interesting, the most important single global phenomenon is related to the presence and condition of water. The spatial and temporal distribution of water temperature, the amount of water in the soil and the atmosphere, the boundaries of snow and ice cover, the extent and state of foliage development, the presence of variaous chemicals in the water effect the electromagentic radiation emitted by the associated surface thus generate a signature of some sort.

In order to utilize this latent potential, a host of basic questions must be answered. What frequency bands, bandwidths, polarization, angle of incidence, revisit times are best for certain observations? What are the radiation levels and their time variations associated with the phenomenon to be measured relative to variations caused by external interferences and measuring system imperfections? What spatial and radiation level (noise temperature) resolution is necessary in order to make the collected information useful? What technologies are necessary to collect and process the data?

The present study will be very limited in scope compared to these general questions. It will address the instrumentation problems associated to the measurement of soil moisture with a meaningful spatial and temperature resolution at a global scale. For this goal only medium term available affordable

technology will be considered. The study while limited in scope, will utilize a large scale antenna structure, which is being developed presently as an experimental model. The interface constrains presented by a single STS flight will be assumed.

The study methodolgy will consists of the following steps: Review of the science requirements; Analyze the effect of these requirements on the selection of the concept. scale, quality and method of operation of the instrument; Present basic system engineering considerations and trade-off related to orbit parameters, number of spacecraft and their lifetime, observation angles, beamwidth, crossover and swath, coverage percentage, beam quality quatity and resoltuion, instrument quantities and integration time; Bracket the key system characteristics and develope an electromagnetic design of the antenna-passive radiometer system. Several aperture division combinations and feed array concepts are investigated to achieve maximum feasible performance within the stated STS constrain.

Next, some mechanical configurations are determined which are compatible with the structural design of the reflector system and can be packaged and developed within the applicable constrains. Finally, the major technology develoment needs are identified.

2. SCIENCE REQUIREMENTS

The requirements presented by space science on observation systems have been studied previously in considerable details. Here only, a summary of these requirements will be given and commented.

The first column of Table 2.1 shows a list of the most interesting physical parameters, _measurands_ to be determined. All of these measurands are derived by determining the noise power level at the output of an antenna terminal for a given relative position between the antenna and a solid angle region occupied by the boundary or volume of the unknown physical quantity. This noise power is proportional to the "noise" or "brightness" temperature of the physical quantity occupying the region. In turn the noise temperature is the product of physical temperature and emissivity or physical temperature can be determined if the other characteristics is obtained by alternative methods. The noise power measurement itself is accomplished relative to the noise power of a reference source.

For a given radiometer (calibrated antenna receiver system) the received noise power is a function of a number of _parameters associated with the measurands_. This allows the deduction of the measurands from the raw noise temperature data. (See second column of Table 2.1.) By setting and calibration of the radiometer, use of other instruments and data available from miscellaneous sources, the radiometric measurement can supply one or more of the unknown data.

The third column of Table 2.1 displays those _instrument and inherent external characteristics_ which influence the quantity and quality of the collected data. These characteristics can be affected by engineering design and are the subject of the present study. Since some of these characteristics cannot be determined easily and they are intricately related to each other,

3

TABLE 2.1

Science requirements and their effects

Measurands	Parameter associated with the measurands	Instrument and external characteristics affecting the obtained data
Soil moisture content	Material composition	Antenna aperture diameter
Water surface temperature	Physical temperature	Aperture field distribution
Water temperature gradient	Frequency of radiation	Accuracy and stability of aperture field distribution
Water surface roughness	Polarization mode and/or angle	Beam efficiency
Wind speed at water surface	Angle of incidence	Circuit loss
Snow boundary	Spatial distribution	Antenna noise temperature
Ice boundary	Surface geometry	Number of beams
Sea water salinity	Depth of penetration	Crossover between beams
Water pollutant content	Time variation of all the above	Beam to beam similarity
Water vapor content		Beam pointing accuracy
Non-precipitating water cloud		Angle of observation
Precipitating water (rain)		Polarization modes
		Number of polarization modes
		Polarization angles
		Orbit height
		Orbit shape
		Orbital volocity
		Orbit variations
		Inclination angle
		Coverage percentage
		Swath
		Revisit time
		Time of observation
		Experiment lifetime
		Receiver noise temperature
		System noise temperature
		Predetection bandwidth
		Dwell time
		Integration time
		Natural background noise
		Man made noise

the selection of an optimum set of instrument characteristics is neither
straightforward no unique. Nevertheless the effect of their variation can be
relatively easily demonstrated and used to derive a reasonable approximation
of the optimum condition

The largest effect of the science requirements on the design is the selection of frequency.

It is known that all materials above absolute zero temperature emit electromagentic radiation. The magnitude of this radiation increases with the molecular excitation (physical temperature) and has local maximums as a function of frequency at the molecular transition lines. When this radiation is observed by an _ideal_ antenna, which has an equivalent solid angle field of view then the total radiation may be decomposed approximately into two parts. The first part is coming from the volume bounded by the antenna aperture, the "walls" of the solid angle region and the surface at the far end of the cell where a rapid change of material distribution occurs. The second part of the radiation is coming from the _surface_ representing the far end boundary of the cell. Depending on the application either the volumetric or the surface radiaiton contains data about the measurand. The two can be separated from each other by proper selection of the observation frequency band.

In the case of a space-based observatory, the cell may be part of the atmosphere and the far end boundary may be the surface of the Earth. The vbolumetric radiation (absorbtion) is due to the permanent electric dipole moment of molecules or permanent magnetic dipole moment of atoms. The primary radiations are associated to water vapor (first resonance around 21 GHz), oxygen (first resonance around 60 GHz), but carbon dioxide, ozone, nitrogen and water vapor have several additional resonances in the 1.5 to 20 micron optical wavelength range. While the first resonance of the oxygen molecule is at higher frequency then for water vapor the atmosphering radiation up to about 14 GHz is caused mostly by oxygen, due to the wider frequency band of this radiation.

The radiation by the surface at the far end of the cell is mostly caused by the presence of condensed water. This water is forming the surface of sea, lakes, rivers or it is absorbed to various exten by the soil.

In final detail this so called surface radiation is not emitted by the surface but ba a second cell, which is beyond the atmosphere-Earth surface boundary. The depth of this cell in the direction of wave propagation associated to the observing antenna, depends on the capability of the electromagnetic wave to penetrate into the second region. At a given frequency this is conveniently characterized by the skin depth. Thus the magnitude of this "surface" radiation is a function of the material characteristics within the volume defined by the skin depth. ("Material characteristics" include the physical temperature.)

According to observations the radiation from the Earth surface is relatively constant and falls into the 50K to 350K range, representing about ±4.2 dB variation relative to the average. When the surface radiation represents the desirable measurand, then its level must be large compared to the volumetric radiation and particularly compared to the variable (water vapor caused) part of the volmetric radiation. Since at, or below $f_U = 7$ GHz the water vapor caused attenuation is less than one-tenth of the oxygen attenuation, this frequency may be considered as the upper limit for determining surface characteristics. Selecting the frequency as much as possible below f_U improves the capability to suppress the effect of volumetric radiation.

Up to this point both the antenna and the environment in the cell was assumed to be ideal. Unfortunately, none of these are true in practice. The assumption, that no external noise sources outside the cell are present is reasonably accurate at higher frequencies, where the ionosphere acts as a shield against extraterrestrial radiation. With decreasing frequency, the

6

ionosphere becomes more and more transparent. For instance, at 1 GHz the minimum (near average) galactic radiation reaches about 5K. This is about one-tenth of the lowest level of the interesting surface radiation. Since the galactic radiation is reflected by the surface under observation it represents an error, limiting the resolution of the measurand. On the basis of these considerations i is customary to define $f_L = 1$ GHz as the lowest practical frequency for measurements of surface radiation.

It may be noted, that for a practical antenna, not all the radiation is coming from a limited equivalent solid angle. Volumetric and surface radiation outside the desired angular region represents a background noise, which further limits the resolution of the measuring system. Finally, man made noise may be generated inside the cell at the far end boundary or outside the observed cell. These could cause errors or altogether eliminate the possibility of measurements.

On the basis of the above considerations WARC 79 allocated a number of frequency bands for radiometric observations. These are listed in Table 2.2. In the primary frequency bands no electromagnetic transmissions are permitted.

TABLE 2.2

Primary frequency band allocations for radiometry

No.	Frequency band (MHz)	Bandwidth (MHz)	Possible measurand
1	1400-1427	27	Soil moisture, salinity
2	2690-2700	10	Sea surface temperature
3	10680-10700	20	Water roughness, rain, snow
4	15350-15400	50	Water vapor, rain, snow
5	31300-31500	200	Oil spills, clouds
6	31500-31800	300	Ice, snow

According to Table 2.2 for surface noise temperature measurements, only two bands are available if the measurements are restricted to the primary frequencies. Among the band of interests, Band 1 has the largest available

bandwidth, thus it ofers the best possible temperature resolution potential. Since the radiation related to the salinity of sea water has a relatively strong frequency dependency, the lowest frequency is the most useful from this point of view. At higher frequencies the sea surface temperature associated radiations become less dependent on salinity. Consequently, Band 2 can be used most appropriately for sea surface temperature measurement. While soil moisture can be measured in Band 2, Band 1 is preferable, because it has a larger skin depth and it is less sensitive to the canopy effect of foliage. Ideally, a system, which has combined soil moisture, sea salinity, and sea surface temperature measuring capability must operate simultaneously or in time sequence in Band 1 and Band 2. It is unlikely that such capability can be economically implemented by using a common sperture. If the common aperture is a reflector or lens, then in Band 1 for an optimum design its spatial resolution is accuracy limited and its temperature accuracy is loss limited. In Band 2 it might be possible to achieve the same spatial resolution, beam number and swath, provided that over the utilized (center) part of the optics the accuracy is better by the frequency ratio of the bands. Unfortunately, such utilization of the optics requires a corresponding increase of feed array size measured in wavelength and number of radiating elements. this in turn increases feed losses, thus reduces the temperature resoltuion. If the common aperture is an array, then the area of the higher frequency band array is only 27% of the area of lower frequency array. The density of radiating elements in the ghiher frequency array is 3.7 times larger. thus even if a dual band element can be desinged, the layout and excitation requirements are different for the two bands. Consequently, the electromagentic part of the array must be independent. Whether they share a common supporting and deployment structure is a matter of design detail.

However, when the complexities related ot the array overlap are weighted against the advantages of saving 27% of the support structure are it is unlikely that an overlaping design can offer sufficient benefits. On that basis it is likely that the combined use of a single structure in Band 1 and Band 2 is not cost effective. for such a case Band 1 is usable for soil moisture and sea salinity measurements only.

The next important characteristics of the radiometer is the spatial resolution, influenced by the science requirement. Table 2.3 summarizes the minimum spatial resolution requirements for the presently considered applications.

TABLE 2.3

Minimum spatial resolution requirements

Measurand	Application	Minimum spatial resolution (km)
Soil moisture	Agriculture	10
	Hydrology	10-25
	Climate	100-200
Sea salinity	Coastal regions	1
	Open ocean	10

It can be seen from Table 2.3 that the measurements of salinity in coastal regions require an order of magnitude better resolution than adequate for most other applications. Since this measurement can be accomplished cost effectively by airplanes, it is not cost effective to burden wider applications systems with this requirement. Excluding the coastal salinity measurement, 10 km spatial resolution is adequate for all other applications.

The relationship between spatial resolution and antenna size is a complicated one. At the outset it must be understood that the spatial resolution by itself does not adequately define the quality of the system since the system

9

parameters define the <u>product</u> of spatial and temperature resolution only. One of these resolutions can be improved at the expense of the other for given antenna dimensions. This phenomenon will be discussed later in more detail.

For the simplest, idealized case, the best spatial resolution can be achieved between two point sources. If two such point sources are 10 km from each other at 573 km distance from the antenna, parallel with the antenna aperture then their distance represents 1° separation. Using a uniformly illuminated circular antenna aperture with 58.4 λ aperture diameter, the 3 dB beamwidth is $\theta_3 = 1°$. The angle between beam maximum and the first null is also approximately 1°.

Assume that the two point sources have $T_1 = 100°$ and $T_2 = 101°$ noise temperatures, respectively, and the temperature resolution of the system is ΔT. If $\Delta T < T_2 - T_1$ then for the given beamwidth the antenna can distinguish the two point sources. It will measure $T_1 \pm \Delta T$ in direction of source 1, $T_2 \pm \Delta T$ in direction of source 2 and $1/2(T_1 + T_2) \pm \Delta T$ in halfway between. The required antenna diameter for this condition is $D = 58.4 \lambda = 1.24$ m at 1413 MHz. If $\Delta T > T_2 - T_1$ then the antenna beamwidth must be reduced in order that a temperature minimum can be observed as the antenna is pointed halfway between the two sources. At the extreme, this minimum is zero, when the antenna beam has simultaniously nulls toward each point source. This requires approximately doubling the antenna diameter to 24.8 m. For this condition the two point sources are spatially resolved independent on the temperature resolution.

When the sources have finite angular extent the spatial resolution may be defined by the antenna beamwidth which produces a detectable increase in the derivative of noise temperature versus angle as the antenna beam moves across the crossove point between two different temperature regions.

10

Figure 2.1 illustrates this situation. In this figure T_1 and T_2 are the actual noise temperatures in angular regions W_1 and W_2.

The dotted line shows the apparent noise temperature at the output of the test antenna as its main beam moves across the observed regions. The magnitude of the $\delta T/\delta\theta$ derivative in the transition region is a function of T_1, T_2, W_1, and W_2 and the shape of the antenna radiation pattern.

As an example, assume that $T_1 = 100°K$, $T_2 = 101°K$, $W_1 = W_2$ $1°K$ and the temperature resolution is $\Delta T = 0.1°K$. What is the necessary antenna diameter for this condition? Before this question can be answereed a practically realizable aperture distribution must be assumed. Select an

$$A + (1 - A)(1 - r^2)^P$$

type distribution with $A = 0.2$ and $P = 2$. In this case the radiation pattern is axially symmetrical and 97% of the total antenna power is within a half cone angle of $\theta_{97\%} \cong 1.27$ Rad/D_λ. Thus the beamwidth of the antenna which contains 97% of the power is $\theta_{97\%} \cong 145.5°/D_\lambda$.
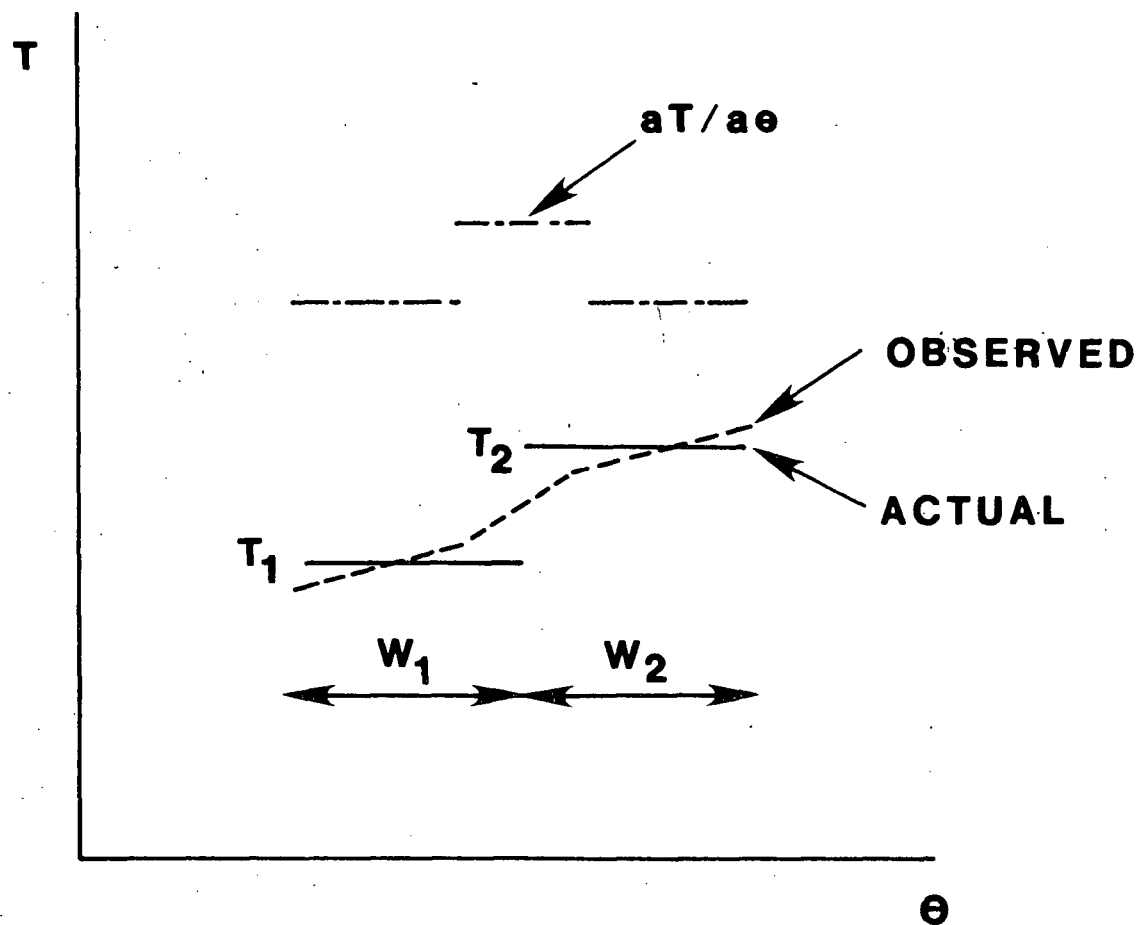
Figure 2.1 - Relationship between spatial resolution and noise temperature distribution.

Figure 2.2 shows the results of pattern integration for this case. As the antenna beam scans the observed regions the noise temperature versus θ function has three points:

$$T_1 = 97.7575°K$$

$$T_{12} = 98.2387°K$$

$$T_2 = 98.7200°K$$

which lie on a straight line as a function of θ. The $T(\theta)$ function falls below this straight line between points 1 and 12 and reaches a value of 97.876°K. This is 0.122°K lower than the value at this angle using the straight line prediction. Since the assumed temperature resolution is 0.1°K such a minimum is detectable and the two regions are resolved. For $W_1 = 1° = \theta_{97\%}$, $D = 145.5 \lambda \cong 30.9$ m. If the temperature resolution is poorer or the beam efficiency is poorer than the necessary antenna diameter is larger. Furthermore, the antenna diameter increases if the orbit height is larger than the 573 km assumed in the example. Additionally, the resolution deteriorates inversely with the cosine of the angle accounted. The combined effect of these factors can cause an increase in the required aperture by as much as 50%. Thus it can be concluded that the antenna diameter for the presently contemplated resolution is in the order of 45 m, while the exact value can be determined only by a more detailed and rather complicated analysis.

In the following, a somewhat different approach will be taken. The antenna diameter will be fixed for the above estimated range in the manner compatible with existing structural development and STS compatibility. Then the obtainable resolution will be calculated for various design conditions.
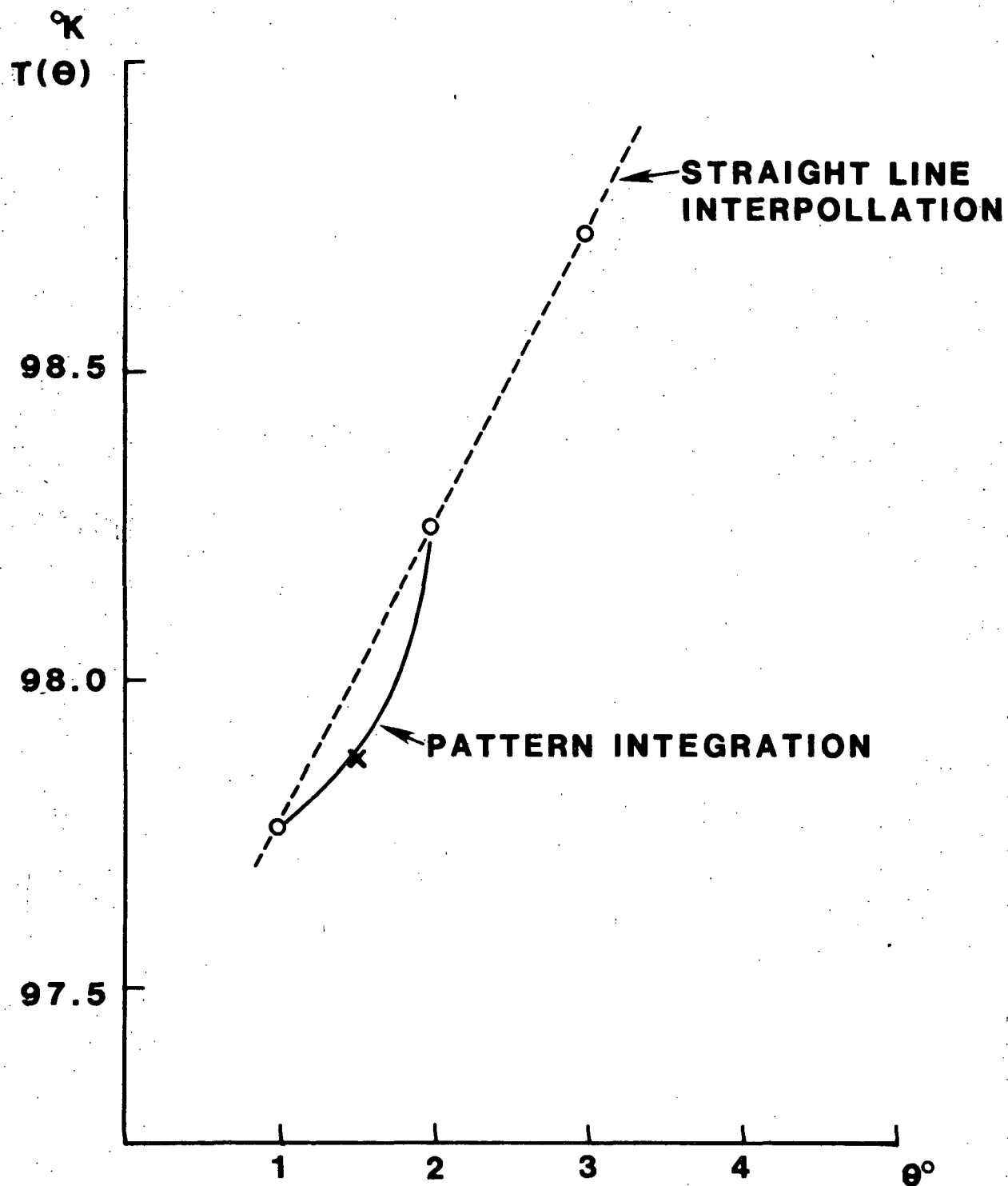
Figure 2.2 - Variation of observed noise temperature versus angle for a
practical antenna pattern.

The science requirements discussed so far, determine an antenna aperture diameter of $D \sim 212\lambda$ for a nominal orbit height of $H = 573$ km, if the associated temperature resolution is approximately $\Delta T = 0.12°K$. This set of $(D_\lambda, H$ and $\Delta T)$ characteristics represent the vasic complexity of the system which has the desired $\Delta R = 10$ km spatial resolution. While the optimization of the $D_\lambda, H, \Delta T$ set is important the basic complexity is determined by ΔR.

Another independent complexity factor is the selection of polarization mode or modes.

The polarization mode of the antenna affects the measurands because the reflection coefficient, thus the related noise temperature is a function of the boundary conditions between two homogeneous region. In the case of the atmosphere and Earth surface boundary the reflection coefficient is different for the parallel and perpendicular electric field component of the incoming eletromagnetic wave. Thus the observable noise temperature is a function of the polarization angle or more generally, polarization mode. Furthermore, in case of a rough surface (like for waves on the surface of the water) the noise temperature is a different function of the surface roughness for different polarization angles. If sensitivity to surface roughness must be minimized then vertical polarization is perferable at a relatively large, fixed incidence angle. This can be achieved by one polarization. If sensitivity to incidence angle must be minimized then the average noise temperature for horizontal and vertical polarization must be calculated. This requires the availability of two polarizations.

The measurement of condensed water (rain) in the atmosphere is based on the scatter mechanism associated to the rain droplets. For this purpose circular polarization is desirable because it achieves near independence on droplet shape.

15

The present application is related to surface noise temperature measurements, thus linear polarization is preferable. For the comtemplated pushbroom type bean structure the antle of incidence varies from beam to beam. Thus it would be desirable to include two orthogonal polarizations. On the other hand, the provision of two polarizations require a doubling of the beam forming network. This approximately doubles the volume required for the feed circuit. A more detailed analysis of the impact of such a requirement shows that dual polarization can be implemented only at the expense of reducing the number of beams in the pushbroom, due to Shuttle space limitations. This is considered as a bad trade off between improved noise temperature measuring accuracy and reduced coverage. Thus, the single polarization system was selected as the baseline for the present study. For this situation "vertical" linear polarization is the preferred polarization mode. It may be noted that the actual polarization at the point of incidence is approaching vertical only for near grazing angle condition. for a nadir direction beam the polarization is always parallel to the surface of the Earth. The general beam in the pushbroom has an intermediate angle (say 45°). If "horizontal" polarization is selected at the antenna, the angle at the surface of the Earth is nearly 0°, independent on the angle of incidence.

The science requirements represent an additional important complexity driver on the radiometer system through the value of the required temperature and spatial resolution product. This can be seen from the following simple calculations:

The temperature resolution is given by

$$\Delta T = \frac{2 \, T_S}{\left(Bt_i\right)^{1/2}}$$

where

$T_S = T_R + T_{Rx}$ is the system noise temperature

B = is the predetection bandwidth = 1/2 of 27 MHz

t_i = is the integration time of the radiometer

In the above expressions

T_R = temperature of the reference load

T_{Rx} = is the noise temperature of the receiver system

$t_i \cong t = \frac{(\Delta R)^2}{vS}$ = dwell time

ΔR = diameter of the footprint (assumed to be circular in shape)

v = orbital velocity projected to the ground $\cong$ 7.6 km/s for H = 573 km

S = swath width

Inserting t_i into the expression of ΔT the $\Delta T \Delta R$ product is

$\Delta T \Delta R = 2T_S \left(\frac{vS}{B}\right)^{1/2}$. It was shown previously that $\Delta T \Delta R < 1^\circ K$ km is desirable

for the present application. For this case the system noise temperature must

be not larger than

$$T_S = 298^\circ K$$

Assuming T_{Rxo} = 40°K front end noise temperature and $\alpha \sim$ 1dB circuit loss

in the antenna $T_{Rx} = 40^\circ + 75^\circ = 115^\circ K$. For this case the reference load

must be $T_R = T_S - T_{Rx} = 183^\circ K$, or better. This may be achievable by a

thermoelectrically colled load. Alternatively, the load may be kept at 293°K

17

room temperature. In this case $T_S = 408°K$ and the achievable temperature resolution deteriorates to $\Delta T = 0.137°K$. If it is desirable to keep the $\Delta T \Delta R$ product at $1°K$ km, then the increase of the load temperature results at 37% increase in antenna diameter! (From 45 m to 61.6 m.)

The above discussions have been conducted for a single beam. In an actual system a number of simultaneous beams must be formed in order to obtain the necessary swath using a single satellite. For a given percentage of coverage revisit time and $\Delta R \Delta T$ product the swath is uniquely determined. Since ΔR is given the number of required beams are

$$n = \frac{S}{\Delta R}$$

Table 2.4 summarizes the realtionship between science requirements and radiometer system complexity on the basis of the above considerations.

TABLE 2.4

Relationship between science requirements and major system complexity

characteristics for L-band radiometer application

Science requirement	Major complexity drivers
Product of spatial and temperature resolution	Antenna diameter in wavelength
Revisit time	Number of beams
Coverage percentage	Orbit height
Independence on angle of incidence	System noise temperature (T_{Rxo}, α, T_R) Polarization modes

For the purpose of the present study the configuration and the overall structural diameter of the antenna is given (hoop column antenna with maximum 118 m structural diameter). Consequently the antenna diameter in wavelength can be influenced only by the number of division applied to the overall aperture. If no subdivision is employed a certain amount of blockage

(scatter) is unavoidable. With the use of subapertures the scatter can be greatly reduced but with increasing number of division the available subaperture diameter for the formation of a beam decreases. At the same time the undesirable coupling between subapertures, due to spillover radiation increases. This limits the number of usable subapertures to about 4. Thus it is adequate to consider singlet, doublet, triplet and quadruplet aperture configurations only. In each case there is a practical upper limit for the feasible number of beams. This is caused by the deterioration of beam quality with increasing scan angle. for small number of subapertures, the avalable subaperture is large and the beamwidth is small. Thus in terms of beamwidth a large number of beam scan is necessary to cover a given swath. This requires rapidly increasing feed clusters for increasing scan angle until the system is limited by deteriorating beam quality, feed losses and feed volume.

For alrge number of subapertures, like the case of the quadruplet, the desired scan angle can be achieved with less feed loss and feed volume. It is clear that this case has poorer spatial resolution, but the variation of the $\Delta R \Delta T$ product as a function of the number of subapertures cannot be predicted without more involved analysis.

On the basis of Table 2.4 the system engineering task for the radiometer can be defined by the selection process for optimum number of subapertures, number of beams, orbit height, system noise temperature and polarization modes if the spatial-temperatue resolution product, revisit time, coverage percentage and dependence on angle of incidence is given.

These system engineering considerations are presented in Section 3.

3. SYSTEM ENGINEERING CONSIDERATIONS

The system engineering considerations leading to optimum selection of antenna characteristics will be presented on the basis of a simplified model. This model characterizes the main physical features of the problem only, yet it is adequate for acceptably accurate trade off analysis.

For the antenna design optimization the relationship between the antenna related coordinate system and the ground related coordinate system must be established.

Figure 3.1 shows the applicable geometry. It is assumed that the satellite carrying the antenna is in point S, at a height h above a spherical Earth with a radius of R_E = 6372.88 km. Furthermore, it is assumed that the satellite moves along a circular orbit with an orbital velocity of v. The projection of the satellite toward the center of the Earth produces a ground trace on the surface of the Earth. The speed of this satellite projection point along the ground trace is v_g.

A point P within the field of view of the antenna on the surface of the Earth can be characterized by the half cone angle, β, which is measured between the direction of nadir and the direction $\overline{SP}$. Alternatively, the position P can be defined by α which is the angle between nadir and the line connecting P with the center of the Earth. The angle of incidence at the location of P for a wave which is traveling from the antenna toward P is δ.

From Figure 3.1 one can derive the following relationship

$$R + h = \frac{R}{\cos \alpha} + R \frac{\tan \alpha \sin \delta}{\cos(\alpha + \delta)} \tag{3-1}$$

or

$$h = R \left[\frac{1}{\cos \alpha} - 1 + \frac{\tan \alpha \sin \delta}{\cos(\alpha + \delta)} \right] \tag{3-2}$$

20

$$L = \{[R(1 - \cos\alpha)+h]^2+(R\sin\alpha)^2\}^{\frac{1}{2}}$$

P

$r = R\sin\alpha$

R

δ

α

$R\tan\alpha$

$R\tan\alpha\sin\delta$

$\alpha + \delta$

α

C

$\dfrac{R}{\cos\alpha}$

$R(1 - \cos\alpha)$

$U = R\,\dfrac{\tan\alpha\sin\delta}{\cos(\alpha+\delta)}$

$\beta = 90° - (\alpha+\delta)$

$M = \quad R(1 - \cos\alpha) + h$

$= \tan^{-1}\dfrac{r}{M}$

$R = 6372.88$ km

h
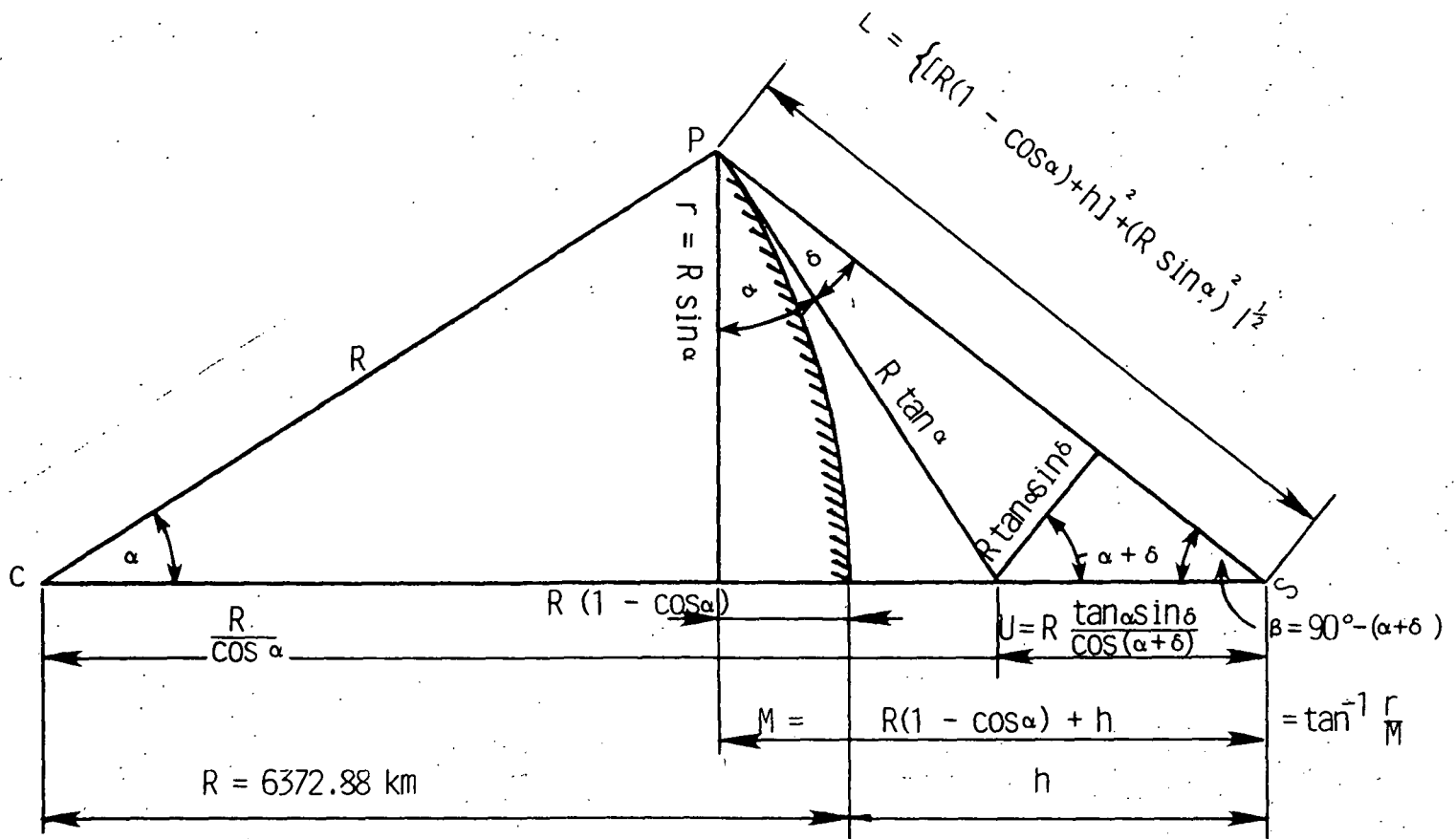
S = location of satellite

P = location of observed point on earth

δ = elevation engle from P to S

β = half swath angle

α = angle between P and S from center of earth

Relationship between h, α, δ and β

$$R + h = \frac{R}{\cos\alpha} + R\,\frac{\tan\alpha\,\sin\delta}{\cos(\alpha+\delta)}$$

$$h = R\left(\frac{1}{\cos\alpha}-1\right) + \frac{\tan\alpha\,\sin\delta}{\cos(\alpha+\delta)}$$

The spot size minor and major dimensions

$$\Delta X_m = L\,\theta_{98\%} \qquad \Delta X_M = \frac{\Delta X_m}{\sin\delta}$$

Figure 3.1 - Geometry of the field of view for a low Earth orbit satellite antenna.

The expression for observable field of view

$$\beta = 90° - (\alpha + \delta) = \tan^{-1} \frac{R \sin \alpha}{R(1 - \cos \alpha) + h} \qquad (3-3)$$

If P is the furthese point to be observed, then β is the half angle of the swath of the satellite.

The distance between the antenna and the point to be observed is

$$L = \left\{ [R(1 - \cos \alpha) + h]^2 + (R \sin \alpha)^2 \right\}^{1/2} \qquad (3-4)$$

If the beamwidth of the antenna is θ_B then n beams are necessary to fill in the 2β swath angle by a contiguous set of beams, thus

$$n = \frac{2\beta}{\theta_B} \qquad (3-5)$$

The θ_B angle on the ground defines an illuminated spot. If the antenna beam has a circular cross section the spot shape on the ground is approximately an ellipse, except for a nadir directed beam for which it is a circle. The major axis of this ellipse is in the plane of Figure 3.1. The minor and major axis dimensions:

$$\Delta X_m \cong L \theta_B \qquad (3-6)$$

$$\Delta X_M \cong \frac{\Delta X_m}{\sin \delta} \qquad (3-7)$$

The definition of θ_B is somewhat arbitrary. Ideally, it should be the angle, which contains the antenna power, which is 4π. A somewhat more practical definition is the angle, which contains 98% of the power for a perfectly accurate antenna. This is called the 98% power angle of the antenna, $\theta_{98\%}$. Using this definition, $\theta_B = \theta_{98\%}$ and the spatial resolution of the antenna, R is

22

$$\Delta R = \Delta X_M = L \frac{\theta_{98\%}}{\sin \delta}$$

$$= \frac{[R(1 - \cos \alpha) + h]^2 + (R \sin \alpha)^2}{\sin \alpha}^{1/2} \theta_{98\%} \qquad (3-8)$$

In order that the satellite maintains its orbital height, h it must move along its orbit with an orbit velocity of v. The travel time for one orbit period for perfect circular orbit is approximately

$$T = 6.987 \times 10^{-6}(hnm + 3440)^{1/2} \qquad \text{siderial hours}$$

$$\qquad (3-9)$$

$$= 0.0250845 \ (h^{nm} + 3440)^{3/2} \qquad \text{solar sec}$$

From the above formulas some basic relationships can be calculated which are needed in the following.

Table 3.1 shows the value of period time and the number of orbits, p_j for j = 1,2,3 and 4 days as a function of orbit height. The corresponding values of v and v_g are also exhibited.

TABLE 3.1

Period time versus orbit altitude for circular orbits

h^{km}	h^{nm}	T^{sec}	T^{Hr}	p_1	p_2	p_3	p_4	km/s v	km/s v_g
300	161.98	5333.28	1.48147	16.200	32.400	48.600	64.800	7.861	7.500
350	188.98	5394.04	1.49834	16.017	32.035	48.053	64.071		
400	215.98	5455.02	1.51284	15.864	31.593	47.593	63.457		
450	242.98	5516.23	1.53229	15.663	31.325	46.988	62.651	7.771	7.414
500	269.98	5577.67	1.54935	15.490	30.981	46.471	61.961		
550	296.98	5639.33	1.56648	15.321	30.642	45.963	61.284		
600	323.97	5701.20	1.58367	15.155	30.309	45.464	60.619	7.685	7.016
650	350.97	5763.32	1.60092	14.991	29.982	44.974	59.965		
700	377.97	5825.66	1.61824	14.831	29.661	44.492	59.323		
750	404.97	5888.22	1.63562	14.673	29.347	44.020	58.693	7.600	7.251
800	431.97	5951.01	1.65305	14.519	29.037	43.556	58.074		
850	458.96	6013.99	1.67055	14.366	28.733	43.099	57.466	7.546	7.199
900	485.96	6077.22	1.68812	14.217	28.433	42.650	56.867		
950	512.96	6140.66	1.70574	14.070	28.140	42.210	56.280	7.493	6.514

From Table 3.1 certain orbit heights can be calculated for which p_j is an integer. In this case the satellite is back to an earlier position with j periodicity. j is the revisit time of the satellite. For such orbit heights the appearance of the subsatellite point at any ground location is a periodic function of time. In the following, only such orbit heights will be considered. The orbit numbers corresponding to integer values of p_j will be designated by k_j.

Tables 3.2 and 3.3 show the period times and orbit heights corresponding to k_i for j = 3 and 4 day revisit times, respectively. Figures 3.2 and 3.3 show the relationship graphically.

TABLE 3.2

Orbit periods and heights for 3 day revisit time

k_3	T^{sec}	h^{km}
48	5400.00	281.338
47	5514.89	375.362
46	5634.78	472.784
45	5760.00	573.801
44	5890.90	678.622
43	6027.91	787.507
42	6171.42	900.677
41	6321.92	1018.421

TABLE 3.3

Orbit periods and heights for 4 day revisit time

k_3	T^{sec}	h^{km}
64	5400.000	281.338
63	5485.714	281.338
62	5574.193	
61	5665.573	
60	5760.000	573.801
59	5857.627	
58	5958.621	
57	6063.158	889.465
56	6171.429	
55	6283.636	
54	6400.000	1153.218
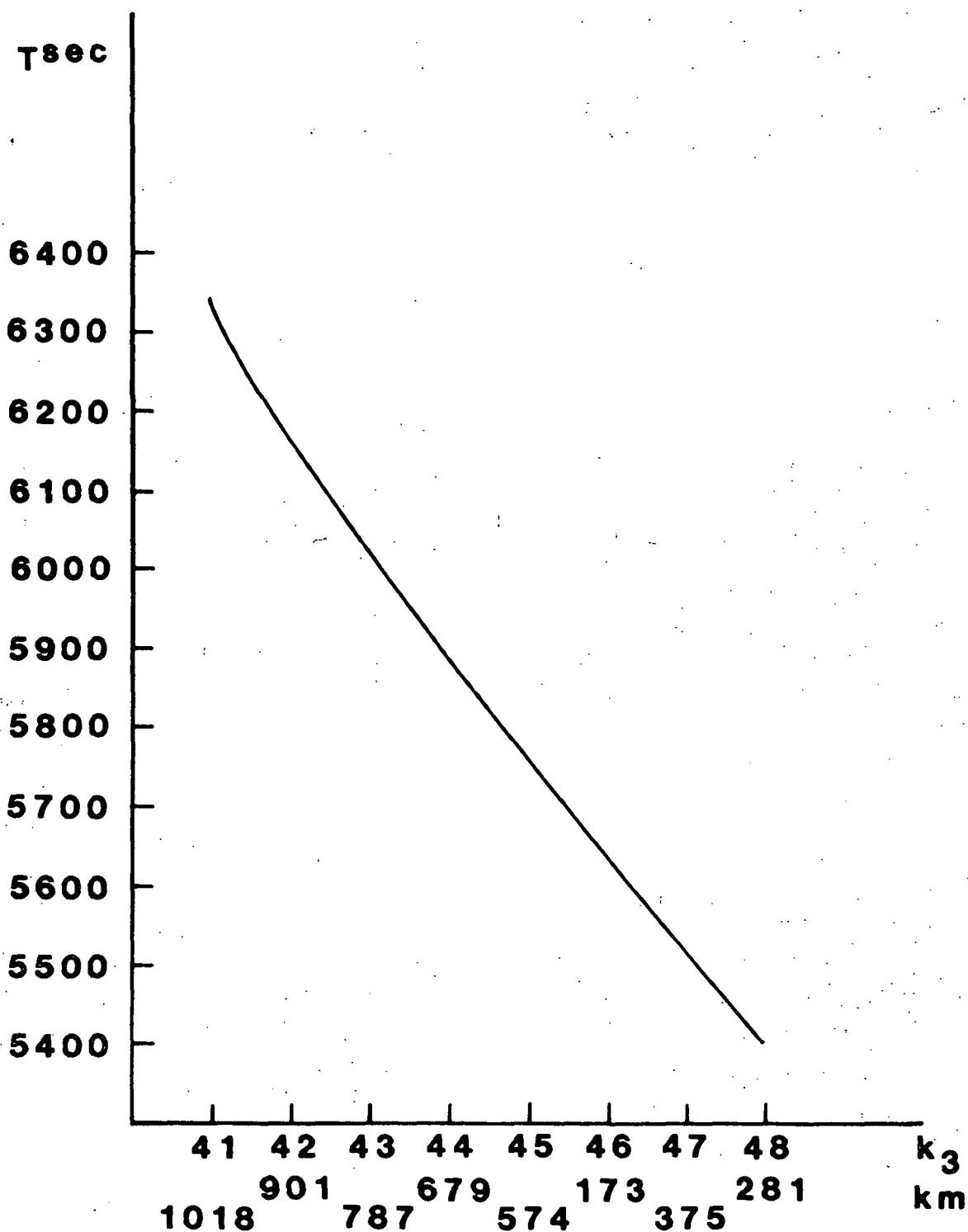
Figure 3.2 - Orbit numbers and period times versus orbit height for 3 day revisit time.
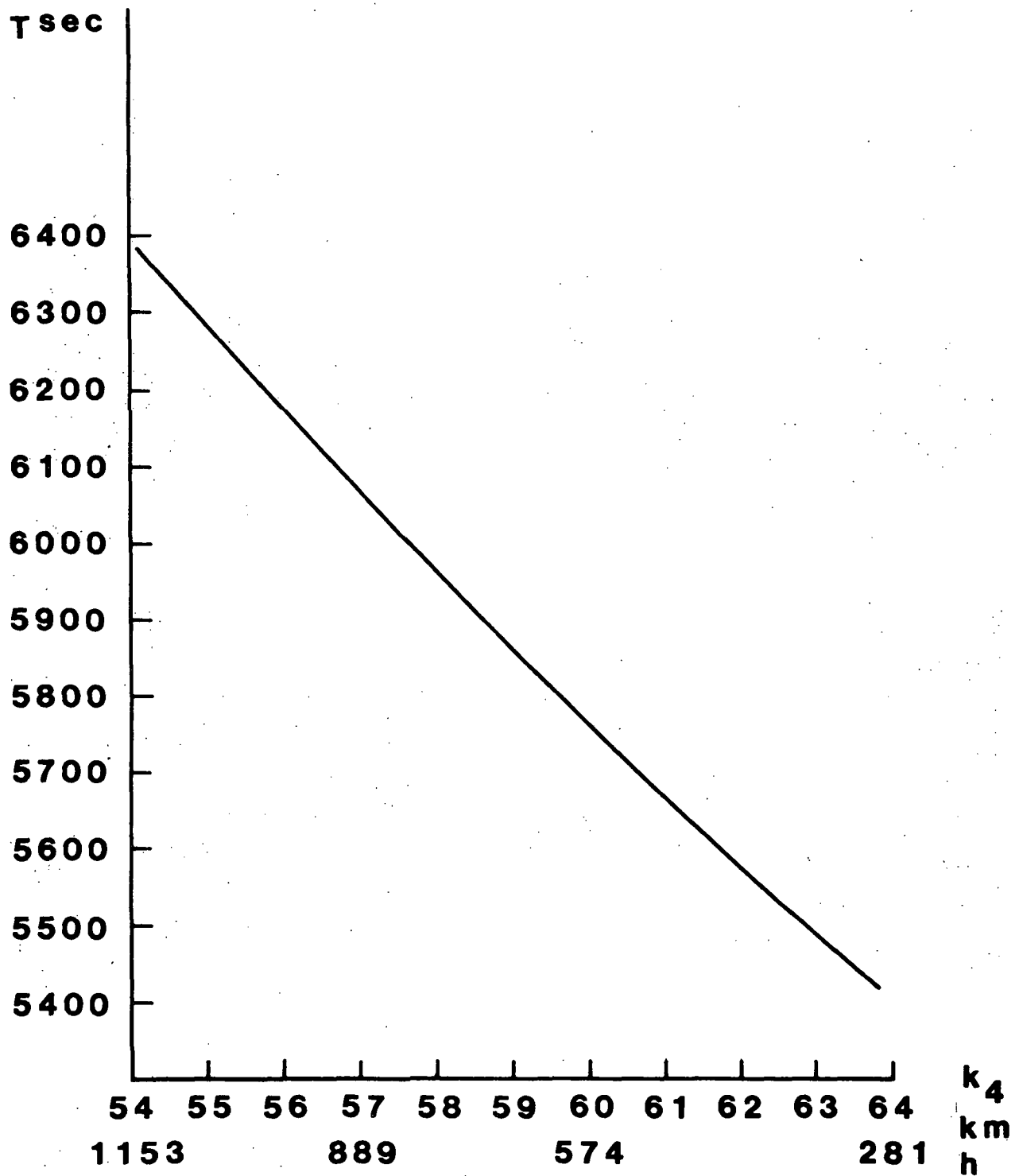
Figure 3.3 - Orbit numbers and period times versus orbit height for 4 day
revisit time.

After one orbit period time, T the subsatellite point on the Earth moves by $K(\phi)$ from West to East, where K is a function of latitude ϕ of the subsatellite point. For a polar orbit ($i = 90°$) this produces $K(0)$ distance between subsequent subsatellite points at the equator of the Earth. For larger latitudes the distance between the traces is less than $K(0)$. Table 3.4 displays the separation between the 0th and 1st orbit traces at $\phi = 0$ (equator) and $\phi = 45$ latitude versus k_3.

TABLE 3.4

Separation between consecutive orbit traces caused by the

rotation of Earth for polar orbit, 3 day revisit time

k_3	h^{km}	$K(0)^{km}$	$K(45°)^{km}$
48	281.3	2500.00	1769.62
47	375.4	2553.19	1807.27
46	472.8	2607.51	1846.57
45	573.8	2664.21	1887.59
44	678.6	2727.27	1928.47
43	787.5	2785.29	1975.39
42	900.7	2850.07	2022.41
41	1018.4	2917.91	2070.54

By definition k_3 orbit occurs in 3 days. Thus the k_3^{th} orbit trace is the same as the 0th. Some of the orbit traces are between the 0th and the k_3^{th} orbit trace and divide the gap K into smaller sections. The situation best can be illustrated by an example.

Table 3.5 shows for $k_3 = 44$ polar orbits the distance from the sub-satellite point of the 0th orbit at the equator and $\phi = 45°$ for various values of the orbit number.

TABLE 3.5

Separation between orbit traces for $k_3 = 44$ for various

orbit numbers (h = 678.6 km)

Orbit no.	Flight direction	$K(0)^{km}$	$K(45°)^{km}$
0.44	N	0	0
29.5	S	454.55	
15	N	909.10	642.82
44.5	S	1363.65	
30	N	1818.20	1285.66
15	S	2272.75	
1	N	2727.27	1928.42
30	S	3181.85	

The geometry of the ground traces and the corresponding coverage area is

exhibited for 3 representative cases:

1. $k = 44$, $h = 678.62$ km, $i = 90°$, $\Delta X_M = 9.2$ km (Fig. 3.4)

2. $k = 43$, $h = 787.52$ km, $i = 90°$, $\Delta X_M = 10.42$ km (Fig. 3.5)

3. $k = 44$, $h = 678.62$ km, $i = 60°$, $\Delta X_M = 9.2$ km (Fig. 3.6)

These figures have been drawn for a scale which is distorted in longitude by

cos ϕ. The periodicity of the segments corresponds corresponds ;to the dotted

lines. The coverage within a segment is calculated for the solid line

boundaries. The swath for the figures is selected so that at the equator the

combination of North and Sourth traces results in 100% coverage. The

corresponding swath is called S_0. For polar (or near polar) orbits the shape

of the uncovered areas are North-South elongated "diamonds". For 60° orbit

inclination these diamonds are approximately square in the vicinity of the

equator. For the condition of Figure 3.4 the maximum uncovered area occurs

around $\phi = 27.5°$. Full coverage is obtained for $\phi > 52.65°$.

Some interesting characteristics can be derived from the displayed

geometries.

$\dot{\omega} = 52.65°$

Boundary of strip

$\phi = 38.52$

Not covered area

Orbit trace

Equator

454.5 km

k = 44
h = 678.62 km
i = 90°
ΔX_M = 9.2 km
$\bar{c}$ for
o ≤ i ≤ 90°

β°	S^{km}	n	$\bar{c}$%	$\phi_M°$
18.51	454.55	54	87.081	52.65
20.41	505	60	88.97	51.85
22.42	560	66	90.86	38.52
24.65	622.9	72	92.70	33.66
30.51	800	89	100	0
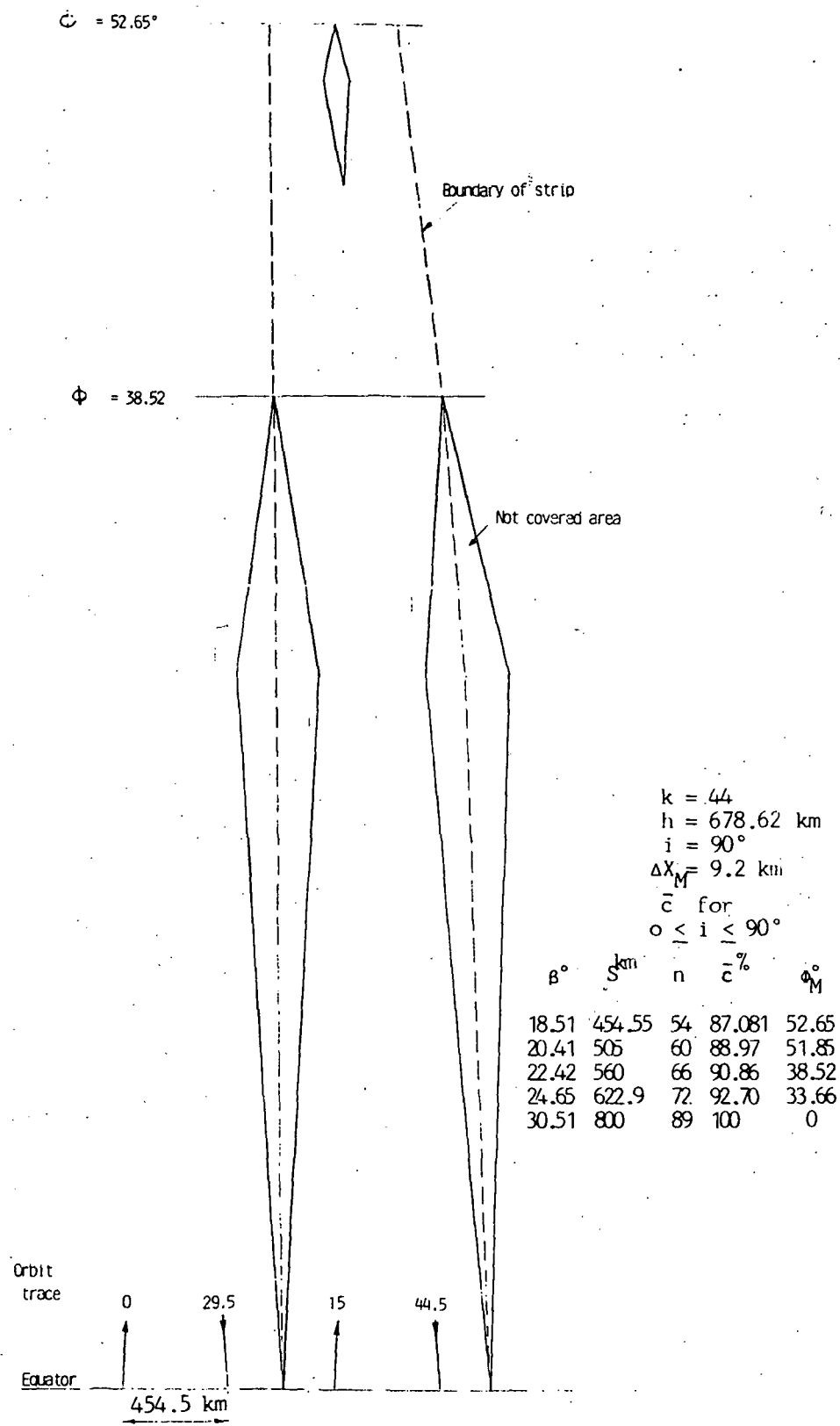
Figure 3.4 – Geometry of ground traces for k = 43,   h = 787.5 km, i = 90°.

k = 43
h = 787.5 km
i = 90°
ΔX_M = 10.42 km

β°	S km	n	c̄ %	$\Phi_M°$
16.37	465.1	48	86.61	52.56
18.41	523.2	54	88.84	51.66
20.12	573.0	59	90.90	38.52
23.29	678.3	69	94.79	31.59
27.46	818.6	81	100	0

0

43.5

4.65.1 km
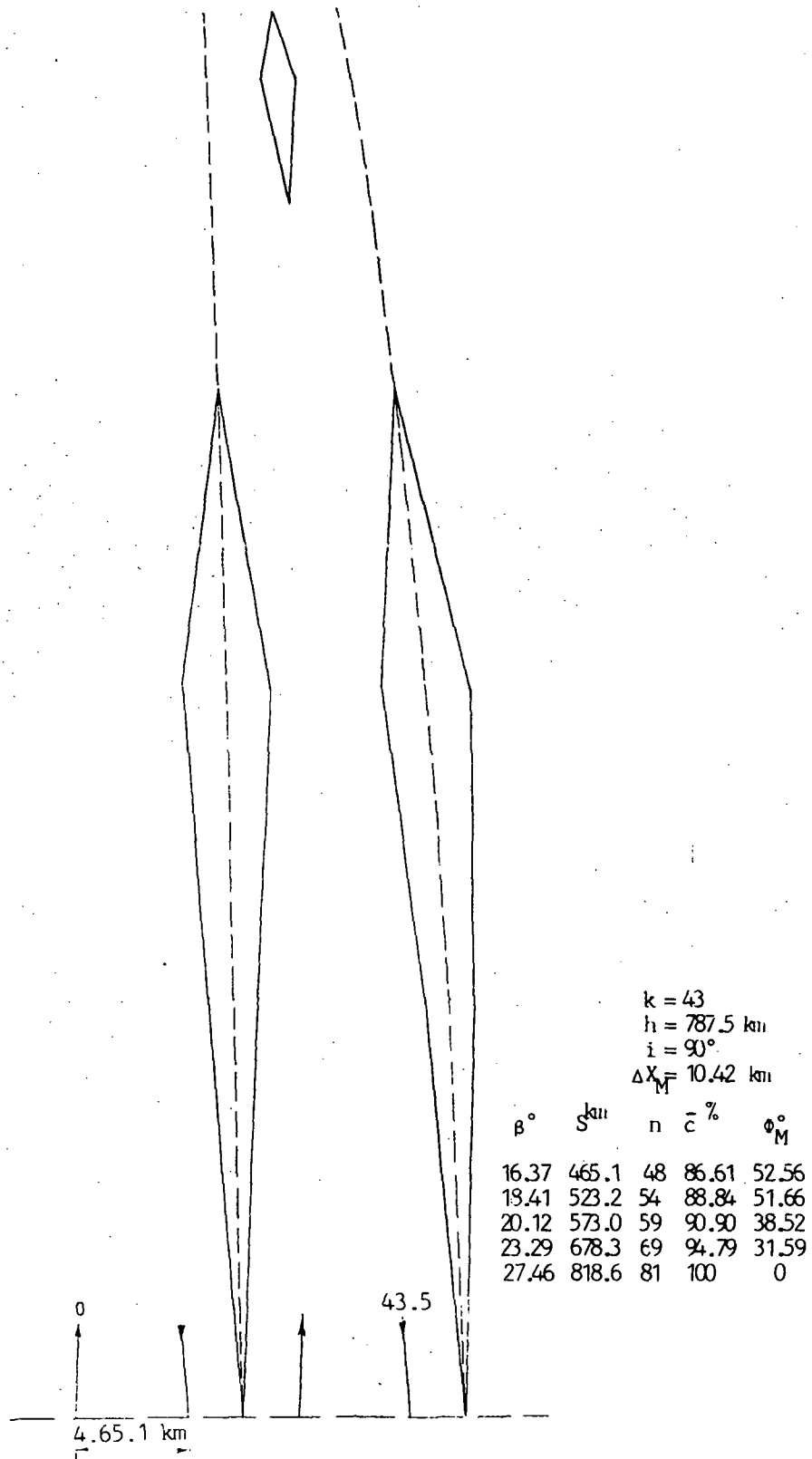
Figure 3.5 - Geometry of ground traces for k = 44 h = 678.62 km, i = 90°.

30

$\phi = 36°$

k = 44 $\bar{c}$ for
h = 678.62 km o $\leq$ i$\leq$60°
i = 60°
ΔX_M= 9.2 km

$\beta°$	S^{km}	n	$\bar{c}^{\%}$	$\phi°_M$
18.51	454.5	54	86.43	49
21.06	522.7	62	92.19	43
26.66	681.7	78	97.11	36

Equator

454.5 km
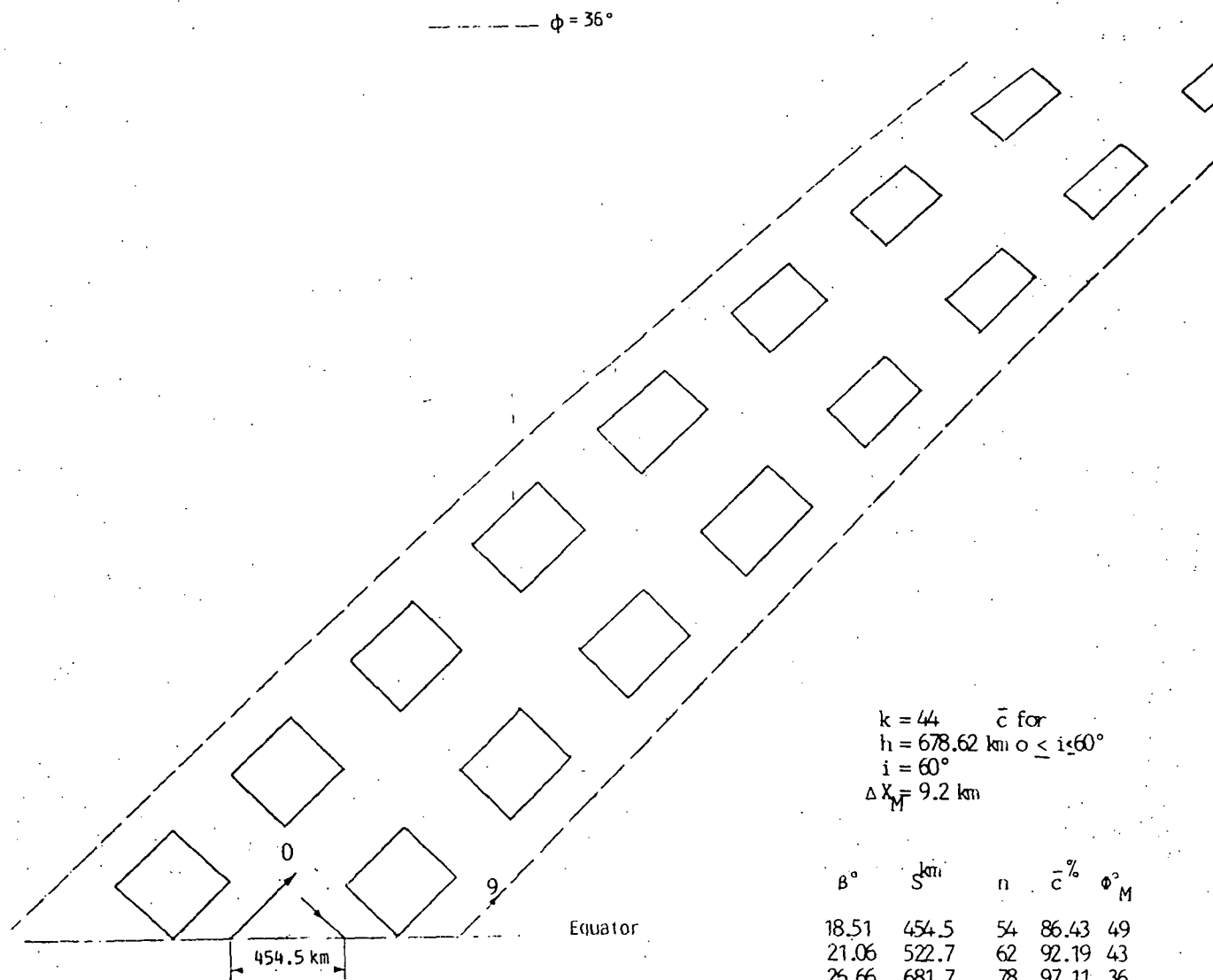
Figure 3.6 – Geometry of ground traces for k = 44,   h = 678.62 km,   i = 60°.

Figures 3.7 and 3.8 show the variation of coverage percentage versus latitude for $i = 90°$ and $60°$, respectively, for $k = 44$ ($h = 678.62$). (In Fig. 3.7 the instanteneous, in Fig. 3.8 the running average of the coverage percentage is shown, where the average is calculated over a range of $\Delta\phi = 4°$.) It can be seen that for $i = 90°$ the first minimum coverage latitude is around $\phi \cong 27°$ while for $i = 60°$ this shifts to $\phi \sim 15°$. Furthermore, with increasing swath the latitude of minimum coverage can be lowered (to about $\phi \sim 10°$ for $i = 60°$, $S = 681.7$ km). With $i = 60°$, $S = 681.7$ km assures a 100% coverage for $36° < \phi < 60°$.

Figure 3.9 exhibits the average coverage for $i = 90°$ as a function of the swath, S. It can be seen that for $k = 44$, $S = 650$ km is needed for 100% coverage. However, for the more realistic swath of 450 km nearly 92% coverage is achievable.

Figure 3.10 presents the achievable average coverage as a function of antenna beams for $\Delta X_M = 9.2$ km spatial resolution. For $i = 90°$ the average is calculated assuming $0 < \phi < 90°$. For $i = 60°$ the average is computed assuming $0 < \phi < 60°$. As expected, the inclined orbit gives a better coverage in its applicable area, provided the number of beams are $n > 55$.

According to Figure 3.11 for $i = 90°$, $n = 50,85.9\%$ and 87.4% average coverage can be obtained with 9.2 km and 10.4 km spatial resolution, respectively. Any further increase of average coverage percentage requires a rapid increase of n.
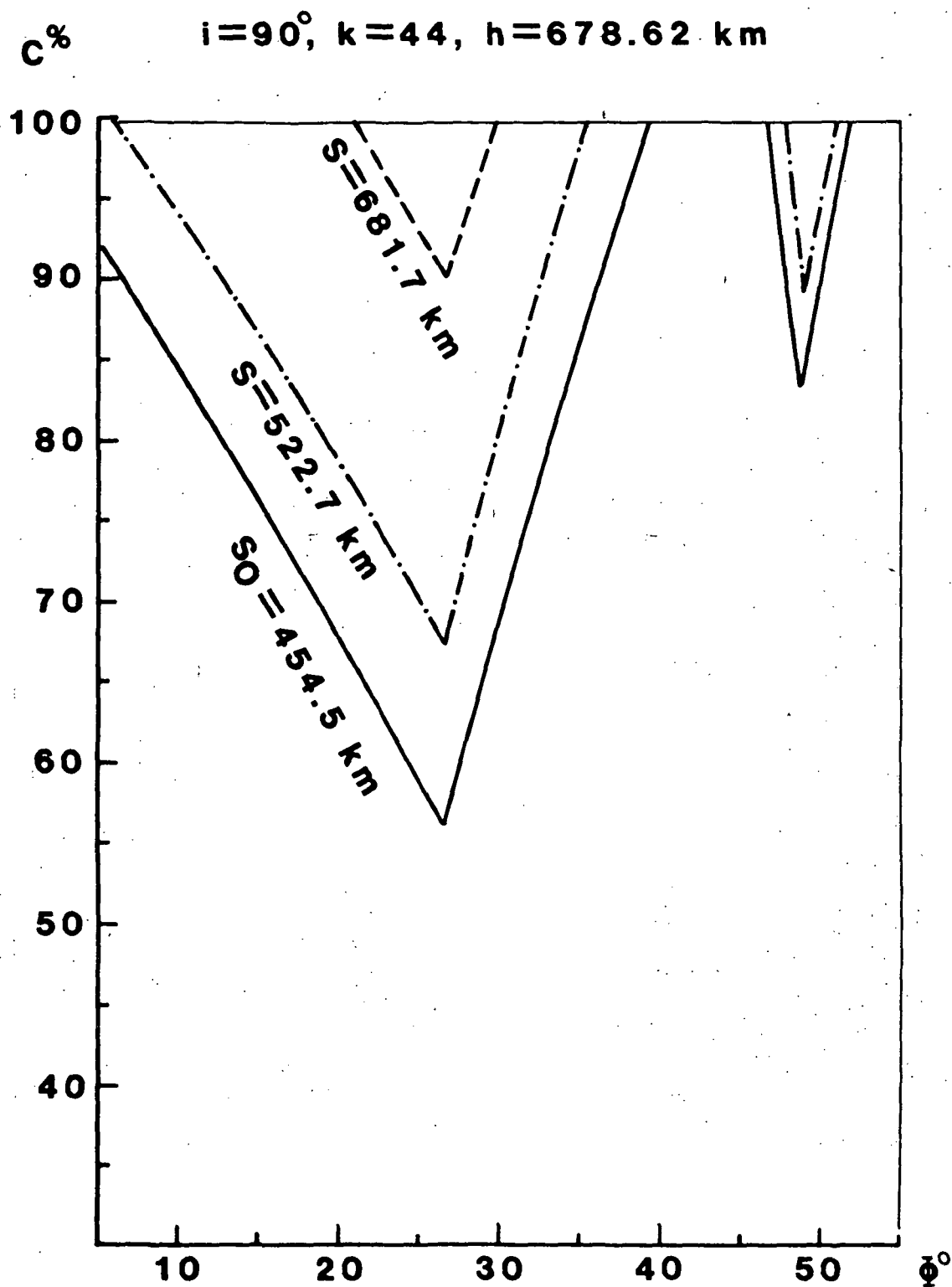
Figure 3.7 – Variation of coverage versus latitude, ϕ for various values of swath, S (i = 90°).
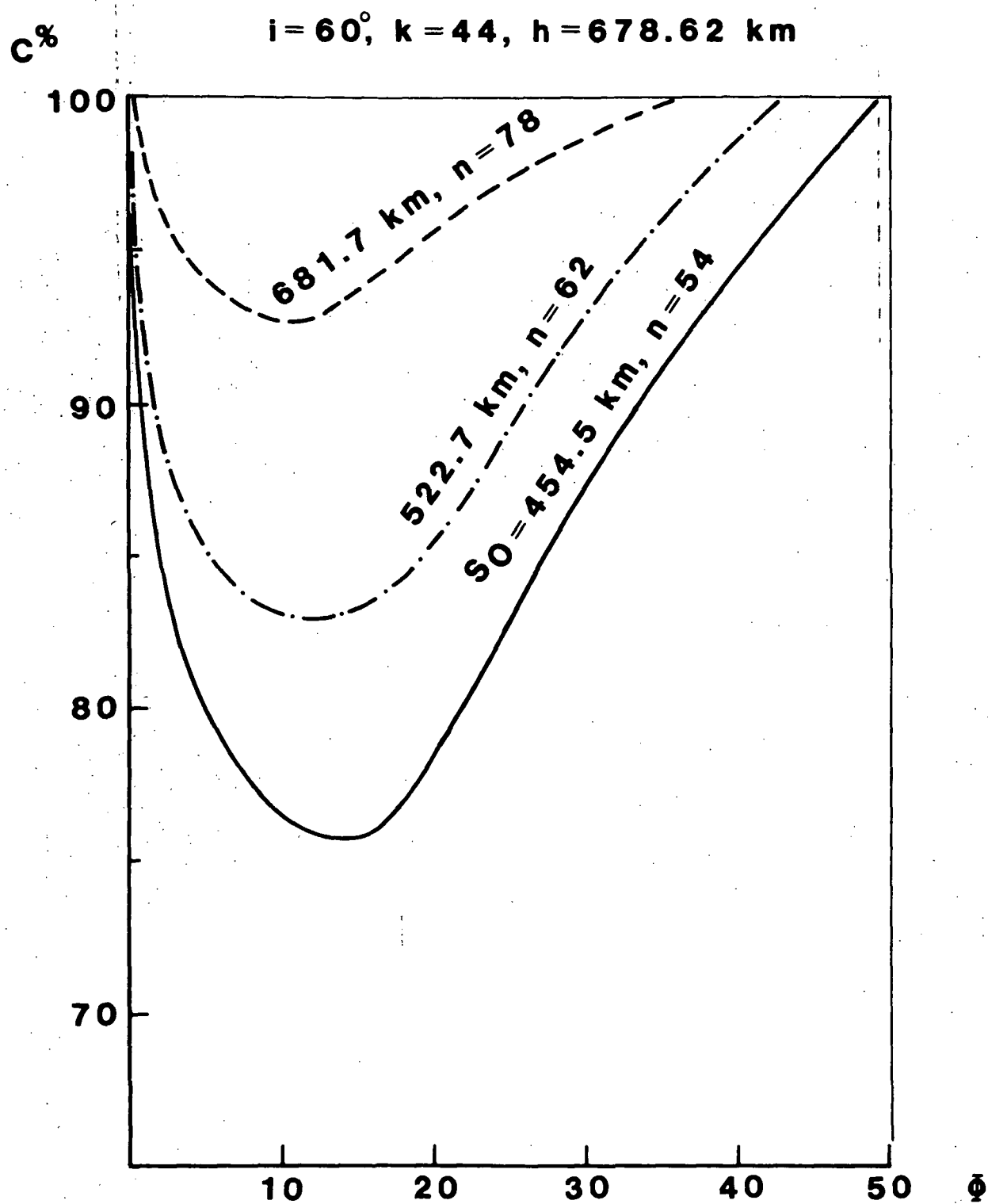
Figure 3.8 - Variation of coverage versus latitude, ϕ for various values of swath, S (i = 60°).

$k_3 = 44$, $h = 678.6$ km
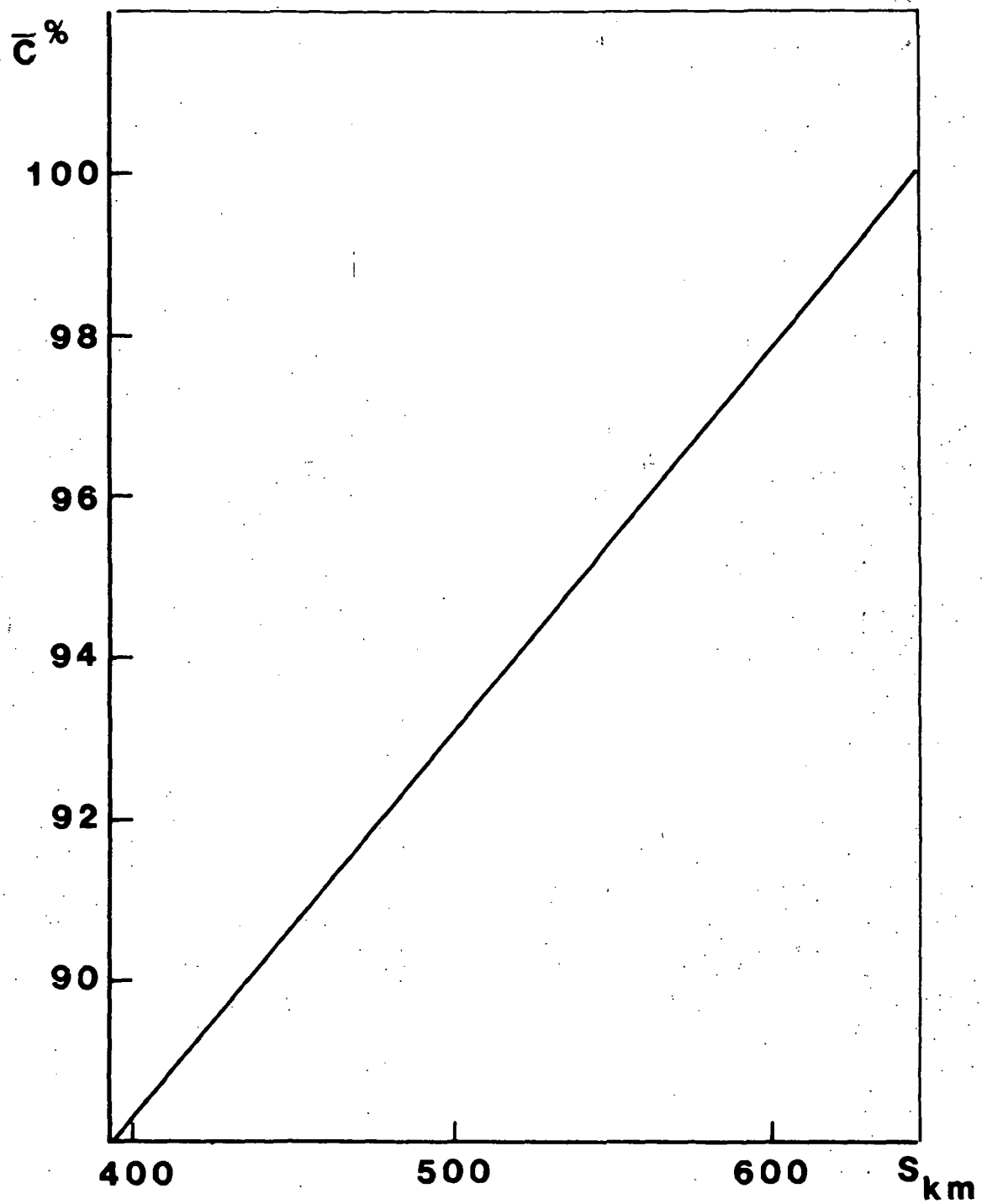
Figure 3.9 – Variation of average coverage versus swath for polar orbit.
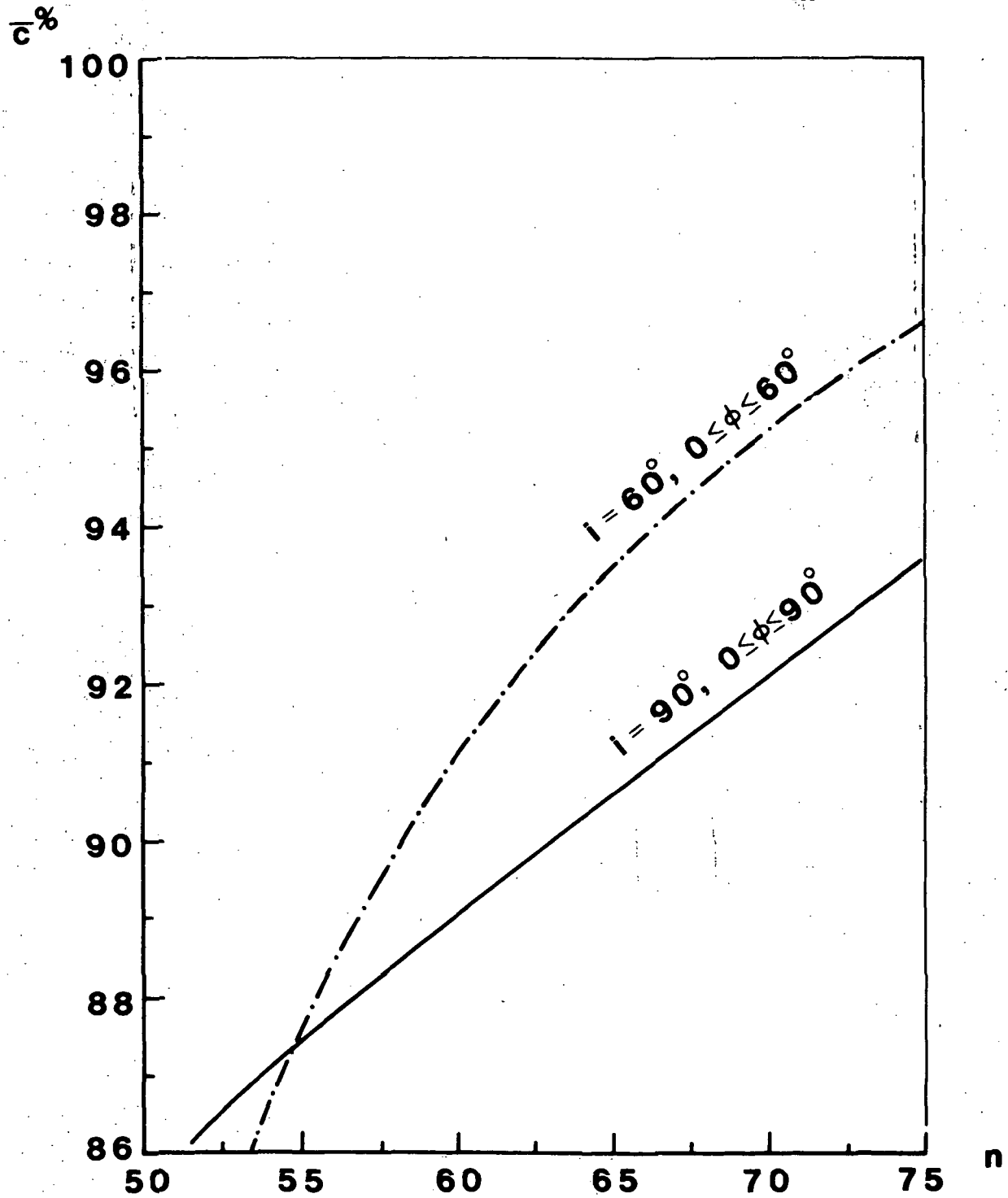
Figure 3.10 - Variation of average coverage versus number of antenna beams for different orbit inclinations.
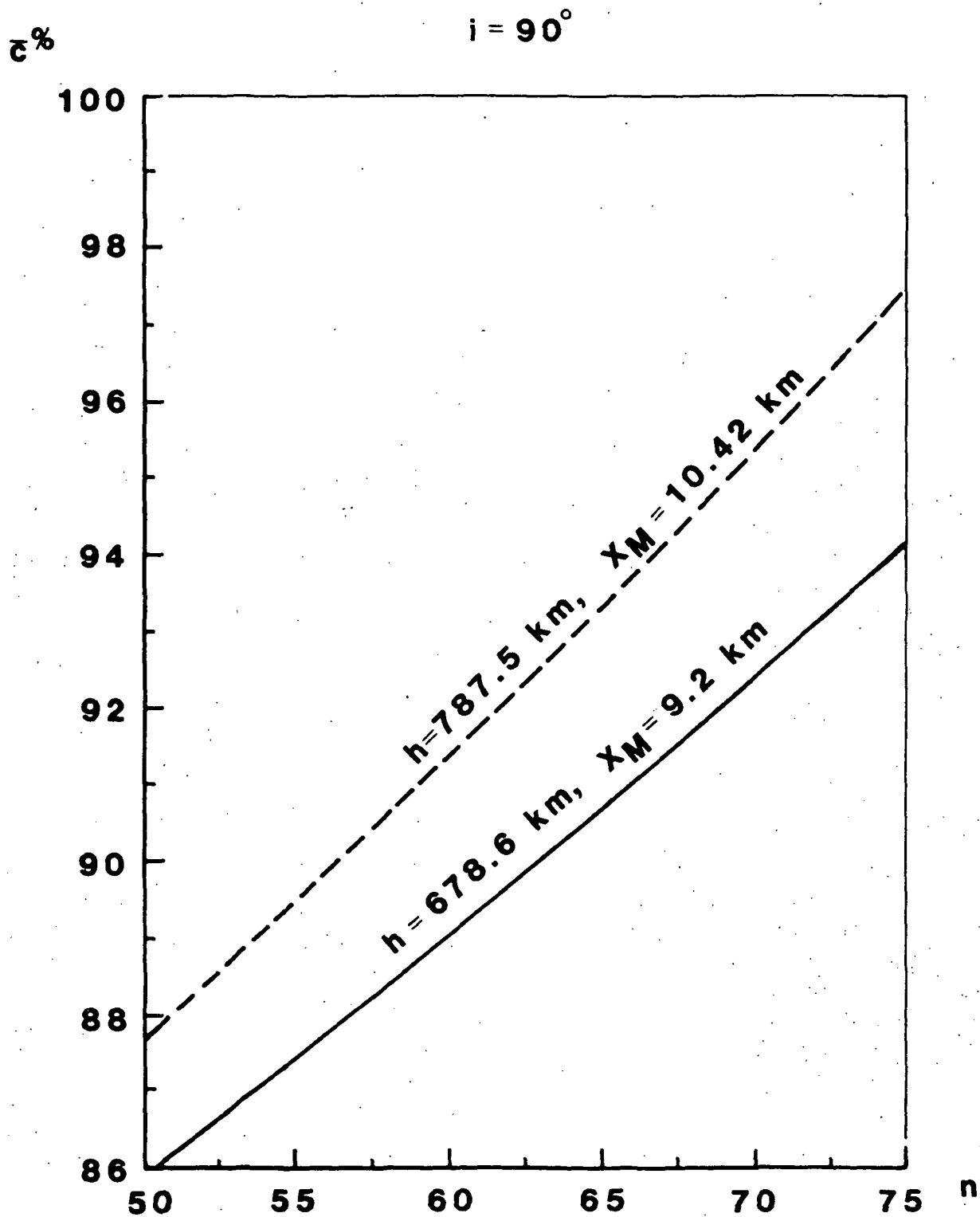
Figure 3.11 - Variation of average coverage versus number of antenna beams for different orbit heights.

Table 3.2 indicates that $k_3 = 48$ results in too small orbit height (unacceptable large atmospheric drag) and $k_3 = 42$ results two large orbit height (unacceptable poor resolution for the given antenna). Thus only $43 < k_3 < 47$ should be considered. Among these values $k_3 = 45$ must be omitted, because it results in ground traces which do not fill the gap between the 0th and 45th orbit. The remaining values for further considerations are $k_3 = 47, 46, 44,$ and 43.

Tables 3.6 and 3.7 display some of the characteristics of these remaining orbits.

TABLE 3.6

Separation between orbit traces for $k_3 = 46$ and various

orbit numbers (h = 472.8 km).

Orbit no.	Flight direction	$K(0)^{km}$	$K(45°)^{km}$
0.46	N	0	0
15.5	S	435.39	
31	N	870.08	615.75
46.5	S	1306.19	
16	N	1741.12	1231.16
31.5	S	2176.53	
1	N	2611.44	1846.57
16.5	S	3046.83	

TABLE 3.7

Separation between orbit traces for $k_3 = 47$ and various

orbit numbers (h = 375.4 km).

Orbit no.	Flight direction	$K(0)^{km}$	$K(45°)^{km}$
0.47		0	0
31.5		425.84	
16		851.86	602.36
47.5		1277.65	
32		1703.73	1204.72
16.5		2129.79	
1		2555.86	1807.27
32.5		2981.65	

On the basis of the previously presented formulas it is possible to calculate the relationship between h, β, α, and δ. For the given orbit height and latitude of an Earth point, Tables 3.5, 3.6 or 3.7 give the applicable $K(\phi)$ separation between orbit traces. From this α can be determined. Then the use of Figure 3.3 yields β. The results are exhibited in Figure 3.12.

Using the above data the design procedure is illustrated by the following example. If $k_3 = 44$, then $h = 678.6$ km. At $\phi = 45°$ latitude the separation between the North directed traces is $K(45°) = 642.83$ km. This corresponds to

$$\alpha = \sin^{-1} \frac{r}{R_E} = \sin^{-1} \frac{0.5\ K(45^0)}{R_E}\ 15 = \sin^{-1} \frac{615.75}{6372.88} = 2.889^0$$

From Figure 3.4

$$\beta \sim 25^0, \quad \delta \sim 63^0$$

Assuming $\theta_B = \theta_{98\%} = 0.6865°$, the number of required beams for contiguous coverage at $\phi = 45°$ latitude is

$$n = \frac{2\beta}{\theta_B} \cong 73$$

If $k_3 = 47$, then $h = 375.4$ km and $K(45°)_{16} = 602.3$ km. For such a case $\alpha = 2.707°$, $\beta \cong 37°$, $\delta \cong 50°$ and $n = 108$.

It can be seen from the example that while the spacing between ground traces is not very sensitive to orbit height the number of necessary beams for contiguous coverage varies rapidly with h.

$D^X = 118$ m, $D = 48.96$ m, $f = 1413.5$ MHz, $A = .2$, $P = 2$, $\theta_{14.5dB} = \theta_{98\%} = .6865°$, $\theta_3 = 3353°$, $D_\lambda = 230.68$, $\lambda = 21.2239$ cm
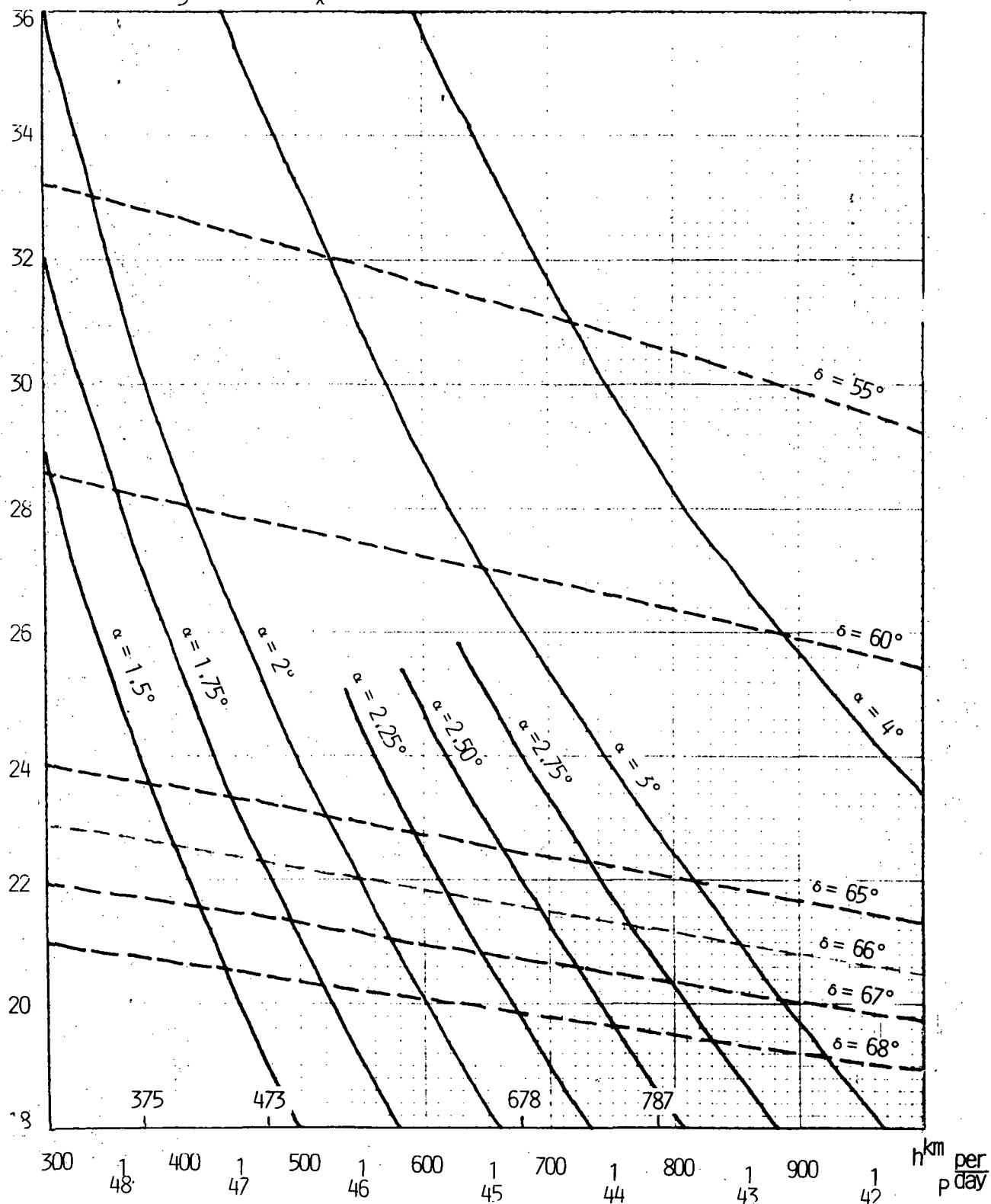
Figure 3.12 – Variation of various field of view characteristics versus number of orbits in 3 day revisit time systems.

The variation of spatial and temperature resolution with orbit height represents the other aspects of the orbit height considerations. This is displayed in Table 3.8 assuming $\theta_{98\%} = 0.6865°$. The same table indicates the orbit separation at the equator and the number of beams necessary for contiguous coverage at the equator when both the North and South traces are utilized.

TABLE 3.8

Resolution and required beam number characteristics for $\theta_{3dB} = 0.335°$, $\theta_{98\%} = 0.686°$, 100% coverage at equator, N and S traces utilized, polar orbit 3 day revisit time.

k_3	h^{km}	$2r^{km}$	$\alpha°$	$\delta°$	$\beta°$	L^{km}	ΔX_m^{km}	δX_M^{km}	n	$v_g^{km/s}$
47	375.4	425.5	1.913	58.77	29.31	434.6	5.206	6.088	84	7.2607
46	472.8	434.8	1.954	63.52	24.52	523.7	6.274	7.009	72	7.1062
44	678.6	454.5	2.043	69.54	18.41	719.5	8.619	9.199	54	6.7972
43	787.5	465.1	2.091	71.54	16.37	825.2	9.885	10.421	48	6.6427

It can be seen from Table 3.8 that the spatial resolution improves rapidly with decreasing h while the speed of suborbital point increases. This reduces the available dwell time, thus temperature resolution. Table 3.9 exhibits the variation of normalized spatial resolution, $(\Delta X_M)_N$, ground speed, $(v_g)_N$, dwell time, t_N, and the product resolution $(\Delta X_M)_N (\Delta T)_N$ as a function of h.

It can be seen from Table 3.9 that for a given antenna the product resolution improves with lower orbit height. Thus it can be concluded that the orbit height must be as small as possible, compatible with the largest n which can be accommodated within the constrains of the launch vehicle.

TABLE 3.9

Variation of the normalized resolution characteristics

k_3	h	$(\Delta X_M)_N$	$(v_g)_N$	t_N	$(\Delta T)_N$	$(\Delta X)_M(\Delta T)_N$
47	375.4	1	1	1	1	1
46	472.8	1.151	.9787	1.176	.9221	1.061
44	678.6	1.511	.9361	1.614	.7870	1.189
43	787.5	1.711	.9149	1.870	.7312	1.251

The problems associated with increasing n can be seen from Table 3.10. This table exhibits the full swath angle, 2β, of the overall antenna system and the maximum scan angle, $\pm\theta_M$, of each subaperture when the overall aperture is divided into N = 2, 3 or 4 subapertures. For this situation the difficulty to make a properly formed beam can be characterized by the $\theta_N = \theta_M/\theta_{3dB}$, normalized scan angle. Note that in Table 3.10 θ_3 is constant. This assumes that the overall diameter of the antenna aperture is increased to keep the subaperture diameters in wavelength constant as the number of subdivisions increases.

TABLE 3.10

Required scan angles for various numer of subapertures, N, assuming

contagious coverage at the equator, $\theta_3 = 0.355°$, N and S traces

utilized, polar orbit, and 3 days revisit time.

k_3	n	$2\beta°$	$2\beta°/N$			$\pm\theta_M°$			$\pm\theta_N = \theta_M/\theta_3$		
			N = 2	N = 3	N = 4	N = 2	N = 3	N = 4	N = 2	N = 3	N = 4
47	84	56.62	29.31	18.87	14.15	14.65	9.43	7.07	43.73	28.14	21.10
46	72	49.04	24.52	16.34	12.26	12.26	8.17	6.13	36.59	24.38	18.30
44	54	36.82	18.41	12.27	9.20	9.20	6.13	4.60	27.46	18.30	13.73
43	48	32.74	16.31	10.91	8.18	8.15	5.45	4.09	24.32	16.27	12.21

It can be seen, that at one extreme, for $k_3 = 47$ (h = 375.4 km) with N = 2 subapertures the antenna must scan $43.73\ \theta_3$. This cannot be achieved

by a focal point feed paraboloid reflector. A paraboloid torus optics may be usable in this case, but such a geometry is characterized by relatively poor reflector utilization and partial blockage. Furthermore such a configuration needs a large subarray per beam even for small scan angles in order to compensate aberations in the optics.

At the other extreme of orbit height range, ($k_3 = 43$, h = 787.5 km) the product resolution is 25% poorer. However, N = 4 subapertures requires 12.21 θ_3 beamwidth scan only. This can be comfortably realized with a relatively large F/D ~ 1.3 and modest size subarrays.

At intermediate orbit height ($k_3 = 44$, h = 678.6 km) N = 3 subaperture requires $\theta_N = 18.3 \theta_3$ beam scan. This results in acceptable beam quality with somewhat larger subarray, thus with an increased size overall feed cluster. Since the feed cluster complexity and volume is roughly proportional with θ_N^2 the overall feed system volume is proportional with $n\theta_N^2$. The normalized bolume of this function is exhibited in Table 3.11.

TABLE 3.11

Relative variation of overall feed system volume with k_3.

k_3	$n\theta_N^2$		
	N = 2	N = 3	N = 4
47	22.447	9.295	5.225
46	13.470	5.980	3.369
44	5.690	2.527	1.422
43	3.967	1.775	1

The feed volume is taken as unity for the $k_3 = 43$, h = 787.5 km and N = 4. The volume increases by 5.225 times as the orbit height is reduced from 787.5 km to 375.4 km. Thus a 25% of improvement in product resolution requires a rapid increase of feed complexity.

For constant k_3 the feed volume increases and the resolution decreases with ddecreasing N.

If $k_3 = 44$ and N is decreased from 4 to 3 then for constant resolution the overall antenna diameter can be reduced by 0.75 while the feed volume increases by 1.777. Provided the feed volume increase is approximately compensated by reduced reflector volume such a trade off could be attractive. This is so because the use of 3 subapertures has structural advantages relative to the 4 subaperture case. However, for a given overall antenna structure size the lightest (smallest volume) feed requires the smallest possible k_3 and the largest possible N.

4. ELECTROMAGNETIC DESIGN

4.1 General Considerations

The basic mechanical concept of the hoop column involves the use of a strong circumferentially located hoop and structurally rigid, axially placed column. Between these elements a set of guywires maintains the static balance. This basic structure supports an electromagnetically reflecting mesh surface, forming the optically necessary reflector shape.

From the point of view of RF design the reflector is the only useful contributor to the antenna. Additional elements like the guywires, the central column, and the feed of the optics represent undesirable elements as far as blockage and scatter are concerned.

It can be shown, that by controlling the number, diameter, attachment location and material of the guywires the blockage and scatter related to these elements can be reduced to a practically acceptable level. On the other hand the location of the column at the structural symmetry axis remains a major contributor to the undesirable effects. Additionally, with increasing number of component beams the feed array represents increasing blockage. This is causing a reduction of pattern quality through lost aperture area and by scattering the intercepted radiation into undesirable angular regions.

The above described limitations may or may not be tolerable depending on the special application. When the antenna must generate one, or a few component beams then the feed blockage itself may be small compared to the scatter caused by the column. Provided that the column is electromagnatically adequately transparent such a design may be considered for pushbroom antennas with limited number of beams and with medium quality sidelobe levels. This configuration is the "singel aperture hoop column antenna" which offers the best possible resolution for a given structural diameter. With increasing

number of component beams the number of subarrays in the feed cluster increases. Additionally, for increasing scan angle the quality of beam formation can be maintained only by increasing the number of elements in the subarrays. This increase the feed blockage until the system becomes blockage limited. Alternatively, it is possible to keep the blockage relatively low by limiting the number of elements in the subarrays. For such situations the system rapidly becomes phase error limited.

It is clear from he above considerations that for large component beam number pushbroom applications the feed blockage and column scatter must be either eliminated or greatly reduced. This requires the offset feeding of the hoop column antenna.

Electromagnetically, the simplest possible offset feeding would require the use of a single aperture offset feed paraboloid. In this configuration the hoop and column maintains the basic structural symmetry as before and the axis of the feed array is directed along the axis of the column. The reflector however, is an offset feed paraboloid, thus it is not axially symmetrical in the polar coordinate system with an axis along the axis o the column. The column is parallel with the direction of maximum feed radiation and the scatter from the column is similar to the already discussed case of single aperture with small number of component beams. However, by increasing the offset, the feed blockage and scatter can be reduced or at the limit eliminated. The implementation of such a system requires a relatively large F/D in order that the shape of the offset paraboloid surface does not deviate considerably from the shape of its best fit, tilted axis symmetrical parabolid. (See Fig. 4.1.) If this condition is not maintained the mechanical implementation of the offset feed paraboloid reflecting surface on a symmetrical hoop column structure becomes impractical or impossible.

46
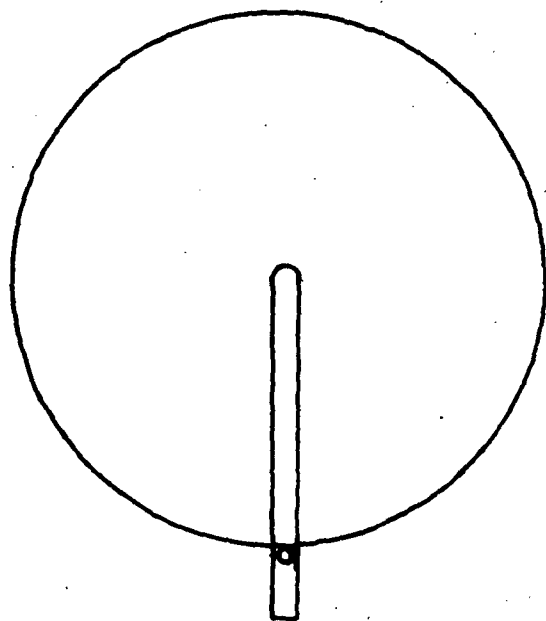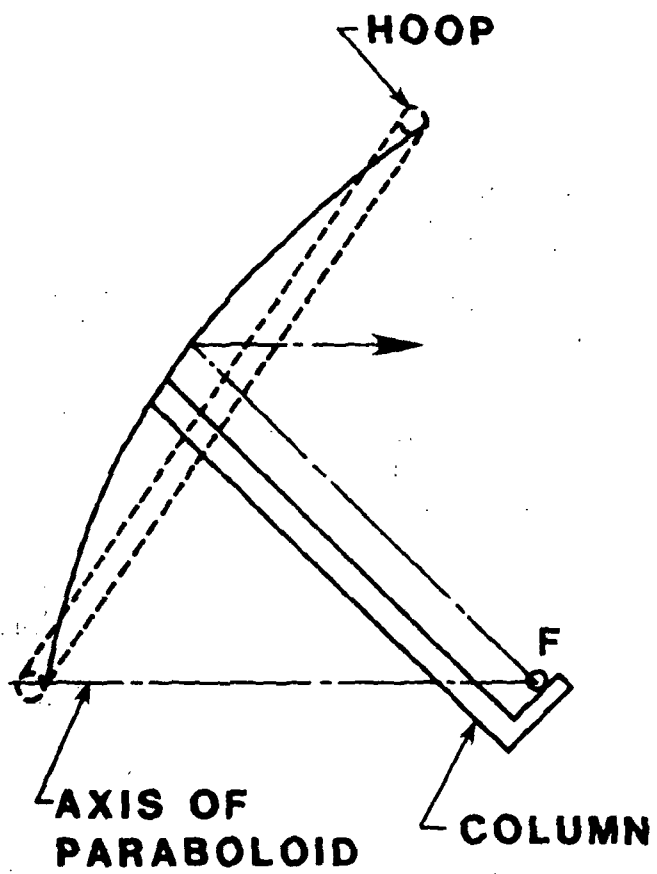
Figure 4.1 - Concept of the single aperture offset feed hoop column antenna.

It can be seen from the above that in a single aperture implementation using a hoop column structure the guywire and feed blockage can be nearly eliminated, while the column scatter can be only reduced. Such reduction requires the use of a highly transparent column and mounting the subarrays of the feed relatively far away from the column.

A further reduction of the scatter requires the subdivision of the overall aperture into a set of subapertures. When the overall aperture is divided into two equal halfs, each is illuminated by its own feed array. This configuration allows the tilting of the feed array axis away from the axis of the column, thus a simultaneous reduction of column scatter and feed blockage. (See Fig. 4.2.) This configuration offers a great deal of design freedom. When the feed array is not tilted the complete hoop column aperture is illuminated and the best resolution is achieved. However, for this case column scatter and feed blockage is maximum. With increasing feed array tilt the scatter and blockage is reduced, but the illuminated aperture for a given taper is decreased and beam width is increased.

A practically interesting special case is when the desired subaperture contours are tangential with each other. Then the corresponding feed arrays are nearly outside the projected subapertures. Feed array tilt beyond this condition allows the compete elimination of feed blockage and the use of separate focal points for the two half reflectors. When the distance between the two focal points is small the combined reflector is still nearly axially symmetrical, this the symmetrical hoop column system offers an efficient supporting structure.
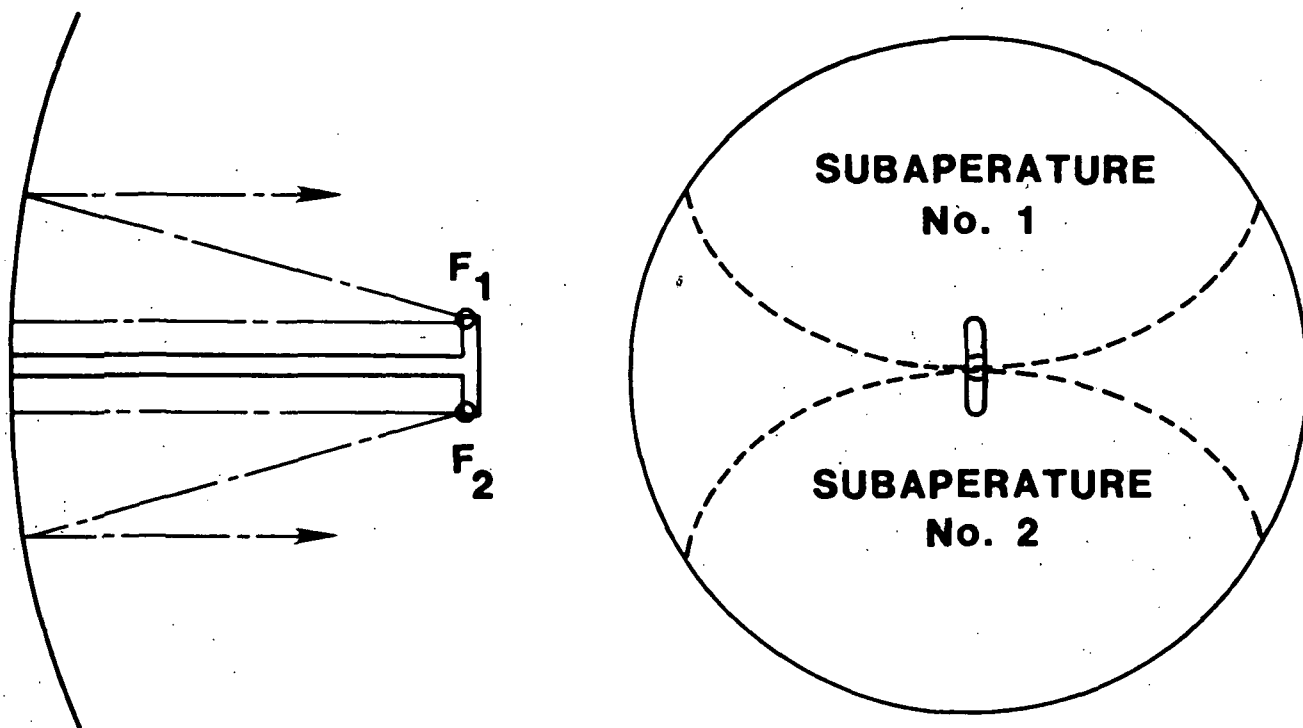
Figure 4.2 - Concept of the dual subaperture offset feed hoop column antenna.

The advantage of the described "double supaperture hoop column antenna" is the individual subapertures are large. Thus comparatively little gain loss occurs relative to the single aperture case. Additionally, the availability of two subapertures allows the assignment of adjacent beams to opposite subapertures, therefore the feed crowding problem is alleviated.

The disadvantage of the double subaperture system is that it provides either an approximately 2:1 aperture aspect ratio or results in a bad utilization of the available overall aperture. The 2:1 aspect ratio by itself is not necessarily an undesirable characteristic. When the dividing line between the subapertures is perpendicular to the direction of flight, the footprint is relatively narrow in the perpendicular to flight direction, resulting in a favorable resolution. On the other hand, it is more difficult to design the subarray for elliptical aperture shape. Additionally, the coverage of the given swath requires a large number of greatly scanned component beams. Acceptable quality beams for this situation requires a large increase of subarray size for large scan angles. This results in large volume for the feed array and the overall system becomes beam number (or feed volume) limited.

Better utilization of the available structure and larger swath angle may be achieved by further subdivision of the overall aperture. Triple quadruple or even higher order subdivision f the aperture may be visualized. (See Fig. 4.3.)

The "triple subaperture hoop column antenna" utilizes three offset feed paraboloid reflector segments. The nominal aperture shape of each of these is circular and the centers of the projected apertures are approximately on an equilateral triangle. For this situation the diameter of the subaperture is 0.48 times the single aperture hoop column antenna (56.81 m for 118 m
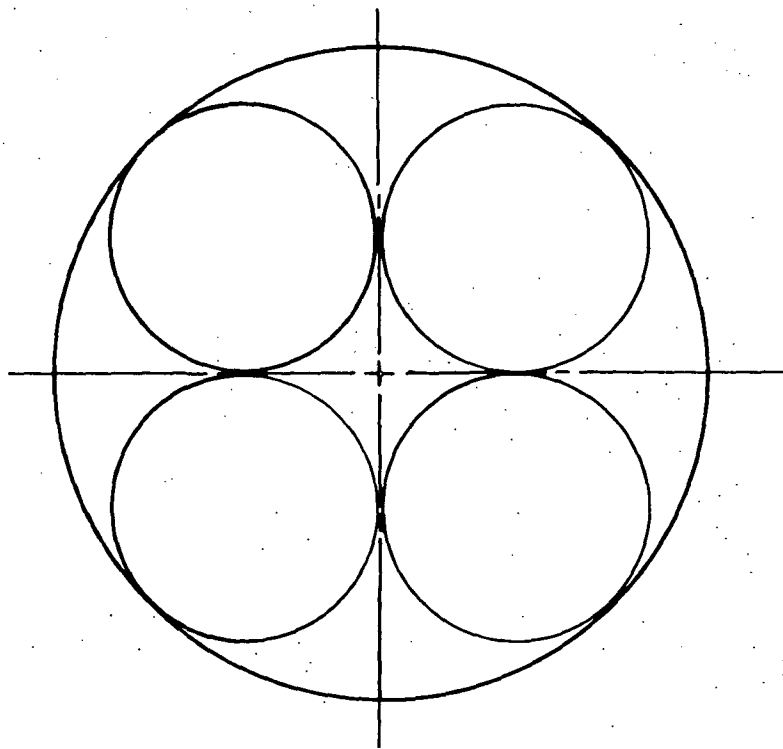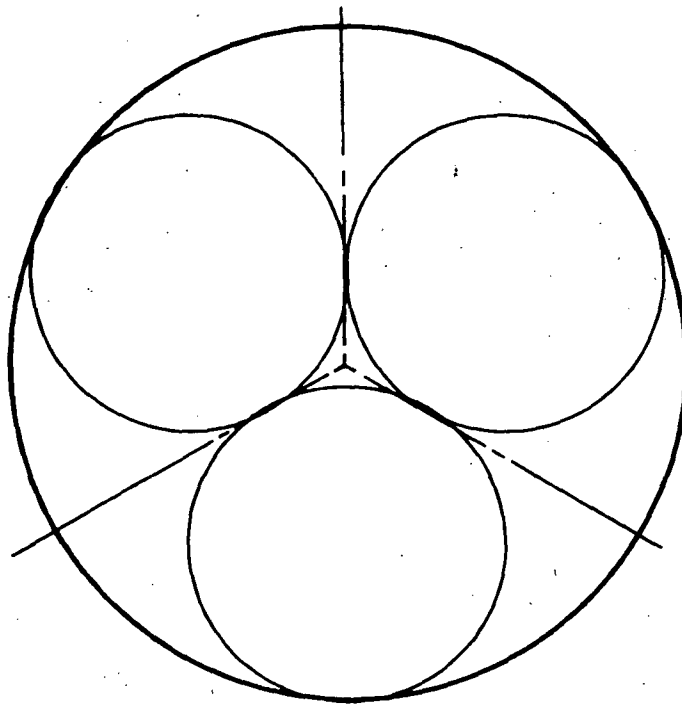
Figure 4.3 - Concept of the triple and quadruple offset feed hoop
column antenna.

structural diameter). The three subaperture utilize 69.52% of the maximum available area.

The configuration creates an unutilized area in the middle of the system. This accomodates the column and part or all of the feed arrays. The axes of the subapertures and corresponding focal points are moved outward from the column, thereby reducing column scatter and allowing more space for the feed arrays. The feed array caused blockage can be further reduced by an additional tilt of the subaperture axes away from the axis of the column. For a pushbroom antenna application one subaperture axis is tilted forward in the plane containing the flight direction and the local vertical. The beams for this subaperture are scanned in the plane perpendicular to the offset of the paraboloid and cover the center part of the desired swath.

The beams for the remaining subapertures are scanned in the plane of the offset and cover the right and left region of the overall swath. The electromagnetic design of the antenna requires two different feeds, however, the overall structure has three planes for which symmetry can be approximately maintained. This allows a simplification of the structural design. Furthermore, the axis of the maximallyscanned beam in each of the three offset reflector segments has to be one third away from the axis of the subaperture relative to the single aperture design. The component beamwidth is about half than for the single aperture (causing 0.48 times poorer resolution) thus the maximum normalized scan angle is about a factor of 6.23 less. This allows a reduction of subarray size, more beams and larger swath.

The disadvantage of this configuration is the reduction of available resolution relative to the single or double subaperture design.

The "quadruple subaperture hoop column antenna" employs a four-way division of the overall aperture. Assuming that the subapertures are equal their diameter is only 0.45 of the structural diameter (53.51 m for 118 m diameter). The four subapertures utilize 82.27% of the maximum area.

The use of four subapertures leaves more space in the center of the system for the feed arrays. Thes axes of the subarrays are on the conical surface in order to further minimize scatter and blockage. Two diagonally opposite axes are in the flight vector - local vertical defined plane, the remaining axes are in the perpendicular to flight plane. The first set of subapertures are associated to the inner left and right side of the swath. In these the beams are scanned in the plane perpendicular to offset. The second set of antennas cover the outer left and outer right side of the swath. In this set the beams are scanned in the plane of offset. Each antenna must be scanned over one fourth of the total swath. Thus the maximum normalized scan angle is about 8.82 times less and the resolution is 0.45 times less than for a single aperture using the same structure. The arrangement results in more beams and larger swath than for the triple subaperture design at the price of an insignificant 6.1% poorer resolution.

It can be concluded that for a larger swath it is advantageous to increase the number of subapertures. On the other hand, with four subapertures it is not practical to keep the tilt angle of the reflector segments approximately identical. This causes a relatively large deviation between the actually required reflector surfaces and the surface of the originial common paraboloid. It is difficult to accomodate the boundary regions between adjacent reflector segments, where large steps are required. Due to these reasons the electromagnetic advantages of the quadruple aperture design are partially negated by increased mechanical design difficulties.

In the following some additional details are given for the single, double, triple, and quadruple subaperture configurations with emphasis on the triple subaperture desing. The triple subaperture concept was selected as the baseline for the present application.

4.2 Single Aperture Concept

The utilization of the hoop column antenna in a single aperture configuration is illustrated in Figure 4.4. In this geometry the governing dimensions are the structural diameter of the hoop, D_s, and the length of the column, L_c. The axis of the column is perpendicular to the lane of the hoop. The hoop and column form a symmetrical structure. Relative to these elements the paraboloid reflector represents an asymmetrical surface. Its axis is in the direction of Y, which encloses an angle ψ_o with the axis of the column. The paraboloid is offset fed. It is characterized by focal distance F and offset Q. Q is selected so that all or most of the feed array is outside the rays associated with the boundary of the paraboloid. In the plane of offset the meridian curve of the paraboloid contains the H, I, and J points, where J, the outer terminating point of the paraboloid, is selected in such a way so that the hoop is not causing blockage. The column is constructed by using lower and upper sections with maximum envelope dimensions t_1 and t_2, respectively. The lattice structure of the column has 25% or better transparency.

For the described configuration a radiating element located at the focal point F_p does not cause blockage. However, the column interferes with the radiation of the element. When the element is moved away from the axis of the column by a distance S, then the beam is scanned in the plane of offset by approximagely $\alpha = \tan^{-1} S/L_c$. When a linear feed array with an axis perpendicular to the plane of Figure 4.4 is placed at distance S then for the

Figure 4.4 – Geometry of single aperture offset feed paraboloid hoop
column antenna.

general element in this array the beam is scanned both in the plane of the offset and in the plane perpendicular to offset. If the plane of offset is the direction of flight then the linear array forms a set of beams in a pushbroom configuration in the plane perpendicular to flight. The plane of the pushbroom is tilted forward or backward relative to the axis of the paraboloid.

With increasing S the shadow cast by the column on the paraboloid decreases while α increases. The first effect reduces scatter, the second deteriorates the beam shape. It will be shown latter that the loss in beam formation is small or comparable to the deterioration caused by the basic beam scan of the pushbroom itself.

The dimensions given in Figure 4.4 are for an antenna, which results in a nominal 10 km spatial resolution with $h = 787.5$ km ($k_3 = 43$) orbit height. For that situation $D_s = 50.95$ m, while $D = 47.85$ m. The effective diameter of antenna is 93.91% of the structural diameter and the antenna utilizes 88.2% of the maximum available aperture area.

Figure 4.5 depicts the boundary of the geometrical blockage associated to the Figure 4.4 geometry. For this figure $S = 1.4$ m is chosen. This represents the closest feed to the column. Additionally, $v_1 = 0.5$ m and $v_2 = 0.2$ m is selected. With 25% column transparency the geometrical blockage caused by the column for the closest subarray is 0.76%. This corresponds to 1.52% total efficiency reduction. For the subarrays, which are further than $S = 1.4$ m away from the column the blockage loss is less, but the scan efficiency is poorer.

It is relatively straightforward to calculate the radiation pattern or gain contours of the above described antenna for a single radiating element. However, for complicated subarrays the computation is quite lengthy.

56
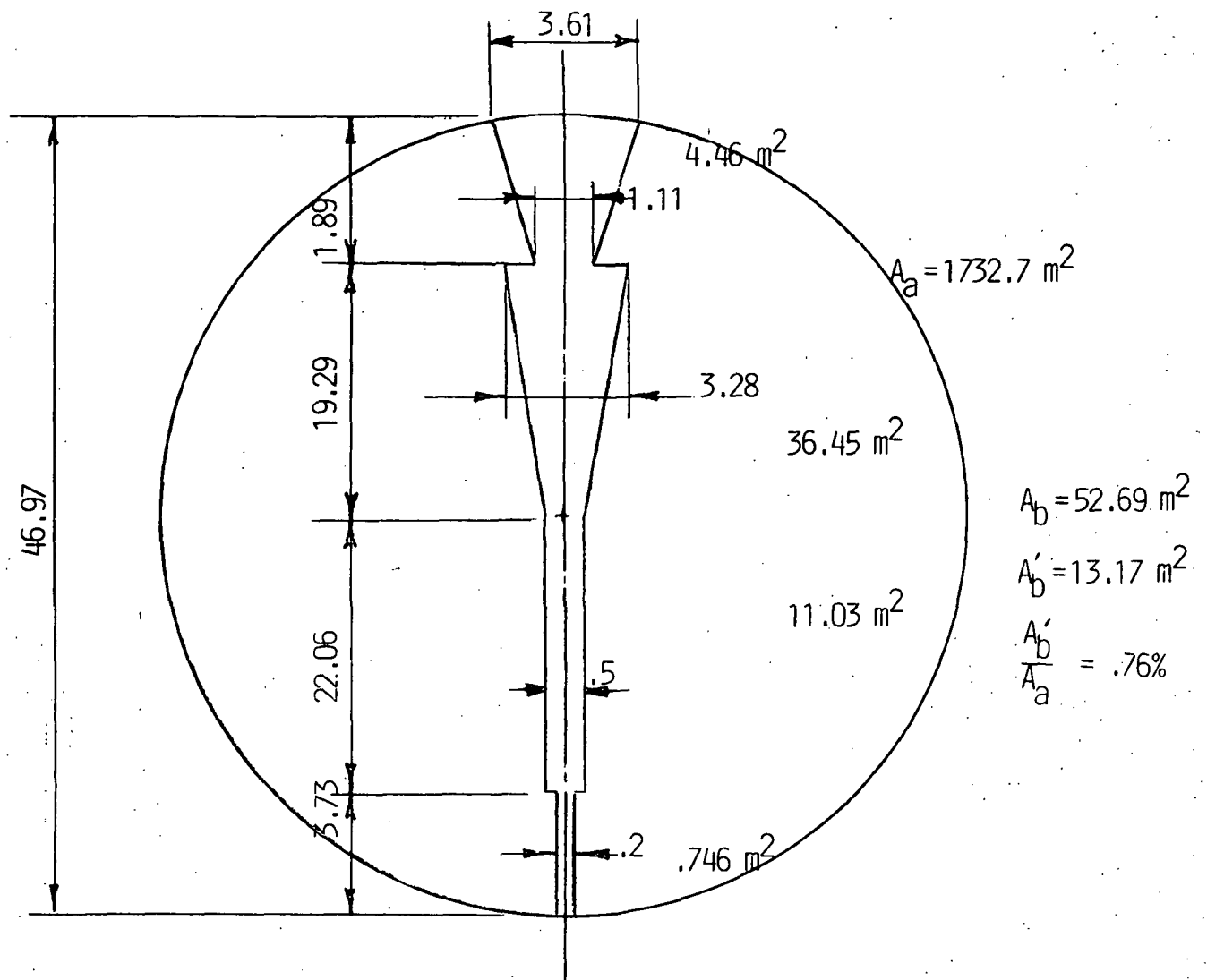
Figure 4.5 - Blockage caused by the column in single aperture hoop column
antenna for S = 1.4 m subarray location.

Additionally, it is somewhat difficult to compare complicated radiation characteristics as a function of different design parameters.

Alternatively, it is easy to construct a computer model which calculates the beam efficiency of the antenna on the basis of the phase distribution in the aperture of the paraboloid. Using Figure 4.4 for a radiating element in point C the path length to a general point on the reflector and to the end point at the edge of the aperture is given by

$$T = [(Y - A')^2 + (X + B)^2]^{1/2} \qquad (4-1)$$

$$T_M = [(Y_m - A')^2 + (X_M + B)^2]^{1/2} \qquad (4-2)$$

where

$$A = S \sin \psi_o, \quad B = S \cos \psi_o, \quad A' = F - A \qquad (4-3)$$

Using the above equations the x,y coordinates of the phase fromt can be expressed as

$$x = X + R \sin \alpha \qquad (4-4)$$

$$y = Y + R \cos \alpha \qquad (4-5)$$

where

$$R = T_M - T \qquad (4-6)$$

Once the phase front is known, the phase deviation relative to a best fit plane wave can be calculated. The results for various scan angles are shown in Figure 4.6. The parameter of the curves is the normalized scan angle $\alpha_N = \theta_M/\theta_3$ where θ_M is the angle between the wave normal and axis of paraboloid and θ_3 is the 3 dB beamwidth of the unscanned beam.

58

F/D = 1.342, Q/D = .0203
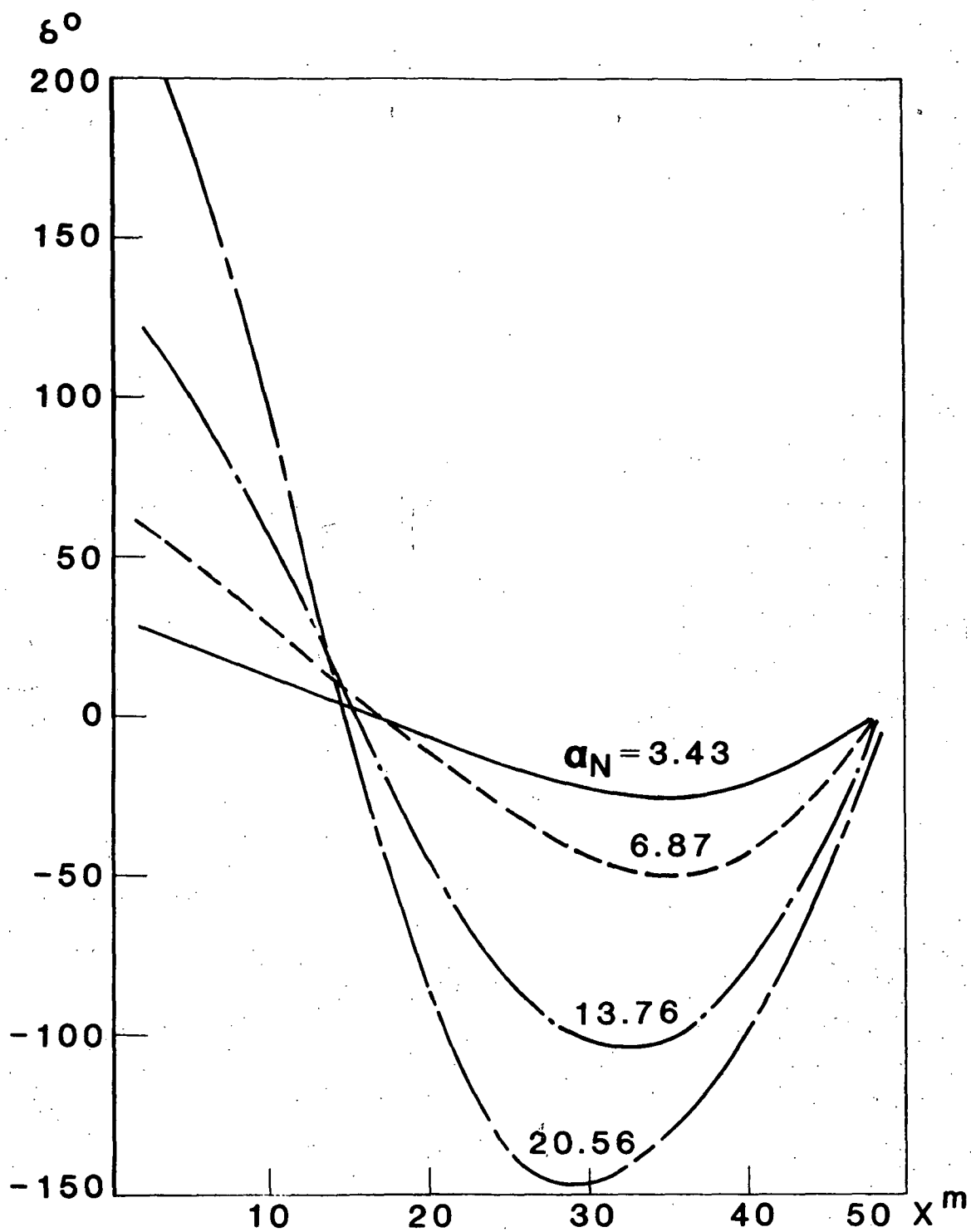
Figure 4.6 – Phase error in plane of offset for various $\alpha_N = \theta_M \theta$ normalized scan angles.

Figure 4.6 assumes the geometry shown on Figure 4.4 and an

$$A' + (1 - A')(1 - r^2)^P \tag{4-7}$$

type of aperture distribution. With $A = -14dB$, $P = 2$, and $\theta_3 = 0.339°$. θ_M is given by the direction of the normal of the best fit phase front.

$$\theta_M \sim \alpha = \tan^{-1} \frac{S}{\psi_o} \tag{4-8}$$

where

$$\psi_o = \frac{F}{\left(\cos \frac{\psi_o}{2}\right)^2} \tag{4-9}$$

It can be seen from Figure 4.6 that the peak value of phase error δ varies between 25° and 225° while α_N varies between 3.43 and 20.56.

The effect of this phase error varies with the applicable amplitude distribution in the aperture. Presently distributions with relatively large aperture taper are of interest. Then for the phase distribution shown on Figure 4.6 the rms phase error can be calculated by using a weighting technique considering the field distribution. The high values of δ in the vicinity of $X_o = 0.95$ m have relatively little effect. The rms value of δ is typically about half of the peak values observable arond $X_1 = 5$ m and $X_2 = 32$ m.

For large scan angles the described procedure predicts relatively large rms phase error. The reduction of this pahse error requires the use of a feed array instead of a single radiating element. When a single radiating element is replaced by 3 radiating elements for the linear array case, then the introduced 2 additional degrees of freedom can be utilized to synthetize 2 nulls in the aperture phase error distribution. When the location of these nulls are selected to coincide with the phase error maximum at X_1 and X_2

then the phase error function contains a total of 5 nulls, provided the location of X_o practically represents a null. The amplitude of the peak phase error for this condition is reduced approximately by 2 relative to the case for the single radiator.

For the actual antenna the phase error occurs not only in the plane of scan, (plane of offset in the above example) but in two dimensions. Thus the above level of phase error reduction requires compensating radiating elements not just on the left and right side of the center element, but all around it. This quality of compensation therefore requires a 7-element feed cluster. An additional approximately factor of 2-phase error reduction requires the addition of two more compensating ring arrays, thus a total of 37 elements. From the rms phase error the scan loss associated to the residual phase errors can be also computed. The gain loss can be expressed relative to the unscanned beam.

For proper normalization it is first necessary to calculate the radiation characteristics of the unscanned beam. Assuming that the basic feed produces an aperture distribution of the type given in equation (4-7), the beam efficiency can be determined from Figure 4.7. Since this is a relative calculation, an arbitrary beamwidth reference can be chosen.

For the present purpose, using Figure 4.7

$$\theta_{98\%} = \frac{156.8_o}{D\lambda} \qquad (4\text{-}10)$$

where $\theta_{98\%}$ is the beamwidth within which 98% of the power associated to the aperture of the ideal paraboloid is contained. This 98% power limit will be considered in the following as the ideal realizable maximum beam efficiency, η_{Bo}. Any other losses, caused by spillover around the reflector, reflector inaccuracy, blockage, scan loss is relative to this upper limit.

61
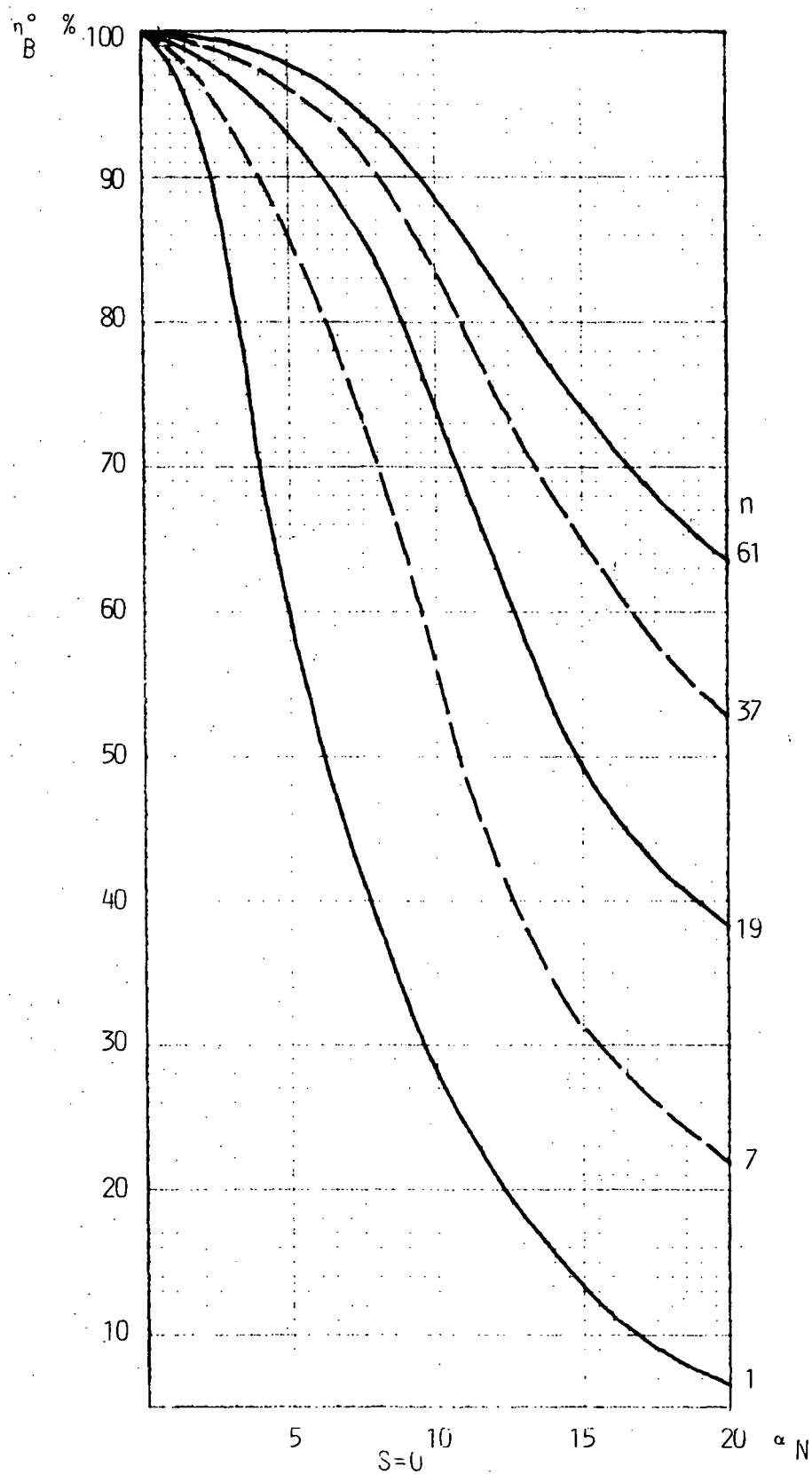
Figure 4.7(a) - Beam efficiency versus normalized scan angle for various array
element numbers and array to column distance.
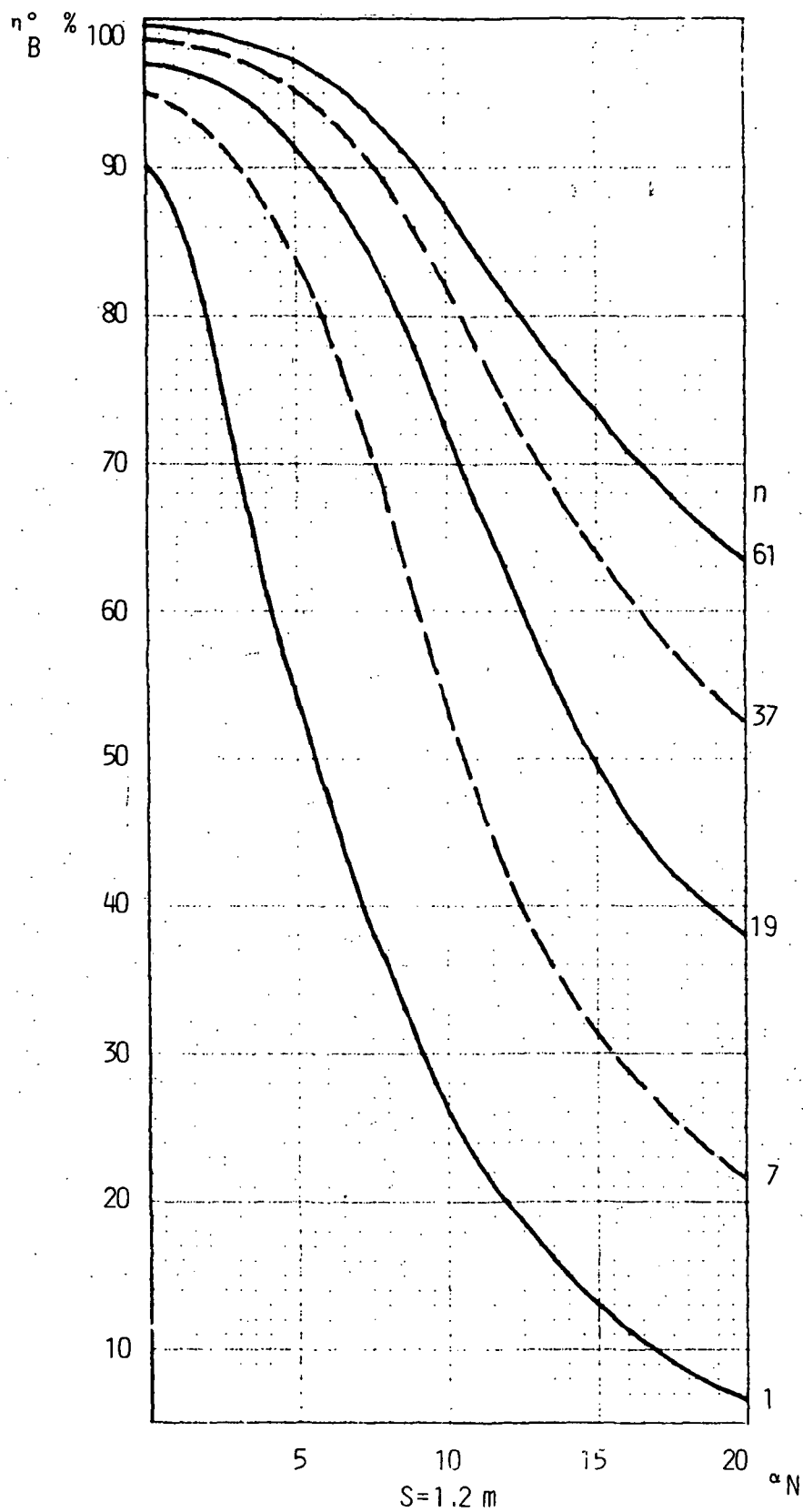
Figure 4.7(b) — Beam efficiency versus normalized scan angle for various array element numbers and array to column distance.
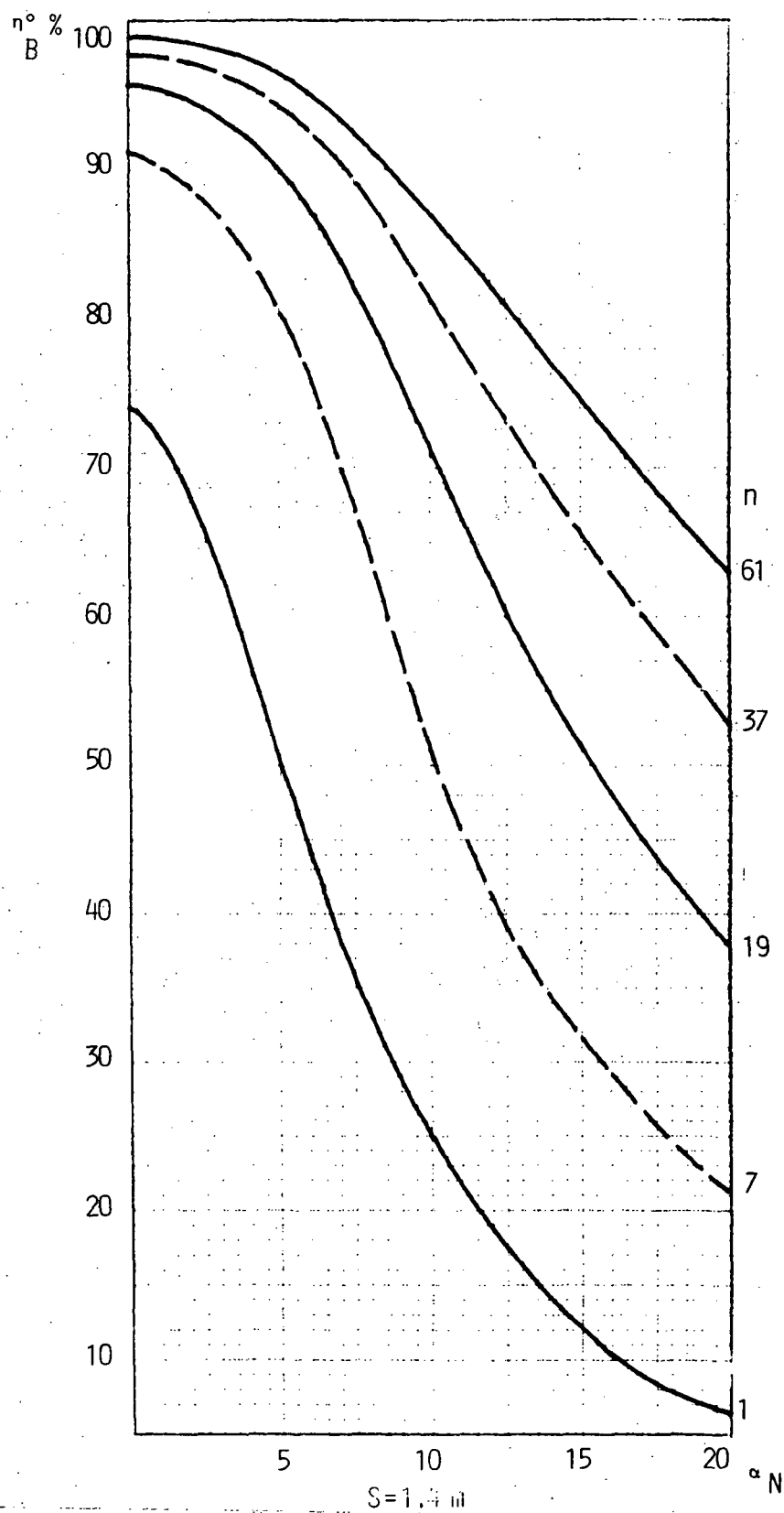
Figure 4.7(c) – Beam efficiency versus normalized scan angle for various array
element numbers and array to column distance.
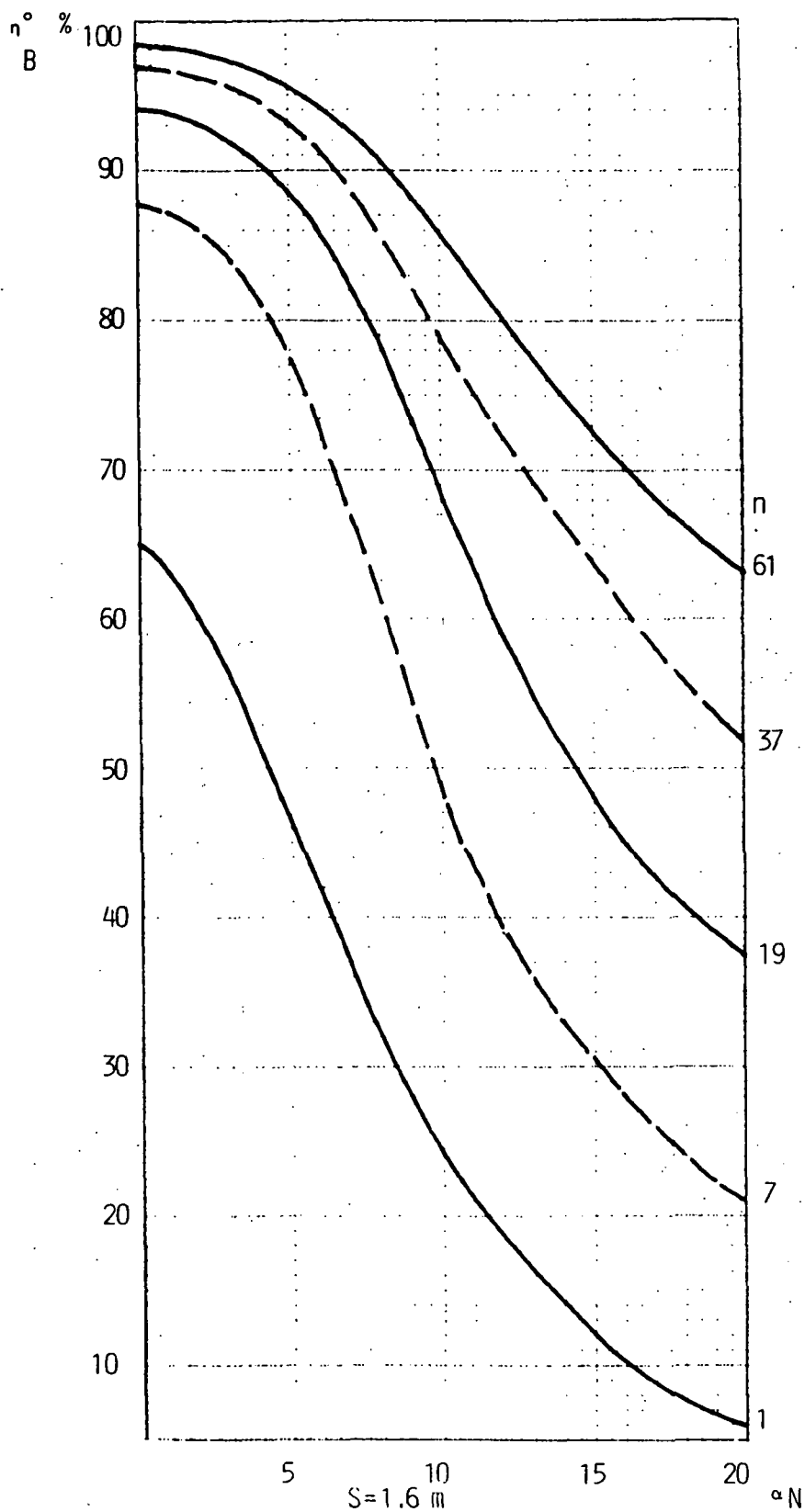
Figure 4.7(d) - Beam efficiency versus normalized scan angle for various array element numbers and array to column distance.

For the above described ideal case $\theta_{98\%} = 0.709°$. The 3 dB beamwidth of the antenna, $\theta_3 = 0.339°$, thus $\theta_{98\%}/\theta_3 \text{ }_{dB} = 2.09$.

It is practical to represent the antenna characteristics as a function of the normalized scan angle, $\alpha_N = \theta_M/\theta_3$. Figure 4.8 shows the calculated gain degradation (scan loss) as a function of α_N for $n = 1, 7, 19, 37,$ and 61 element subarrays for the case when the arrays are synthetized to give the described null distribution in the aperture phase front in the paraboloid. It can be seen that when 1 dB scan loss is tolerated the antenna can be scanned up to $\alpha_n = 13$ with $n = 61$. For such a conditions the swath of the antenna is $\beta = 2 \alpha_N \theta_3^\circ = 8.81°$.

The total beam efficiency for an ideal paraboloid with no spillover radiation is

$$\eta_B = \eta_{Bo} \eta_S \tag{4-11}$$

In Figure 4.7 S is the distance between the axis of the paraboloid and the line connecting the center of the subarrays in the pushbroom feed configuration. The highest possible efficiency is achievable for $S = 0$, but in this case the blockage is very large. $S = 1.4$ m seeam to result a practically acceptable geometrical blockage of 0.86%. (See Fig. 4.9.). Such a blockage cause $P_{B\ell} = 1.72\%$ loss of total power. When this blockage is considered, then the modified form of equation (4-11) becomes

$$\eta_B = \eta_{Bo} \eta_{B\ell} \eta_S \tag{4-12}$$

If one desires to achieve $\eta_B = 85\%$ then for $\eta_{Bo} = 98\%$ and $\eta_{B\ell} = (100 - P_{B\ell})\% = 98.28\%$, the tolerable η_s is 88.25%. This allows $\alpha_N \sim 10$ or $\beta = 6.78°$ swath.
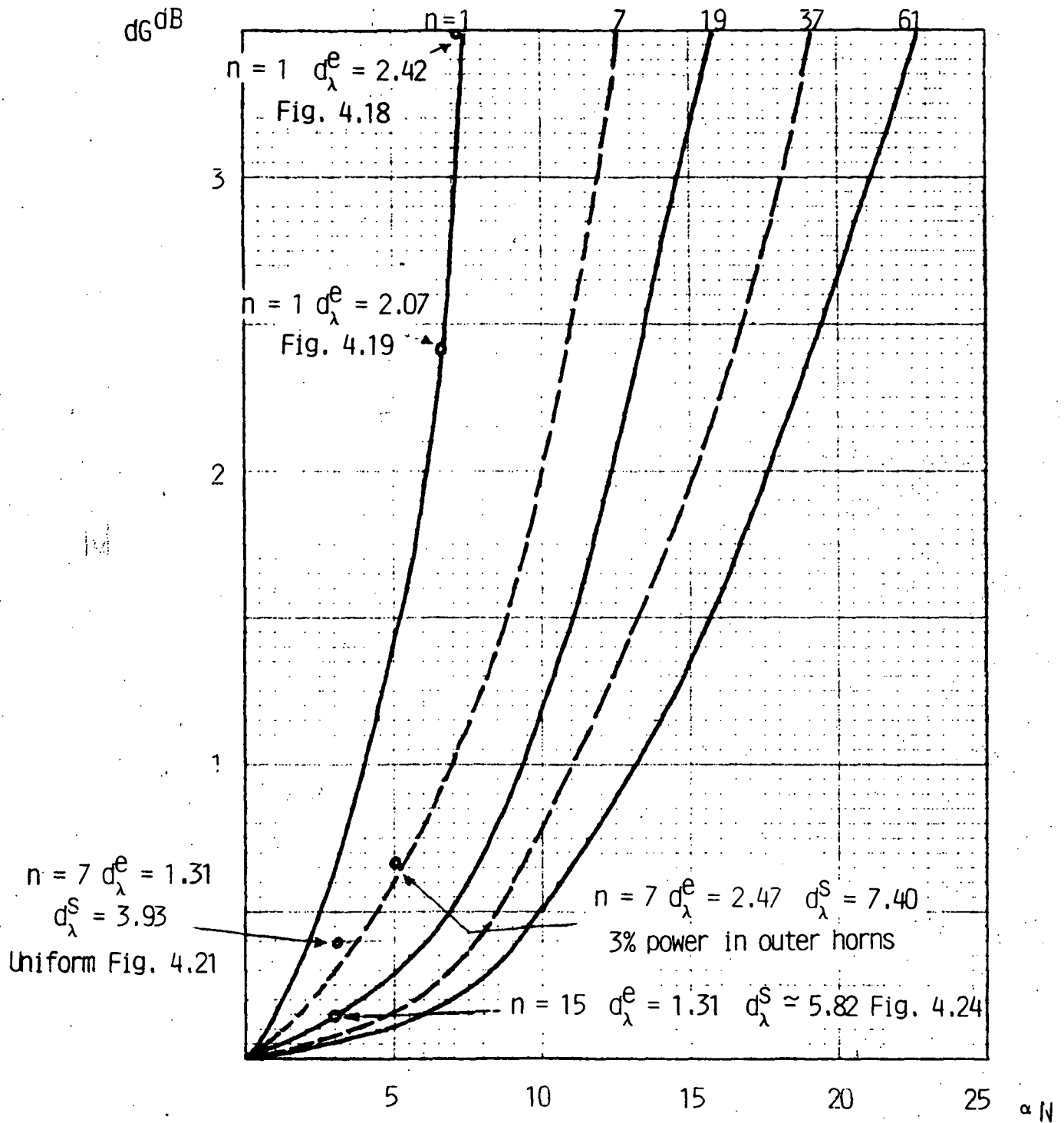
Figure 4.8 – Scan loss versus normalized scan angle for various feed array element numbers.

N = 33, 25% column transparency
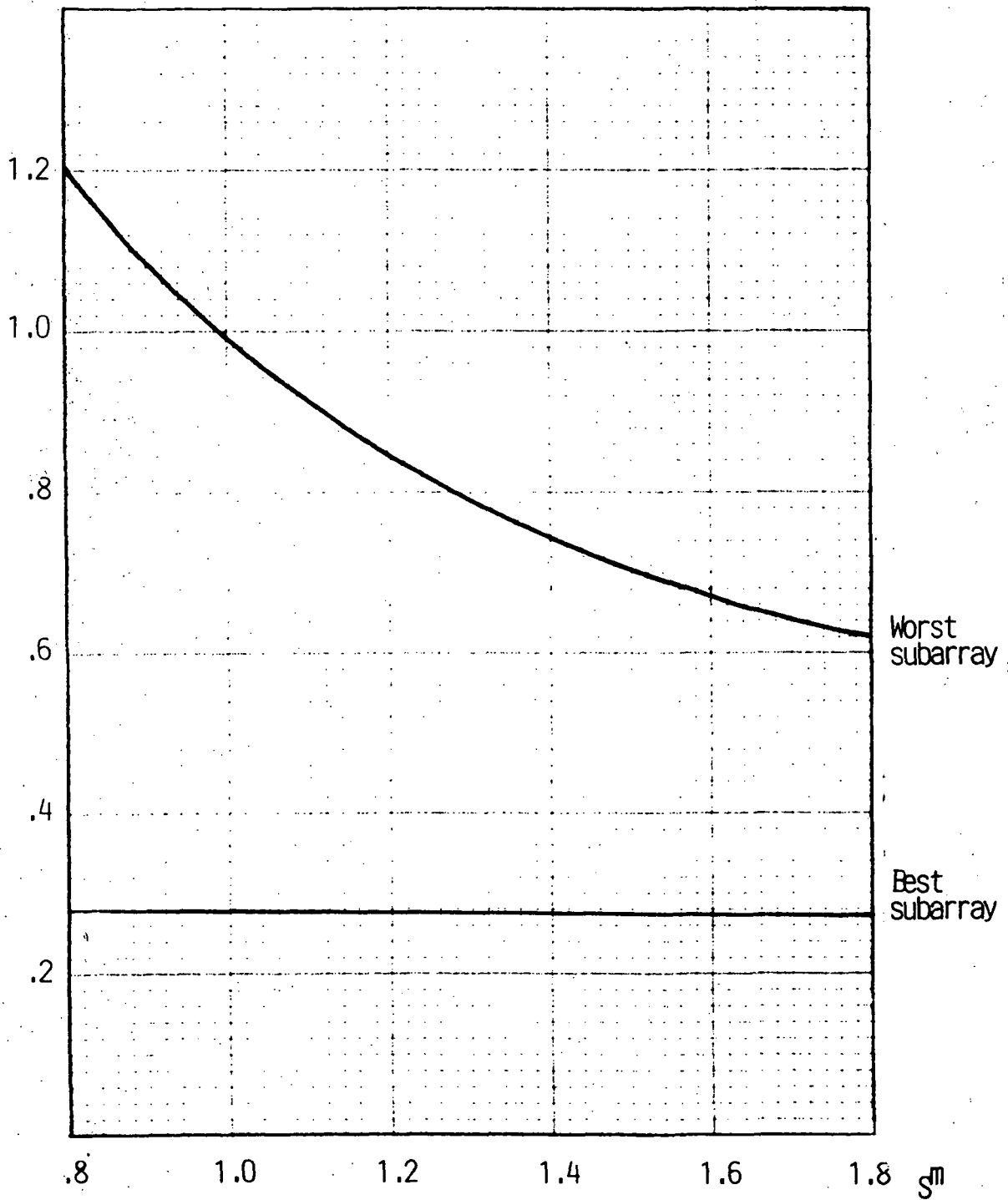
Figure 4.9 – Variation of geometrical blockage versus S.

Figure 4.10 gives another representation of the above data. It shows the number of required elements in a subarray for a given swath angle β and scan efficiency, η_s. $S = 0$ is assumed for displaying this effect. It can be seen from this figure that the number of elements in a subarray is very sensitive to the required efficiency for large β values. For instance if $\beta = 6°$ is required an improvement of scan efficiency from 80% to 90% requires to increase the elements in the subarray from 19 to 47. Since the complexity of the feed array is proportional with n such an improvement increases the antenna complexity fy a factor of 2.47.

In a practical antenna the feed array complexity must be minimized by selecting the minimum number of elements for each subarray for a given range of beam efficiency.

Figure 4.11(a) shows the variation of beam scan efficiency and the size of applicable subarrays for various subranges of the total swath for $S = 0$. The figure also shows the number of subarrays s of each type. According to this figure for $\beta = 11.18°$ swath a total of 31 subarrays are needed to achieve $\Delta X_m = 8.98$ km spatial resolution with h = 787.5 km height. The scan efficiency at the edge of swath decreases to about 71% while the average scan efficiency is approximately 83%. The above case is not practical, because $S = 0$, thus would suffer from high blockage. Figure 4.11(b) shows the situation when $S = 1.4$ m. This case does not allow the use of n = 1 type "subarrays" thus only n = 7, 19, 37, and 61 is employed. This increases the total number of radiating elements. Furthermore, the average scan efficiency is reduced to approximately 81%. However, the worst case efficiency is still nearly 71% and the average blockage is approximately 0.5%.
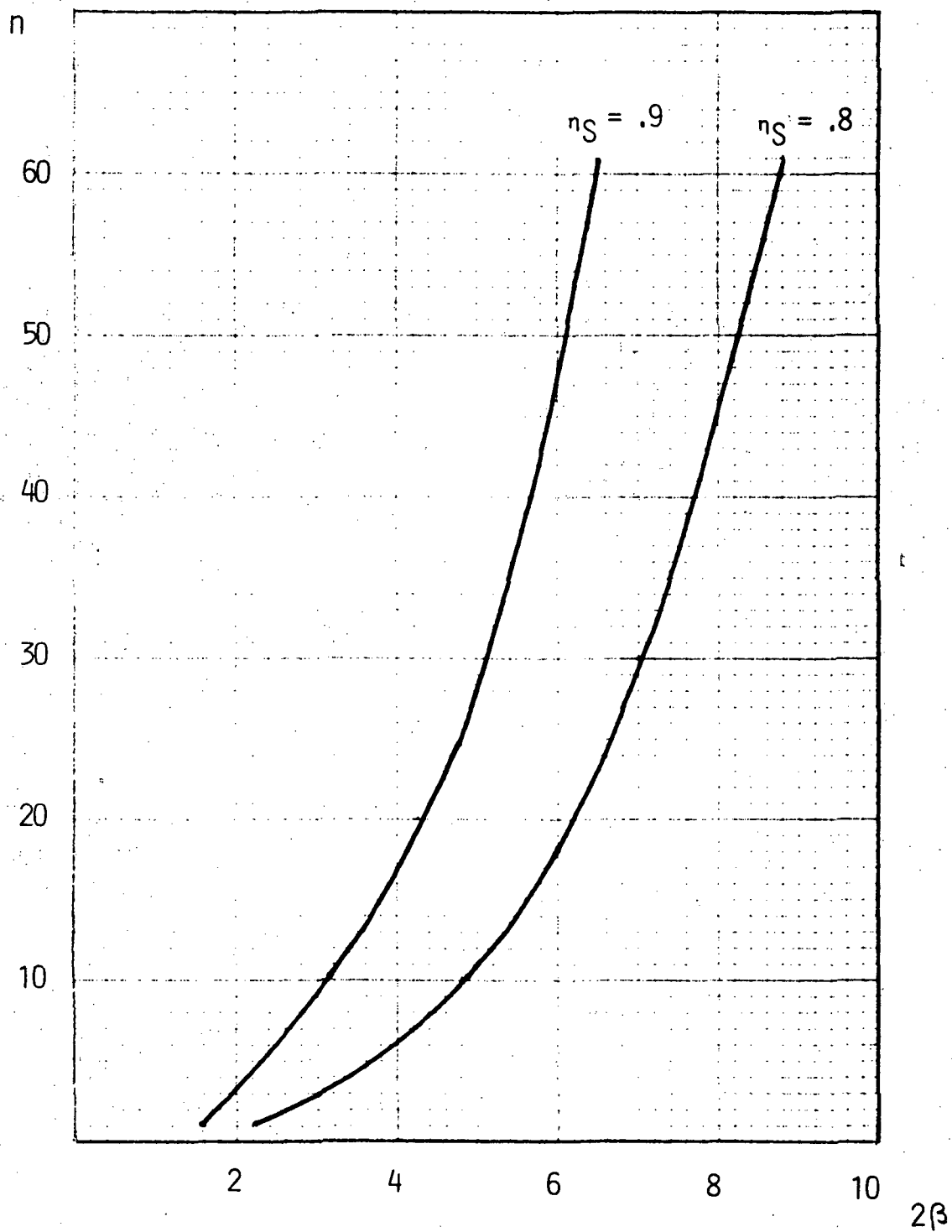
Figure 4.10 - Required radiating element number n versus total swath angle
2β   for η_B = 0.8 and 0.9   beam scan efficiency.
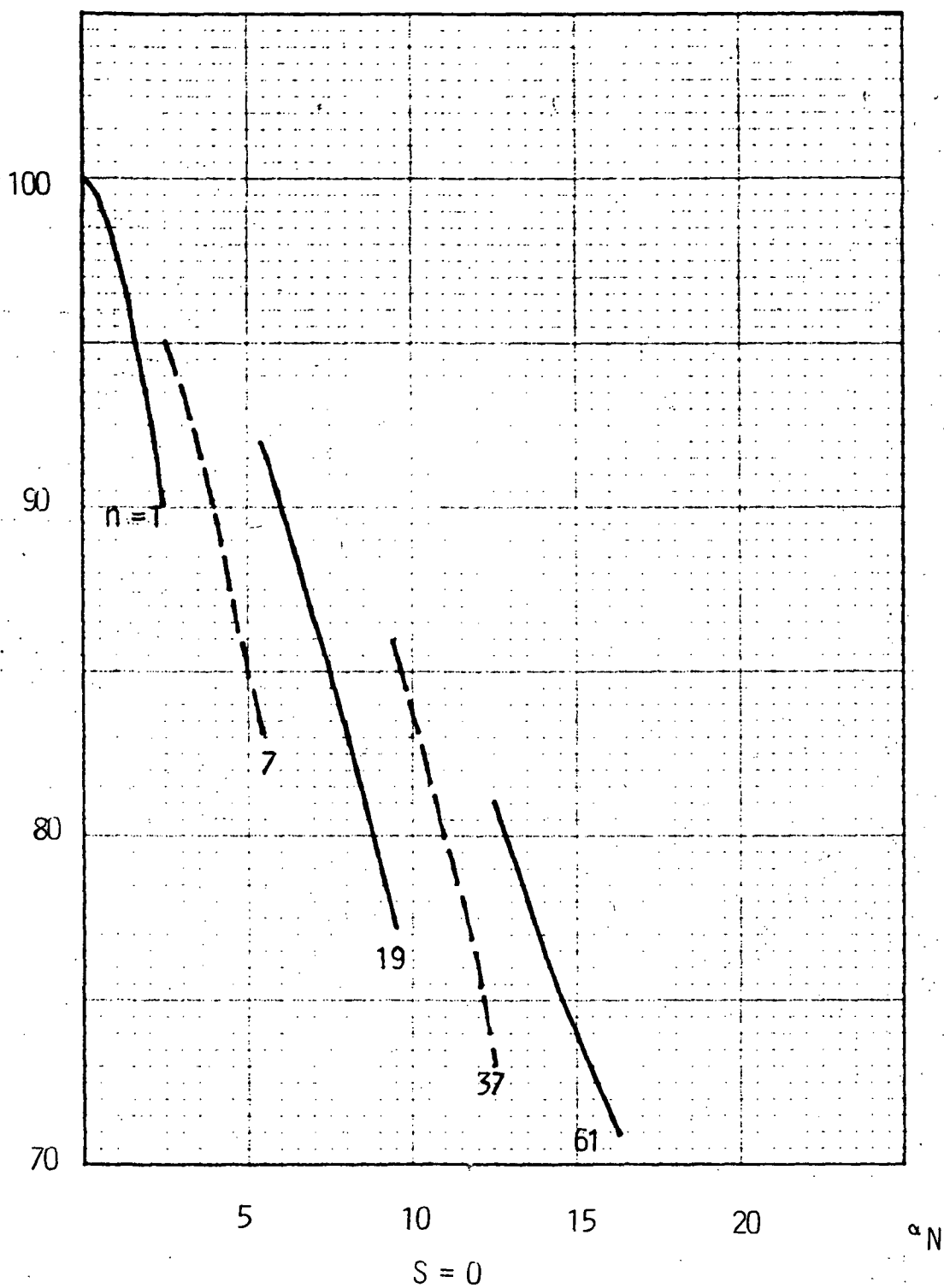
Figure 4.11(a) – Variation of beam scan efficiency and feed cluster size to cover $\beta = 11.18°$ with $N = 33$ beam for $S = 0$ a.
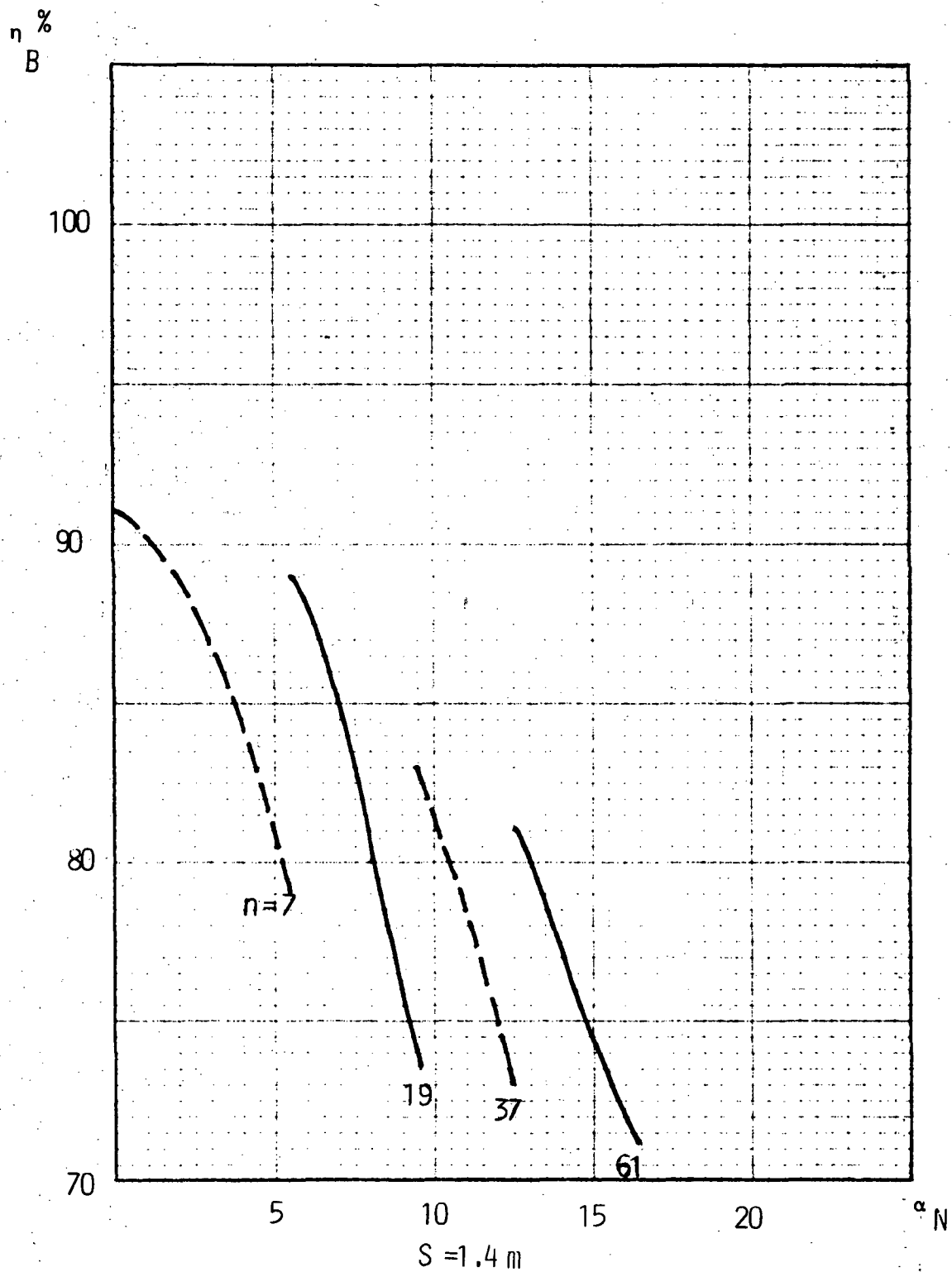
Figure 4.11(b) - Variation of beam scan efficiency and feed cluster size to
cover β = 11.18° with N = 33 beam for S = 1.4 m.

The variation of blockage as a function of S is inidcated in

Figure 4.9. This figure assumes that the rest of the geometry is as shown in

Figure 4.4 and the antenna is designed for β = 11.18° swath (N = 33). Then

the worst blockage occurs when a subarray is closest to the column, the least

blockage is applicable for the maximally scanned beam. The calculation

assumes 25% transparency for the column. This is an average transparency.

The transparency is a function of the structural design of the telescoping

column and can not be accurately calculated until a particular design is com-

pleted. However, the transparency is generally improving with increasing S

and scan position. For a given S the actual geometrical blockage is closer

to the worst case for the small scan angles and lcoser to the best case for

large scan angles. In order to make the blockage less dependent on the trans-

parency it is prudent to select relatively large S.

Up to now the beam efficiency characteristics of the antenna have been

analyzed as a function of the number of radiating elements (feed points) n,

associated to a subarray. n determines the freedom for the synthesis, (the

number of points where the aperture phase front coincides with the pahse front

of the plane wave). Additionally, the location of the radiating elements in

the feed array must be selected.

In the following it assumed that all subarray elements are identical and

they form a hexagonal grid. Furthermore, the envelope diameter of the un-

scanned subarray is large enough that the subarray is capable to produce the

required distribution in the aperture of the paraboloid characterized by

A^X = -14 dB and P = 2.

Figure 4.12 shows the results of the calculation for radiating element

diameter d_λ^e, and subarray diameter d_λ^s, as a function of n. The selection

73
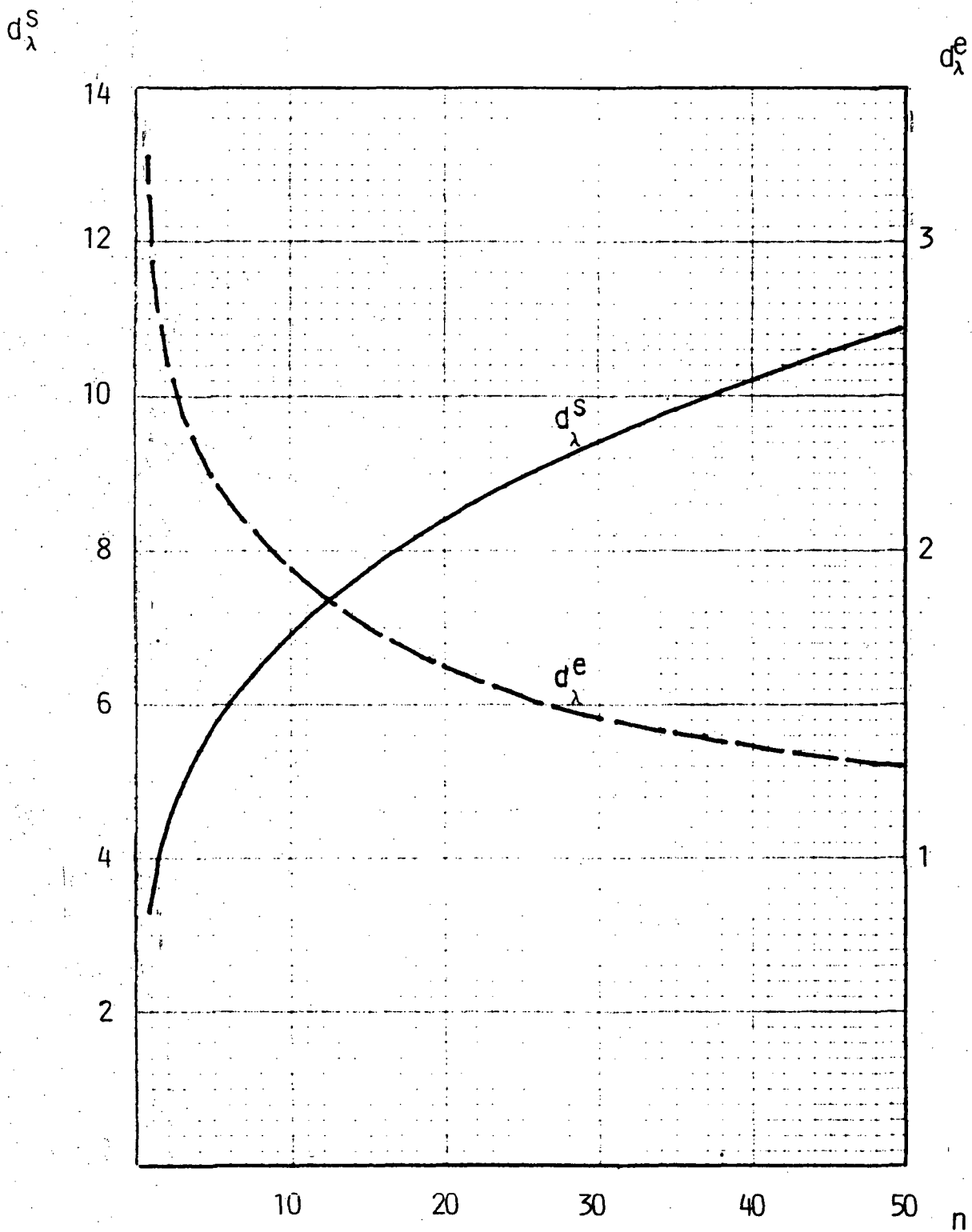
Figure 4.12 – Variation of radiating element diameter d_λ^e and subarray diameter d_λ^s versus n.

results in a realizable implementation, which avoids supergaining (d_λ^e too small) and grating lobes (d_λ^e too large). However, it does not represent a geometry, which maximizes the beam efficiency. The execution of a full optimization is quite time consuming and results in a slightly larger d_λ^e for larger n. However, it is concluded that the value of such optimization is academical, because it requires a larger overall array, than can be implemented within available space.

As was shown before the n values of interest are between 7 and 61. For such cases the subarray diameter varies between 6.32 λ and 11.45 λ. Thus the partial compensation of scan effects requires a 1.81 times increase of subarray diameter within the range of scan.

On the basis of the previous calculations Table 4.1 summarizes the main characteristics of the feed array for S = 0 and S = 1.4 m. The table shows the number of subarrays, s; feed points per subarray, n; total feed point per type of subarray, q; d_λ^e, d_λ^s, the number of patches, P, necessary to realize a given d_λ^e diameter radiating element and the total number of patches, t, used for each type of subarray.

It may be noted, that the selection of the number of patches to realize a given radiating element diameter must satisfy the geometrical requirement of patch resonance and avoidance of grating lobes. Figure 4.13 shows the layout to realize the d_λ^s diameters used in Table 4.1.

The complexity of the overall feed array is characterized by the number of feed points, by the total number of patches and by the surface area on which they array is built. The minimum array complexity is achieved when S = 0, which results 87.56 m^2 active array surface and t = 4153 patches. Due to blockage this is not acceptable for small scan angle subarrays.
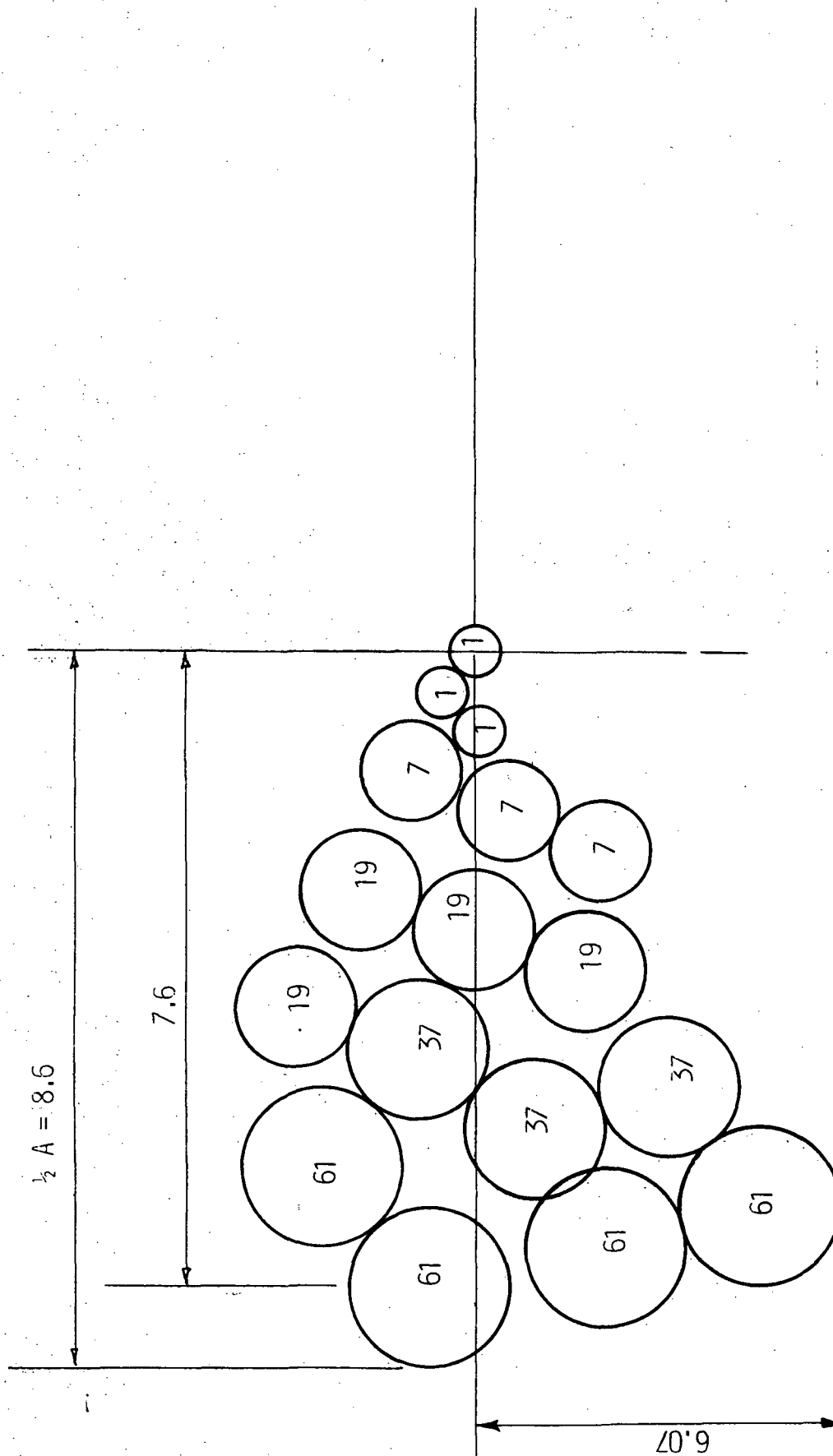
Figure 4.13 - Realizable feed layout for single aperture design.

Dimensions in m

½ A = 8.6

7.6

6.07

However, the $S = 1.4$ m feed array position results in only a small increase of complexity yielding 92.77 m^2 active array surface and $t = 4408$ patches. The feed array layout shown on Figure 4.16 refers to this case. It can be seen from this figure, that due to the support requirement of the active array surface the actual array surface is 128.35 m^2. This is 6.29% of the overall aperture of the hoop column structure and 7.41% of the antenna aperture. It is clear, that such a large array apertue area cannot be accomodated in a symmetrically feed paraboloid. However, with the offset feed reflector, the array blockage is eliminated and only the column related 0.5% (average) blockage remains.

It must be emphasized, that all the above data are derived on the basis of a relatively simple mathematical model.

In order to assess the accuracy of the utilized model some additional exact calculations have been performed for a limited number of examples.

Figures 4.14 and 4.15 show the gain contours for a singlet ($n = 1$) using $d_\lambda^e = 2.42$ at $\alpha_N = 0$ and 7.2, respectively.

TE_{11} mode excitation is assumed in the aperture. The calculated scan loss is $\delta G = 3.5$ dB for this case, while the simple model predicts $\delta G = 3.4$ dB. (See Fig. 4.8.) The gain contours of 4.14 indicate that the extent of significant pattern distortion due to scan extends to an angular radius of $\sim 2\theta_3$ from the main beam maximum. Thus the compensation of such a scan caused distortion would require at least two rings of elements around the center element. This results in a 19-element array for which Figure 4.8 predicts a relatively negligible 0.5 dB of scan loss.

Figure 4.16 shows other data points corresponding to $n = 1$, $d_\lambda^e = 2.07$, and $\alpha_N = 6.6$. The exact scan loss is $\delta G = 2.42$ dB for this case, practically identical to the approximate value. (See Fig. 4.8.)
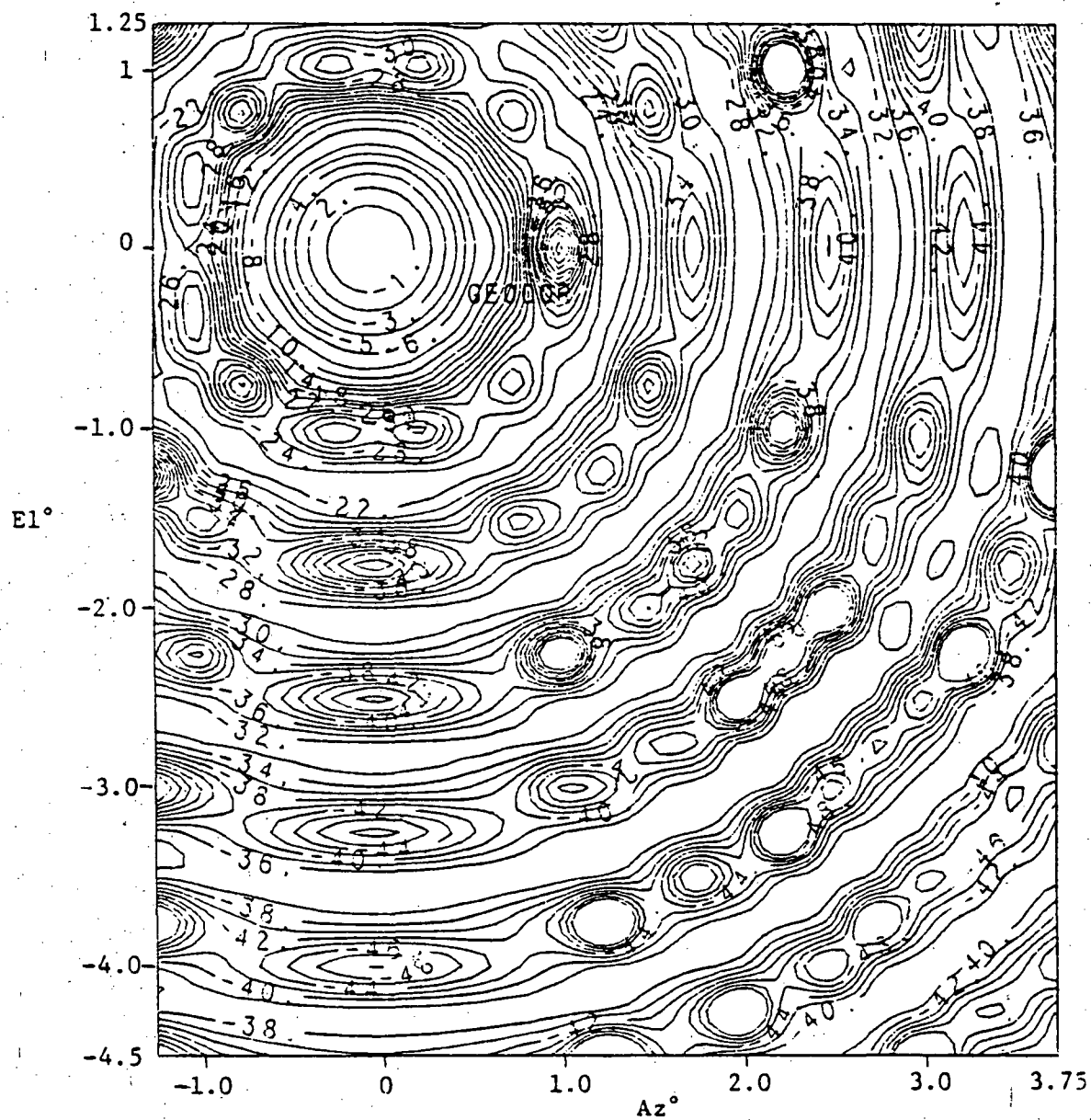
$$D_{\lambda} = 75.6$$

Figure 4.14 - Gain contour of singlet feed $d_{\lambda}^{e} = 2.42$, $\alpha_N = 0$.
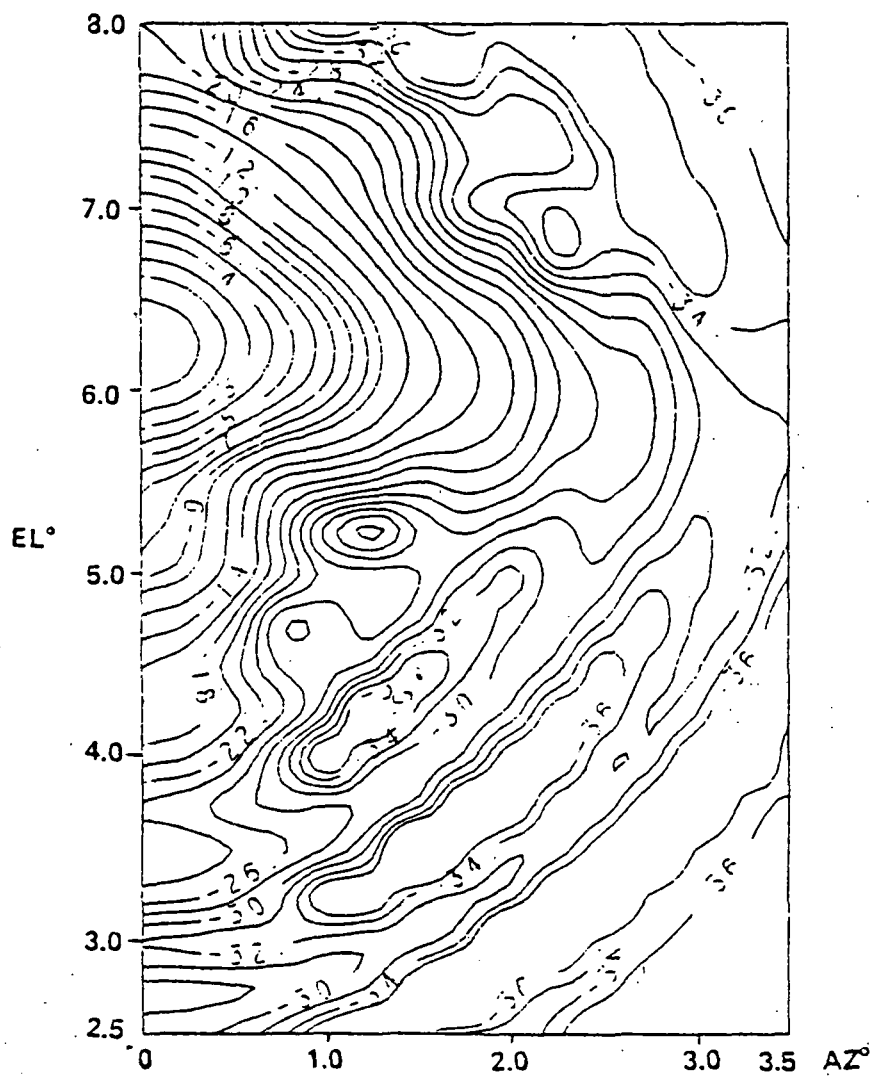
$D_\lambda = 79.48$

Figure 4.15 - Gain contour of singlet feed, $d_\lambda^e = 2.42$, $\alpha_N = 7.2$.

$$D\lambda = 162.53$$

Figure 4.16 – Gain contour of singlet feed, $d_\lambda^e = 2.07$, $\alpha_N = 6.6$.
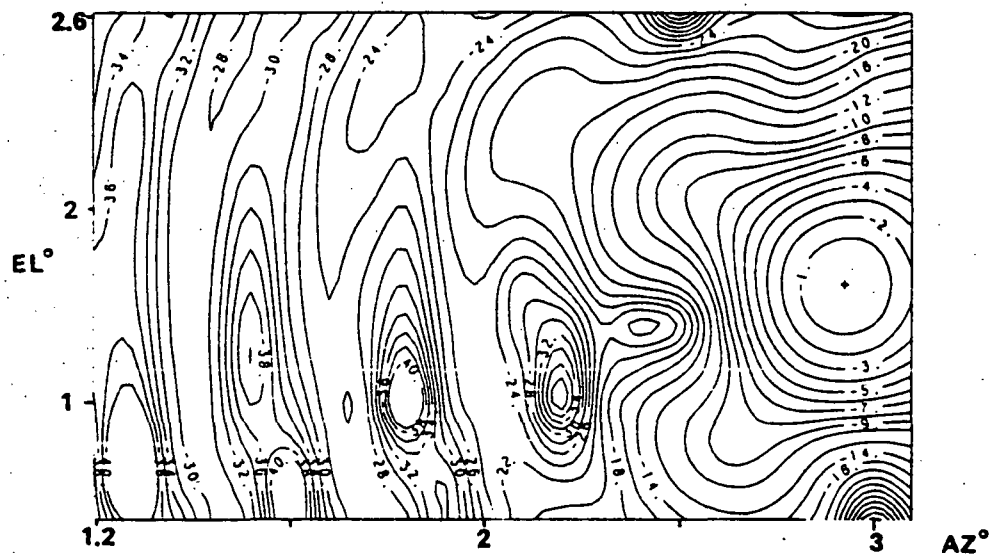
The character of the gain contour is very similar to the one shown in Figure 4.15. However, the two figures together prove that the scan loss for a singlet for large α_N is very sensitive to α_N. Significantly, the two exact data point defines very closely the same scan loss slope as the approximate model. The calculations also indicate that the diameter of the radiating element has relatively minor effect.

Figure 4.17 gives an example for a 7-element cluster utilizing an average of 3% power on the outer ring of radiators. In this case $n = 7$, $d_\lambda^e = 2.47$, $d_\lambda^s = 7.4$, and $\alpha_N = 5.04$. The scan loss is $\delta G = 0.66$ dB versus $\delta G = 0.60$ dB obtained using the approximate calculations.

Figure 4.18 presents the results for a uniformly excited 7-element array using $d_\lambda^e = 1.31$, $d_\lambda^s = 3.93$, and $\alpha_N = 3$. The exact scan loss is $\delta G = 0.40$ dB verus 0.3 dB using the approximate model.

Finally, Figure 4.19 prsents the exact results for $n = 15$, employing $d_\lambda^e = 1.31$, $d_\lambda^s = 5.82$, and $\alpha_N = 3$. The predicted scan loss is $\delta G = 0.15$ dB, the same value as calculated from the approximate model using $n = 19$. (See Fig. 4.8.)

It can be concluded from the above calculations that the accuracy of the approximate model is well within the accuracy limits necessary for tradeoff calculations.

In summary, the single aperture concept results $\Delta X_M = 9.5$ km spatial resolution, when $D_s = 50.95$ m structural diameter is utilized and $h = 787.5$ km. The antenna is capable to form $N = 33$ beams with an average beam efficiency of 81% provided the paraboloid surface is exact. 33 beams cover a swath of 11.18°, which for a polar orbit would result in 59% coverage. Thus in an operational configuration, 2 spacecrafts would be needed to provide practically complete coverage.

$$D_\lambda = 75.37$$

Figure 4.17 - Gain contour of septet feed, $d_\lambda^e = 2.47$, $d_\lambda^s = 7.4$, $\alpha_N = 5.04$.
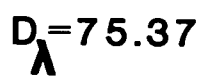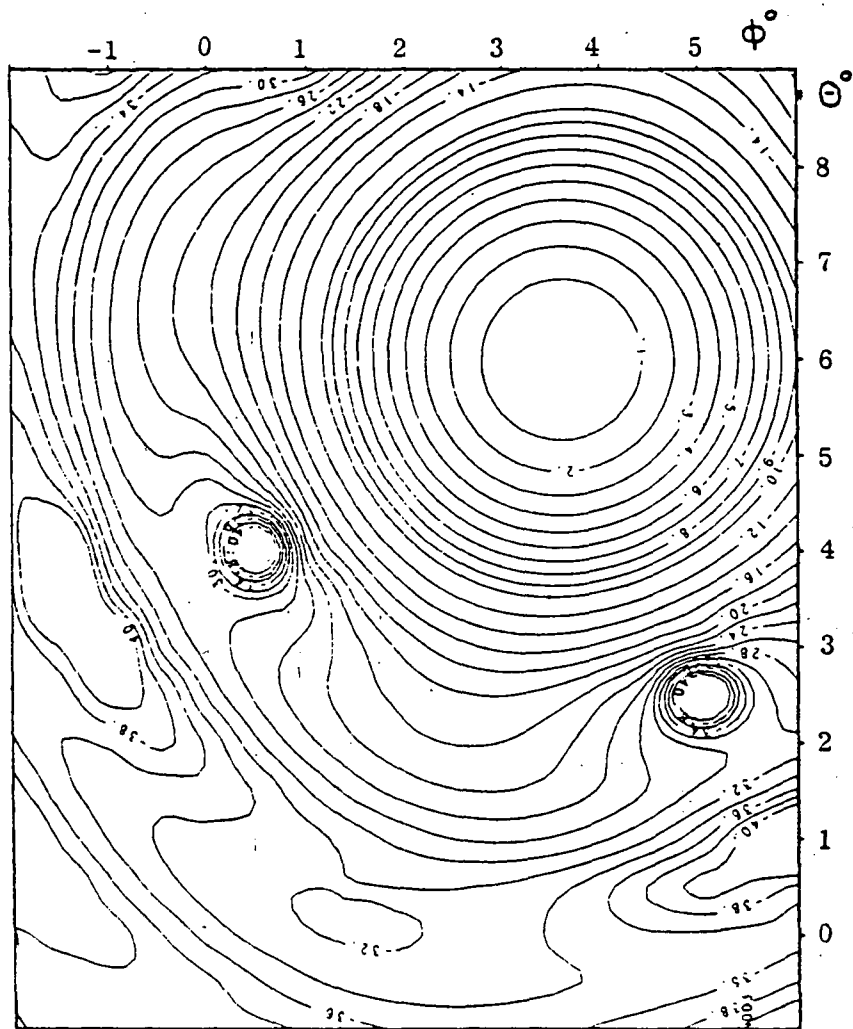
$$D_\lambda = 27.34$$

Figure 4.18 - Gain contour of septet feed, $d_\lambda^e = 1.31$, $d_\lambda^s = 3.93$, $\alpha_N = 3$.
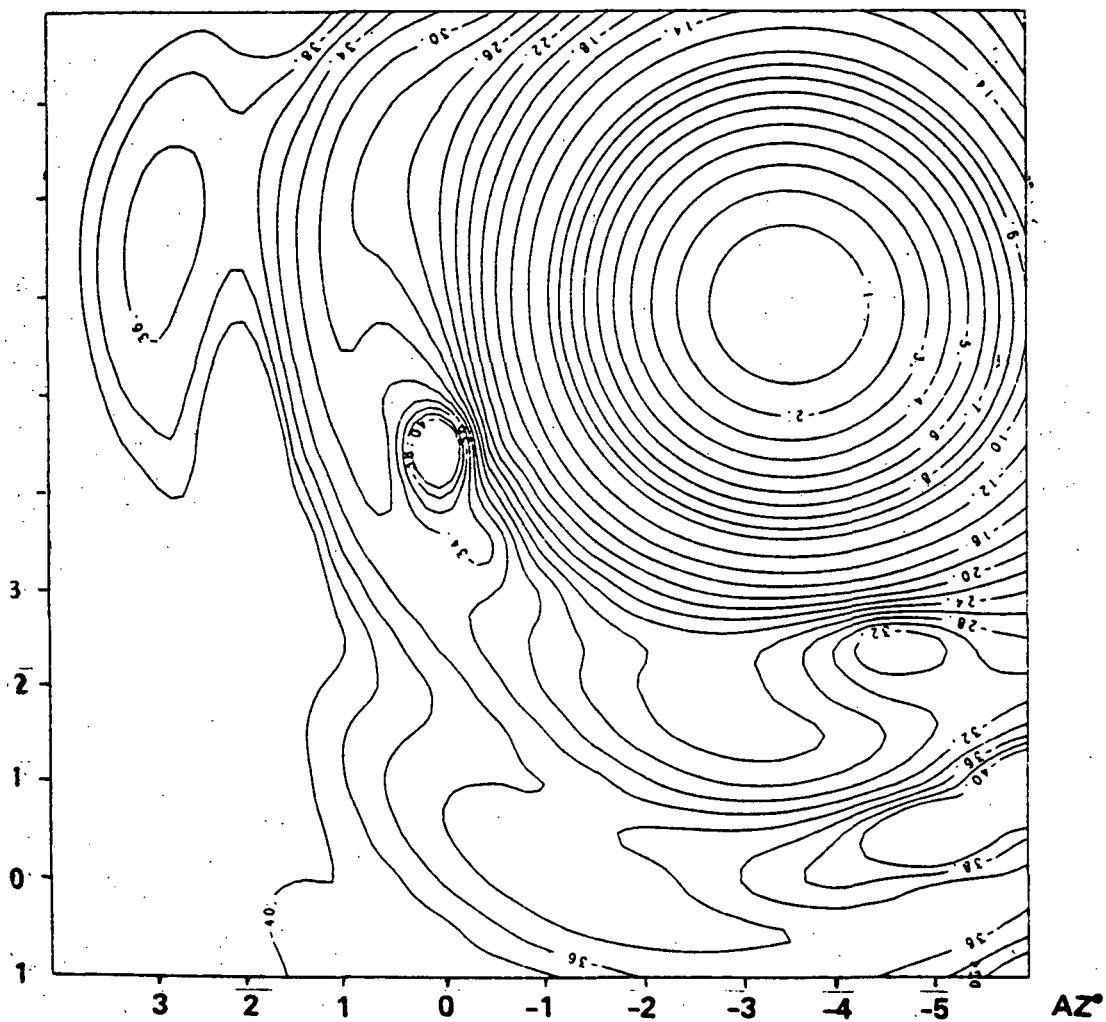
$D_\lambda = 27.34$

Figure 4.19 – Gain contour of 15 element feed, $d_\lambda^e = 1.31$, $d_\lambda^s = 5.82$, $\alpha_N = 3$.

It is interesting to note that $X_M = 9.5$ km resolution with the above type of antenna is achievable if $D = 15$ m, $h = 375.4$ km, and $f = 2288$ MHz. Such a combination can be implemented as a scale model Shuttle experiment to verify the orbital characteristics of a single aperture design.

4.3 Double Aperture Concept

There are a numer of configurations by which the beam number limitation of the single aperture concept can be reduced. Figure 4.23 shows geometries utilizing two subapertures. In these configurations the structural diameter of the antenna is adjusted in such a manner, that the spatial resolution of the system is maintained at approximately 10 km. This requires an approximately two fold increase of the structural diameter relative to the single aperture concept discussed in Section 4.2 and shown in Figure 4.4.

Figure 4.20 exhibits the aperture layout of the antenna utilizing subapertures A and B. These are displaced relative to each other in the direction of flight. The apertures are realized by identical offset feed paraboloid segments, with axes parallel to the axis of the column and with focal points at F_A and F_B, respectively. The subarrays of the feeds are displaced in the perpendicular to flight direction. For such a situation the beams of subapertures A and B are capable to cover the same cell. The configuration has no more scan capability than the single aperture concept depicted in Figure 4.4. However, it eliminates the direct blockage by the column. Furthermore, the subarrays can be placed closer to the column, thus they require less supporting and deployment structure. The two subapertures can be utilized to reduce feed crowding, or introduce dual polarization, dual frequency band or two antenna receive/transmit capability.

85
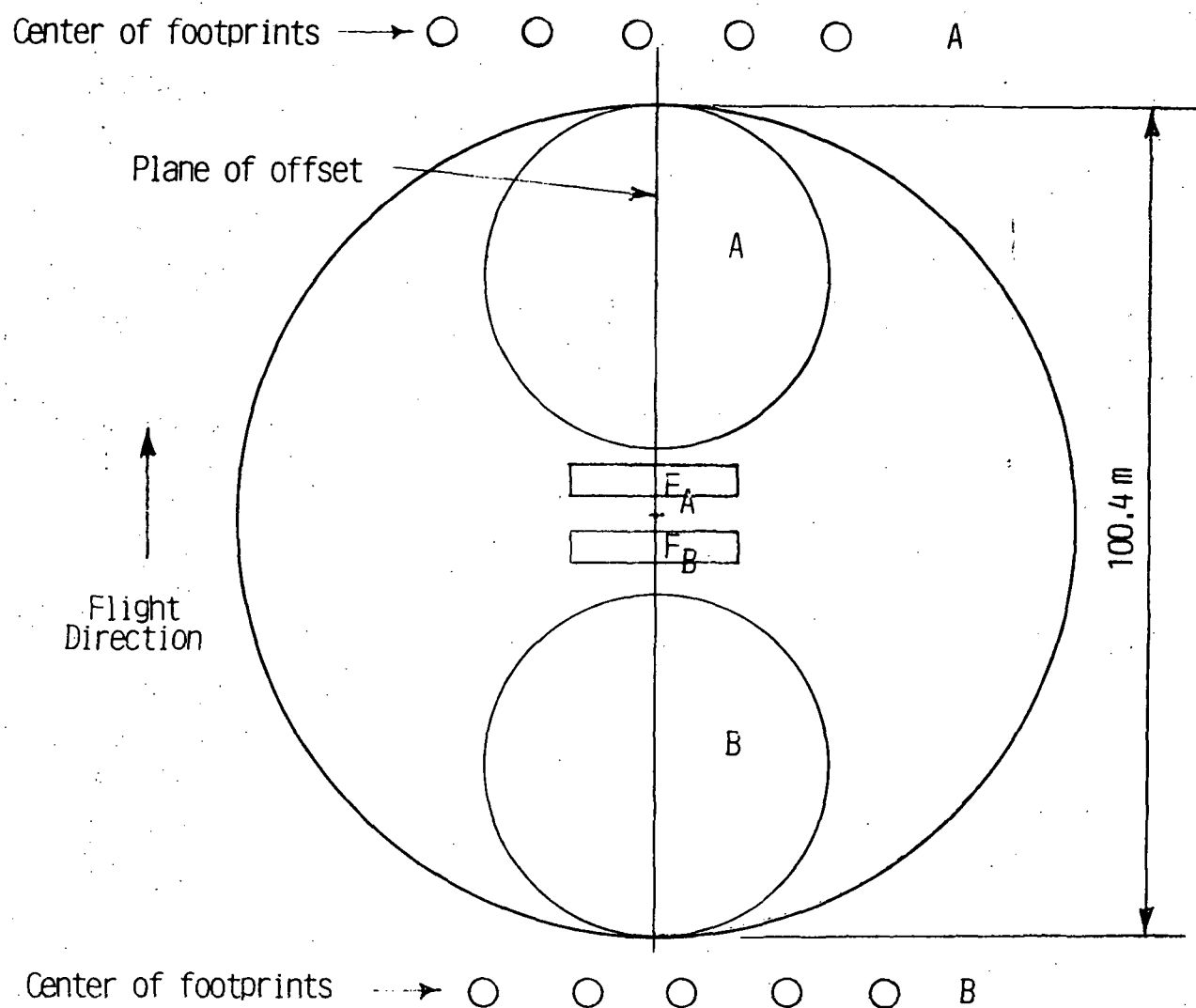
Figure 4.20 - Double aperture antenna concept employing symmetrical configuration.

In the arrangement shown in Figure 4.21, the plane of offset is rotated by an angle γ relative to the plane of flight. This allows to scan the beams from subapertures A and B to the right and left from the flight plane, respectively. Consequently, for a given subarray size and quality of beam the configuration nearly doubles the achievalbe swath. In practice a full doubling of the swath may not be possible, because there is not enough space to package the feed within the constrains of the spacecraft. Nevertheless the arrangement can accomodate increased number of beams relative to the single aperture configuration.

The difficulty of this setup is the implementation of the necessary paraboloid reflector segments. In order to maximally utilize the available structure it is desirable to illuminate the entire half of the reflector in Figure 4.21 for the "forward" beams and the lower half for the "backward" beams. However in this case due to the large distance between focal points F_A and F_B a relatively large step develops at the border between the two reflector segments. This causes a mechanical implementation difficulty and undersirable diffraction. The diffraction effect can be reduced by more illumination taper, but this decreases the aperture efficiency and increases the beamwidth.

Figure 4.22 shows a compromise. This eliminates the step between the reflector segments yet it retains some of the advantage of the Figure 4.23(b) setup. The layout is similar to the one shown in Figure 4.23(a), but the entire space craft is rotated by τ angle relative to the flight direction and the axes of the reflector segments are tilted in the plane of offset away from the axis of the column. In this situation the beams from subaperture A are titled forward relative to the flight direction in the left hemisphere. The net result is a set of footprints on each side of the flight path.

Center of footprints → ◯ ◯ ╱◯ ◯ ◯ A

Plane of offset

A

F_A

Flight
Direction

F_B

B

Center of footprints → ◯ ◯ ◯ ◯ ◯ B
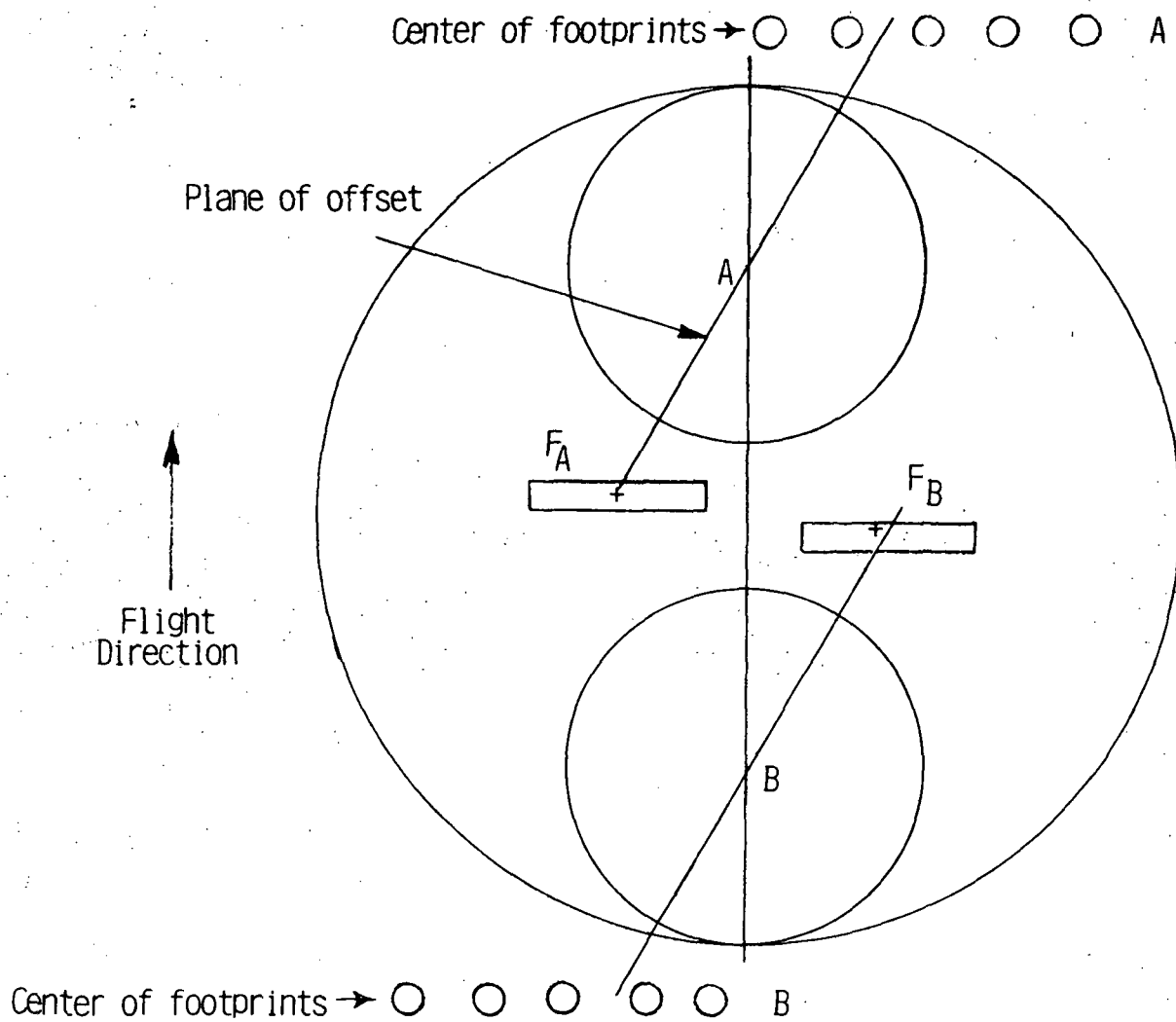
Figure 4.21 - Double aperture antenna concept employing rotated offset planes.

88

C-2
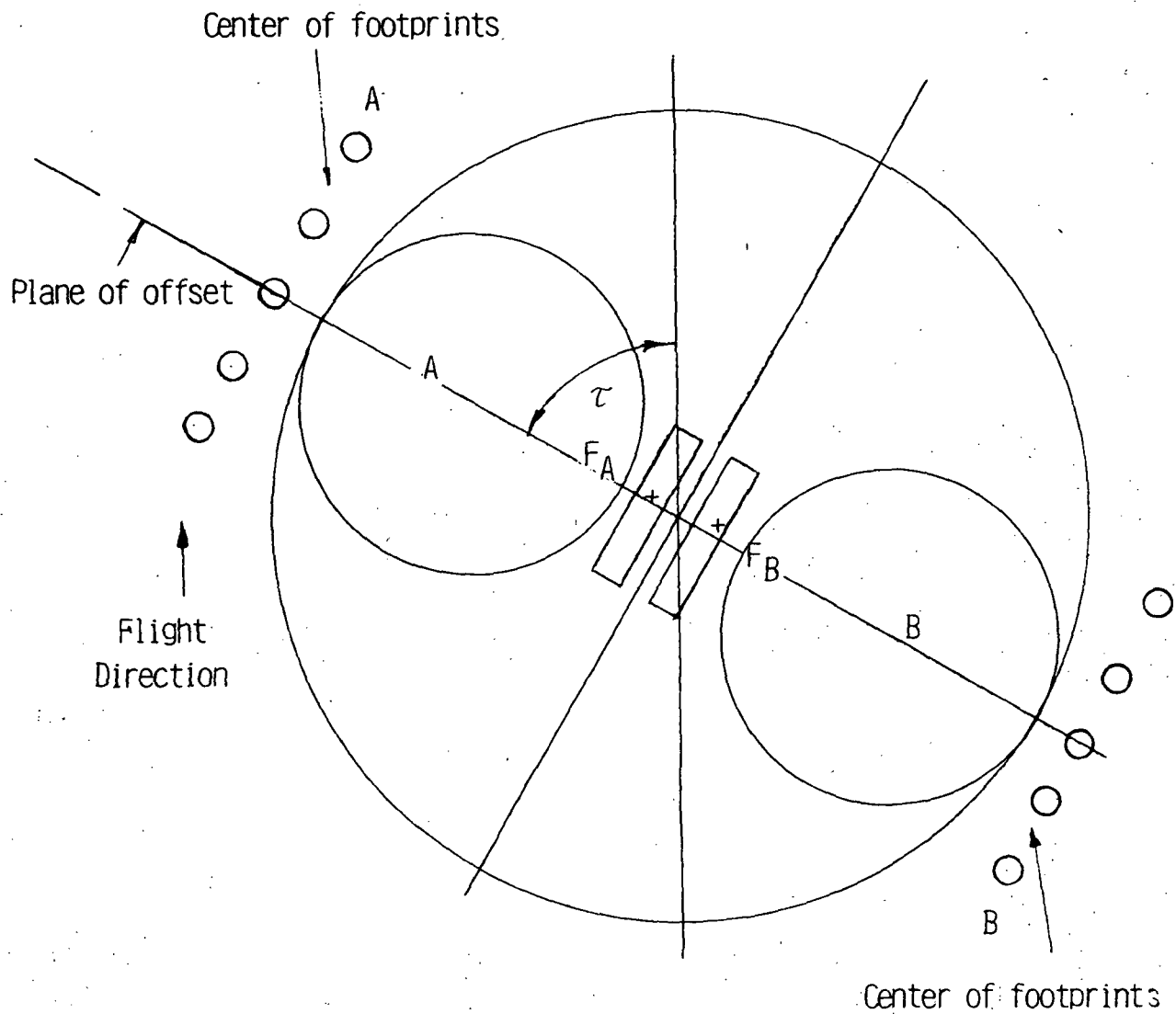
Figure 4.22 – Double aperture concept employing rotated aperture relative to flight direction.
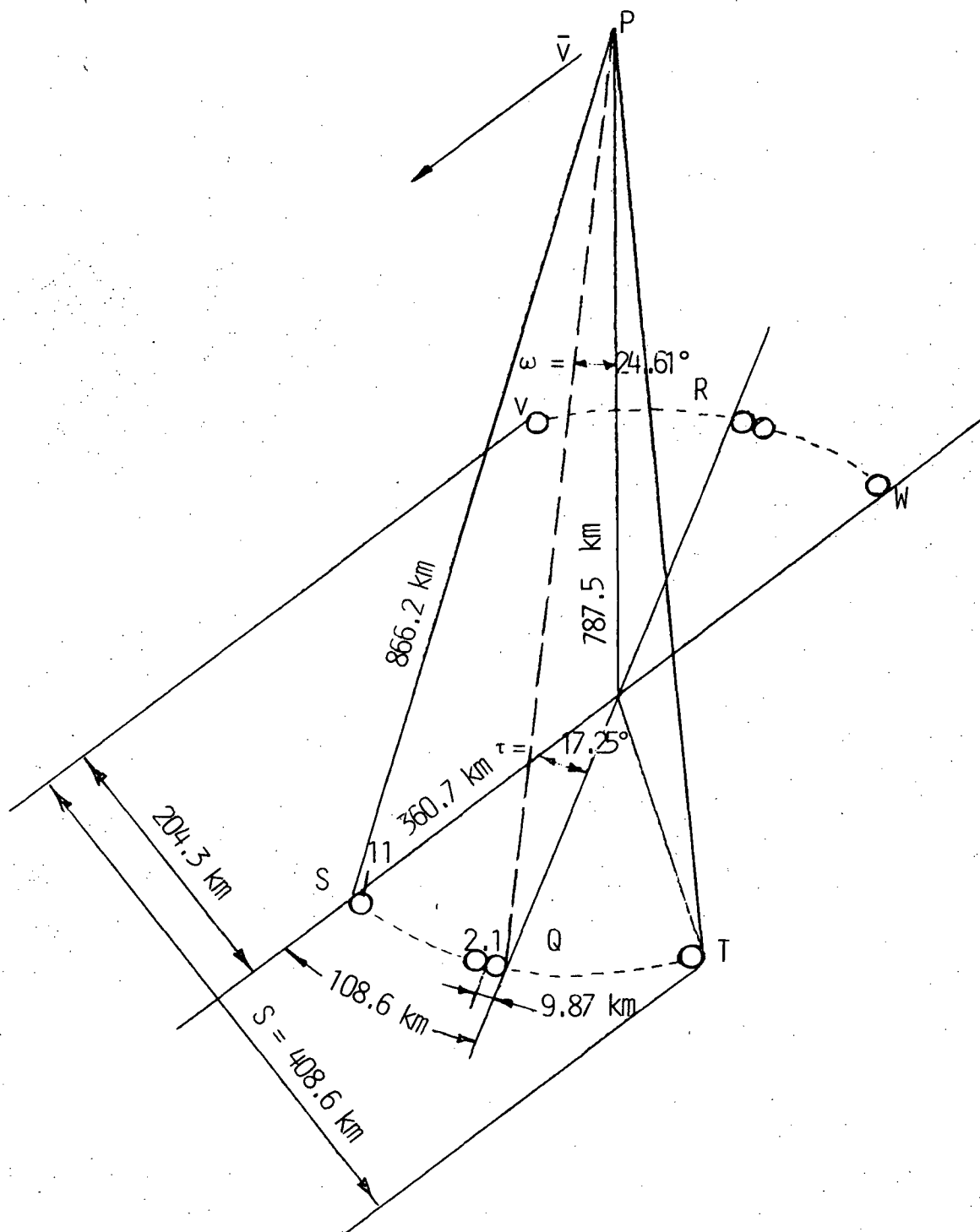
Figure 4.23 — Footprint geometry of the Figure 4.22 double aperture antenna.

The structure has two symmetry planes, simplifying the electrical and mechanical design. There is a sharpe edge, but no step at the intersection of the reflector segments. The total swath is typically two times larter than for the equivalent single aperture.

In the following the configuration depicted in Figure 4.22 will be further analyzed.

Figure 4.23 exhibits the geometry of the footprint assuming $h = 787.5$ km and a subaperture diameter of $D = 47$ m (these are similar values to the ones used in the example for the single aperture implementation). The offset of the paraboloid reflectors is in the PQR plane which is rotated by $\tau = 17.25°$ relative to the vertical plane containing the flight vector $\bar{v}$. When the axis of the two paraboloids in the PQR plane are tilted by $\pm\omega = 24.61°$ then the footprint of a beam at Q has a minimum dimension of $X_m = 9.87$ km. This corresponds to the $\theta_{98\%} = 0.653°$ beamwidth of the ideal, unscanned beam. The maximum dimension of the footprint is $X_M = 10.86$ km.

The centers of the footprint are on a circle with 360.7 km in radius measured from nadir. The footprints from subaperture A are on the SQT arc on the left side of the ground track while the footprints from subaperture B are on the VRW are on the right side of the track. Assuming ±11 scan position (N = 44 beams) the total swath is $S = 408.6$ km.

Figure 4.24 shows the geometry of optics necessary to implement this beam configuration. The upper part of the figure displays the profile of the offset feed paraboloid reflector in the plane of offset for one of the subaperture implementation. The second subaperture is symmetrical relative to this. The paraboloid axis is tilted by $\omega = 24.61°$ relative to the axis of the column. Its focal point is 1.4 m away from the axis of the column in order to assure the necessary clearence between the feed array and column.
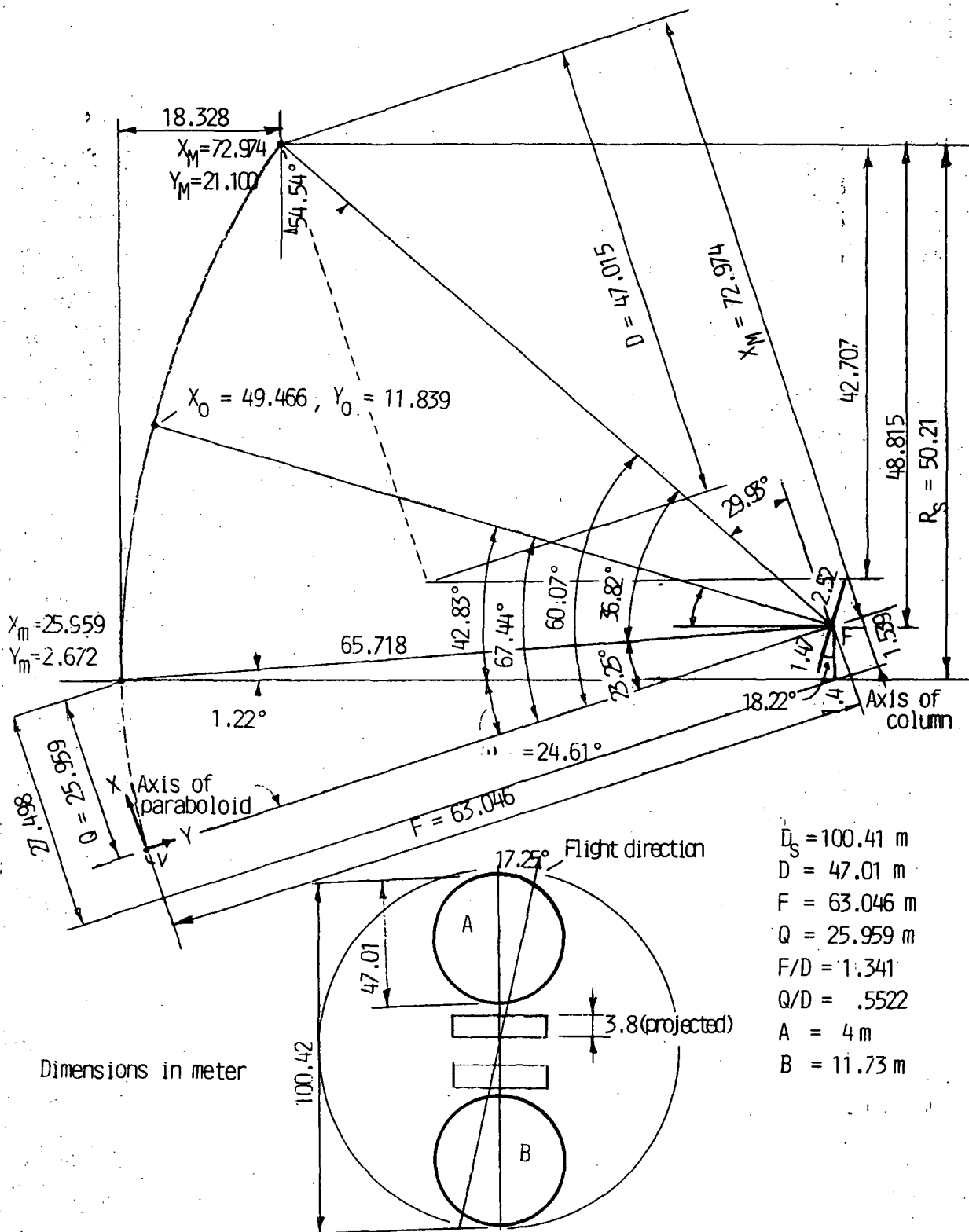
Figure 4.24 - Geometry of optics of the Figure 4.22 double aperture antenna.

F = 63.064 m is selected, for which the required D = 47.01 m subaperture diameter yields F/D = 1.341. These selections result in a structural diameter of D_s = 100.42 m. The two subapertures utilize 43.83% of the achievable structural aperture area assuming that the projected subaperture shape in the direction of the electrical axis is a circle. A little better utilization is possible if the subaperture shapes are elliptical.

The nominal feed array width is A = 4 m (in the plane of offset) and its length is B = 11.73 m.. Further details are exhibited in Figure 4.25. The center of the feed array does not coincide with the focal point in order to minimize the clearence requirement for the feed and the necessary offset Q for the paraboloid.

The system has a comfortable large F/D. This is advantageous to maintain good quality for the scanned beams. However, it has a large Q/D = 0.552, which reduces the achievable beam efficiency. The large Q value is the consequence of the large ω value, which is necessary to accomodate the selected number of beams, N = 44. In the vicinity of N = 44 A/D is approximately proportional to N. Thus a reduction of N to 40 reduces Q/D to ~0.5. For such condition an overall improvement of the quality of all beams is possible at teh expense of about 10% swath reduction.

The optics shown in Figure 4.24 is scanned perpendicular to the plane of the drawing. Since the beam centers must be $\theta_{98\%}$ away from each other and the subarray size must be increased as the beam is scanned a staggering of the subarray layout is necessary in the direction of flight. (See Fig. 4.25.)
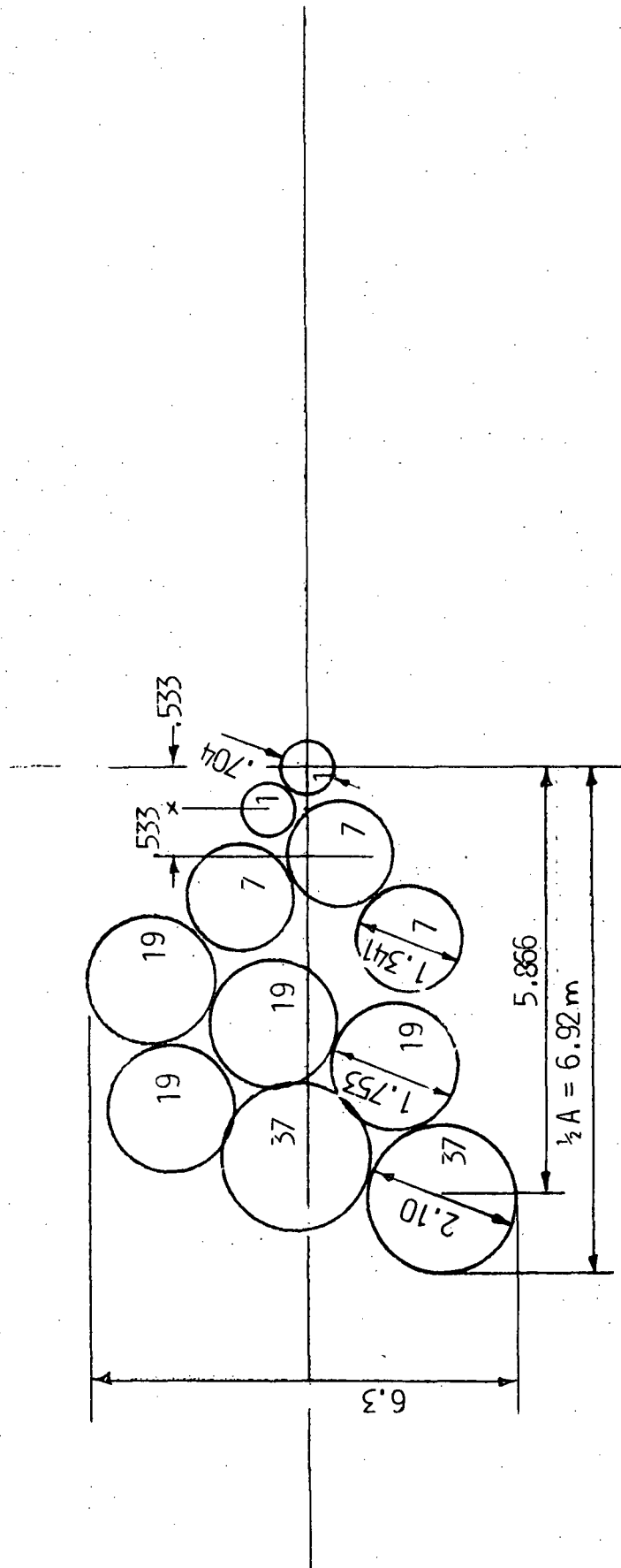
Figure 4.25 - Feed array layout of the Figure 4.22 double aperture antenna.

Table 4.2 contains some of the subarray characteristics. According to theis table, four different types of subarrays are necessary, containing 1, 7, 19, or 37 radiating elements. The radiating element designs are similar to the ones shown in Table 4.1, except for the 37 element subarray. For this a slight reduction of diameter is necessary to fit the subarray within the available overall array diameter. $N = 44$ requires 84.77 m^2 active array area within the nominal 93.84 m^2 overall feed aperture surface. 4600 patches are needed to implement the system.

It is interesting to compare these figures with the corresponding values for the $N = 33$ beam, single aperture system. It can be seen that the array surface is considerable less for the two aperture cases (93.84 m^2 versus 128.35 m^2) while the number of patches increases from 4408 to 4600. The main difference of course is a drastic increase of structural diameter to 100.4 m from 50.95 m. The 1.97 times increases structuraldiameter yields 1.33 times more swath, reduced column scatter and generally better beam efficiency. The beam efficiency variation as a function of scan position is shown in Figure 4.26. The average beam efficiency is $\bar{\eta}_B$ 87.6% instead of the 81% calculated for the single aperture system. The resultant swath results in approximately 85.5% coverage.

It is interesting to compare the structural characteristics of a single aperture system, using two spacecrafts with a dual aperture system using one spacecraft for approximately equal performance. This is shown in Table 4.3.
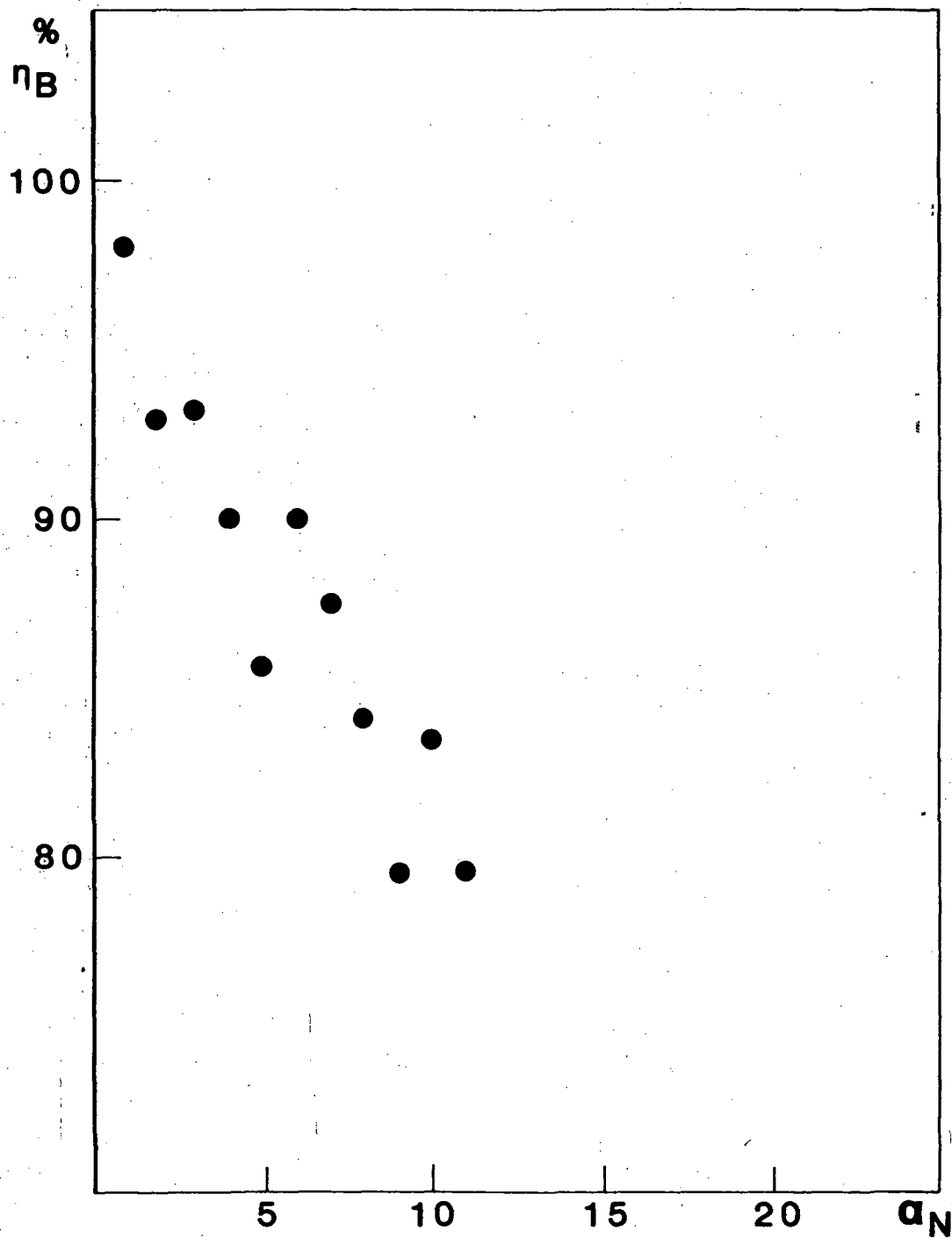
Figure 4.26 - Variation of beam efficiency with scan position of the
Figure 4.22 double aperture antenna.

TABLE 4.3

Comparison between the one and two subaperture systems

System	Total structural aperture m^2	Total feed surface m^2	No. of patches	Average beam efficiency %	No. of beams	Coverage %	X_M km	Weight Ref.	Feed kg	Total
Single aperture 2 space-craft	4077.6	256.7	8816	81.0	66	83.2	9.5	542	1027	1569
Dual aperture sapce-craft	7916.9	93.84	4600	87.7	44	85.5	10.9	1053	375	1428

In Table 4.3 the coverage for the two spacecraft system is calculated on the basis of a simple product probability model. It is believed that with proper orbit optimization near 100% coverage is achievable for the two space-craft system, thus this system has at least the same coverage as the dual aperture system. It is clear from Table 4.3 that the main difference between the two systems is in the total weight and complexity related to the reflector surfaces and feed arrays. Assuming 0.133 kg/m^2 and 4 kg/m^2 for the weight of the reflector and feed, respectively, the total weight to be placed in orbit for the reflector and feed components is 1569 kg and 1428 kg, respectively. While these total weights are comparable it is obvious that the launch weight of the single aperture system is about a factor of 2 less. Additionaly, the single aperture system has better reliability (due to spacecraft redundancy). The differences in beam efficiency, coverage and resolution are small compared to the inaccuracy of calculation, thus they may be considered as approximately equal. On the basis of the above considerations both the single and dual sperture implementations can be potential solution for the desired system.

4.4 Triple Aperture Concept

4.4.1 Geometry

The main difficulty of the dual aperture concept is the relatively large paraboloid offset requirement (Q/F = 0.55). The offset can be reduced (by approximately a factor of two) if the structural aperture is divided into three subapertures. For this situation the number of beams can be further increased or/and their quality improved at the expense of some further increase of the structural diameter.

Figure 4.27 shows the front view of the aperture, while Figure 4.28 displays the geometry of the No. 1 reflector segment in the plane perpendicular to scan. Figure 4.29 gives the geometry of the No. 2 reflector segment in the plane of scan.

In this configuration three reflector segments are implemented within the overall structural envelope. Each of these reflectors are offset feed paraboloids.

The offset plane of the No. 1 reflector segment is in the plane of flight, which is also a symmetry plane of the overall antenna. The axis of this paraboloid in the selected example is parallel to the axis of the column and has a focal distance of $F_1 = 65.989$ m. Its focal point is 2.5 m away from the axis of the column and its offset is characterized by a $A/D_{11} = 0.152$. Assuming a structural diameter of $D_s = 118$ m the above selection provides a subaperture diameter of $D_{11} = 49.057$ m in the direction of flight and $F/D_{11} = 1.345$. It can be seen that the subaperture diameter and F/D_{11} ratio of this geometry is practically the same as for the analyzed two subapertures system, but the Q/D_{11} ratio is greatly reduced.
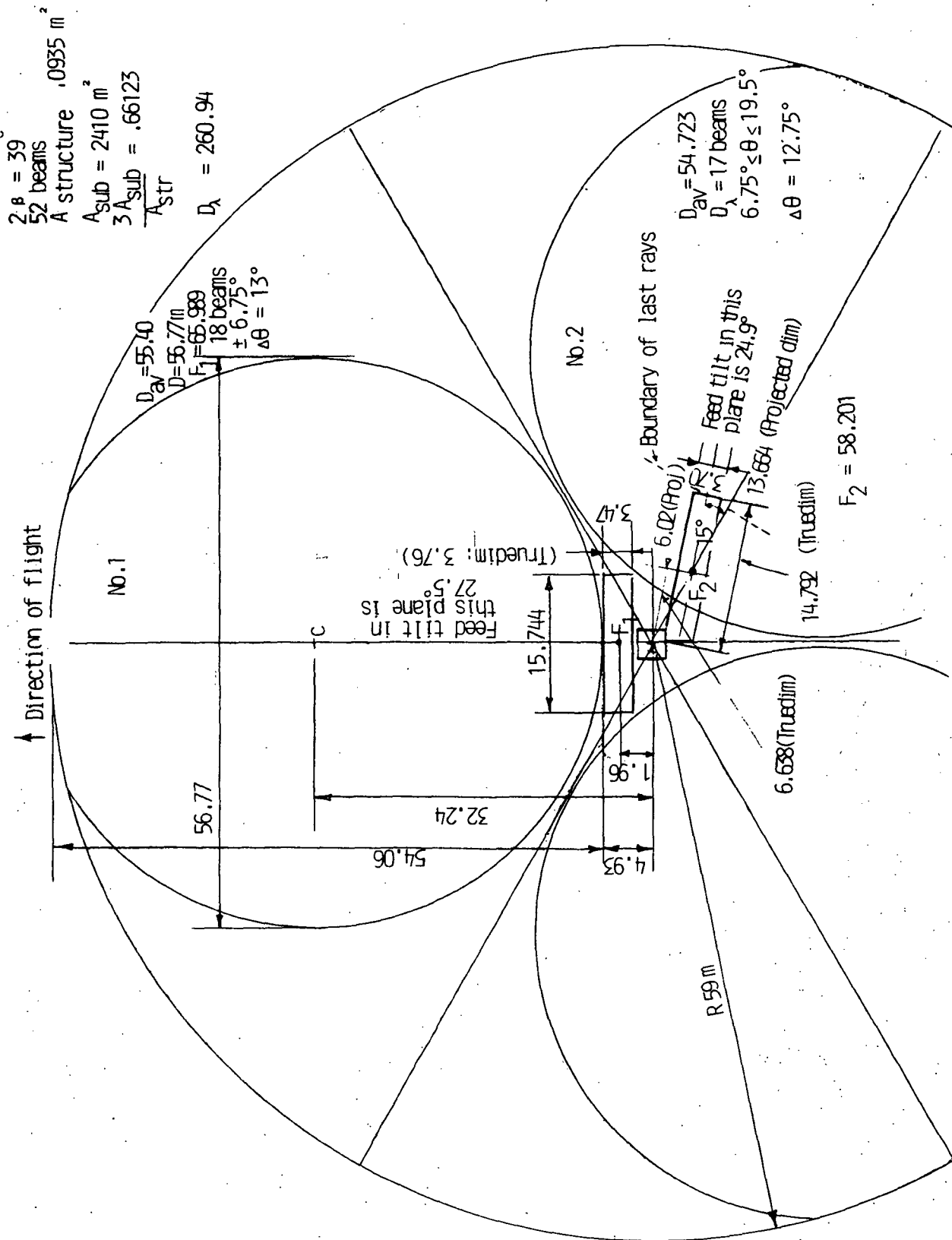
Figure 4.27 - Geometry of optics of the triplet aperture antenna, front view.
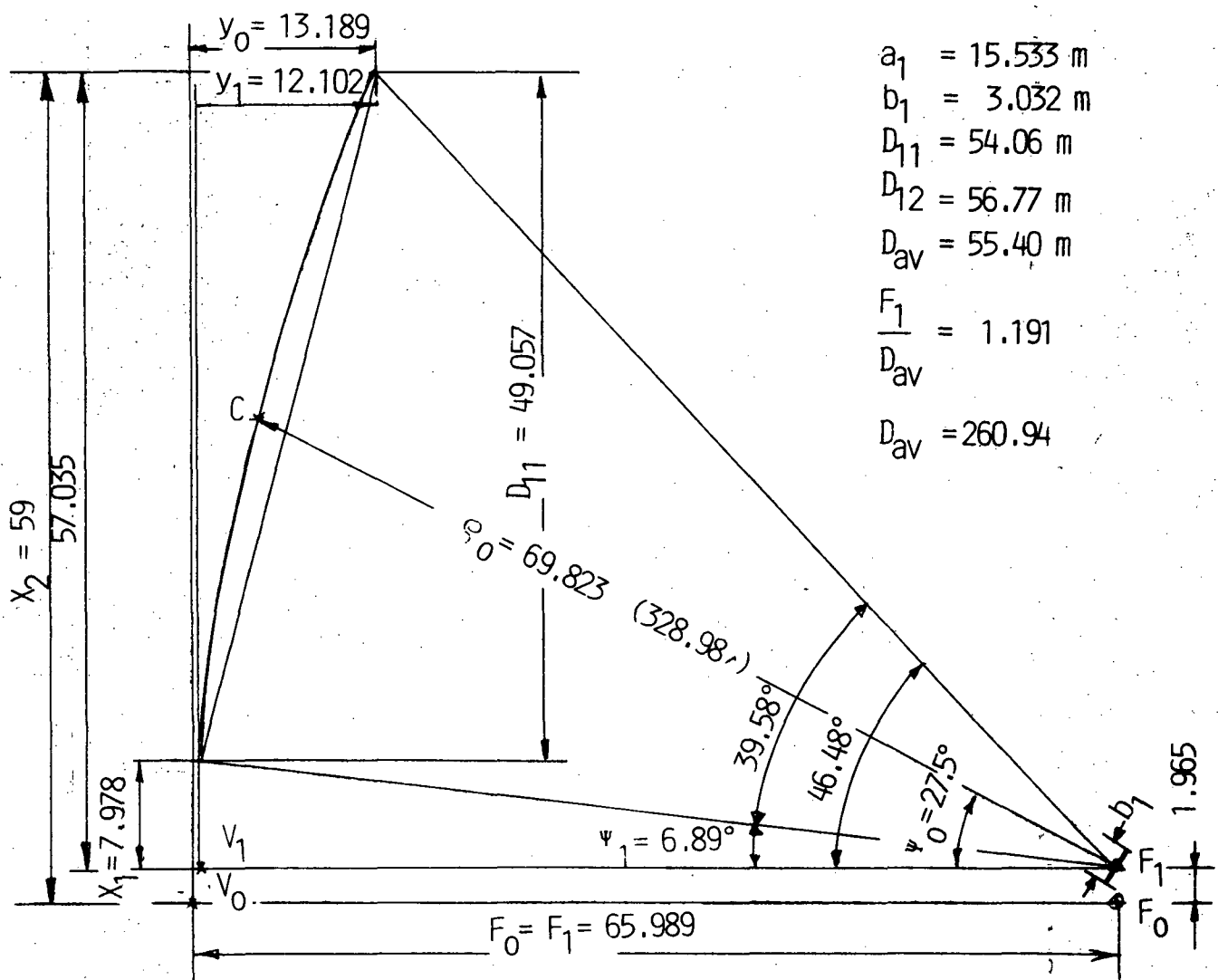
Figure 4.28 – Geometry of optics of the triplet aperture antenna for No. 1 reflector in plane of scan.
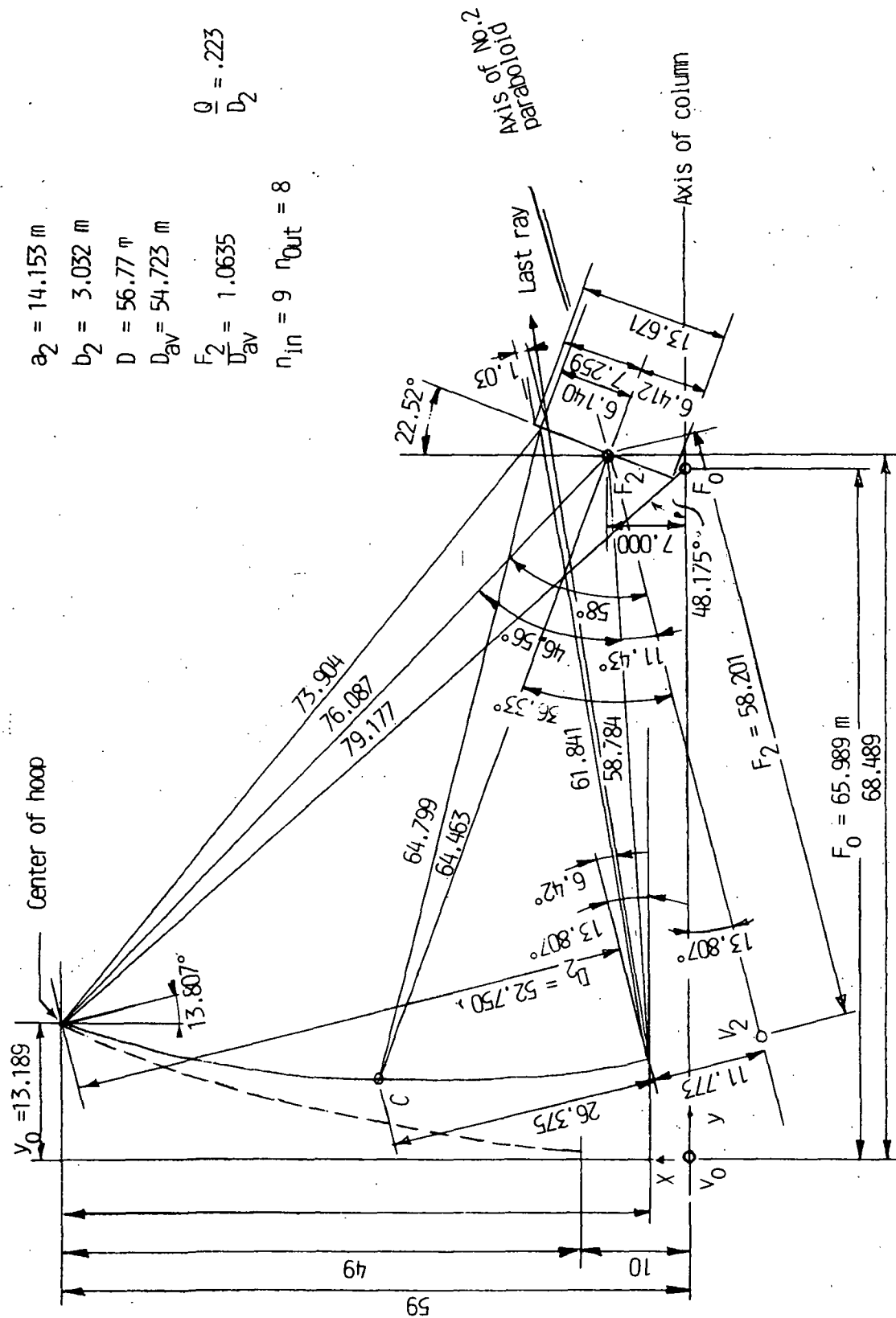
Figure 4.29 - Geometry of optics of the triplet aperture antenna for
No. 2 reflector in plane of scan.

The No. 1 reflector provides the beams for the center part of the composite swath. In order to achieve this the beams are scanned perpendicular to the plane of offset. This is accomplished by a feed array, with a nominal rectangular envelope of $A = 15.53$ m length and $B = 2.69$ m width, when projected to the structural aperture plane. Within this array envelope a total of ± 9 beam positions are accomodated covering a total of $\pm 6.75°$ swath.

The minimum diameter of the utilized aperture is D_{11}. However, allowing some increased spillowver radiation around the hoop, the effective utilized aperture can be slightly increased. The optimum equivalent subaperture diameter than is $D_{1av} = 55.4$ m.

The No. 1 and No. 1 subaperture geometries are symmetrical to the flight palne, thus it is enough to discuss the No. 2 system only. The offset plane of the corresponding parabolid encloses $120°$ angle with the flight plane. The axis of this paraboloid is tilted by $13.807°$ away from the axis of the column. (See Fig. 4.29.) The unscanned beam of this reflector is at $13.81°$ from the unscanned beam of reflector No. 1.

The beams of reflector No. 2 cover the right side of the swath. This can be accomplished if the reflector is scanned in the plane of offset. That requires a clerence of the large dimension of the feed array, thus a larger offset. The combination of larger offset and the tilt of paraboloid axis reduces F_2/D_2. For the selected geometry $D_2 = 52.75$ m, $F_2 = 58.20$ m, $Q_2 = 11.7$ m resulting $F_2/D_2 = 1.10$ and $Q_2/D_2 = 0.223$. As in the case of reflector No. 1 it is feasible to increase the effective aperture diameter to $D_{2av} = 54.72$ m, by allowing some increased spillover radiation.

While it is possible to place the large dimension of the feed array into the plane of offset the footprint geometry can be improved if the feed array is tilted by $15°$ relative to this plane. In such a configuration the plane of

scan is only 15° away from the perpendicular to flight direction, thus the covered swath increases and a slight improvement in spatial resolution is feasible. Furthermore, such rotation results in more compact feed array packaging. figure 4.27 shows this configuration. According to the detailed analysis, a feed array with $A = 13.67$ m and $B = 3.03$ m envelope dimension can accomodate a total of 17 beams with acceptable quality. These beams cover the 6.75° to 19.5° part of the overall swath.

The entire 3 subaperture system requires 10935 m^2 structural aperture area. Out of these the No. 1 subaperture utilizes 2410.5 m^2, the No. 2 and No. 3 subapertures 2×2351.7 m = 4703.4 m^2, thus the total utilized aperture is 7113.9 m^2 (65.06%). The system is capable to produce $18 + 2 \times 17 = 54$ beams within a total swath of $2\beta = 39°$.

It may be noted, that the design shown in Figures 4.27 through 4.29 can be somewhat simplified by making the geometry of the three reflector segments identical. Then the main reflector system ahs three symmetry planes, 120° apart from each other. In this configuration the axis of the No. 1 reflector is 13.807° forward tilted and its F/D ratio is reduced from 1.345 to 1.1. The consequence of these changes is a reduction of beam quality and an additional deterioration of resolution. In this scheme the feed design is still different for the No. 1 and No. 2 reflectors. It is believed that the advantage in simplifying the mainreflector design is not justifying the deterioration of electrical performance, thus the single symmetry plane appraoch was selected for the baseline design.

4.4.2 Main Characteristics

For the optics geometry given in Figures 4.27 through 4.29 the main characteristics of the antenna have been calculated for N = 54.

The results are in Table 4.3. The following is the definition symbols in this table.

m = beam number

$\Delta\theta_s$ = separation between beam centers in plane of scan

θ_s = scan angle

X = distance between focal point and phase center of subarray in plane of scan

X_λ = X/λ

n = number of elements in subarray

A = edge taper in subarray

P = from factor of subarray taper for A+ $(1-A\ (1-r^2)^P$ type aperture distribution

d = diameter of subarray

η_s = spillover efficiency

A_{ant} = taper at edge of paraboloid

$\theta_3, \theta_{10}, \theta_{15}$ = 3 dB, 10 dB and 15 dB angle of main beam without considering scan caused nonlinear phase errors

η_{Bo} = beam efficiency for indicated beam crossover levels without phase errors

η_B = beam efficiency with scan caused phase errors for ideal surface accuracy

$\eta_{B\Delta}$ = beam efficiency due to practical surface (Δ = 3.82 mm, rms = 0.018λ,rms)

η_{BR} = resultant beam efficiency with scan errors, surface errors but neglecting cable scatter

104

Table 4.3 – Main Characteristics of Triplet Subaperture Radiometer

Δ = 3.85 mm = .154 inch, rms

Beam m	$\Delta\theta^\circ_s$	θ°_s	X^m	X_λ	h	A^{dB}	P	d^{nom}_λ	$d^{act.}_\lambda$	d^m	$\eta^{\%}_s$	A^{dB}_{ant}	θ°_3	θ°_{10}	θ°_{15}	$\eta^{\%}_{Bo}$	$\eta^{\%}_B$	$\eta^{\%}_{B\Delta}$	$\eta^{\%}_{BR}$	$d^m_{env.}$
						Subarray characteristics							without	phase errors						
1	.60	.30	.365	1.719	18	14	2	3.78	4.16	.883	98.5	14	.293	.516	.614	98.1 at 13.52dB	97.6	94.8	92.5	1.25
2	.62	.90	1.096	5.162	20	14.75	2.1	3.93	4.36	.925		15.1					96.1		91.1	1.32
3	.64	1.52	1.853	8.728	22	15.5	2.2	4.09	4.58	.972		16.2					94.7		89.8	1.38
4	.66	2.16	2.663	12.401	25	16.25	2.3	4.24	4.79	1.017		17.3					93.2		88.3	1.47
5	.68	2.82	3.439	16.198	28	17.00	2.5	4.40	5.02	1.066		18.4					92.2		87.4	1.56
6	.70	3.50	4.270	20.112	31	17.75	2.6	4.55	5.23	1.110		19.5					91.2		86.4	1.64
7	.72	4.20	5.127	24.148	35	18.50	2.7	4.71	5.46	1.159		20.6					90.2		85.5	1.74
8	.74	4.92	6.010	28.307	38	19.25	2.8	4.86	5.69	1.208		21.8					88.3		83.7	1.82
9		5.64	6.932	31.660	41	20.00	3.0	5.02	5.92	1.257	99.5	23.0	.335	.607	.725	94.5 at 14.39dB	86.6		82.1	1.88
																	Av.		87.42	
10 (9)	.76	7.39	6.582	31.002	41	20.00	3.0	5.07	5.33	1.12	99.6	26.0	.353	.635	.751	98.8 at 14.64dB	80.1		75.9	
11 (8)	.74	8.15	5.719	26.987	38	19.25	2.8										83.2		78.9	
12 (7)	.72	8.89	4.881	22.989	35	18.50	2.7										84.0		79.6	
13 (6)	.70	9.61	4.067	19.156	31	17.75	2.6										85.0		80.6	
14 (5)	.68	10.31	3.277	15.434	28	17.00	2.5										86.9		82.4	
15 (4)	.66	10.99	2.623	12.354	25	16.25	2.3										89.8		85.1	
16 (3)	.64	11.65	1.767	8.321	22	15.50	2.2										91.9		87.1	
17 (2)	.62	12.29	1.046	4.929	20	14.75	2.1										93.3		88.4	
18 (1)	.62	12.91	.349	1.644	18	14.00	2.0	3.46	3.76	.794	98.6	17.5	.311	.537	.636	98.6 at 14.25dB	93.9		89.0	
19 (1)	.62	13.53	.349	1.644	18	14.00	2.0										93.9		89.0	
20 (2)	.64	14.15	1.046	4.929	20	14.75	2.1										93.3		88.4	
21 (3)	.66	14.79	1.767	8.321	22	15.50	2.2										91.9		87.1	
22 (4)	.68	15.45	2.623	12.354	25	16.25	2.3										89.8		85.1	
23 (5)	.70	16.13	3.277	15.434	28	17.00	2.5										86.9		82.4	
24 (6)	.72	16.83	4.067	19.156	31	17.75	2.6										85.0		80.6	
25 (7)	.74	17.55	4.881	22.989	35	18.50	2.7										84.0		79.6	
26 (8)		18.29	5.719	26.987	38	19.25	2.8										83.2		78.9	
																			Av. 83.41	

Left-margin annotations:

Feed No.1
$\bar{R}_1 = 65.989$ m   f = 1413 MHz
$\rho_{c_1} = 69.823$ mλ = .212314 m
$D_\lambda = 260.94$
$\phi_{ac_1} = 20°$

Scan: 75° to flight

Feed No.2
$E_2 = 58.201$ m $\phi_{ac_2} = 23.28°$
$\rho_{c_2} = 64.463$ m $D_\lambda = 257.75$

For the calculation in Table 4.3 the number of elements in the subarray have been increased with scan angle in a nearly monotonous manner. For small scan angles the envelope diameter of the subarrays is somewhat larger than in the example shown in Table 4.1. Such an increase is feasible without significant increase in complexity, (the supporting surface for these elements must be provided anyway for structural reasons). The choice results in some improvement in beam efficiency for small scan angles relative to the case in Table 4.1. For large scan anbles the subarray diameter is reduced. This compromize is introduced because otherwise it is not feasible to increase the beam numbers from 44 to 54 due to feed packaging limitations. In the case of reflector No. 1 the reduced subarray size for large scan angles does cause a moderate deterioration of beam efficiency, while the average beam efficiency is about the same as for the case shown in Table 4.1. For reflector No. 2 the deterioration is larger, because the optics has a lower F/D and the beams are scanned to a general position relative to the plane of offset. The average beam efficiency of the system is about the same as for the case in Table 4.1 because the maximum scan position is only 9 instead of 12. When the surface accuracy of the reflector is considered (Δ = 3.82 mm, rms) then the resultant beam efficiency of the system is 85.4%. It can be concluded that the 3 subaperture system is capable to produce similar beam efficiency and spatial resolution to that of the 2 aperture system, but with a 54/44 = 1.33 times increased swath. These results, however, require a structural diameter increased by 118/100.4 = 1.175.

It can be seen from Table 4.3 that with increasing scan angle the beamwidth of the scanned beam increases. This is an inherent characteristics associated to the increasing aperture phase error and increased aperture taper. In reflector No. 1 the 15 dB beamwidth (approximately equal to the

beamwidth within which 98% of all the radiated power is contained) varies between 0.164° and 0.725°. The angular separation between beam centers is adjusted to these angles and varies between 0.60° and 0.74° in order that the maximum practi al swath is realized. The combined swath of the 3 subaperture system is $2\beta = 37.20°$ using the subarray locations given in Table 4.3. According to Figure 3.11 the 54 beam system gives $\bar{c} = 88.8\%$ average coverage for $H = 787.5$ km orbit height.

The worst resolution occurs for the maximally scanned beam of reflector No. 2. In the plane of paraboloid offset the footprint dimension is 10.87 km, while in the perpendicular direction it is 10.32 km. The best resolution is for the minimally scanned beam of reflector No. 1. This footprint has approximately 8.44 km diameter. It may be mentioned that due to the synthesis procedure selected for the subarray excitation optimization, the deterioration of beam efficiency with scan angle has only a second order effect on the achievable spatial resolution. The main beam widening effect comes from the increased aperture taper.

The above technique assures, that the deterioration of spatial resolution with scan angle is only $10.87/8.44 = 1.29$. At the same time, the deterioration in noise temperature resolution is considerably more. For the minimally scanned beam of reflector No. 1 7.5% of all power is outside the defined footprint. For the maximally scanned beam of reflector No. 2 24.1% of the power is outside the beam. The deterioration in lost power is given by the $24.1/7.5 = 3.21$ ratio. Not much can be done against the deterioration of beam efficiency in the 3 subaperture system for the selected N. A larger F/D or better formed beams would require larger feed array, which cannot be accomodated in the given STS envelope. Thus an improvement in temperature resolution can be achieved only by a reduction of the number of beams.

It must be noted, that the above beam efficiency calculation assumes no spillover loss around the reflectors. Actually the calculated spillover efficiency varies between 98.5% and 99.5%. This efficiency component further reduces the gain but practically it does not influence the noise temperature resolution of the antenna since this radiation component generally does not hit the surface of the Earth. Thus the effect of spillover efficiency is neglected in the above beam efficiency calculations.

4.4.3 Feed Design

The major implementation problem of the soil moisture measuring radiometer system is concerned with the design of the feed array. While the structural complexity related to the antenna optics is characterized by the diameter of the hoop and accuracy of the reflecting surfaces once this problem is solved, the optics may be usable for a number of missions. The feed array on the other hand is specific for a given application and its design must be developed individually for each mission.

The dimensions of the feed array are an order of magnitude less than that of the reflector. However, its weight per area ratio is typically two order of magnitude larger thus the reflector and feed array weight is comparable. Since for space application weight is usually proportional to complexity and cost, it can be suspected that the design, fabrication, and test complexity of the feed is comparable to that of the reflector.

The feed for the present application includes the radiating elements, the beam forming network, the radiometer receiver and the support-deployment mechanism. The design of each of these subsystems is relatively complicated and are strongly dependent on each other.

108

In the following a brief outline of these design problems will be given. No attempt will be made to derive a fully optimized design. However, it is believed that the presented examples are representative to actually achievable designs.

The first step of the feed design is the development of the overall feed array layout. This layout is characterized by the subarray phase centers associated to the individual beams. In Table 4.3 the location of the phase center in the direction of the long dimensions of the overall array is given by X; where X is the distance from the center of the overall array. Since the subarray dimension in the direction of X is generally larger than the separation between phase centers, the subarrays must be displaced in the perpendicular to X direction in order to avoid subarray overlap. (Overlap in principle can be utilized and may be actually implemented in an actual design to some limited situations for the purpose of reducing the overall envelope of the feed array. However, such technique is greatly increasing complexity and loss and will not be considered in the following.) For the given X values and subarray nominal diameter, d the location of the subarray phase centers can be calculated. Figures 4.30 and 4.31 show these locations for feed No. 1 and No. 2, respectively, on the basis of the data displayed in Table 4.3. It can be seen that the phase centers of adjacent beams are separated by $\pm$ displacements in the Y direction and the displacements increase with increasing scan angles. That causes increased width for the array with increasing distance from the focal point, a structurally undersirable feature. In order to assure structural stability the center part of the array must be properly streamlined, causing a less than ideal utilization of the available surface to support radiating elements.
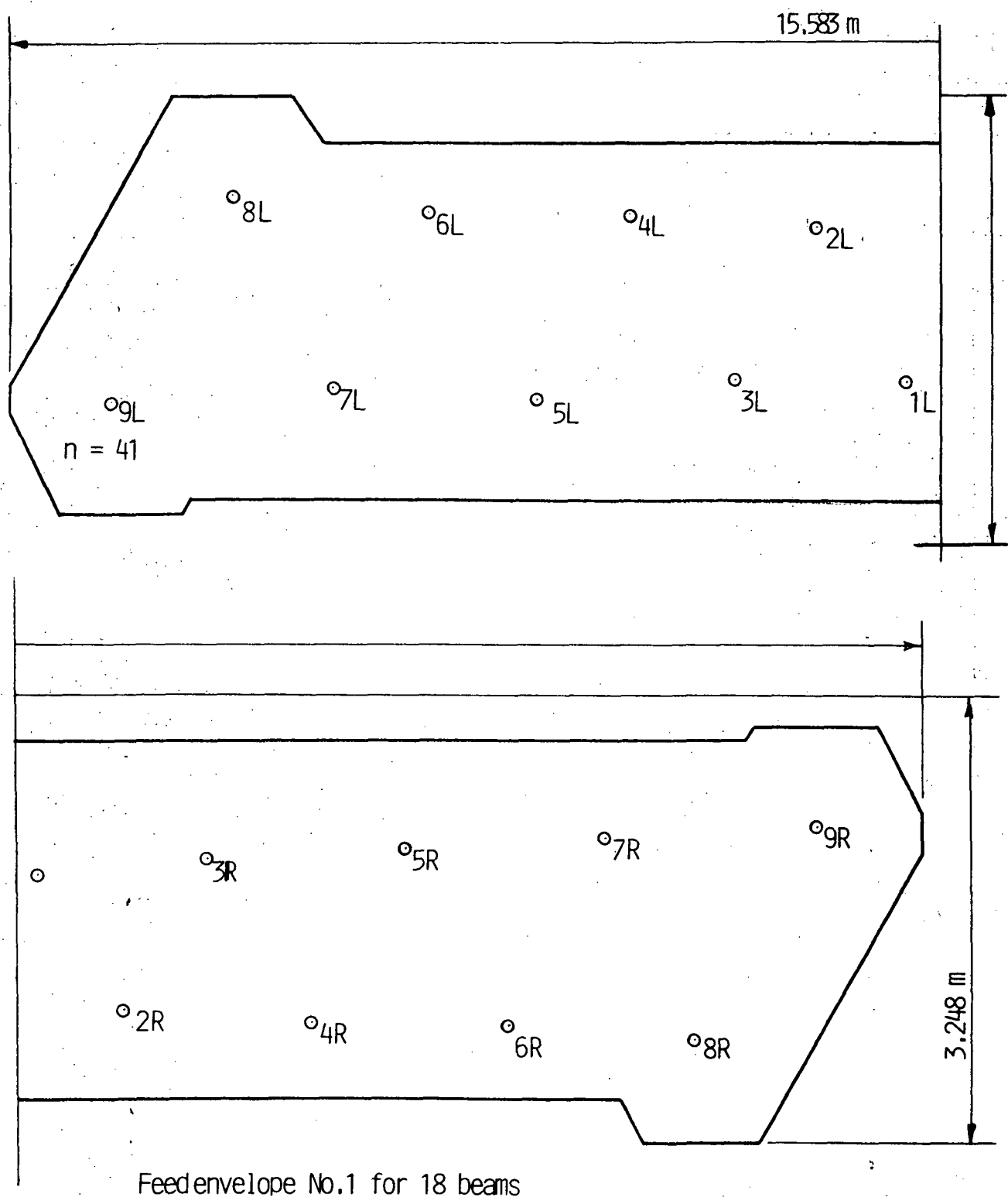
Figure 4.30 – Conceptual layout of the No. 1 feed array for triplet aperture antenna.

14,153 m

8L   6L   4L   2L

9L   7L   5L   3L   1L

outside section

1R   3R   5R   7R

2R   4R   6R   8R

3,248 m

inside section
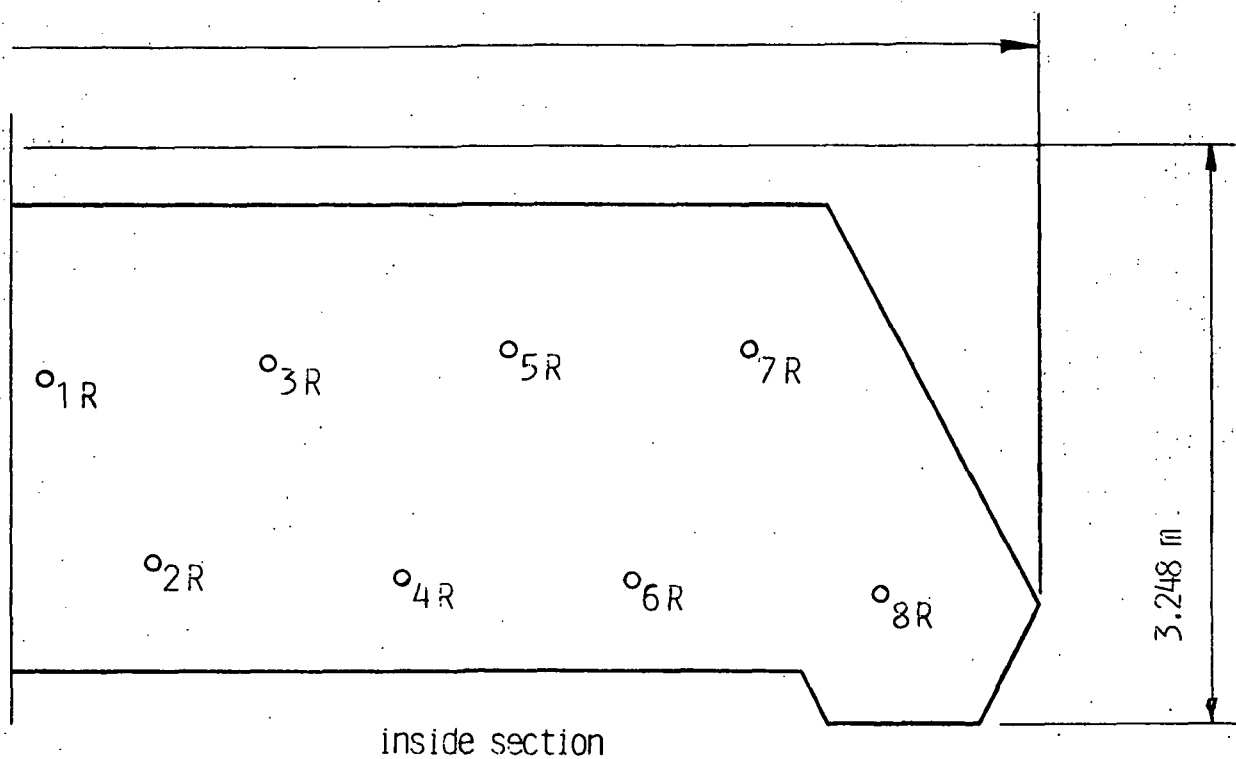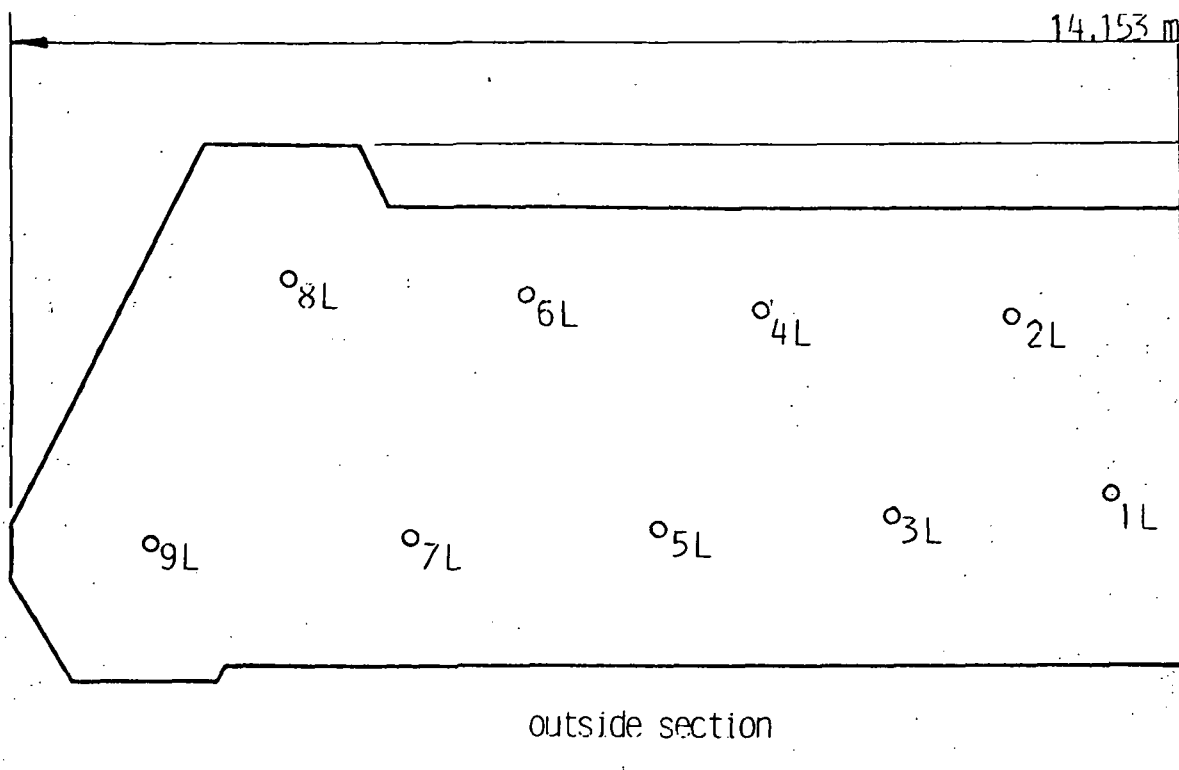
Feed envelope No.2 for 17 beams

Figure 4.31 – Conceptual layout for the No. 2 feed array for triplet
aperture antenna.

111

Figures 4.30 and 4.31 indicate that the layout for the feed arrays is similar. However, the layout for feed No. 1 is symmetrical, while the layout at feed No. 2 (in fine detail) is not. There are 9 different subarrays in feed No. 1 while all 17 subarrays are different in feed No. 2. This requires ideally 26 different subarray designs.

In actual practice some standardization might be possible. Selecting an identical, compromized symmetrical layout for both feeds changes the beam center locations only slightly. Furthermore, a compromize excitation for corresponding elements might be acceptable at the expense of some reduction of beam efficiency. In this case a minimum of 9 subarray designs are adequate. Finally, by replacing two adjacent subarray designs by the more complex of the pair, a total of 5 subarray designs might suffice.

The next step is the determination of the subarray layouts. Generally the quality of beam formation for a subarray improves iwth increasing number of radiating elements, n and with increasing subarray envelope diameter, d.

The determination of n,d and the complex amplitude excitaion of the elements requires a series of pattern synthesis for each subarray within an n,d matrix. The first approximation of the optimum n and d values can be determined by the following steps:

1) Calculate the secondary pattern gain contours by placing a single radiating element at the location of the desired subarray phase center.

2) Select the gain contour which corresponds to the acceptable secondary pattern sidelobe level.

3) Place additional radiating elements around the original element in such a way that the corresponding component beam centers form a sufficient grid within the selected gain contour.

4) Determine the element excitations using the minimax procedure which reduces maximum gain and given sidelobe level in the vicinity of main beam.

5) Calculate beam efficiency.

6) Stop if beam efficiency is acceptable, and

7) Increase n and d and repeat the procedure unitl beam efficiency is above desired value.

The above procedure is not terminated, because with increasing n and d any less than unity beam efficiency can be achieved. Thus, it is necessary to consider two additional constrains. The first constrain is that the loss in the BFN increases with n. This yields a specific n for which the beam efficiency of the lossy antenna is maximum. The second constrain is the practically acceptable subarray size. This presents an upper limit for acceptable n. The above constrains cause a reduction of achievable beam efficiency with increasing scan angle.

The results of the above calculations and some additional practical considerations are shown in Figure 4.32. It is assumed for this figure that the radiating elements are placed into a hexagonal grid. For each subarray the grid size is given by the desired overall subarray envelope dimensions, by the realizable descrete number of radiating elements and by the minimum element distances due to resonance, mutual couling and grating lobe considerations. The actual envelope shape of the subarray layout is determined by the gain contour shape in the secondary pattern and by the criteria to avoid feed overlap. It can be seen from Figure 4.32 that the feed points of the smallest such array (n = 18) are within a 1.2 n × 1.80 m envelope, while the feed points of the largest subarray (n = 41) are within 1.7 m × 1.62 m.

Figures 4.33 and 4.34 show the layout of the integrated array utilizing the geometry of the subarrays given in Figures 4.30 - 4.32. It can be seen
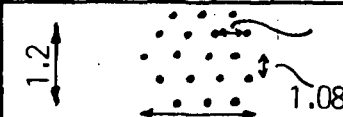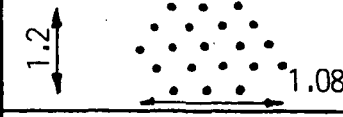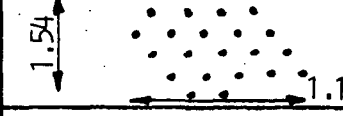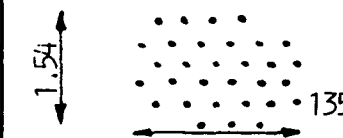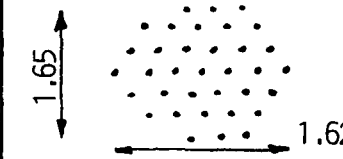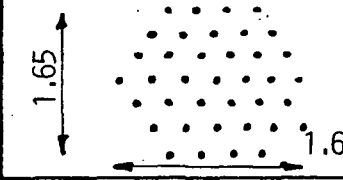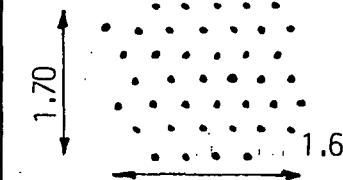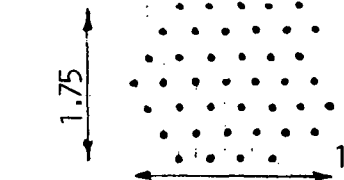
n	No.2 feed (75° plane)	No.1 Feed (Symmetrical beam distribution)
18	1.2 / 1.08	Same
20	1.2 / 1.08	Same
22	1.30 / 1.08	Same
25	1.54 / 1.17	Same
28	1.54 / 1.3	1.75 / 1.3
31	1.54 / 135	Same
35	1.65 / 1.62	Same
38	1.65 / 1.62	Same
41	1.70 / 1.62	1.75 / 1.3

Figure 4.32 – Subarray layouts necessary for the feed arrays of the triplet antenna.

Figure 4.33 - Layout of feed array No. 1 for triplet aperture antenna.

Figure 4.34 – Layout of feed array No. 2 for triplet aperture antenna.

116

that the array supporting surface is well utilized, however, some further increase of subarray sizes is feasible if a more refined design shows sufficient benefit. Unfortunately, for the last 4 beam positions any substantial subarray size increase would cause subarray overlap. It must be noted, that if such an overlap involves low level excitation elements then the effect of increased internal noise temperature may be tolerable for better sidelobe control. However, generally such an overlap must involve frequency or time division techniques. (For instance if a radiating element must be shared between beam 8 and 9, such sharing may be achieved by switching the element back and forth between the two subarrays. In this situation the contribution of this element on an integrated basis will be 3 dB less than a full time available element. This can be compensated by increasing the amplitude excitation of the element by 3 dB. Similar effect can be achieved if the element is not switched but its power is divided equally between the two subarray.)

The next step of the subarray design is the selection of the radiating element. The most convenient radiating element for linear polarization is the printed resonating patch. There is great freedom in the selection of patch geometry from rectangular to elliptical contours of which the square and circular shapes are special cases. Table 4.4 shows the conditions of first resonance for rectangular patch geometry.

TABLE 4.4

Conditions of first resonance with rectangular patch

a_λ	b_λ	a/b
0.2567	0.3054	0.8404
.3315	.3034	1.0920
.4813	.3016	1.5959
.7613	.2994	2.5547
1.0050	.2988	3.3629

It can be seen from Table 4.4 that for a/b ~ 1 (square patch) the element resonates if b ~ 0.304 λ = 6.45 cm. The equivalent circular patch has a diameter of d = 0.387 λ = 8.21 cm. These resonant dimensions can be reduced by dielectric loading, but the resonant dimensions can not be increased. For the described subarray layouts shown in Figure 4.32 the radiating element separation is typically in the order of 1λ. Thus, a single patch may not fill in the area contemplated for the readiating element. This could cause undersirable grating lobes. Based on these considerations, it may be desirable to use more than one combined patches as a single radiating element. Figures 4.35, 4.36, and 4.37 show examples for radiating elements, which are composed from 1, 3, and 12 patches, respectively. These patches are usable for up to 1, 1.5, and 3 wavelength separations between radiating elements. The patches in these configurations are combined into a single radiating element by a microstrp line, which is printed on the same substrate as the radiating element. This solution has the advantage of simplicity, but the stripline segments contribute to the radiation and cause some asymmetry in the element radiation pattern. These asymmetries can be reduced by the rotation of the radiating elements relative to each other within the subarray. further reduction of this effect is possible for the present application due to the large number of elements even in the smallest subarray. Based on these considerations the above patch combining techniques seem to be acceptable.

The next step in the subarray design is the selection of the BFN layout. The typical criteria for this is minimum weight, loss and cmplexity with acceptable structural and thermal performance.

Singlet Patch
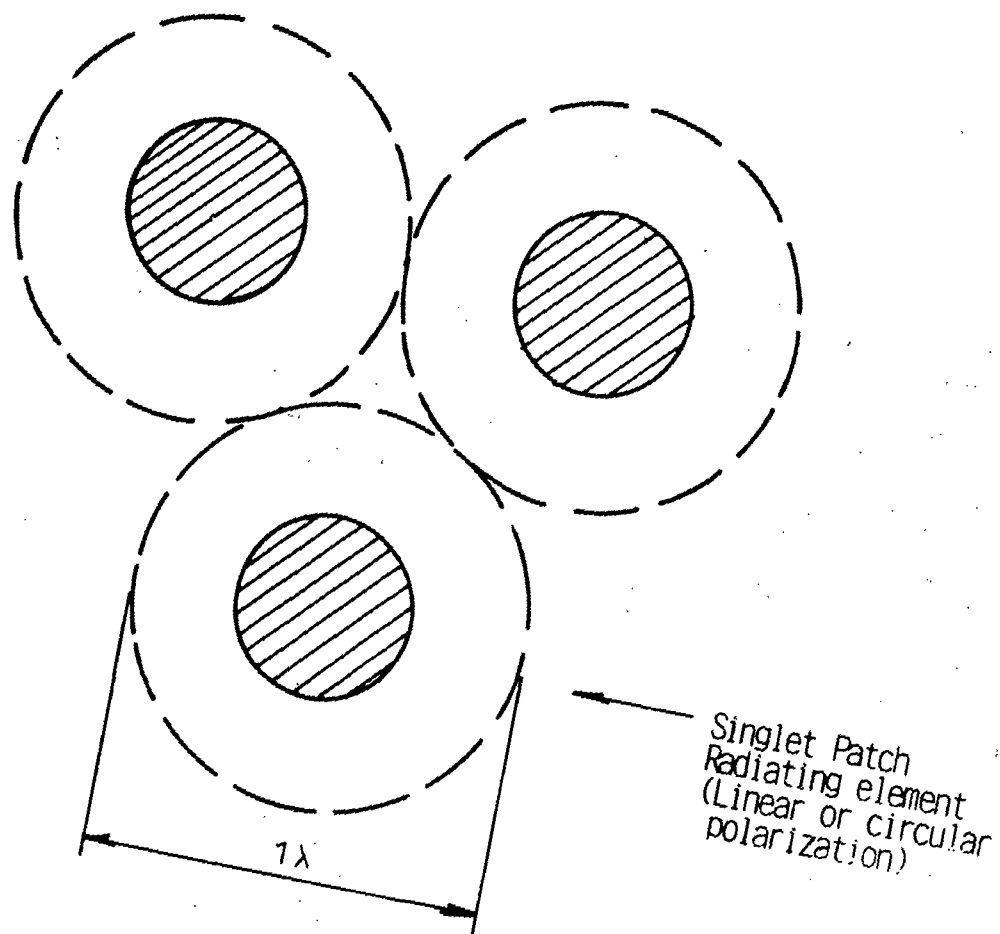Radiating element
(Linear or circular
polarization)

1λ

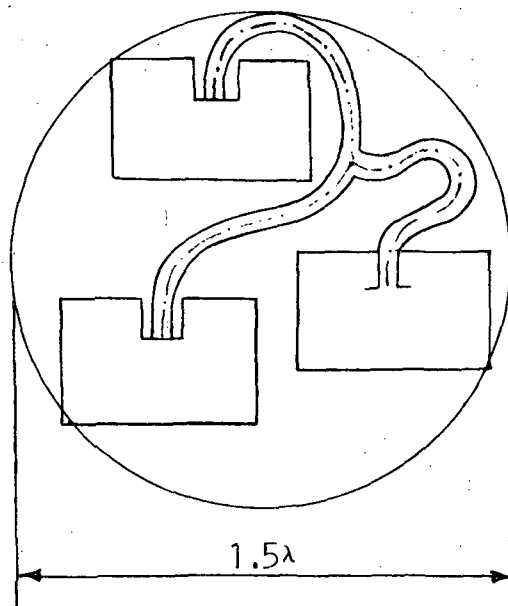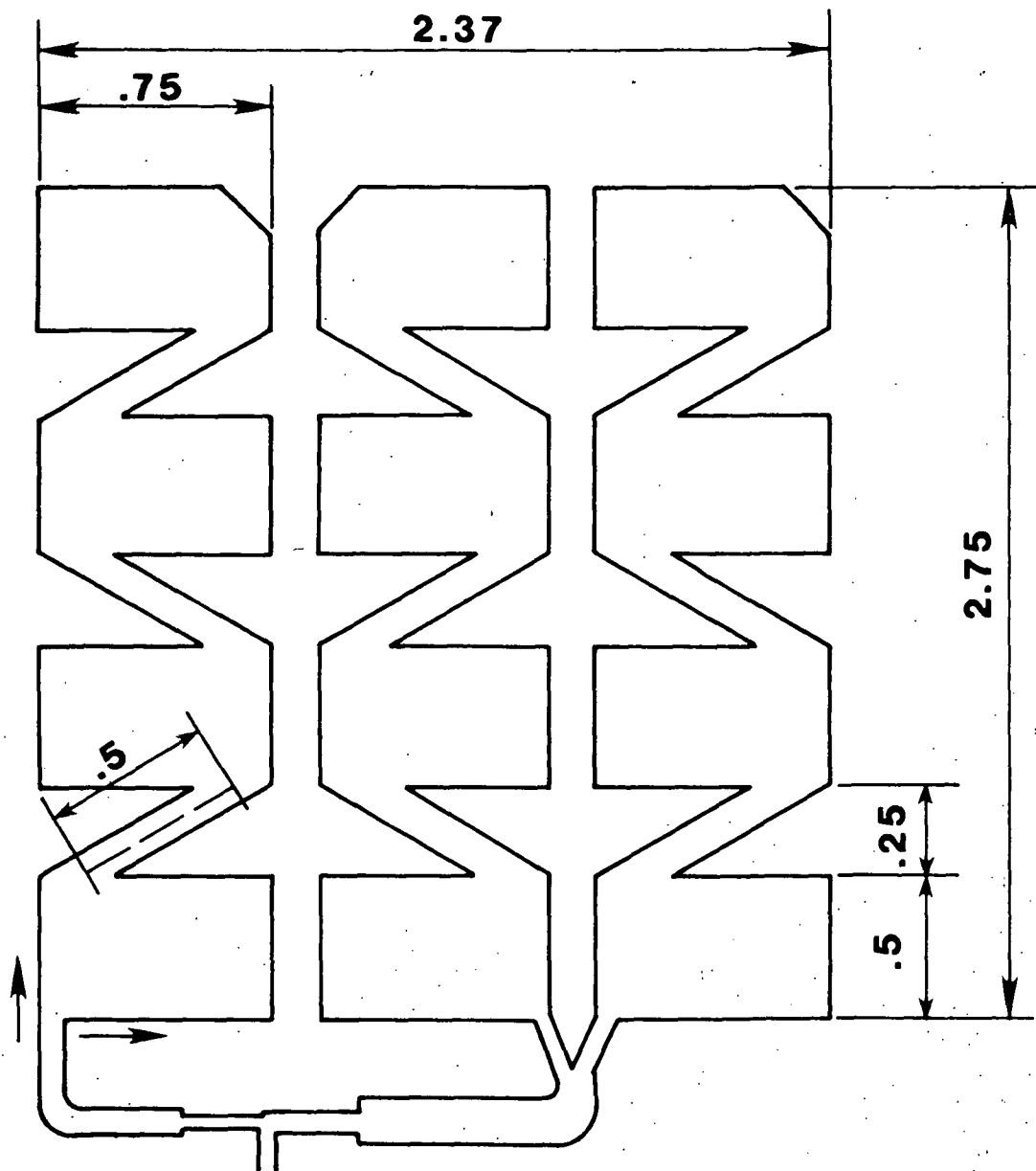Figure 4.35 - Composite radiating element for 1λ element separation.

119

Figure 4.36 - Composite radiating element for 1.5λ element separation.

DIMENSIONS IN WAVELENTH

Figure 4.37 – Composite radiating element for 3λ element separation.

Low weight requires minimization of the nuber of printed layers on which the BFN is implemented and the use of minimum thickness substrates. In order to achieve the above, the area for the stripline must be minimized. This requires the minimization of stripline center conductor width, as defined in Figure 4.38. With decreasing w and constant stripline height b the impedance of the stripline increases rapidly and becomes very tolerance sensitive. If additionally b is also reduced, the loss increases (see Fig. 4.39). Thus a reduction of weight is always accompanied byb increased losses. In other words a given loss defines the real estate requirement for the stripline.

Another parameter which effects the BFN design is the separation between radiating elements. For larger element separation more space is available for the striplines, thus their loss per unit length decreases. At the same time, the length of the lines increases which increases the loss. The optimum selection requires a detailed design optimization.

In the following two design approaches are compared. The first approach is shown for the n = 41 element subarray. This is based on the use of as much as possible real estate in order to reduce losses. The approach leads to a relatively large number of multilayer boards. While the loss within one board is relatively low, the connecting lines between the tandem connected boards increase the combined loss. This design is analyzed for d = 1.18λ and d = 1λ radiating element envelope diameter. The second approach is shown for n = 18 and n = 41 element subarrays. The goal of this approach is a single board BFN implementation. The loss in this case is determined by the available area for striplines and power dividers. It must be noted that in each case a considerable part of the total loss is associated with the delay lines, which are necessary to implement the essentially equal phase excitation of the radiating elements.
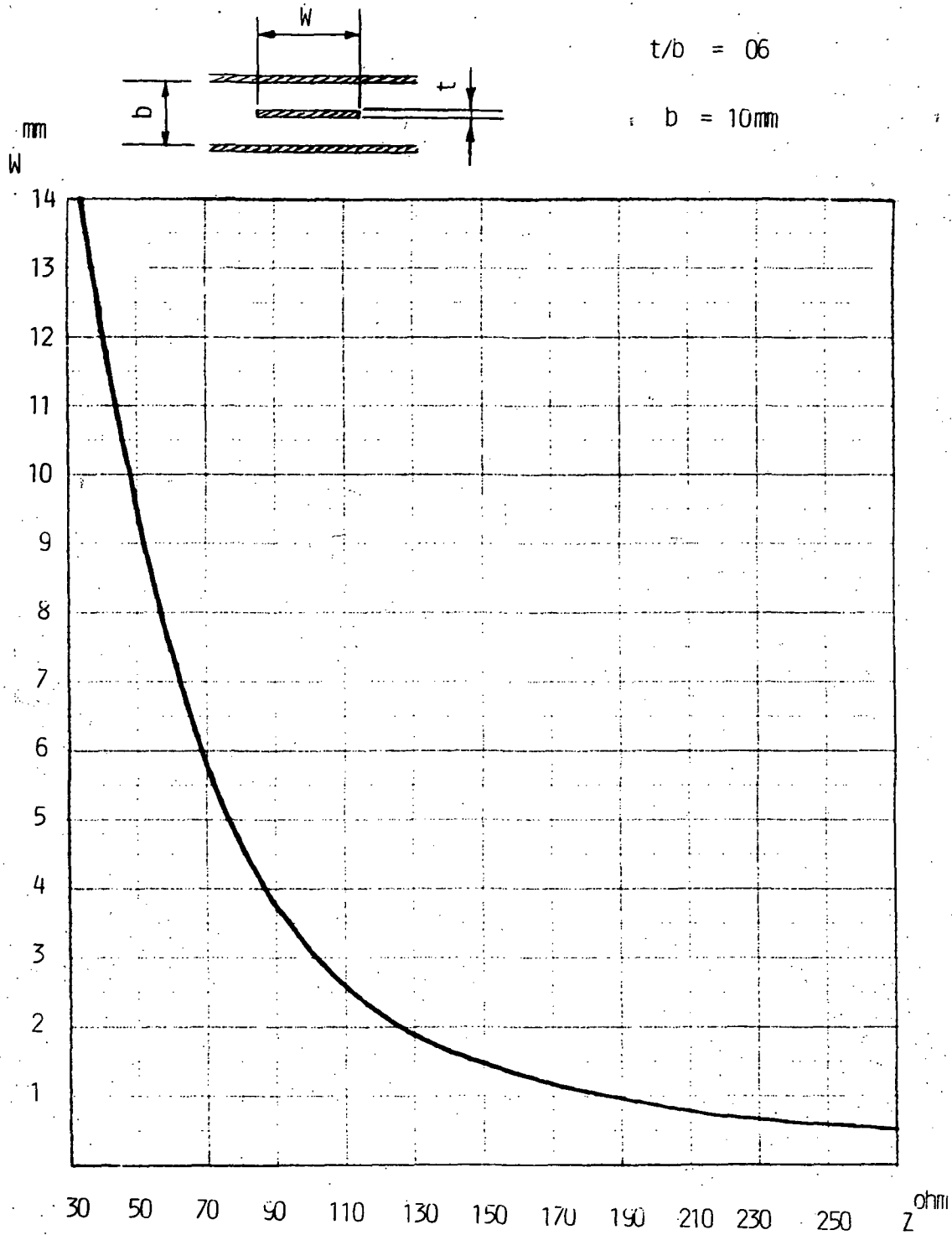
122

Figure 4.38 - Variation of stripline area requirement with stripline impedence.

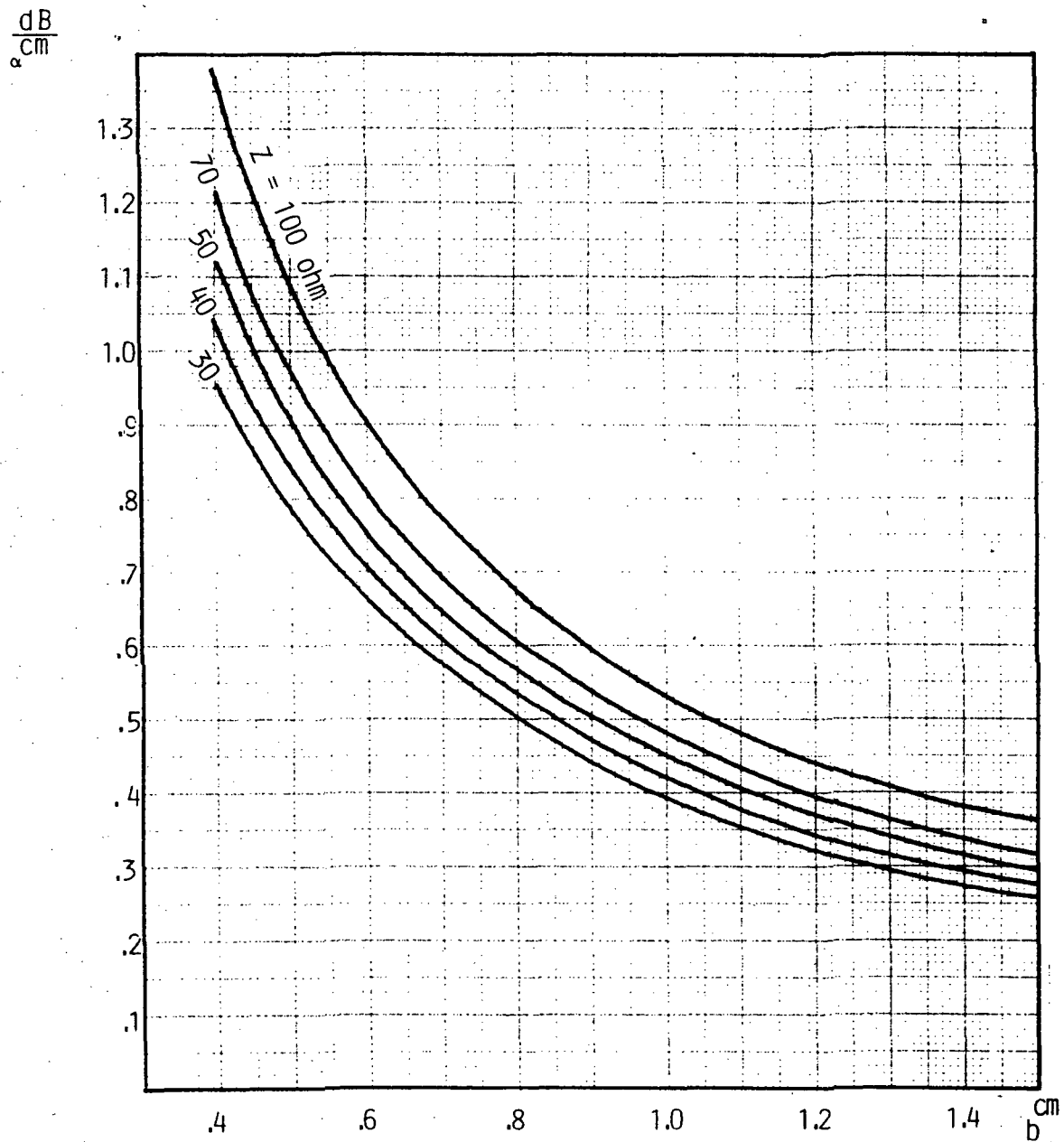$$f = 1.413 \text{ GHz}$$
$$t/b = .01$$

Figure 4.39 - Variation of stripline loss with stripline thickness.

Table 4.5 displays the main characteristics of the multiboard design. This design utilizes a triplet radiating element as shown in Figure 4.40.

TABLE 4.5
Subarray geometry for $n = 41$ radiating elements
(For max. scan [beam 9] in triplet antenna configuration.)

Design 1: $d^e = 1.18\lambda$, triplet element, (LP)

$d_{subarray} = 6.13\lambda$

$\alpha_{BFN} = 0.413$ dB

Design 2: $d^e = 1\lambda$, singlet element (LP or CP)

$d_{subarray} = 5.20\lambda$

$\alpha_{BFN} = 0.363$ dB

Sandwich thickness in each case is 8.93 cm.

Figure 4.41 shows the layout of the radiating elements of the subarray. These are supported by board No. 5. Figure 4.42 presents the corresponding BFN block diagram. This network is broken down into four separate boards. Figures 4.43 through 4.46 give the basic layout of these boards. It can be seen that the layout of these boards allows a generous allowance for the individual striplines. Figure 4.47 shows an example for the cross section geometry, to minimize losses. It can be seen that the total calculated loss in the BFN is 0.41 dB, including hybrid and connecting coaxial line losses. The overall ass'y thickness, shown in Figure 4.48 is approximately 3.1 inch. This accomodates the radiometer boxes.

Similar calculation have been conducted for $d = 1\lambda$. In Figure 4.49 the layout of Board No. 1 is included only. The arrangement results a loss of 0.36 dB, which is only slightly less than for the $d = 1.18\lambda$ design. It can be calculated that the achievable loss in the BFN for the investigated range of d is not very sensitive to radiating element separation.

A somewhat more detailed analysis have been performed for the single board BFN implementation.

Adjacent triplet
radiating element

Triplet patch radiating
element (Linear polarization)

Input

1.8λ

Radiating element design
for 1.18λ separation
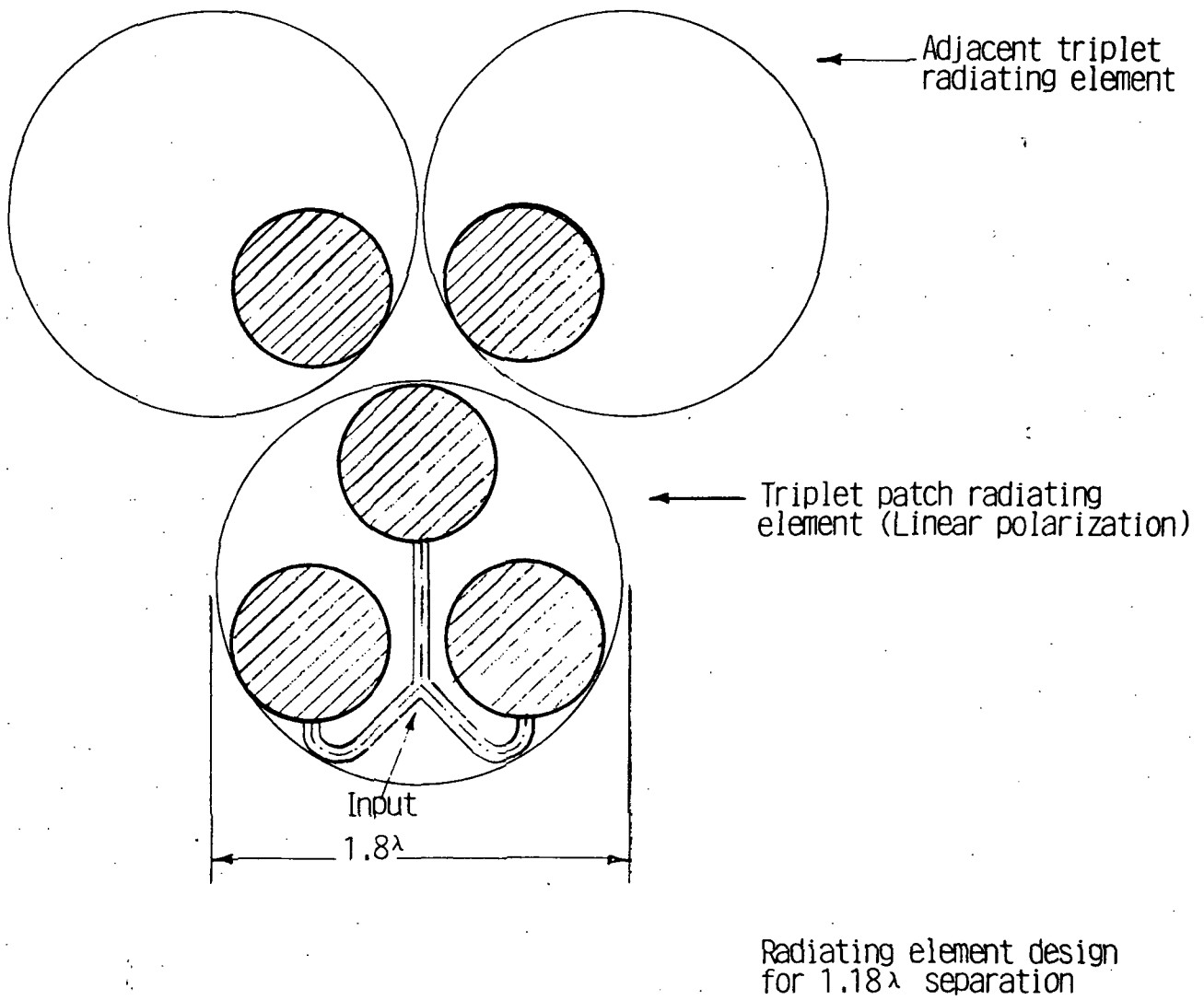
Figure 4.40 – Composite element layout utilized for linearly polarized
41 element subarray design.
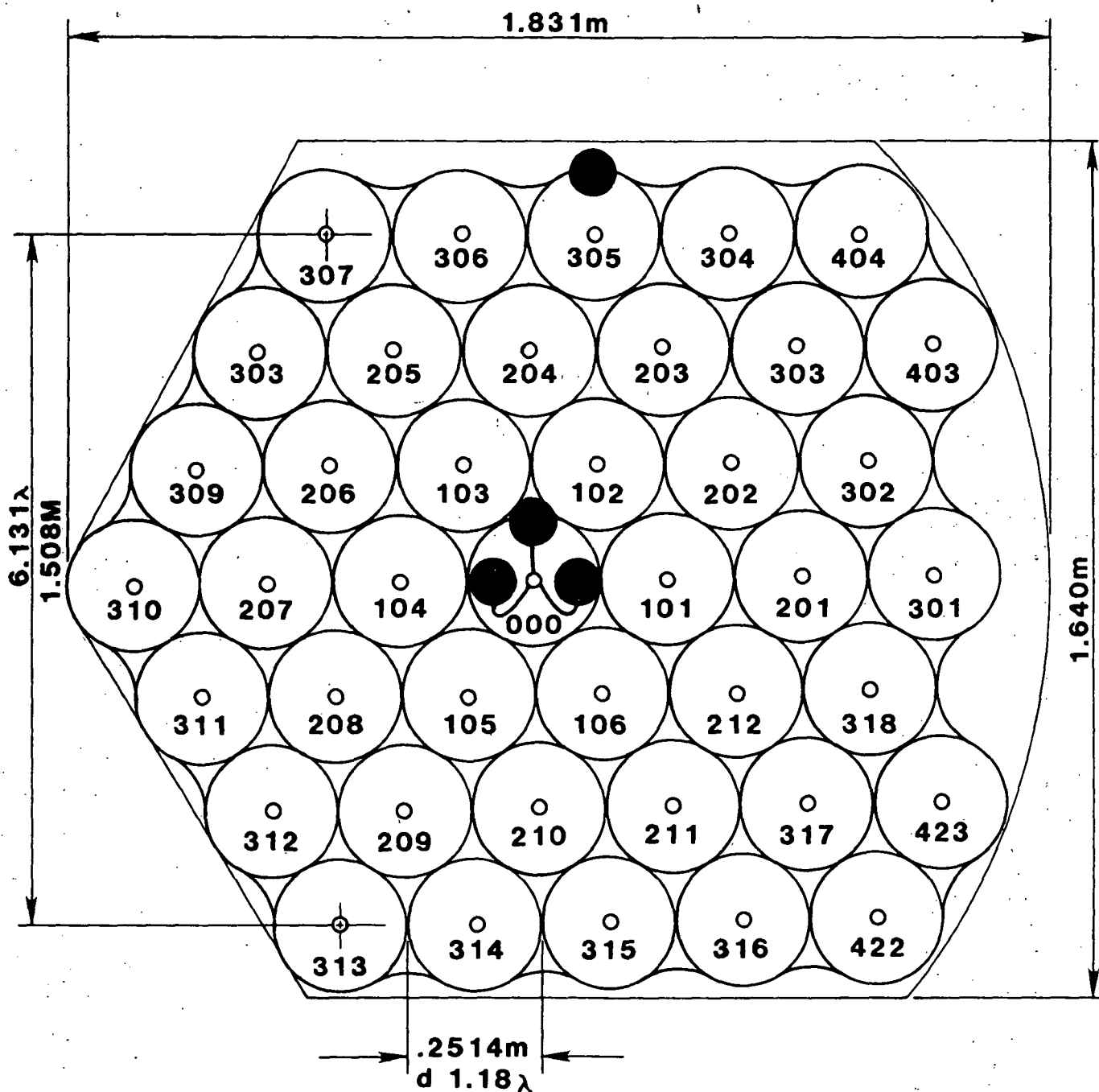
Figure 4.41 – Subarray layout for multilayer, n = 41 element subarray design (board 5).
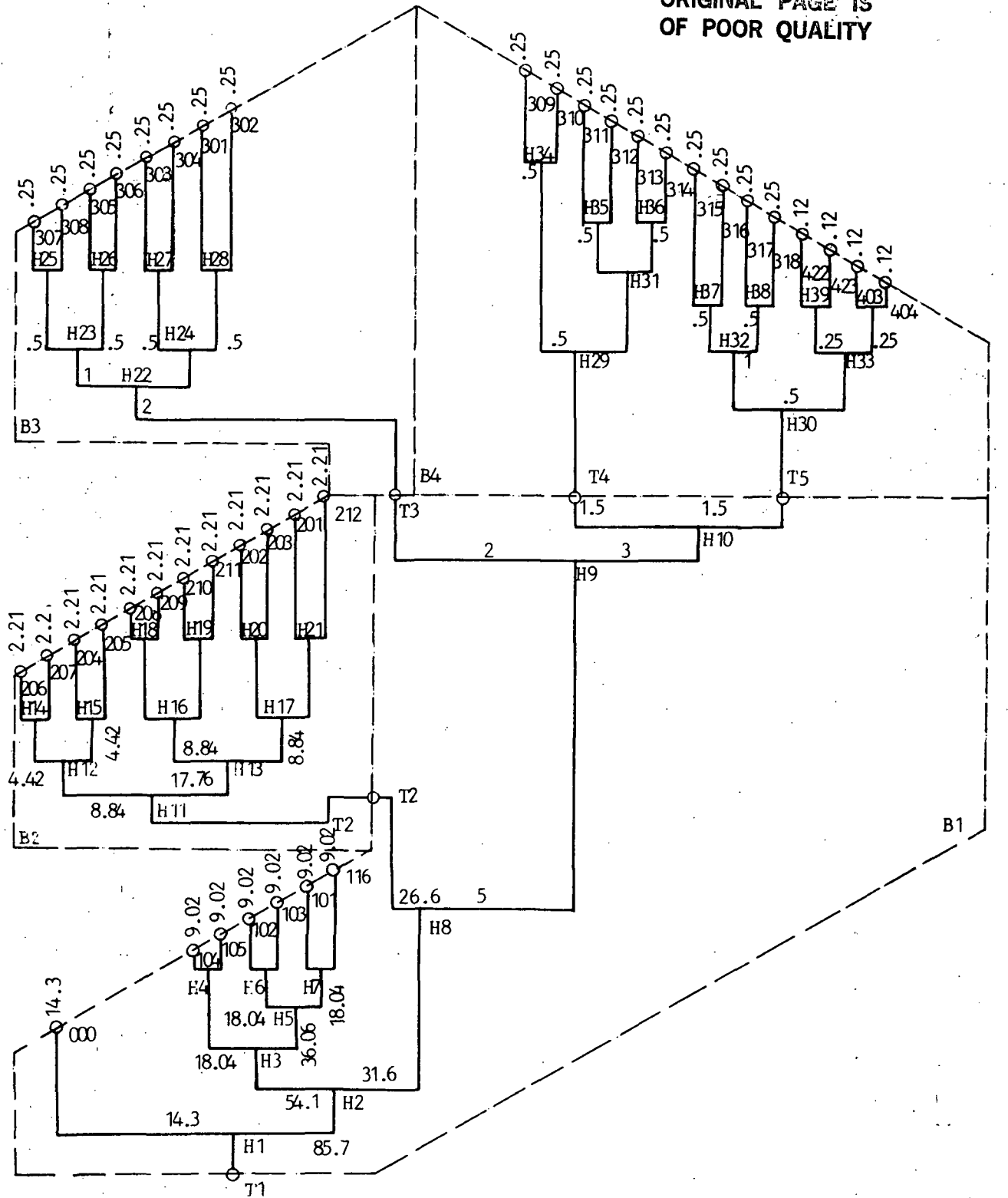
Figure 4.42 – Block diagram of BFN for the n = 41 element subarray of the No. 1 feed, multilayer implementation.

128
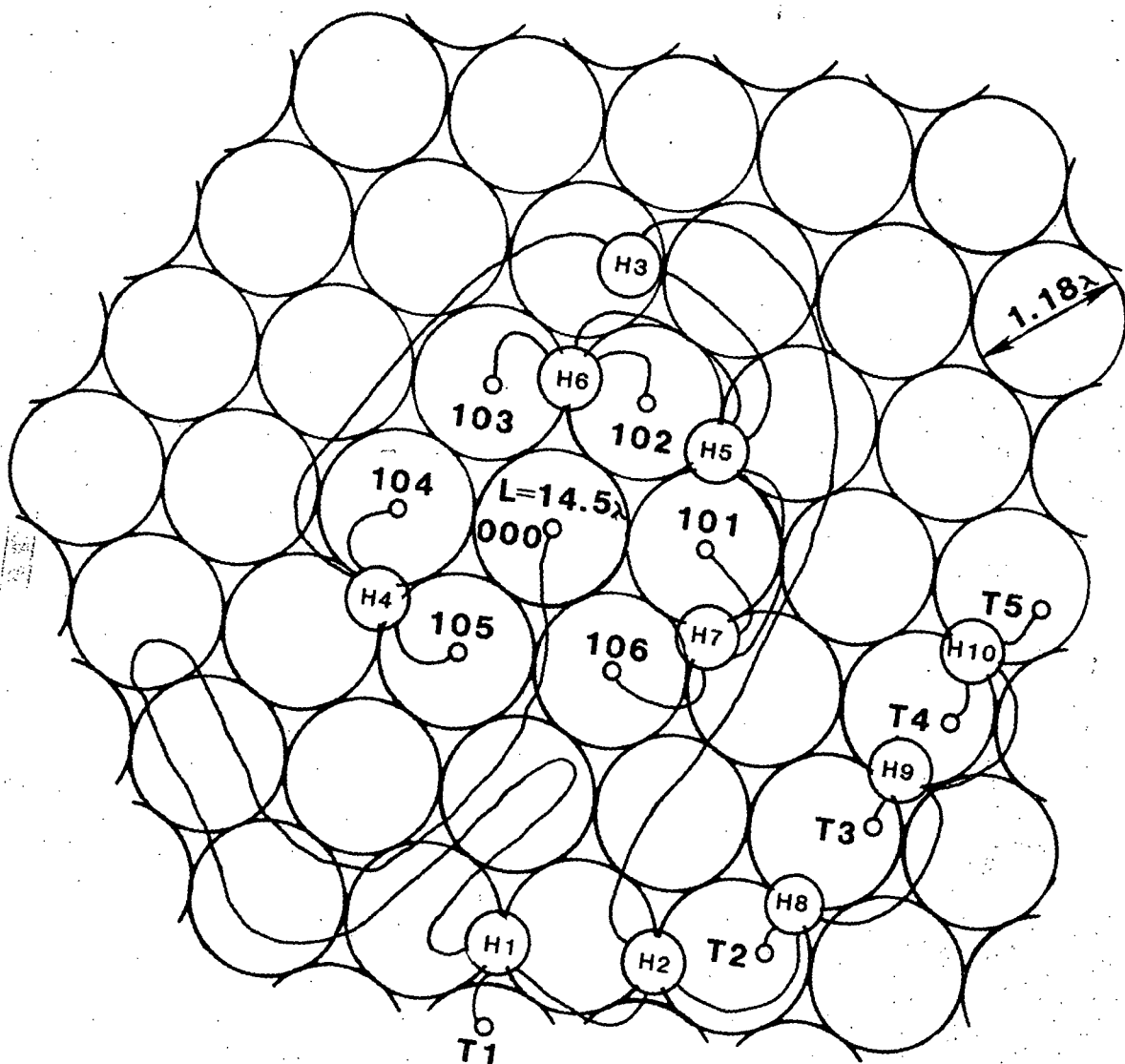
Figure 4.43 — Layout of Board 1, for d = 1.18λ.
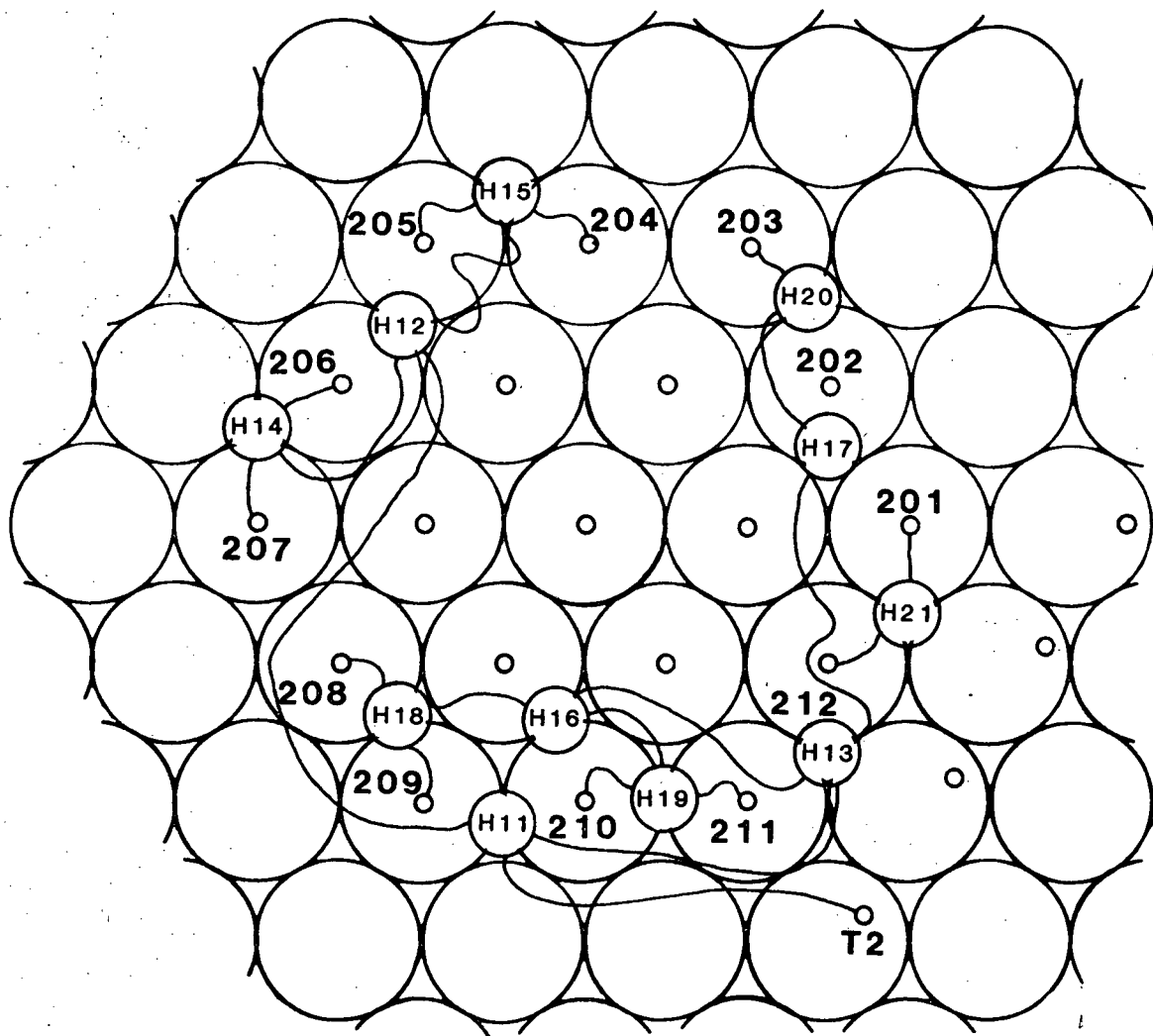
Figure 4.44 – Layout of Board 2, for d = 1.18
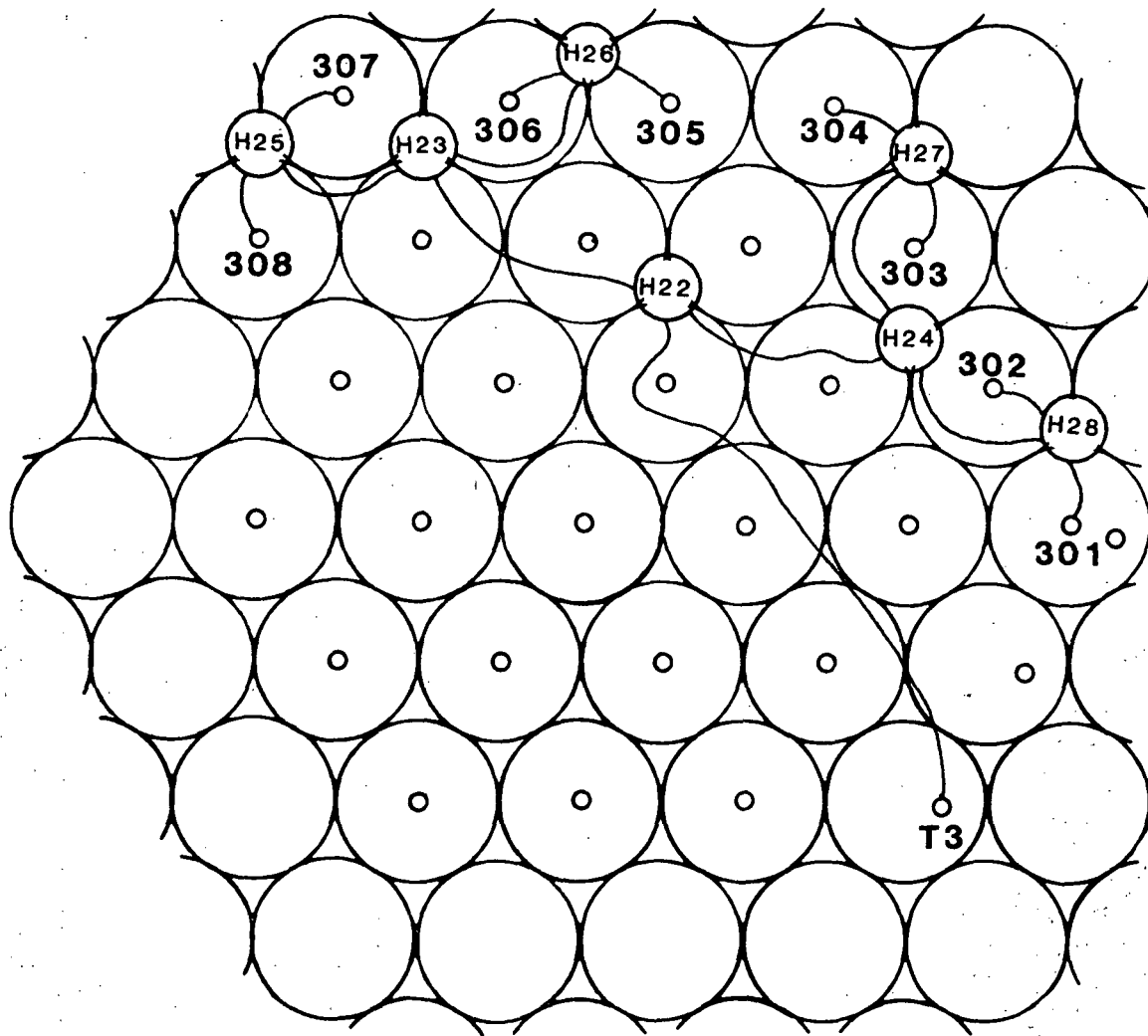
Figure 4.45 — Layout of Board 3, for d = 1.18λ.
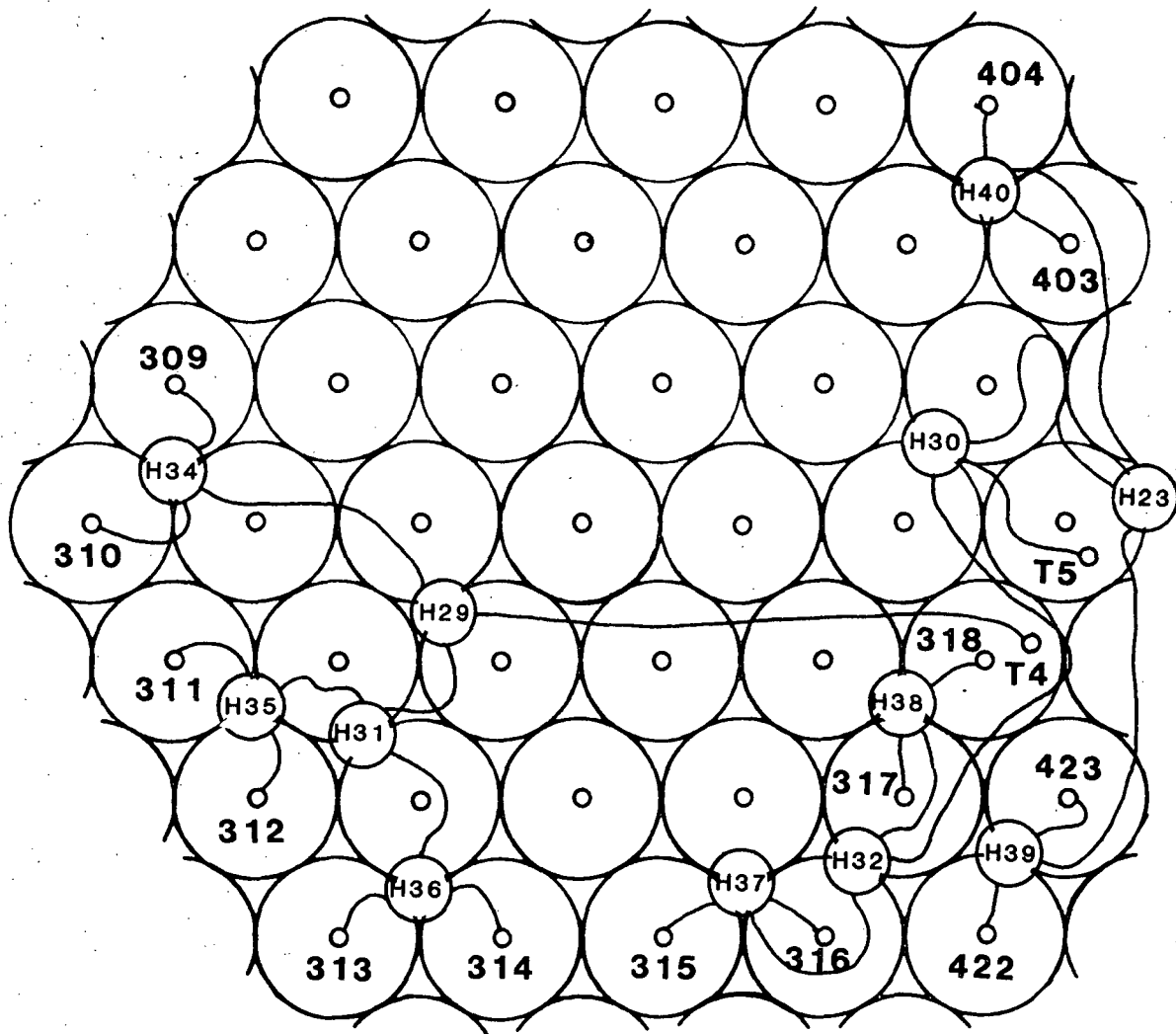
Figure 4.46 – Layout of Board 4, for d = 1.18λ.
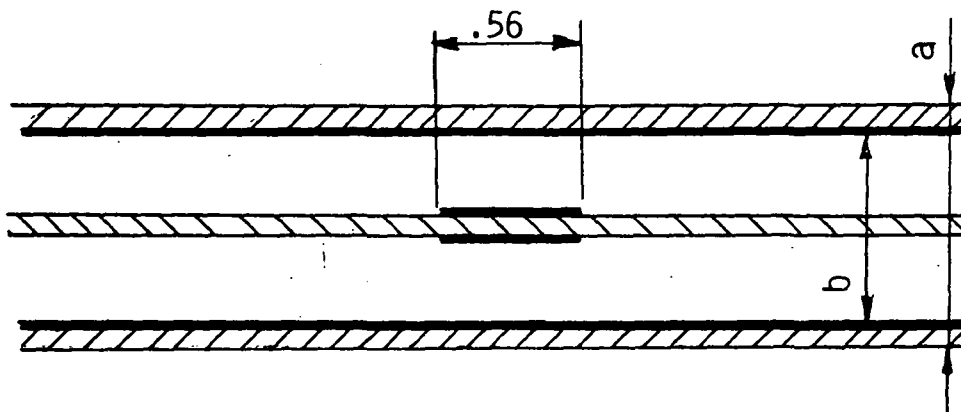
$$a = 1.57 \text{ cm}$$
$$b = 1.27 \text{ cm}$$

BFN path length to input of triplet radiating element for
$d = 1.18$, $n = 41$: $L = 14.5\lambda, f = 143$ MHz, $\lambda = 21.31$ cm

Loss characteristics:

Line loss ($L = 3.08$ m, $\alpha_0 = .055$ dB/m)	$\alpha_L = .169$ dB	
Total hybrid losses (.05 dB/Hybrid)	$\alpha_H = .234$ dB	
Coaxial lines (.005 dB/section)	$\alpha_C = .010$ dB	
Total BFN	$\alpha_{BFN} = .413$ dB	

Thickness characteristics:

Radiating element ($\lambda/8$ above ground)	2.65 cm
4 BFN boards	6.28 cm
Maximum array thickness	8.93 cm
Array thickness at radiometer box (3 layers)	7.36 cm
Radiometer box height allowing 6in= 15.24 cm	
overall ass'y thickness	7.88 cm = 3.1 in

Figure 4.47 – Cross section geometry of BFN stripline and applicable loss
characteristics.

Dimmensions in mm
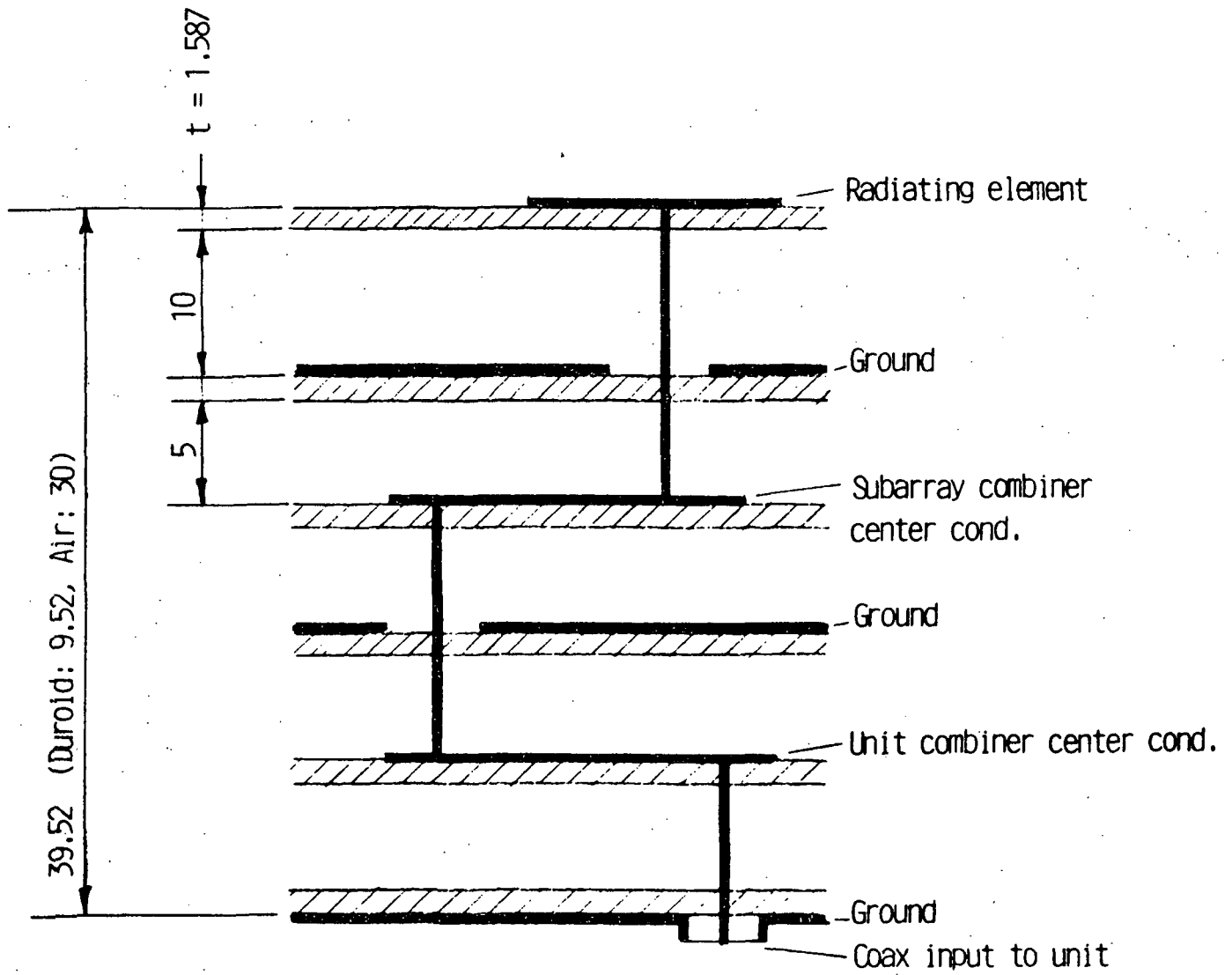
Figure 4.48 – Cross section of the integrated multilayer BFN.
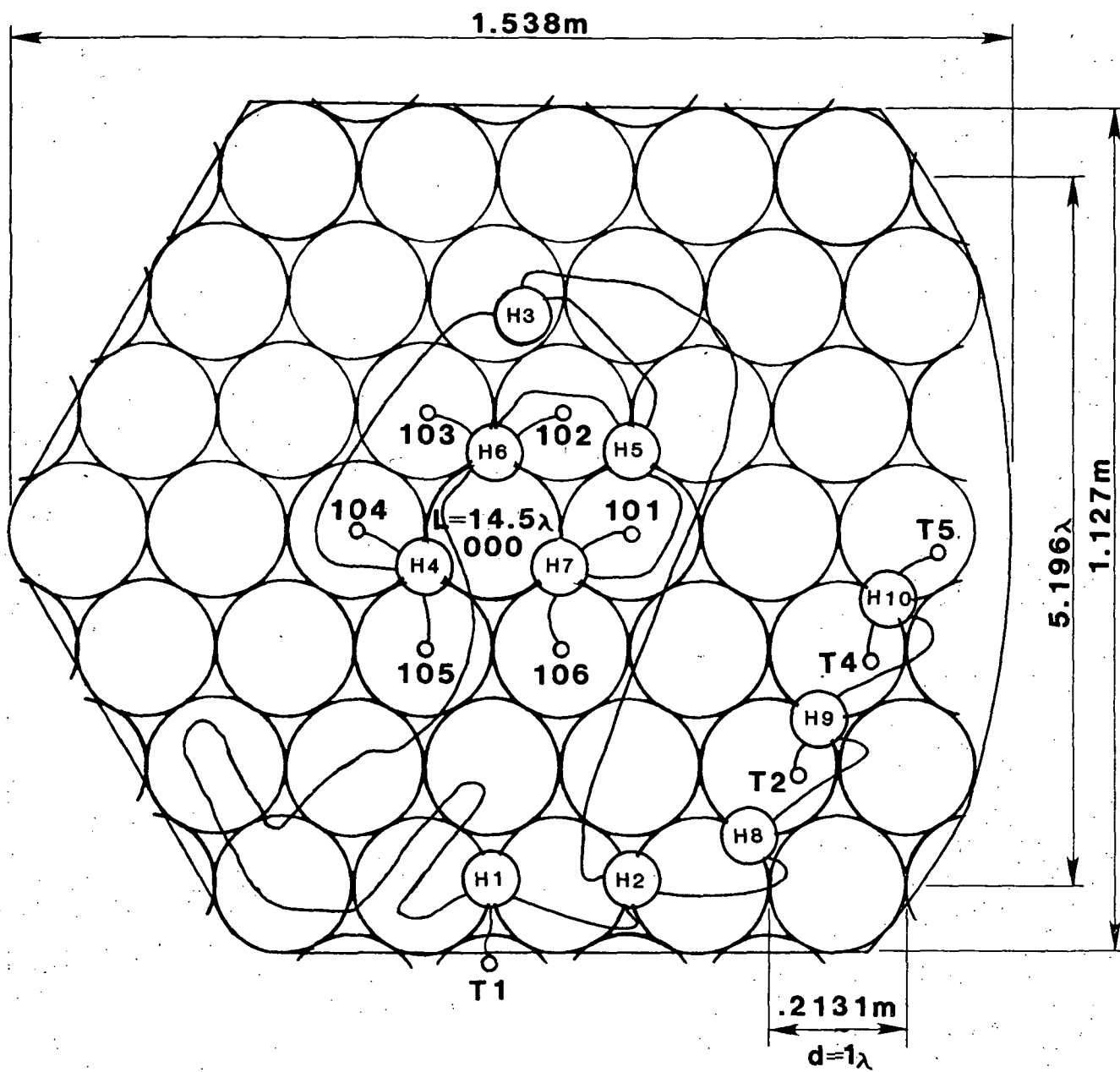
Figure 4.49 - Layout of Board No. 1 for d = 1λ.

Figure 4.50 shows the block diagram of the circuit for the n = 18
element subarray of the No. 1 feed. This subarray contains a center element,
a complete first ring of radiators and a nearly complete second ring of radia-
tors. The table in Figure 4.50 shows the applicable excitation values for
these elements. The implementation of these excitations requires six dif-
ferent types of hybrids. Assuming b = 1 cm, t/b = 0.06 the radius of the
ring hybrid is r = 0.2387λ = 5.064 cm. The loss in the hybrid increases with
the required power division ratio. For instance if the power ratio is 5.24 :
1 then w_o = 12.2 mm, w_2 = 11.7 mm and w_1 = 0.6 mm. For this case the
loss α = 0.0044 dB per ring hybrid. This is negligible compared to mismatch
and unbalance losses, which can be kept less than 0.05 dB.

Table 4.6 shows the geometry of the ring hybrids for the required power
ratios.

TABLE 4.6

Characteristics of ring hybrids at 1413 MHz for b = 15 mm

No.	Power ratio	Z_2(ohm)	Z_1(ohm)	w_2(mm)	w_1(mm)
H 13	1	70.71	70.71	11.10	11.10
H 1	1.016	70.15	71.27	11.25	10.95
H 2	1.049	69.06	72.44	11.40	10.50
H 6	2	55.90	111.80	15.82	4.50
H 4,H 5	5.24	50.92	266.82	17.82	.96
H 3	6.98	50.50	352.50	17.92	.48

Terminal	Level dB	Power	Rel.Power in ring	Normalized element power
1	0	1	1	.2539
2,3,...7	3.8	.4169	2.501	.1058
8,9,...18	14	.0398	.438	.0101
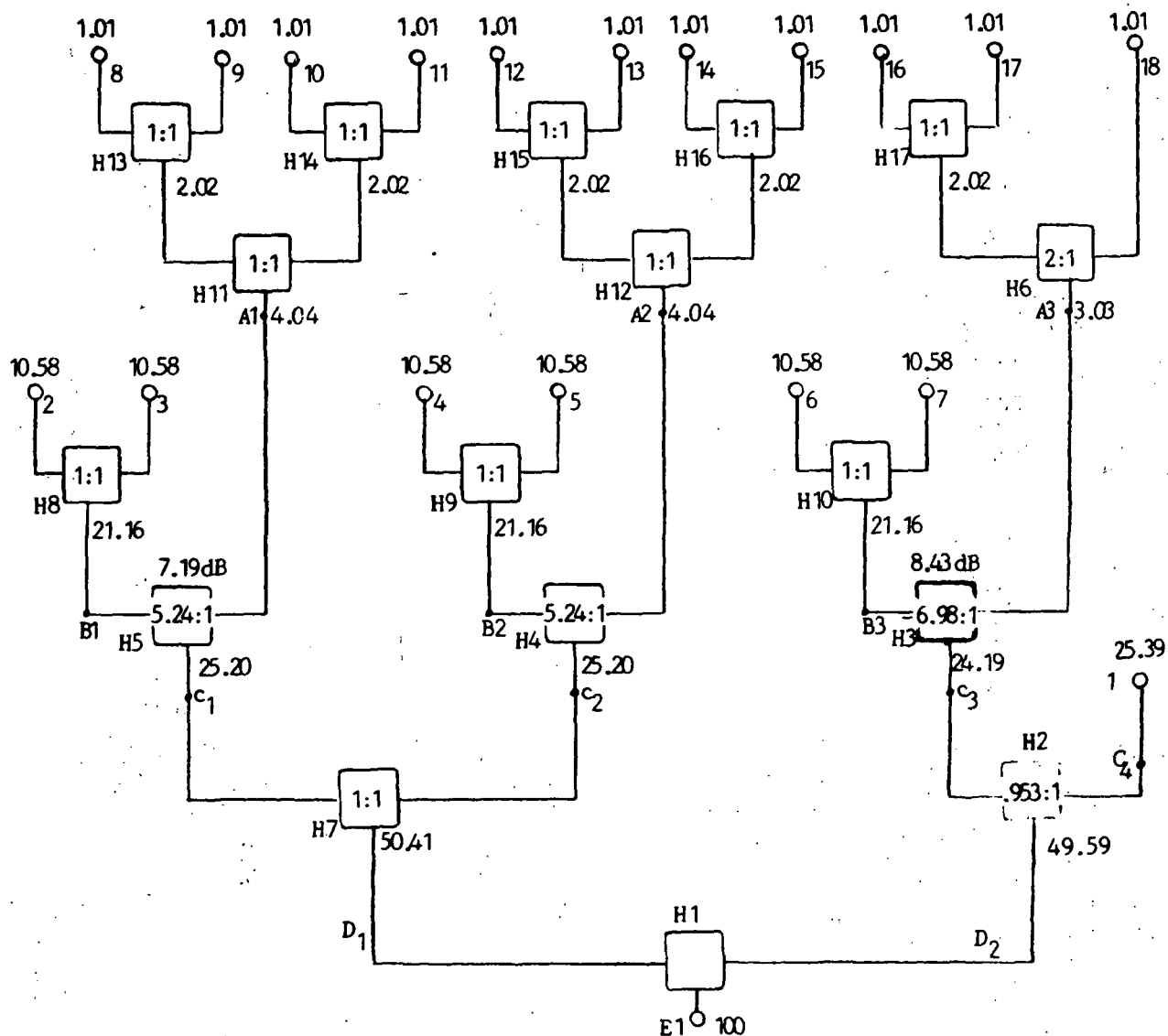
Figure 4.50 – Block diagram of the BFN of the n = 18 element subarray of the No. 1 feed, single layer implementation.

Figure 4.51 shows the block diagram for the n = 41 element subarray.
Figures 4.52 and 4.53 display the layout of the BFN for the n = 18 and
n = 41 element cases. The figures prove that it is possible to construct a
center conductor layout in the n < 18 < 41 element range on a single board!
This is a very significant result, because it has a major implication on the
realizable thickness of the overall feed array. On the basis of these
results, it is possible to determine the loss, volume, and weight character-
istics of the overall feed array. Some of these characteristics are
summarized in Table 4.7 and in Figure 4.54.

4.5 Quadruple Aperture Concept

The quadruple aperture concept employs a four way division of the overall
structural aperture. This type of optics have been investigated in great
detail previously for the Land Mobile Satellite application. However, in the
present case the shape of the feed array is much more elongated, which in-
creases the angle between the axis of the column and the axes of the sub-
apertures. consequently, from a optical point of view this case is more
closely related to the triple aperture concept discussed in Section 4.4.

Figure 4.55 shows the front view of the optics, while Figure 4.56,
Figures 4.57, 4.58, and 4.59   the geometries of the reflector profile and
the layout of a feasible feed array.

Since the characteristics of this configuration are similar to that of
the 3 aperture case, it will not be discussed here in detail. However, the
main feature of this optic, like increased beam number capability and larger
steps at subaperture boundaries at adjacent reflectors must be emphasized.

Figure 4.51(a) - Block diagram of the BFN for the n = 41 element subarray of the No. 1 feed, single layer implementation.
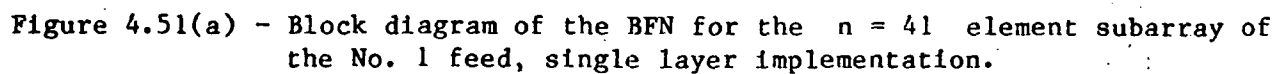
Terminal	dB	Power	K	Power in ring	Normalized ring power	Normalized element power
1	0	1	1	1	.1158	.1158
2,3,...7	1.5	.7079	6	4.2474	.4921	.0820
8,9,...19	6.3	.2344	12	2.8128	.3259	.0271
20,21,...37	15.3	.0295	18	.5310	.0615	.0034
38,39,..41	20	.0100	4	.0400	.0046	.0012

Figure 4.51(b) – Power distribution for feed shown in Figure 4.51(a).

Figure 4.52 — Layout of the BFN (center conductor) for n = 18.

141
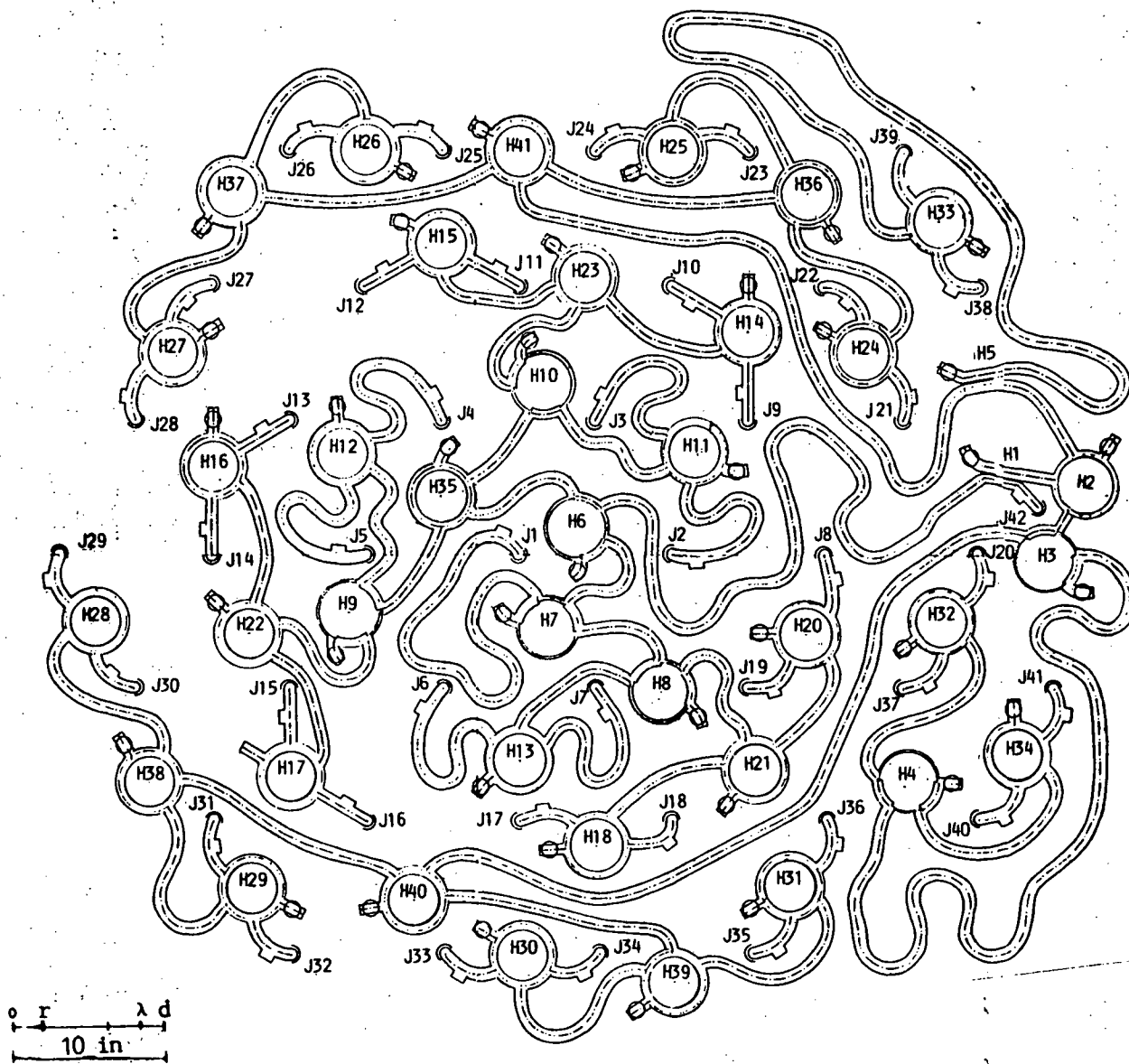
Figure 4.53 – Layout of the BFN (center conductor) for n = 41.

Dimmensions in mm

V = 1
t = .5
b = 10
p = .03
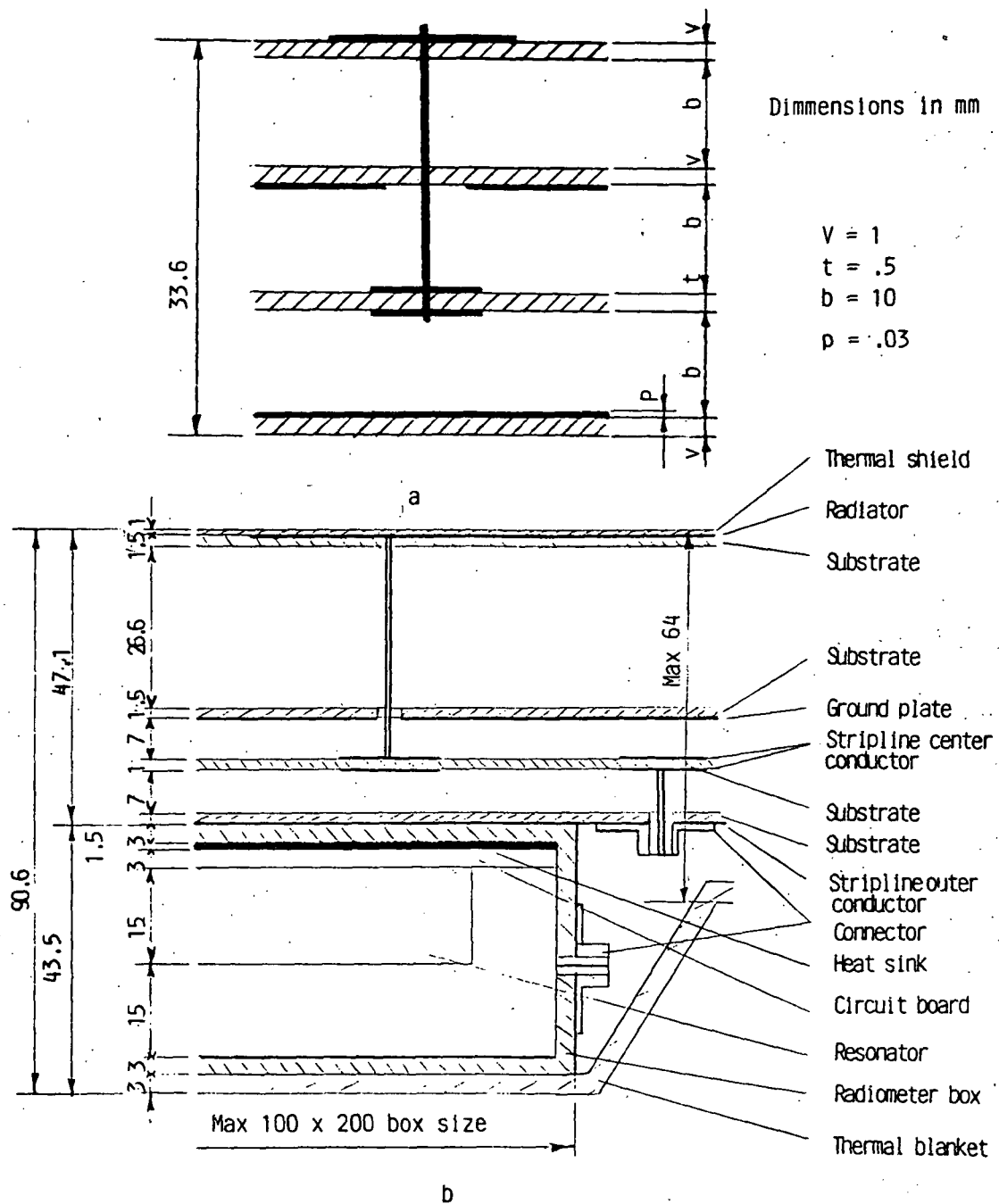
Figure 4.54 - Cross section of the feed panel. (a) Optimized for minimum loss (b) Optimized for overall radiation performance.

143
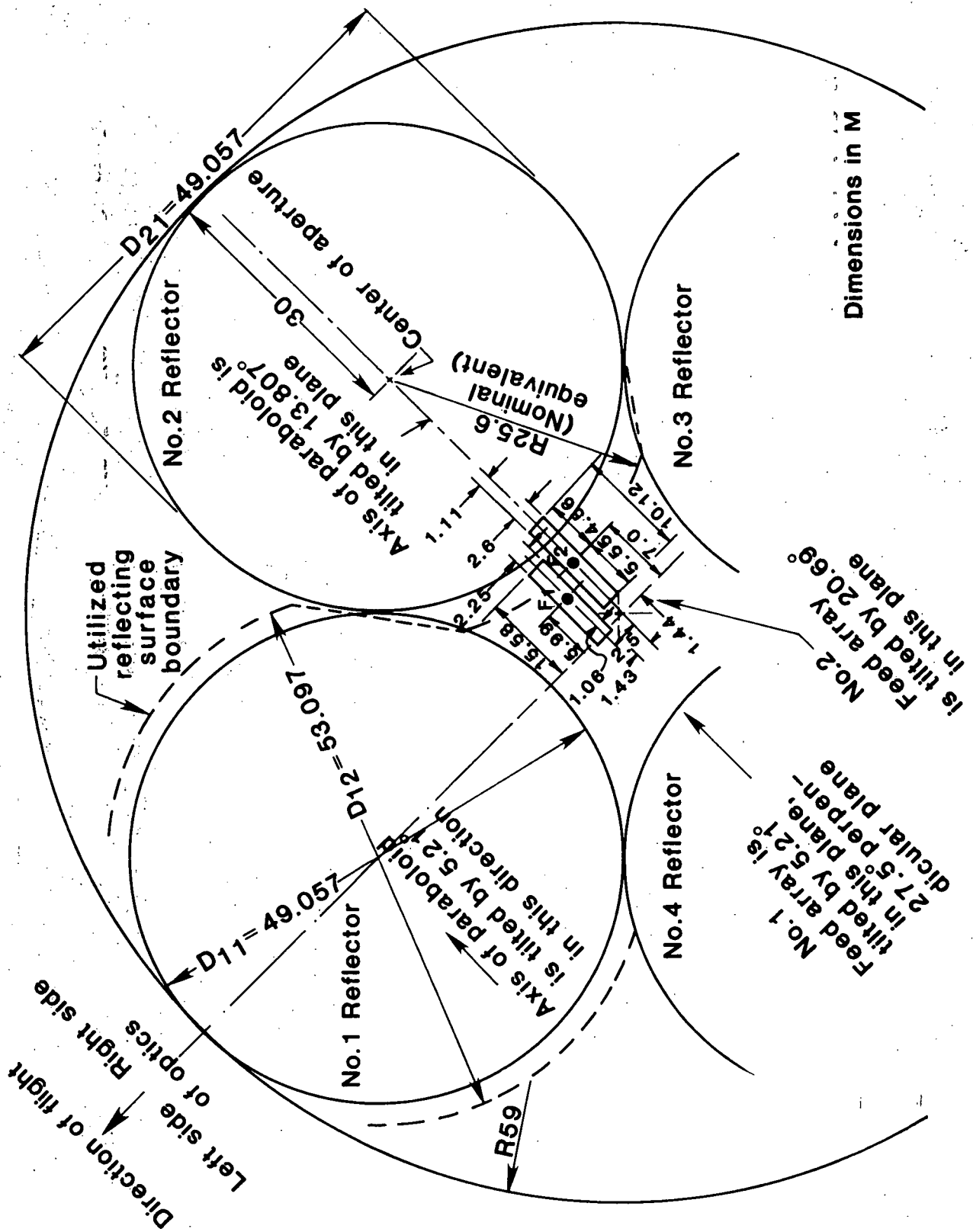
Figure 4.55 – Geometry of optics for the quadruplet antenna, front view.

144

Figure 4.56 – Geometry of optics for the quadruplet antenna No. 1 reflector in plane of scan.
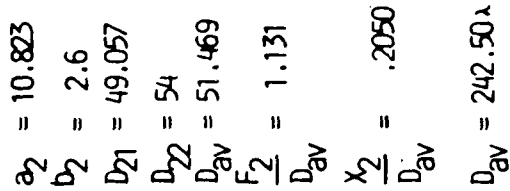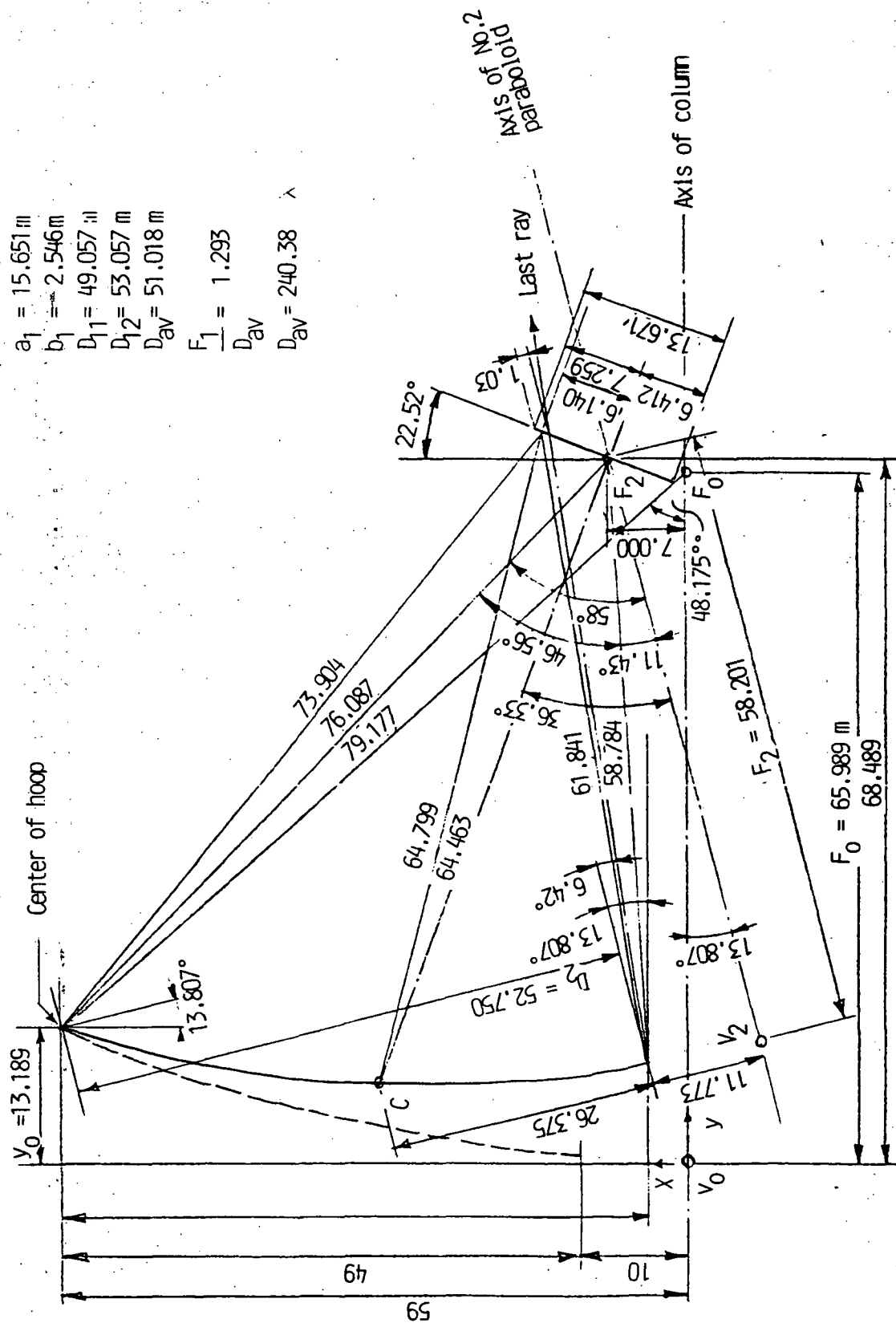
Figure 4.57 – Geometry of optics for the quadruplet antenna No. 2 reflector in plane of scan.

$a_1 = 15.651$ m
$b_1 = 2.546$ m
$D_{11} = 49.057$ m
$D_{12} = 53.057$ m
$D_{av} = 51.018$ m
$\dfrac{F_1}{D_{av}} = 1.293$
$D_{av} = 240.38$

Axis of No. 2 paraboloid
Axis of column
Last ray
Center of hoop

22.52°
1.03
13.671
6.412 7.259
6.140
F_2
F_0
7.000
48.175°
58°
46.95°
11.43°
36.33°
73.904
76.087
79.177
64.799
64.463
61.841
58.784
$F_2 = 58.201$
$F_0 = 65.989$ m
68.489
6.42°
13.807°
$D_2 = 52.750$
13.807°
11.773
26.375
v_2
y
v_0
x
13.807°
$y_0 = 13.189$
C
49
10
59

146

Figure 4.58 - Geometry of feed array for quadruplet antenna, feed No. 1.

Dimensions in wavelength

$\lambda = .21224$ m

Phase center of sub-array

Symbols - indicate centers of patches

Sym. plane of feed array

d_{av}/λ	8.0	7.25	6.6	6.0	5.75	5.60	5.50
U_p/λ	27.807	23.529	19.254	14.973	10.695	6.417	2.139
m_p	36	30	26	22	20	18	16
θ_M	4.84	4.10	3.35	2.61	1.86	1.12	.37
p	7	6	5	4	3	2	1
Patch symbol	.	$\odot$	+	.	$\odot$	+	.

$n_1 = 2\, p_M = 14$

$2 \sum_1 m_p = 336$

$a_1 = 73.744\lambda = 15.651$ m

$b_1 = 12\lambda = 2.546$ m

$\Delta\theta_1 = .75°\ (\theta_{12.3\ dB} \to n_{B_0} \sim 95\%)$

$\beta_{T_1} = 2\theta_M + \Delta\theta = 10.43°$

$\dfrac{\theta_M}{\theta_b} = 13.44$

147

d_{av}/λ	7.6	7.0	6.5	6.0	5.6	5.3	5.1
u_p/λ	23.607	19.975	16.343	12.7711	9.080	5.448	1.816
m_p	40	32	28	26	24	20	18
θ_M°	4.477	3.791	3.103	2.414	1.725	1.035	.345
p	7	6	5	4	3	2	1
Patch symbols	$\cdot$	$\odot$	$+$	$\cdot$	$\odot$	$+$	$\cdot$

$n_2 = (p_M)_{in} + (p_m)_{out} = 7 + 6 = 13$

$\Sigma m_p = 336$

$a_2 = 51\lambda = 10.823$ m

$b_2 = 12.25\lambda = 2.6$ m

$\Delta\theta_2 = .69° \ (\theta_{11.5dB} \rightarrow {}^n B_0 -92.5\%)$

$\beta_{T_2} = 8.95°$

$(\beta = \beta_{T_1} + \beta_{T_2} = 19.38°)$

$\dfrac{\theta_M}{\theta_3} \equiv 12.44$

Figure 4.59 – Geometry of feed array for quadruplet antenna, feed No. 2.

4.6   Summary of Tradeoff Considerations

In order that the various configurations can be compared, the main requirements like spatial reaolution (approx. 10 km), temperature resolution (approx. 0.5°K), revisit time (3 days), was kept the same for the various systems while the coverage percentage was set to better than 80%.

For these conditions the orbit height is approximately 678 km, while orbit inclination can be varied between relatively wide limits.

Under these situations, the most important system parameter is the number by which the overall structural aperture is divided to obain relatively blockage free subapertures.

During the study this was selected as $M = 1,2,3$, and 4 leading to the terminology of single, double, triple, and quadruple hoop-column antenna configuration.

It was recognized early in the development of the hoop-column antenna concept, that for multibeam configuration, applications were both linear dimensions of the feed array are large, the optics must be offset in oder to reduce or eliminate the feed array blockage caused scatter. One such optics is the quadruple subaperture configuration.

In the case of push broom radiometers, where the feed array envelope defines a highly elongated, approximately rectangular aperture more freedom exists in the optics design. For such feeds it is possible to offset feed the reflector even without subdividing the structural aperture $(M = 1)$. The scatter under these situations is caused mostly by the column and this can be controlled by the distance between the center of the feed array and the axis of the column.

In all the investigated cases, the main structural elements (column and hoop) remain symmetrical, but the geometry of the reflecting mesh surface exhibits various degrees of asymmetry.

For the single aperture case the structure and its associated cable system supports a single offset feed paraboloid. The axis of this paraboloid is at an angle relative to the axis of the column and the normal to the feed axis is essentially parallel to the axis of the column.

For the dual aperture case the reflector is either two, parallel axis paraboloid or two, parallel axis torus and the feed is two, highly elongated array, located close to the symmetry plane of the reflector system.

For $M \geq 2$ more than two paraboloid sections are utilized in an offset configuration, with separated and generally tilted axes relative to each other.

For a given spatial resolution the smallest antenna diameter is possible with $M = 1$. In such a system there is a practical beam number, n which can be accomodated, because with increasing scan angle the beam efficiency deteriorates to a possible lowest acceptable value, while the area and complexity of the feed subarray corresponding to the maximally scanned beam reaches its upper practical limit.

As M increases the following consequences can be observed:

1. The antenna structural diameter increases

2. The number of possible beam increase

3. The coverage percentage improves

4. Complexity of feed reduces

5. Beam efficiency for constant number of beams improves

The above situation was analyzed for a number of cases. Since such an analysis is relatively complex some simplifications have been introduced.

While these simplifications effect the accuracy of the results they do not change the basic conclusions for the trend. Table 4.8 shows some of the results of these calculations.

For $M = 1$ two system alternatives are shown, using one or two identical spacecrafts, respectivley. The two spacecrafts case is introduced to make the coverage achievable with the resultant system comparable to the $M = 2$, 3, and 4 systems.

It can be seen that in the single spacecraft alternative this configuration results in a 4 to 5 times reduction in structural aperture area relative to the remaining cases, but the required feed aperture area is nearly the same. The drawback of this system is the low number of beams and consequent low percentage of coverage. such a system is probably ideal for an early demonstration flight, when high coverage percentage is less important.

All $M > 1$ cases represent a large increase in structure aperture diameter. While the $M = 2$ requires the smallest of these large apertures the achievable number of beams is relatively modest. The main difficulty in this system is the feed subarray design for the large scan angle beams. Detailed subarray topology studies indicate, that a single layer suspended stripline power divider is feasible only up to approximately 41 radiating elements. Beyond this multiple layer power dividers are necessary causing an increase in array thickness, which probably cannot be implemented within the single STS flight constrain. This limits the achievable beam efficiency at the maximum scan. Note that the indicated "average" beam efficiency in Table 1 does not fully characterize the quality of the system. The actual beam efficiency for the maximally scanned beam is considerably poorer.

The $M = 3$ case requires even more structural aperture diameter and somewhat larger feed array area. However, the achieved number of beams is

larger, the spatial resolution is better and the beam efficiency is higher. While there is an 18% increase in beam numbers relative to M = 2 the number of radiating patches is reduced to 95.6%, thus the individual subarray designs are easier. Furthermore, the feed array is divided into three instead of two packages, which could make its deployment simpler. The reflecting surface geometry has three symmetry planes, which make the mesh system design relatively simple.

the M = 4 case represents an RF design refinement relative to the M = 3 case, but ath the expense of added mesh design complexity. This system has only two reflecting surface symmetry planes and has large steps in the reflecting surface at subaperture boundaries.

According to Table 1 this system can use a relatively small overall feed array area and a somewhat lower number of radiating patches. This is the consequence of the reduced beam scan requirement for the individual subapertures. At the same time this configuration offers some improvement in beam efficiency. Overall this case has poorer resolution and more structural complexity than the M = 3 case. It appears that with these deteriorations the improved beam efficiency is not an adequate justification for this system.

On the basis of the above presented comparison it appears that M = 1, 2, or 3 have all some merits for a practical system. Since M = 2 and 3 are not drastically different from a structural point of view any of these two can be selected as a representative system for a multiple aperture configuration. Since M = 3 requires a larger structural diameter, this may be selected as the upper limiting case from mechanical point of view. The other extreme is the M = 1 case, which represents the ultimate feed complexity requirement.

TABLE 4.8

Summary of tradeoff analysis results

No. of subapertures	No. of Spacecraft	Structural diameter m	Total structural aperture area m^2	Total feed array area m^2	No.of patches	Average beam efficiency %	No.of beams	Coverage %	Spatial resolution km
1	1	50.9	2038.8	128.3	4408	81.0	33	64	9.5
1	2	50.9	4077.6	256.7	8816	81.0	66	83.2	9.5
2	1	100.4	7916.9	93.8	4600	87.7	44	85.5	10.9
3	1	118	10935.9	127.7	4398	84.5	52	86.5	9.2
4	1	118	10935.9	69.81	4200	88.7	48	86.5	10.2

5. CONFIGURATION DESIGN

5.1 Introduction

The configuration desing of the feed for the radiometer antenna involves a number of well defined steps. These include:

1. Radio frequency – mechanica – thermal desing of the feed arrays

2. Integration of the radiating structure – radiometer panel assemblies

3. Design of panel deployment subsystem

4. Analysis of dynamic behavior

5. Calculation of geometrical inaccuracies

6. Reliability analysis

In the following discussions the above problems will be outlined at conceptual levels only and they will be restricted to the three aperture configuration. Details have been investigated only to determine feasibility of various concepts and approximate weight of the overall assembly.

5.2 Interfaces Influencing the Configuration Design

In the triplet aperture antenna a total of 52 feed arrays must be implemented and correctly located within the overall optical system. According to Figure 4.32 and Figure 5.1, there are a total of 11 types of radiating arrays, each consisting of a set of printed radiators, a printed power divider board and two solid surface conductors acting as ground planes. It is assumed that these four layers are deposited on kevlar substrates and separated by layers of honeycomb or structural foam. They are integrated with their radiometer units, associated heat sink and packaged for overall thermal stability. A typical construction concept for such a configuration is shown in Figure 5.2. The weight per unit area for the present purpose was determined from actually achieved values on a 19 radiating element construction.
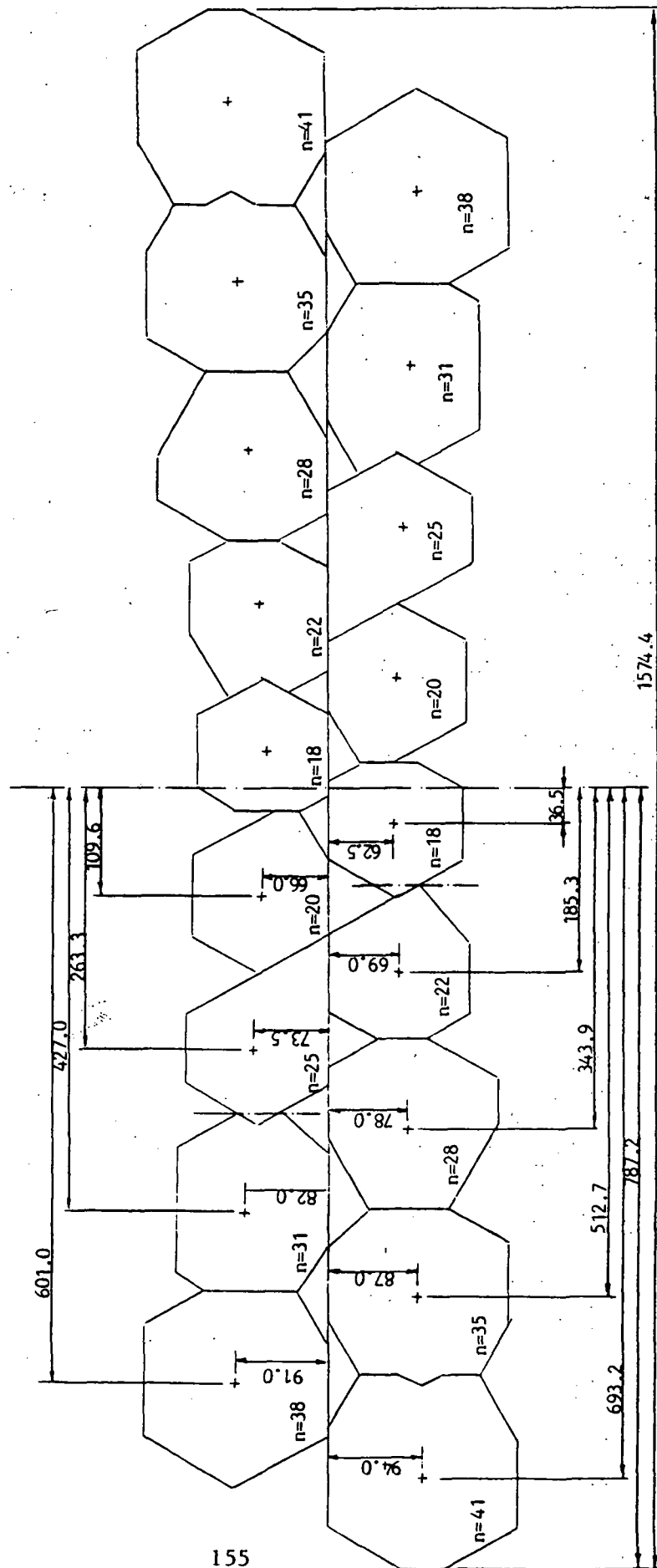
FEED PANEL NO. 1

Dimensions in m.

Figure 5.1a - Layout of feed panels
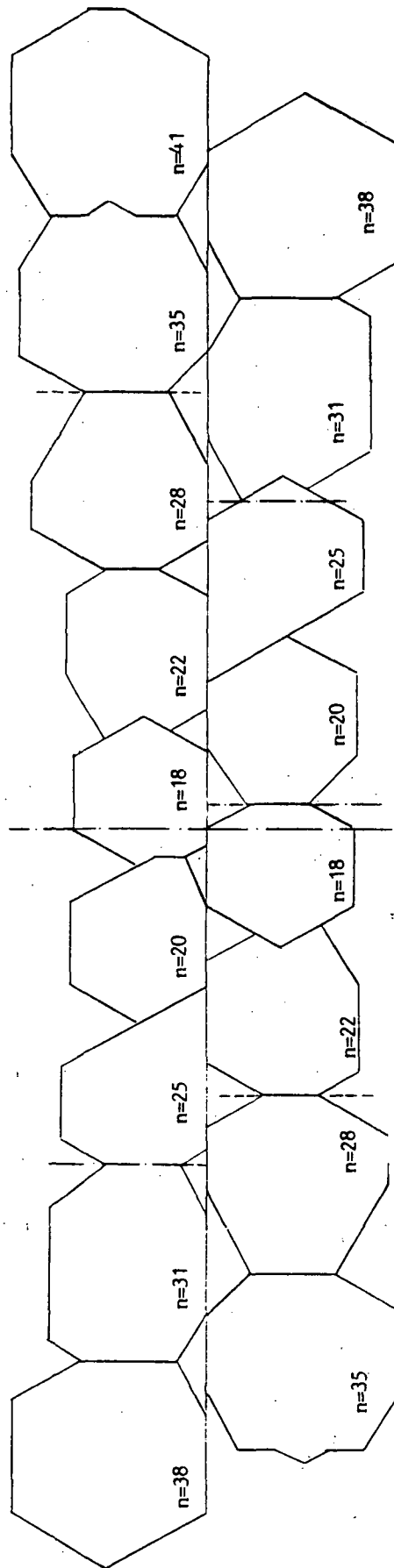
FEED PANELS 2 AND 3
Dimensions in m.

Figure 5.1b - Layout of feed panels

The feed panels are labeled: n=41, n=38, n=35, n=31, n=28, n=25, n=22, n=20, n=18, n=18, n=20, n=22, n=25, n=28, n=31, n=35, n=38

HIGHLY REFLECTIVE
WHITE PAINT(EMISSIVITY=.98)

FIBERGLASS & KAPTON
MULTILAYERED COMPOSITE
HEAT SHIELD

FOAM
INSULATION

HONEYCOMB ISOLATORS

SUN FACING SIDE
RADIOMETRICALLY
TRANSPARENT AREA

FOAM INSULATION

ANTENNA
AND
FEED NETWORK

POSSIBLE
RADIATOR
LOCATION

RADIOMETER ELECTRONICS
AND
THERMAL CONTROL SYSTEM
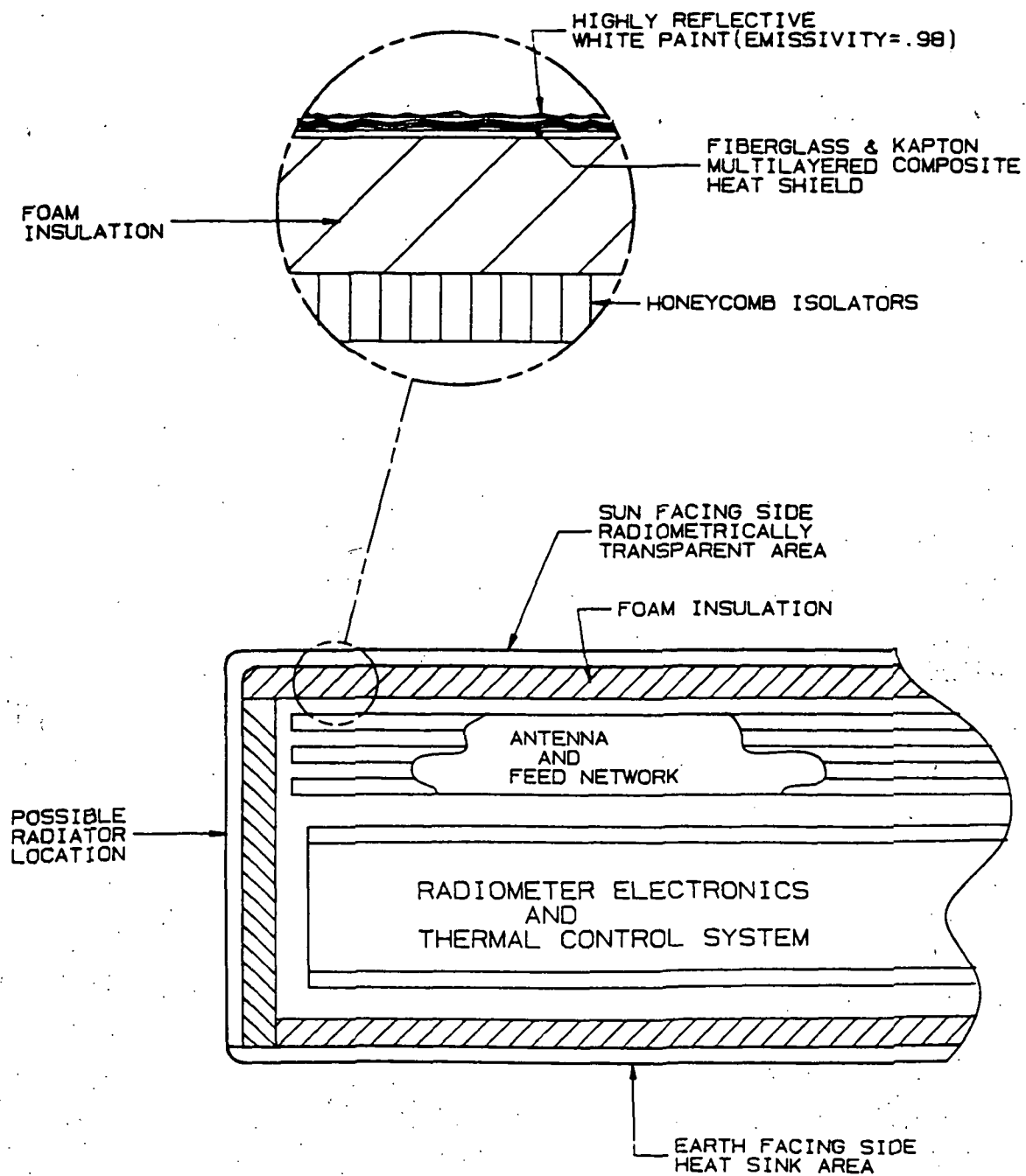
EARTH FACING SIDE
HEAT SINK AREA

Figure 5.2 - Typical cross section of feed panel

157

In a practical design, several arays may be integrated into subpanels of the overall feed. However, from the point of view of testing, ground handling, and sparing, it is advantageous to maintain separability of the feed arrays for each beam. Utilizing this concept, an independent array support frame is necessary into which the feed arrays are separately integrated. Such a frame can be added without any major weight penalty, because the final rigidity of the structure is determined by the contributions of the integrated panel structure and frame structure.

The configuration of the frame structure is strongly dependent on the necessary thicness of the panels, the subdivision of the overall feed into subpanels, the deployment concept and the overall space availalbe in the cargo bay of the STS.

The L-band radiometer payload can be divided into two major subsystems: optics and feeds. For the triplet antenna the weight and volumne of these subsystems are close to each other. They can share the available payload space in the Shuttle cargo bay in two conceptually different ways:

1. The optics subassembly occupies an inner cylinder and the feed is wrapped around it in a cylindrical annulus.

2. The optics and feeds are mounted in an end to end configuration, each occupying a larger diameter but shorter length cylindrical space.

In the following these two basic concepts and some variants of them will be presented.

5.3 Wrap Around Feed Packaging

Figure 5.3 shows the basic geometry of the wrap around packaging. The available space is determined by the 3.34 m outside envelope requirement of the stowed 118 m diameter hoop column optics and the 4.438 m inner envelope defined by the STS cargo bay. Assuming that each of the feed panels of the
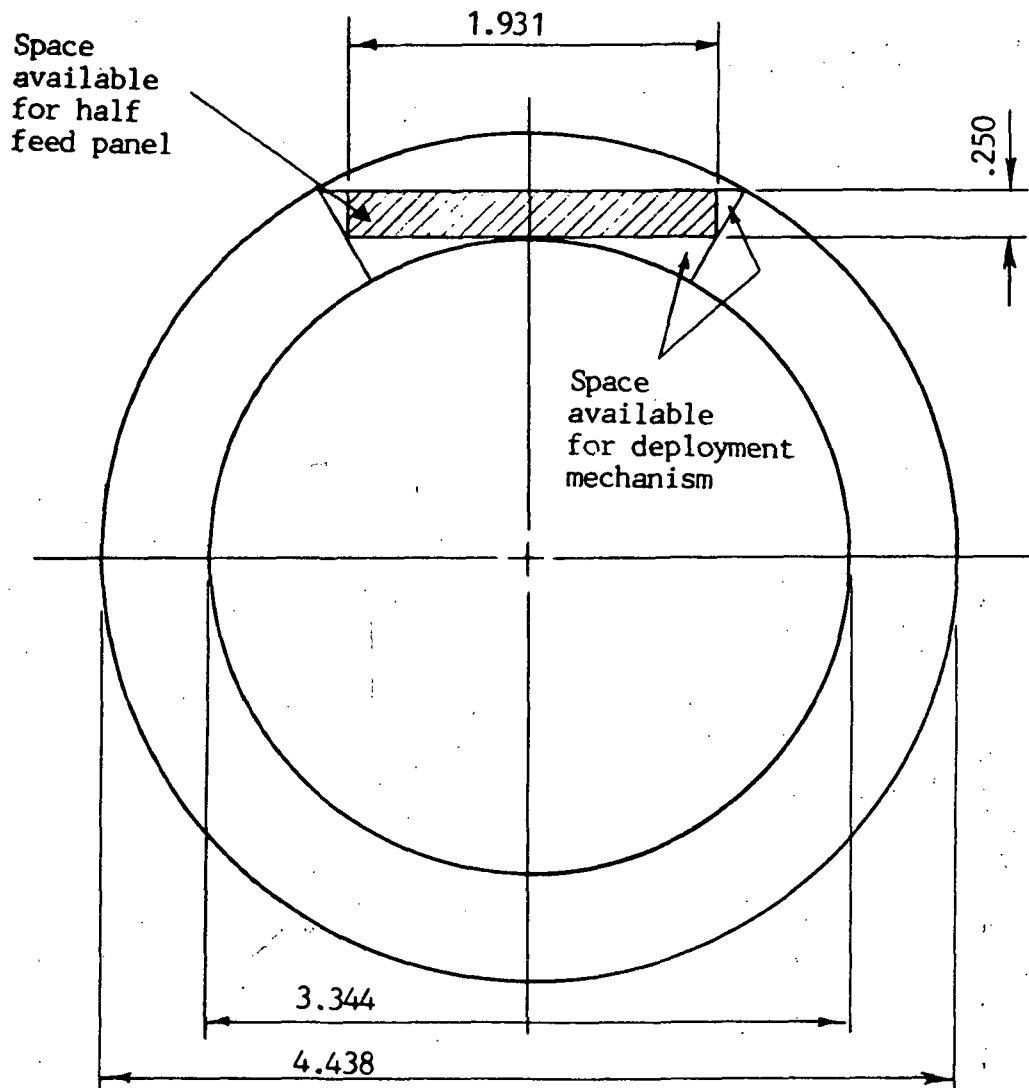
Dimensions in m.

Figure 5.3 - Geometry of wrap around feed packaging. (One of six half panels is shown.) Maximum axial length is 15.744 m.

triplet antenna are divided along the longitudinal symmetry axis the available

cross section for each of the six subpanels is 1.931 m × 0.25 m. According to

Figures 4.33 and 4.34, the maximum width f these subpanels is 1.88 m, thus

this scheme allows 5.1 cm clearence for the width f the panels. According to

Figure 4.54, the thickness of the RF portion of the panel is 9.06 cm. Thus

the above scheme allows 15.4 cm space for the thickness of the panel support-

ing frame and deployment mechanism. It must be noted that an additional

4.35 cm thickness clearence is available at places which are not occupied by

the radiometer boxes. The provided space appears to be adequate with some

margins of safety for the support frames and deployment motors.

There are numerous combinations, a panel stowed in the above defined

space can be deployed into its operational position. the various methods can

be compared on the basis of the number of deploymnet steps involved, the total

volume and weight requirement, achievalbe accuracy and reliability. It is

assumed in the following that the feed deployment follows the deployment of

the optics.

Figure 5.4 shows the deployment sequence for one possible concept (method

No. 1). Due to the fact that feed No. 1 and feed No. 2 and No. 3 are

different in shape and operational position their deployment involve different

mechanism configurations.

Figure 5.4(a) exhibits the steps needed for the placement of feed No. 1

In stowed condition this feed is attached to a U-shaped structure. One arm of

the U is insode the telescoping tower attached to the end of the column.

Because of the necessary long length (7.87 m) of the U structure it is

necessary to retain the end of the panels during the Shuttle flight.

Step 1: Telescope along axis of column by 7.87 m translation

Stow

Step 2: Flatten array by ± 30° rotation

Step 3: Rotate array by 90° rotation
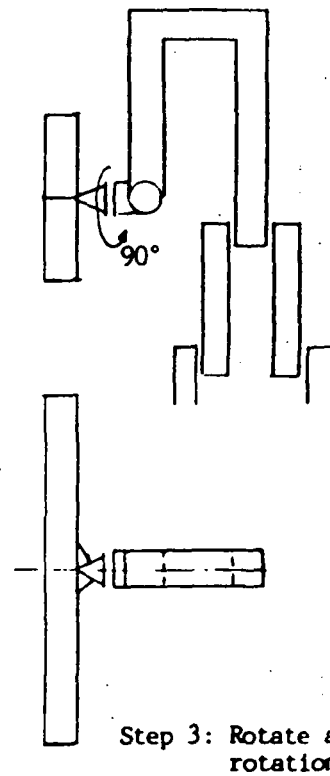
Figure 5.4(a) - Deployment of feed No. 1 of wrap around configuration.

Step 4: Turn array by 62.5° to operational position

Dimensions in m.

Figure 5.4(b) − Deployment concept for feed No. 1 in wrap around configuration

The first step is the release of this retainment, followed by the deployment of the U structure. During this step the feed makes a 7.87 m translatory movement along the axis of t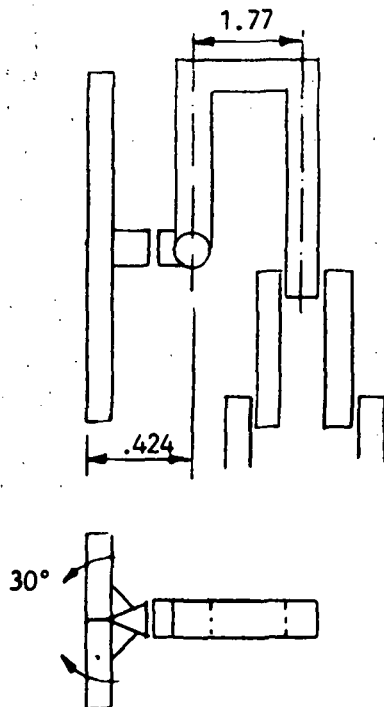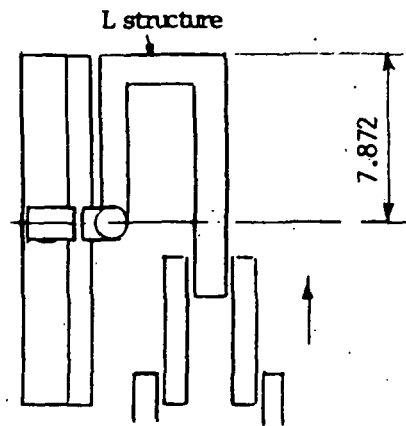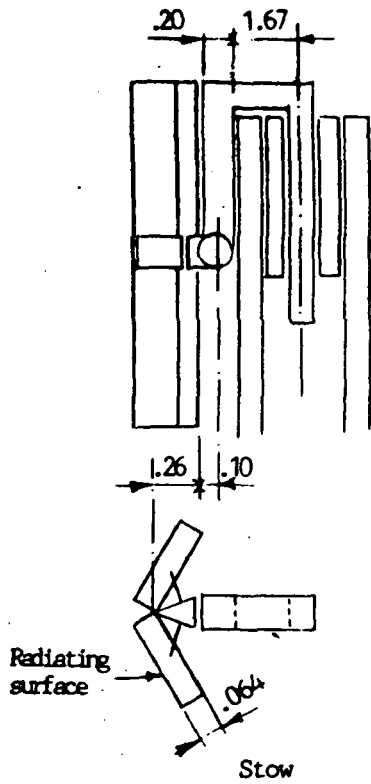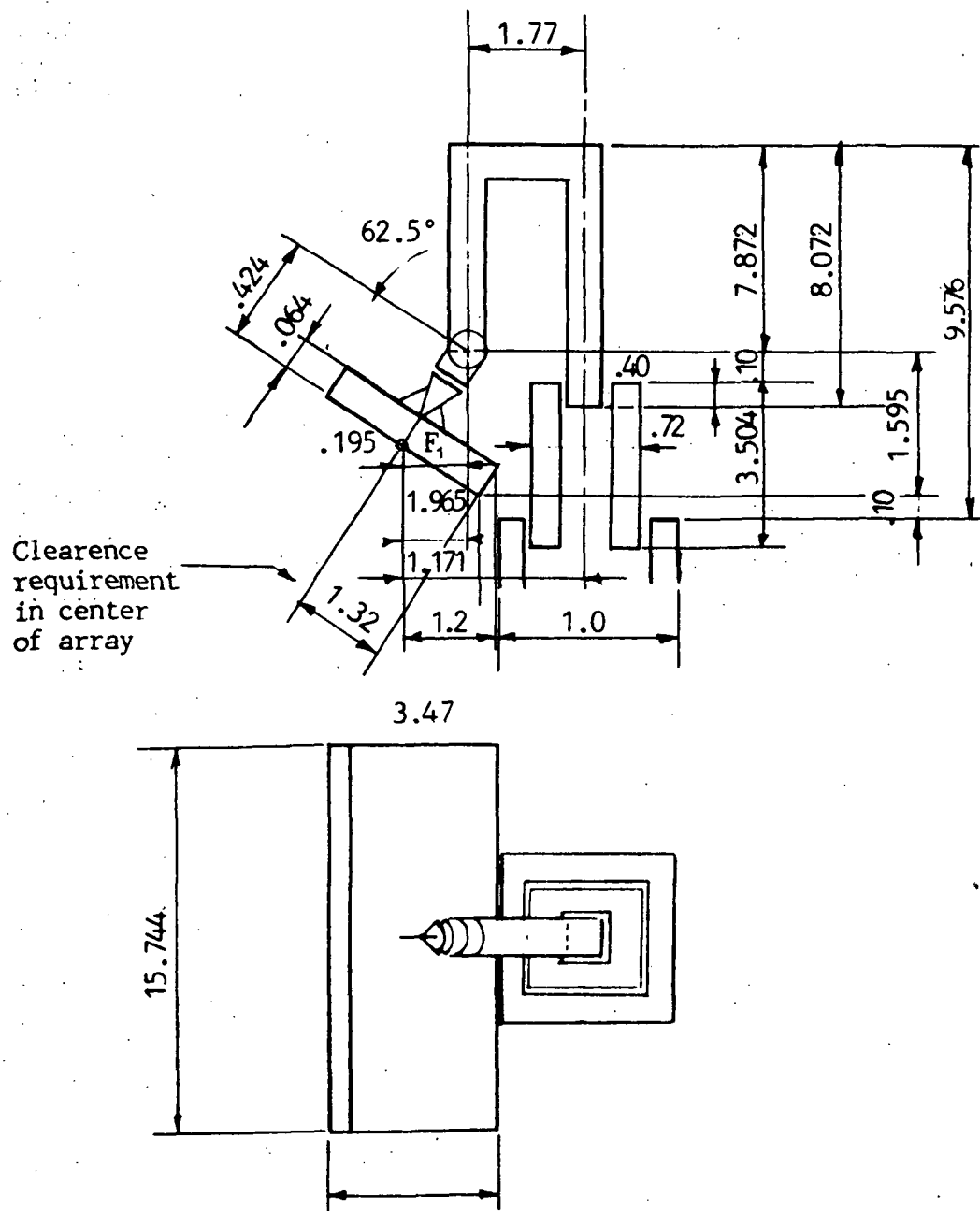he column. This is achieved by telescoping action. This movement along the axis of the column. This is achieved by telescoping action. This movement can be coupled to telescoping of the end section of the column, which is part of the optics deployment. Thus this step may not require an additional motor and its reliability is not part of the feed deployment reliability budget.

The second step is to flatten of the two half panels into a single planar panel. This involves a +30° and -30° rotation of the half panels and can be achieved symmetrically by a single motor operating a dual linear actuator or spring coil if retrieval is not necessary. At this point the longer dimension of the feed is still parallel to the axis of the column.

The third step is a 90° rotation of the overall feed assembly. During this phase the normal to the radiating structure is directed perpendicular to the column, outward from the axis of the reflectors.

The fourth step is a 62.5° inward rotation of the feed panel. This step assures the final orientation as well as the final positioning. The center of the feed panel is a 1.965 m from the axis of the column, at the F_1 focal point of the No. 1 subaperture.

Omitting the initial transloational movement the above deployment scheme involves the use of three stepper motors providing the flattening (30°), orientation (90°), and alignment (62.5°) rotations, respectively. Noe of these rotations appear to be excessive. Furthermore, since the optics utilizes a large F/D none of the rotational accuracy has a major influence on the beam efficiency of the system. The inaccuracy of step 2 has some second order effect on axial focusing and may be used for independent fine focusing

of the two half panels. (Addiitonal axial focusing adjustment may be achieved by step 1 for one of the three feed arrays.) The nominal 90° rotation provided by step 3 is vital for the operation of the system, but an error in this rotation has only second-order effect on the locations of the beams relative to the beams produced by feed No. 2 and No. 3.

Finally, the rotaion achieved by step 3 determines the location of the field distribution relative to the nominal in the offset feed paraboloidal subaperture. A small error in this rotation has only second order effect on the shape of the secondary pattern. It can be concluded that the only relatively critical deployment is step 1. 1 cm error in this step procudes a peak quadratic error of approximately 4.71° in the paerture of the paraboloid. 1 cm macimum positioning error for the telescopic mechanism seem to be realizable during initial deployment representing 1.5×10^{-4} of the nominal focal distance.

The above factor is at least an order of magnitude larger than the applicable thermal expansion coefficient. Consequently, thermal effects are not expected to play a major role in the axial focusing (beam shape) characteristics of the system. It can be concluded that the presented deployment concept is feasible from kinematic and accuracy point of view.

The described flattening, orientation, and alignment operations can be provided in a number of slightly different manner. Figure 5.5 compares the described method No. 1 to an alternative (method No. 2). In this the flattening operation is applied only to one half panel. This does not save a motor but eliminates one set of linear actuators. Additionally, if this operation fails, one half panel is still in the right location and only 9 out 18 beams are lost. The price of this improved reliability is that the rotation needed for the half panel is larger (58.2°) and the alighnement maneuver requires
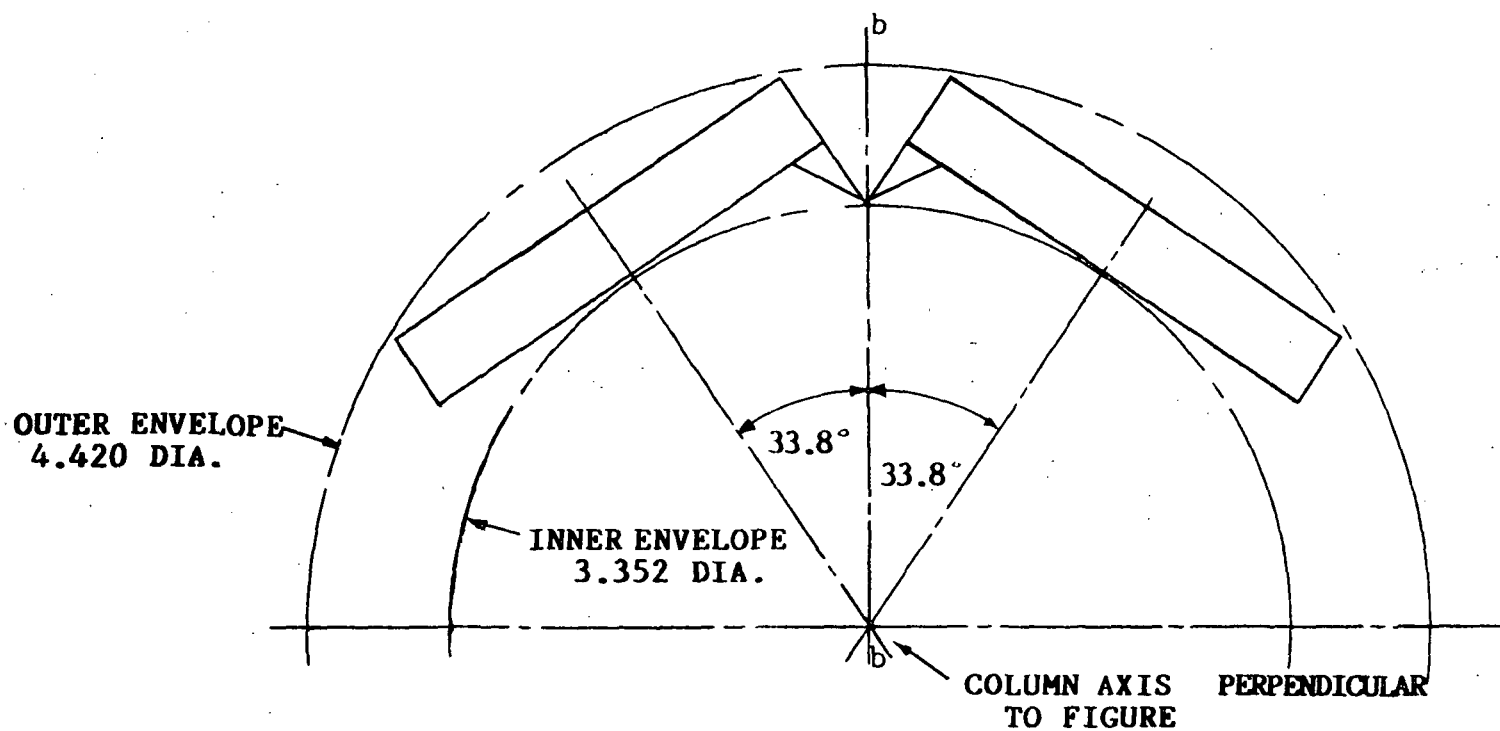
STOWED POSITION

Dimensions in m.
(Subalternative A)

Figure 5.5(a) – Alternative deployment of feed No. 1, wrap around
configuration.
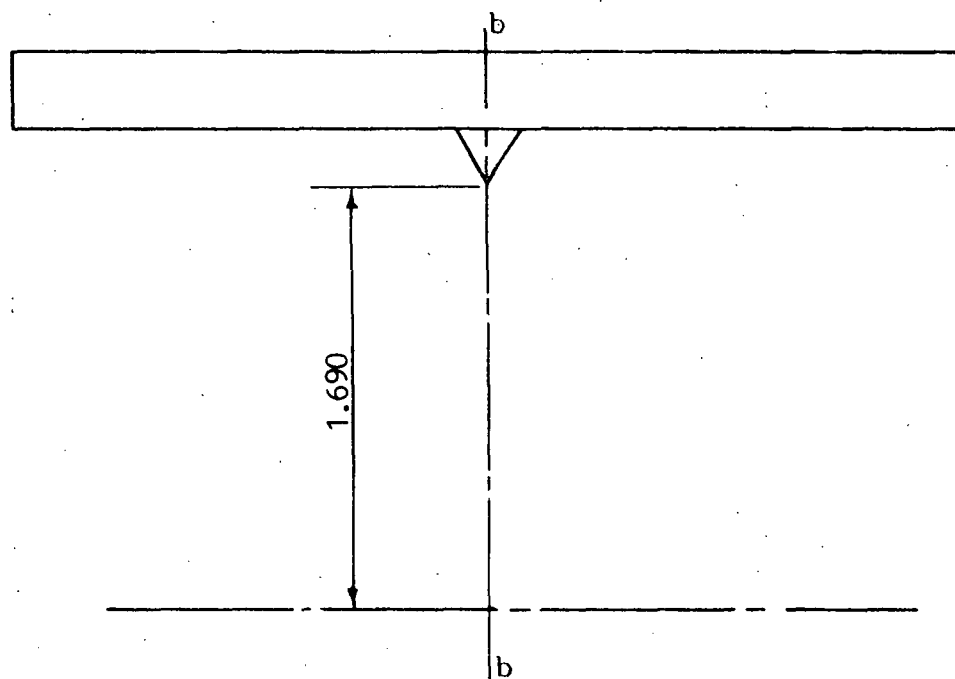
**PANEL OPENED AND ROTATED
90° ABOUT b-b AXIS**

Dimensions in m.
(Subalternative A)

Figure 5.5(b) — Alternative deployment of feed No. 1, wrap around configuration.

62.5° CW

F=65.989

1.690
REF.

1.965

PANEL ROTATED 62.5°

DEPLOYED POSITION

Demensions in m.
(Subalternative A)

Figure 5.5(c) - Alternative deployment of feed No. 1, wrap around
configuration.

1.934

29.1°

29.1°

b

b

INNER ENVELOPE
3.352 DIA.

COLUMN AXIS & PERPENDICULAR
TO FIGURE

OUTER ENVELOPE
4.420 DIA.
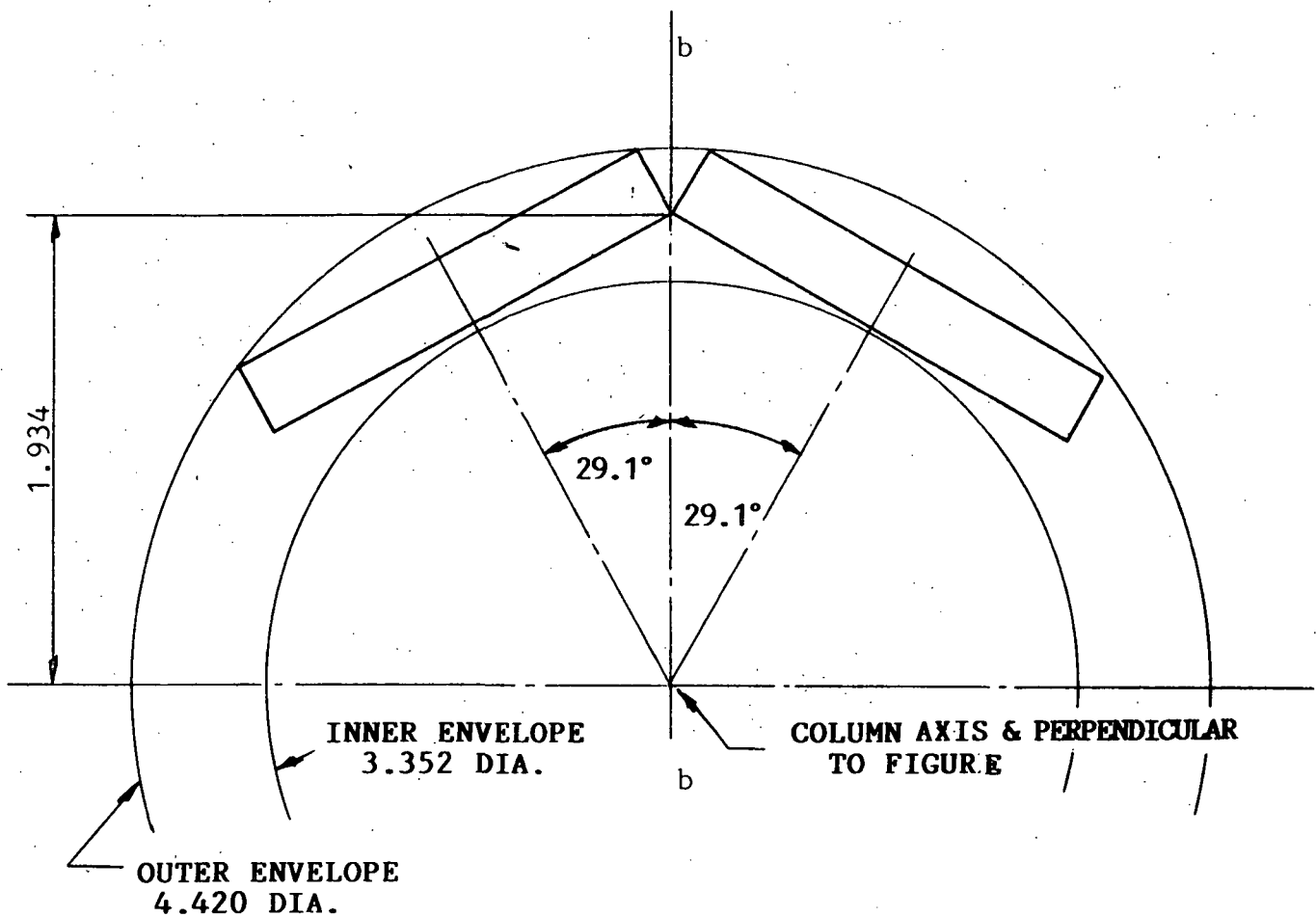
STOWED POSITION

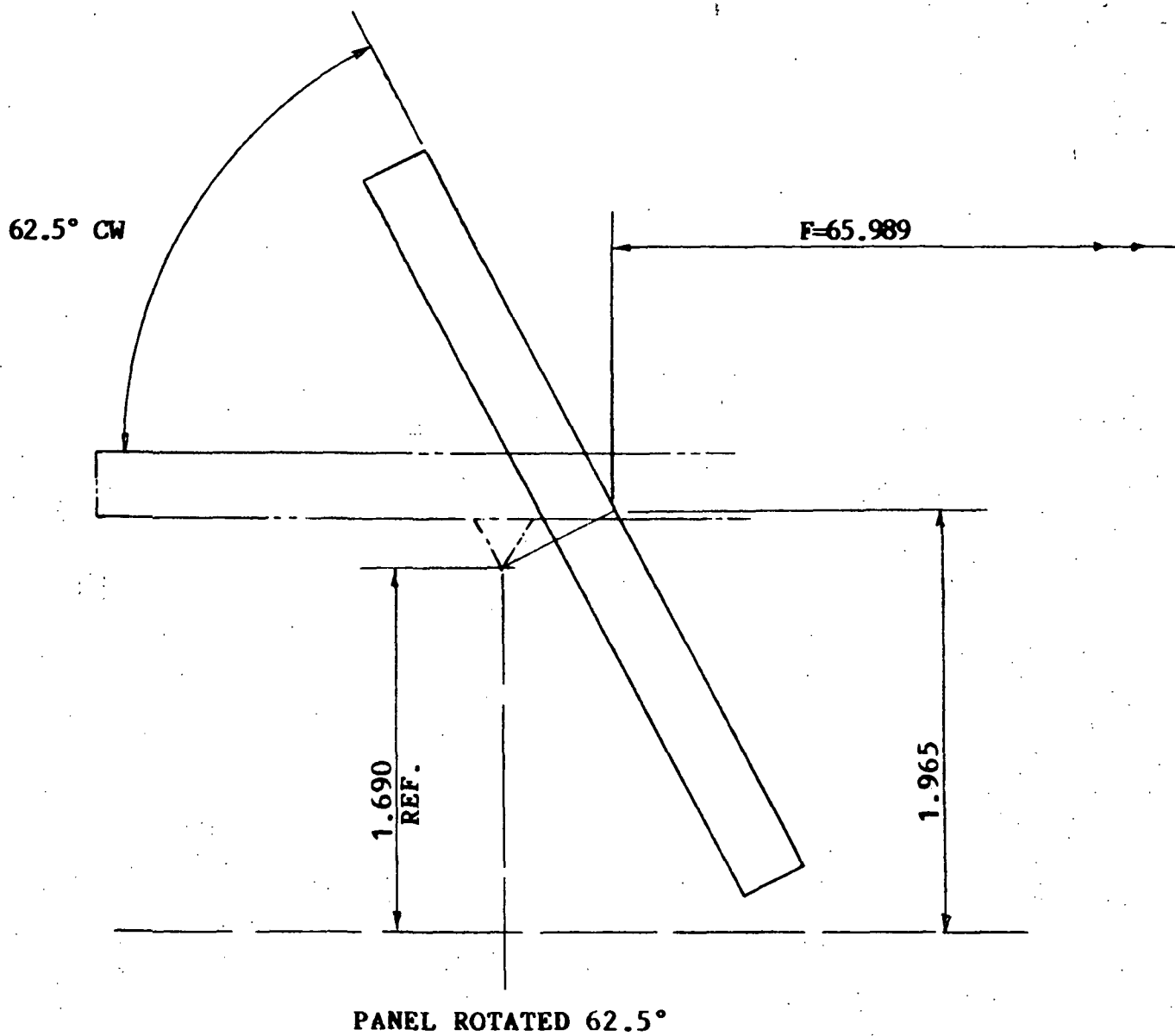Dimensions in m.
(Subalternative B)

Figure 5.5(d) – Alternative deployment of feed No. 1, wrap around
configuration.
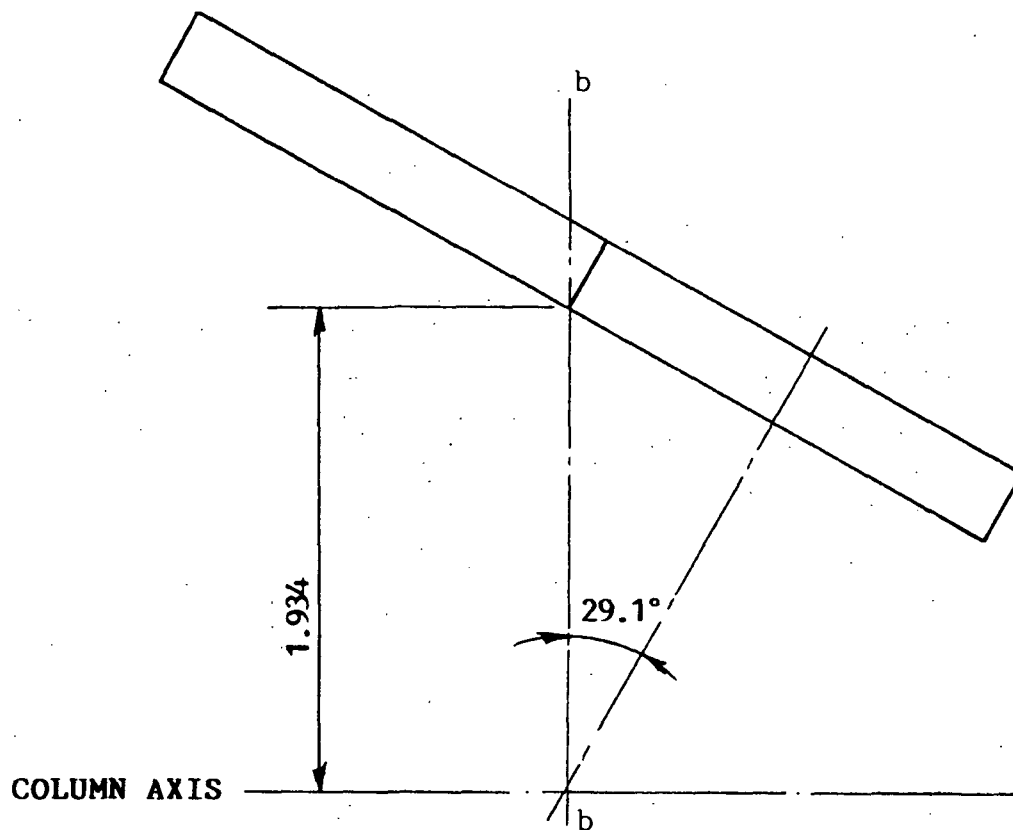
PANEL OPENED AND ROTATED 90° ABOUT b-b AXIS

Dimensions in m.
(Subalternative B)

Figure 5.5(e) – Alternative deployment of No. 1, wrap around configuration.

33.4° CW

F=65.989

27.5°

0.110

LINEAR

1.934 REF.

1.965

COLUMN AXIS
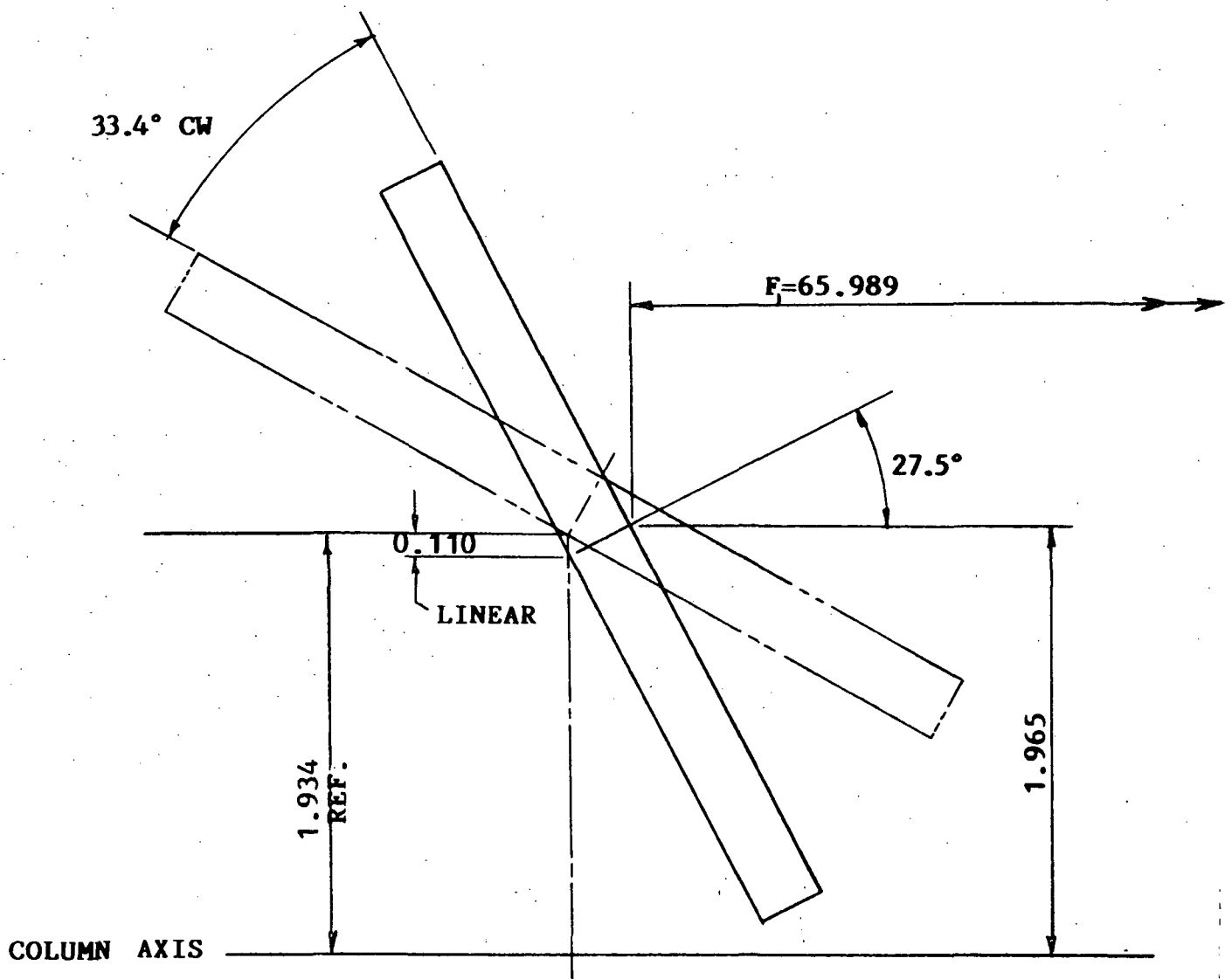
**PANEL ROTATED 33.4° AND TRANSLATED
INBOARD 0.110**

DEPLOYED POSITION

Dimensions in m. (Subalternative B)

Figure 5.5(f) - Alternative deployment of feed No. 1, wrap around
configuration.

two steps: a 33.4° rotation and a 0.11 m translation perpendicular to the axis of the column. In practice, however, the last step can be omitted, because the associated (flight direction) displacement of the beams is only 0.095° or $0.32\theta_3$ which has a negligible effect on beam shape, beam efficiency or coverage. It can be concluded that the compared two methods require about the same total rotation and both are feasible. The choice between the two can be made on the basis of more favorable mechanical design details.

The deployment of feed No. 2 is in principle simpler than that of feed No. 1 because it does not involve the linear translation of the U structure. One possible concept is exhibited in Figure 5.6. The first step is the flattening operation, which involves a nominal 60° rotation of the half panel. This may be achieved by the mechanism employed in Step 1 for method 2 of feed No. 1. However, for feed No. 2 the radiating surface of the panel is on the inside in the stow configuration, thus the mounting of the deployment mechanism may require some compromise if standaridization is attempted. The second step is a 15° rotaion assuring the orientation of the plane of the array perpendicular to the plane of scan. Finally, the alignment operation is achieved by a nominal 112.5° rotation in the plane of scan. It may be noticed that the rotaional tolerance requirements of the first two steps are not very critical. However, the last rotation has a major effect on axial defocusing caused by the displacement between the center of the panel and F_2. Again, if 1 cm error is tolerated at the center of the panel for axial defocusing the final rotation must be accomplished with 0.082° accuracy. If a 1 cm error is tolerated at the center of the maximally scanned feed array then the rotational error cannot exceed more than approximately 0.04°. Assuming, that the location tolerance of the supporting telescopic arm is also 1 cm. The above condition causes a total of 2 cm peak error for the phase center location of

the worst (maximally scanned) beam. The associated peak quadralic error for this condition is a relatively large 18.8°. However, since the beam shape of the maximally scanned beam is relatively poor even in the absence of this error the additional damage is negligible and the system performance is not deteriorated much further. From mechanical point of view the achievement of maximum 0.04° rotational error is still a difficult criteria for this deployment scheme.

Figure 5.7 exhibits another method to achieve the above deployment. This method uses a U-sphaped structure similar to the one described for feed No. 1. Using this concept, the first step is the translation of the U structure; second step is flattening achieved by symmetrical ±30° rotaions; third step is displacement of the center of the panel; fourth step is tilt parallel to the operational aperture plane; fifrh step is alignment of the long axis of panel into the plane of scan by 15° orientation. This method intorduces an additional step in the deployment sequence, but reduces the effect of angular alignment tolerances. For 1 cm axial error in the middle of the panel the step 3 rotation must be only 0.082° accurate. If step 4 is also 0.082° accurate then 1 cm additional error is introduced for the position of the last subarray. Since the two errors are independent their most probable combined peak error is 1.4 cm. for a combined 1 cm maximum error this scheme allows 0.058° peak rotational errors in the motor positions of step 3 and step 4.

1.672

.768

14.792

.064

1.0

Radiating surface

Sym. plane

Stow

Step 1: Flatten array by 60°
rotation

1.672

1.572

.862

F₂

22.5°

Radiating
surface

.20

3.56

Step 2: Position array by 15° rotation

7.0

13.801 (Proj)

.682

.18

F₂

(6.920 to F₂ true length)

Proj: 6.138

Step 3: Orient array to operational
position by 112.5° rotation
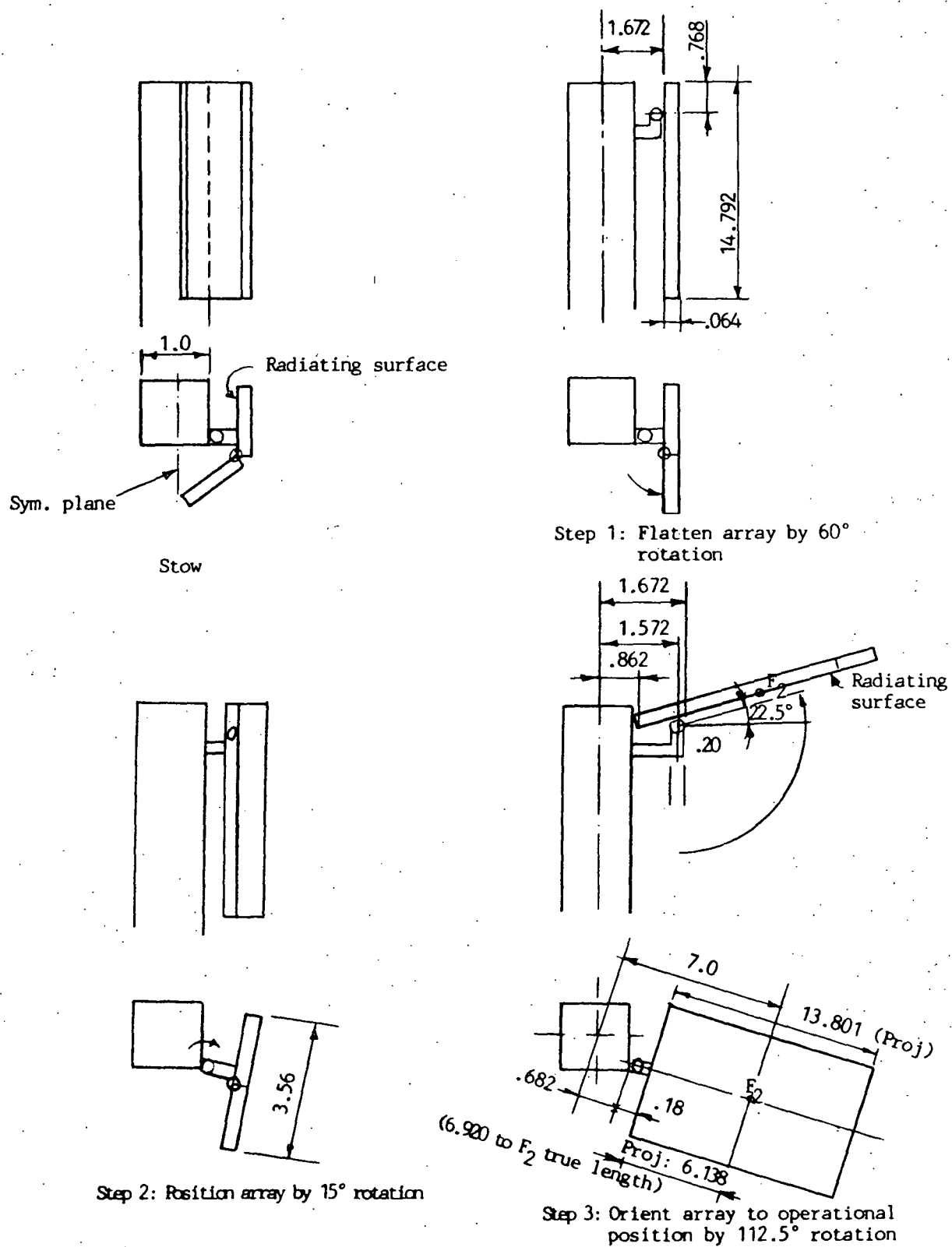
Figure 5.6 – Deployment concept for feed No. 2 in wrap around configuration.

173

OUTER
ENVELOPE
2.210 DIA.

INNER
ENVELOPE
3.352 DIA.

1.934

30°

STOWED POSITION

Dinmension in m.
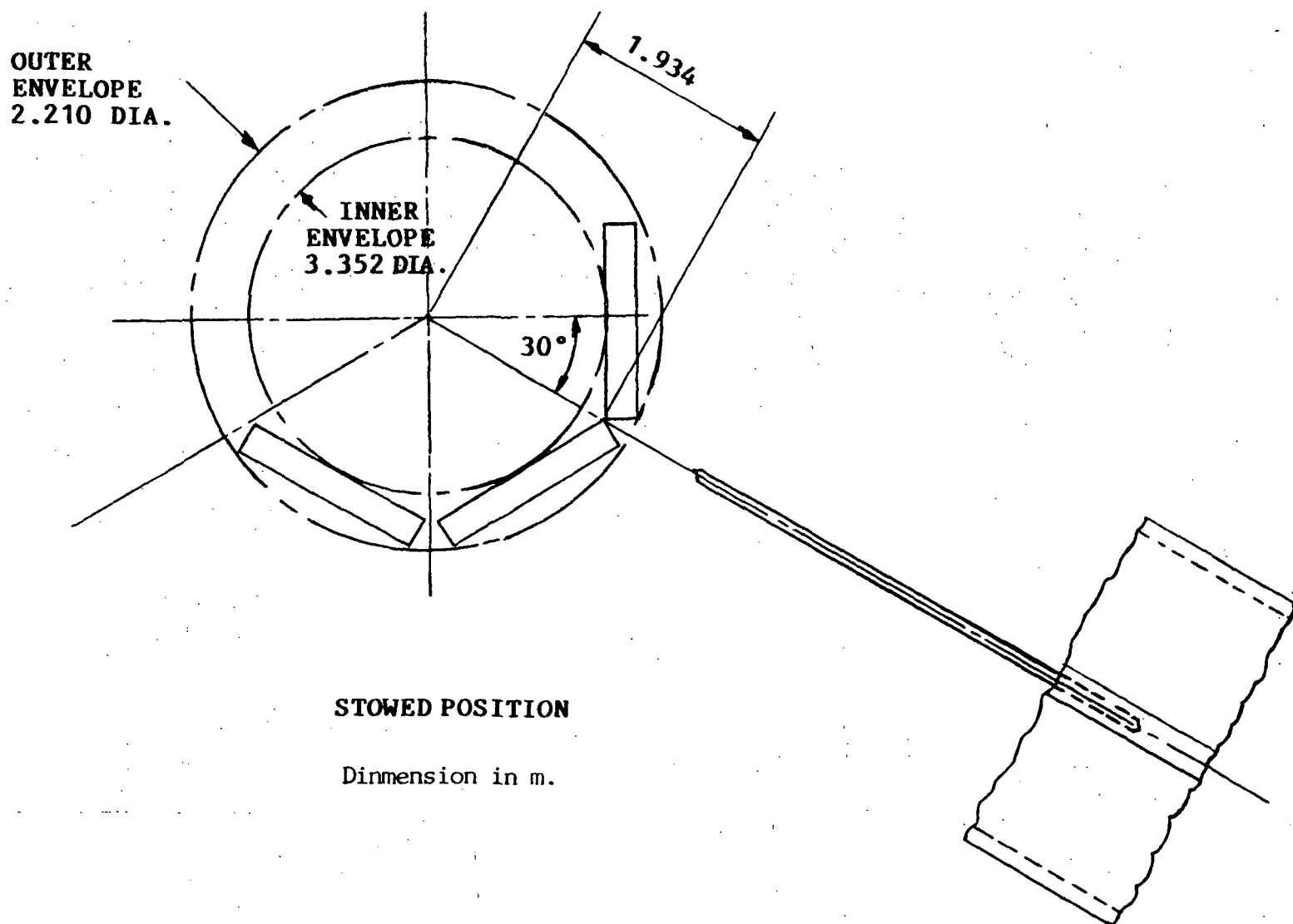
Figure 5.7(a) – Alternative deployment of feed No. 2, wrap around configuration.

PANEL OPENED,EXTENDED AND ROTATED 15° ABOUT c-c AXIS
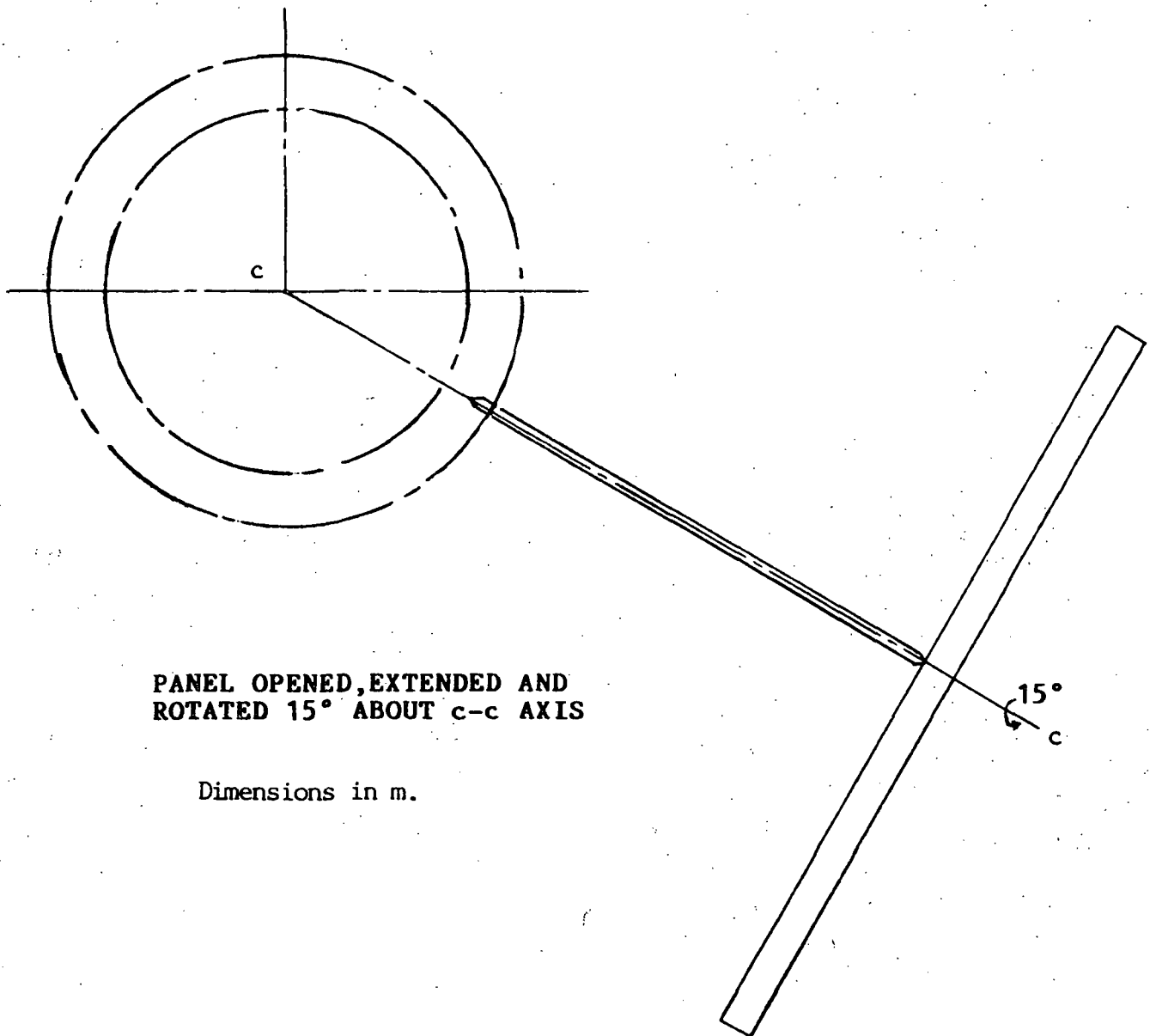
Dimensions in m.

Figure 5.7(b) - Alternative deployment of feed No. 2, wrap around configuration.

**PANEL ROTATED 67.48° ABOUT b-b AXIS
AND ROTATED 24.9° ABOUT a-a AXIS**

Figure 5.7(c) – Alternative deployment of No. 2, wrap around configuration.

176

VIEW A-A   DEPLOYED POSITION

Dimensions in m.

Figure 5.7(d) - Alternative deployment of feed No. 2, wrap around configuration.

177

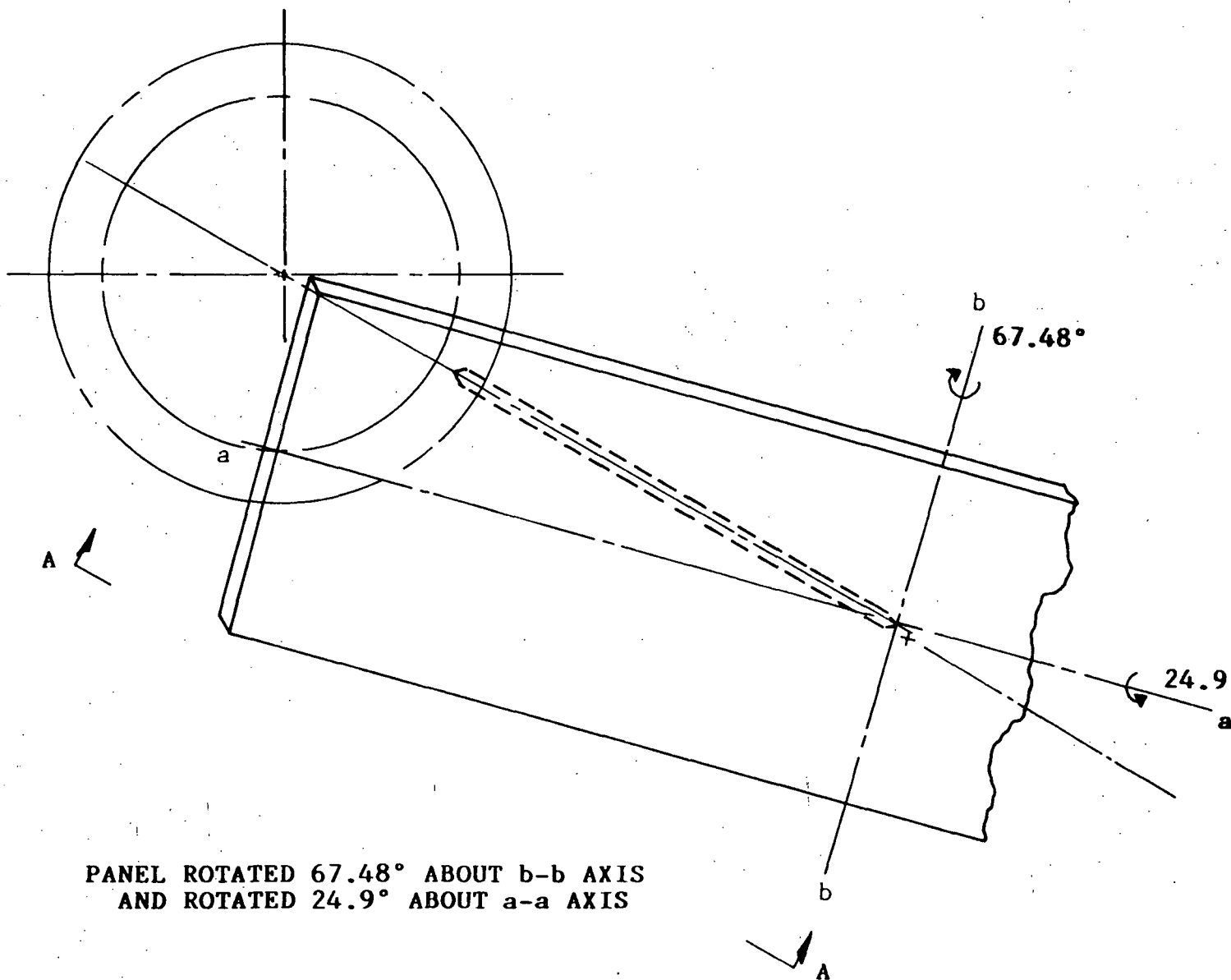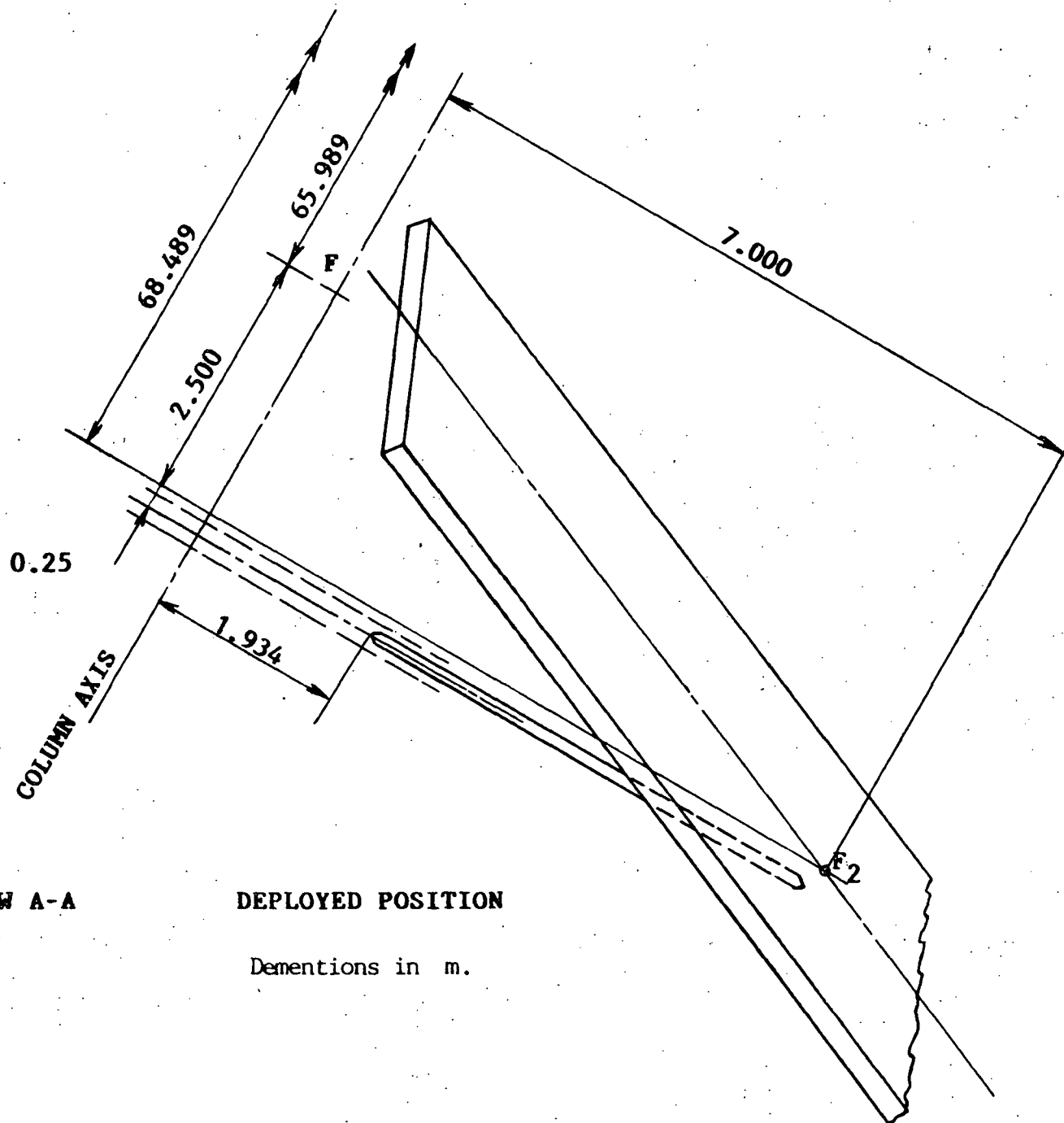## 5.4 End-Mounted Feed Packaging

The end-mounted feed packaging concept is particularly advantageous for los and medium orbit applications (like the L-band radiometer) where the booster rocket in the STS occupies a relatively short length of the cargo bay. In such a configuration the hoop column antenna may occup a larger diameter volume. This could ease it mechanical design and/or improve its accuracy.

Figure 5.8 shows the assumptions for the stowage space of the feed package. It is assumed that in such a configuration the feed interfaces with the hoop column structure at the top of the telescoping column.

The space depicted in Figure 5.8 is divided for the three feeds as shown in Figure 5.9. Each feed is folded in an accordion fashion into a nominally 3.76 m tall, 4.43 m wide and 0.434 m thick package. These three packages are stowed side by side with 0.1 m clearance between them. The largest diameter for this condition is 4.245 m. This fits into the assumed envelope. The free folded feed packages are mounted on an interface structure which contains the pivoting axes for the feeds.

Figure 5.10 exhibits the folded layout of feed No. 1. The overall panel id idvided into four nominally equal subpanels. A total of three internal motors (or spings) are needed to flatten this assembly. The deployment of such a configuration is well studied in the art and is similar to solar array deployment schemes or the one used for SAR phased arrays. Some additional complications are introduced presently by the interleaved nature of the subarrays (see Figure 5.1), but this can be handled by properly selected pivot axis locations.
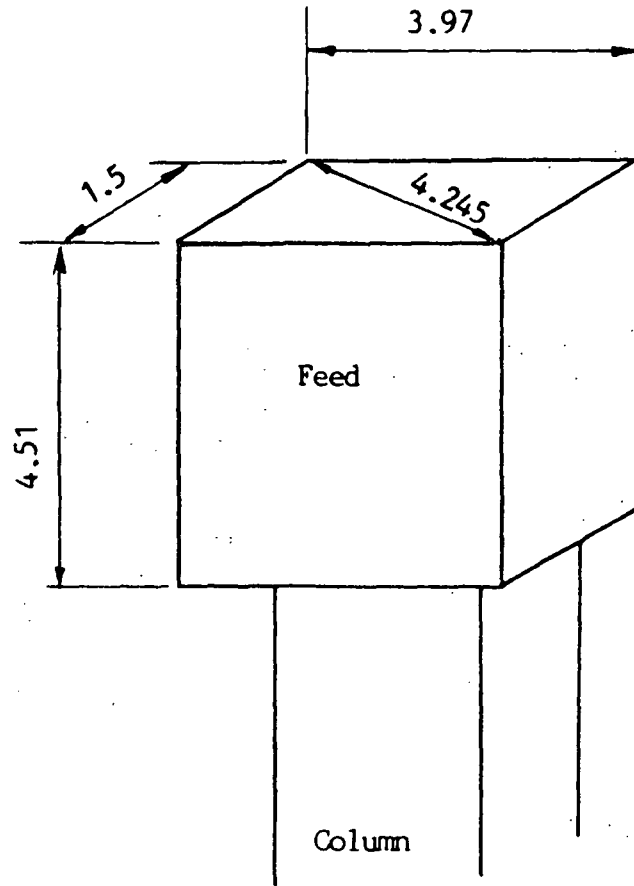
Dimensions in m.

Figure 5.8 - Envelope of stowed feed in end-packaged configuration.
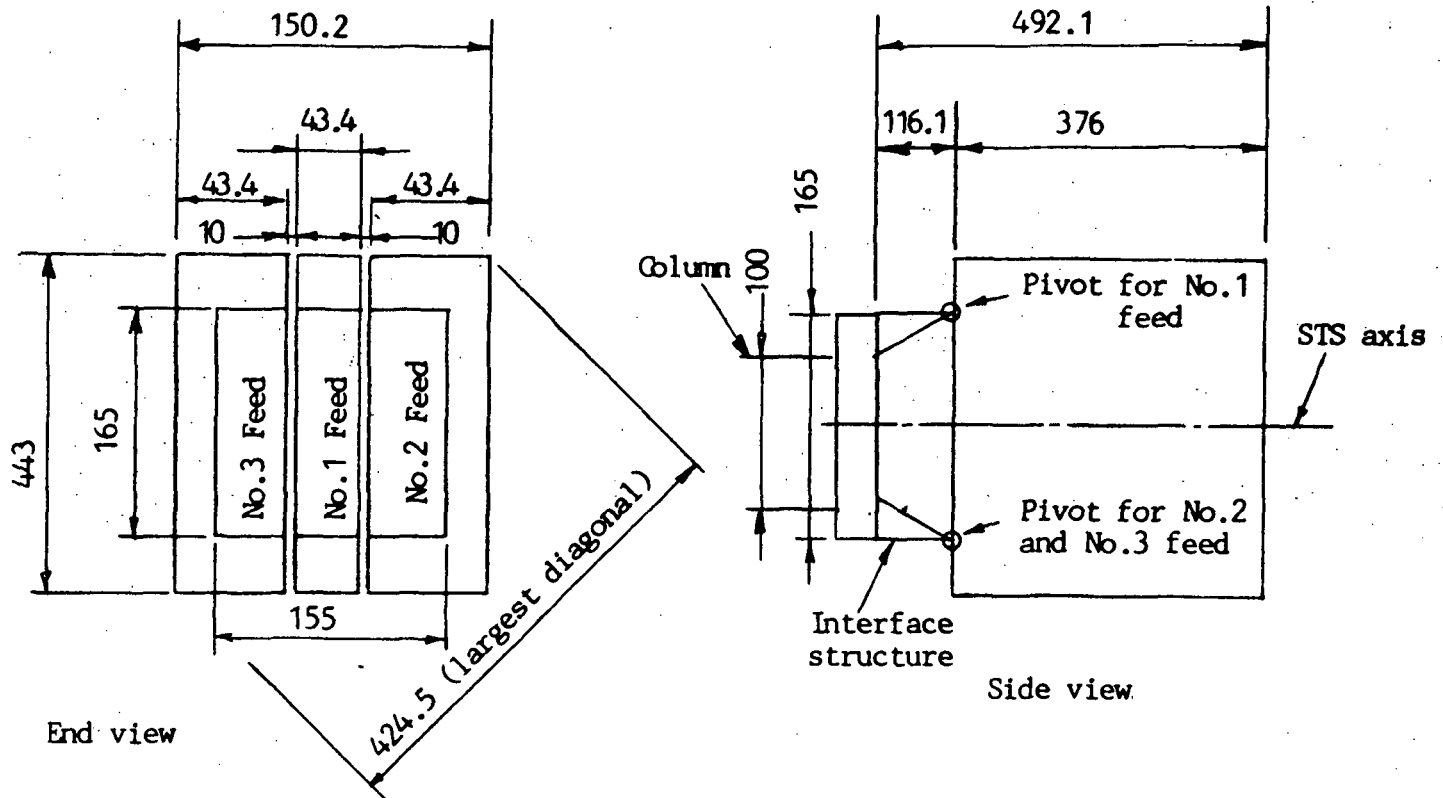
Dimensions in cm

Figure 5.9 – Internal details of feed package in stowed condition (end-packaged configuration).

Dimensions in cm

Note: Overall dimensions are approximate, actual panel
boundary is along subarray boundaries.

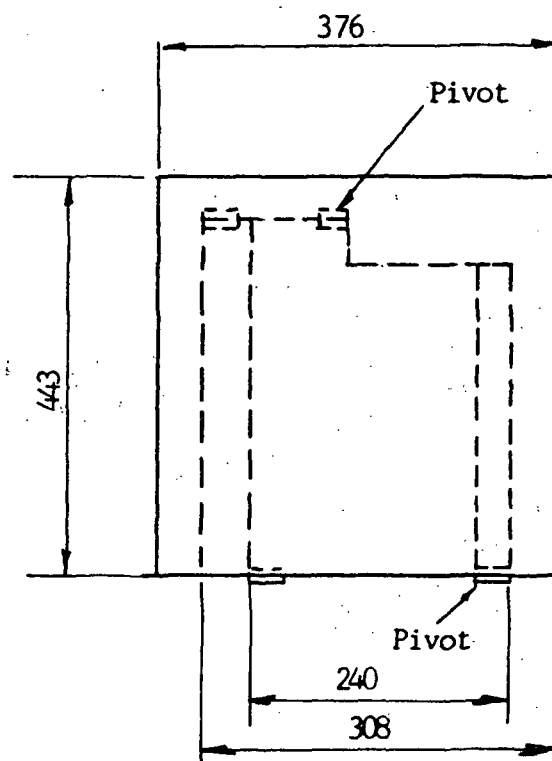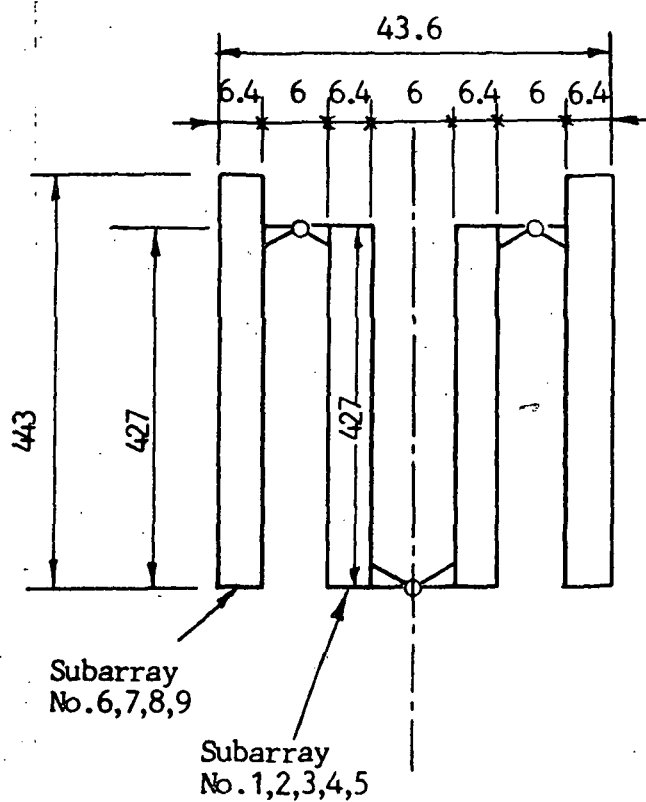Figure 5.10 - Accordion type packaging of array panel for feed No. 1.

The deployment sequence can be followed in Figure 5.11. For feed No. 1 the first step is a 90° rotation of the feed package. This is followed by step 2 which is the flattening operation of the panel. Note that a 1 cm axial position accuracy for the center of the panel requires only 0.304° rotational accuracy, provided that the interface structure location is perfect. A total of four motors are required for this deployment.

For feed No. 2 and 3 the first deployment step is the 90° rotation, like in the case of feed No. 1. The second step is the 15° rotation to bring the package into the plane of scan. The last step is flattening. This scheme requires five motors. Additionally, the flattening involves the support of the panel at one end with the associated tolerance problems as discussed in conjunction with the wrap around packaging. The final deployed configuration is shown in Figure 5.12.

5.5 Weight Estimate

On the basis of the previously outlined configuration concepts, a preliminary weight estimate can be devleoped for the overall 118 m diameter hoop column radiometer antenna. The results for the wrap around feed packaging configuration are summarized in Table 5.1.

The overall antenna consists of two main subsystems: optics and feeds. The optics are made up from the hoop column and reflector; the feed may be subdivided into radiators, radiometers, support frames, and deployment mechanism.
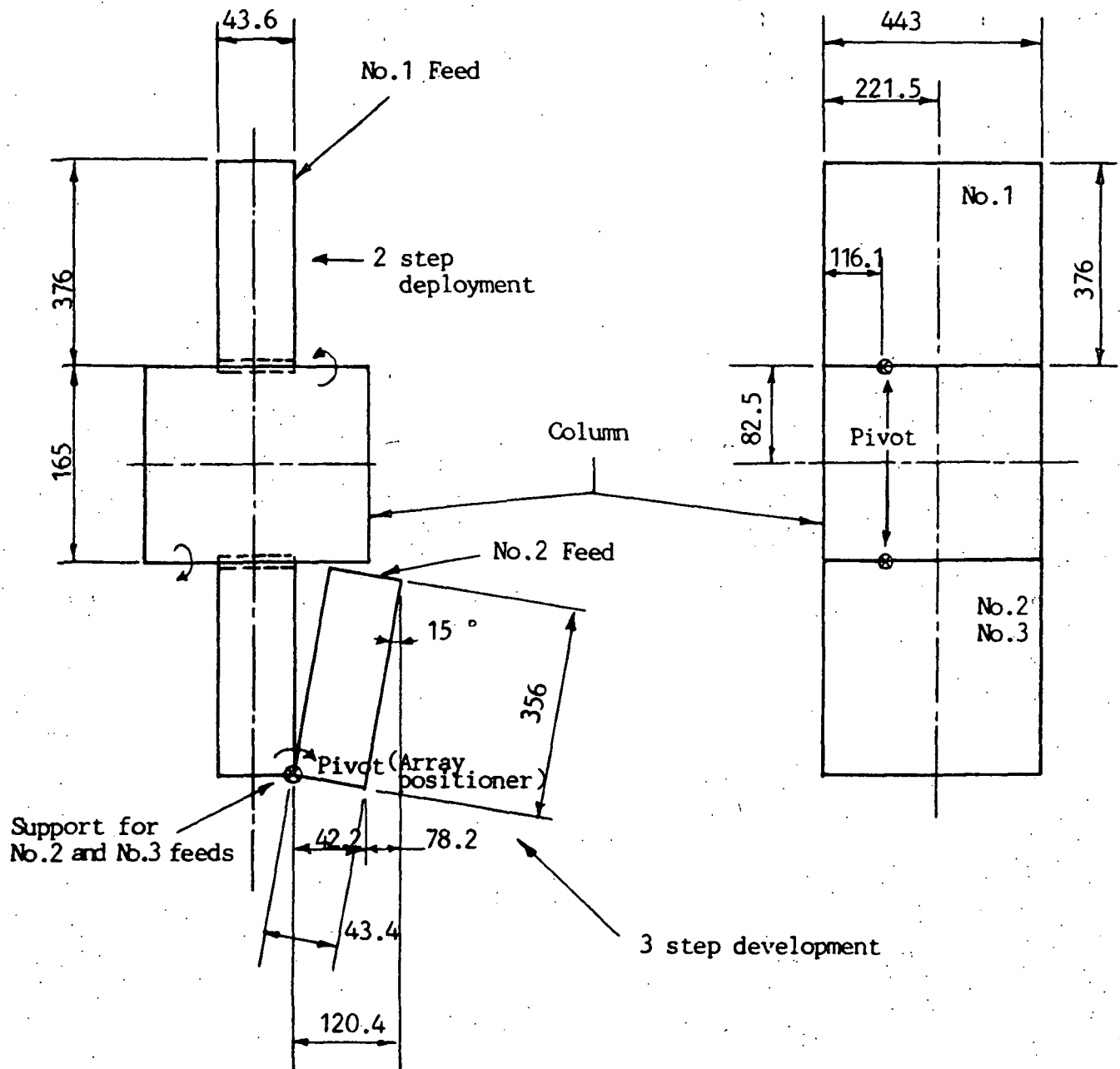
Figure 5.11 - Steps of deployment for No. 1, No. 2, and No. 3 feeds
(end-packaged configuration).

Figure 5.12 – Final deployed configuration for feeds.

TABLE 5.1

Preliminary weight estimate for the 118 m diameter radiometer system

(weight in pounds)

Optics		2188 (25.8%)
Hoop	628	
Column	1340	
Reflector	220	
Feeds		6282 (74.2%
Radiometers	312	
Support frames	1554	
Deployment mechanisms	180	
Total		8470

The following comments can be added to Table 5.1. The weight of the optics subsystem is obtained from an earlier study.[1] Since this study was relatively extensive the accuracy of these calculations are thought to be within ±15%.

The largest single item in the total budget is the weight of the radiating structure. The cross section of this element is shown in Figure 4.54 and the area and number of subarrays is displayed in Figures 4.32, 4.33, and 4.34. The radiating structure is composed of 4 plated substrates, a thermal shield and an interconnecting honeycomb support.

The total thickness of the substrates and thermal shield is 0.6 cm. At a specific weight of 2.15 this represents 1.29 g/cm^2 = 2.628 lb/ft^2. The thickness of the total honeycomb is 4.11 cm. Utilizing the weight characteristics of 1 in. honeycomb with y_4 cells the weight of the honeycomb is 1.199 lb/ft^2.

[1] P. Foles "RF Characteristics of the Hoop Column Antenna for the Land Mobile Satellite System Mission." (Foldes Incorporated, NASA Contractor Report 3842, Contract No. NAS1-17209, November 1984)

C-3

On the basis of the above data, the integrated feed panel weight is 3.827 lb/ft^2, neglecting the weight of the plating. Table 5.2 shows the weight breakdown of the various feeds of the 52 subarray system.

TABLE 5.2

Subarray panel weight characteristics

No. of radiating elements	Area (m^2)	Qty.	Total area (m^2)
18	1.127	4	4.508
20	1.368	6	8.208
22	1.496	6	8.976
25	1.697	6	10.182
28	1.911	6	11.466
31	2.112	6	12.672
35	2.378	6	14.268
38	2.601	6	15.606
41	2736	6	16.416

Total subarray area   102.3 (1106.9 ft^2)

Total subarray weight   1921.6 kg = 4236.4 lb

Specific weight   3.83 lb/ft^2

The above calculated weights may be compared to the weight calculated from an actually constructed similar feed panel used in the ground based 15 m diameter hoop column antenna experiment. This calculation results in 5616 lb or 32.5% more than the figure in Table 5.2. However, considering the fact that in the referenced panel, no significant weight reduction effort was employed, the discrrepancy is not very large. Another reference point may be the weight study results of an 1.49 m × 14 m = 20.9 m^2 synthetic aperture radar phased array.[2] This resulted in 2.91 lb/ft^2 for the feed panels, a figure considerably better than shown in Table 5.2. On the basis of the above indications, it is estimated that the accuracy of the weight values shown in

[2] P. D. Patel, G. Sequin, P. Foldes "Radarsat Passive Planar Array Study" (SPAR Aerospace Ltd., RML-009-83-130, DSS Contract No. OSR83-00068, April 1984)

Table 5.2 is within ±20%. It is far more difficult to estimate the remaining part of the feed without a detailed structural and kinematic analysis. For the purpose of weight calculation it is assumed that the panels are supported by a lattice type triangular truss structure, each of which weights 300 lb (Qty 3 required). The assembly is held together by two rings (unit weight 126 lb) and six struts (unit weight 30 lb). The deployment mechanisms utilize a total of nine motor-actuator assemblies, with an average weight of 20 lb each. The accuracy of these calculations is estimated at ±25%. On the basis of the above assumptions the weight of the radiometer system is 8470 ± 1444 lb.

5.6 Thermal Considerations

There are two types of thermal problems which are affecting the design and operations of the radiometer system.

The first group of problems are possible thermal failure mechanisms. Most of these may occur during the deployment of the system. They could take the form of seizures in the linkages or actuators with the result of partial or complete deployment failures. However, due to the partitioned nature of the overall feed a complete deployment failure has very low probability. The overall feed is divided into groups of 17 + 17 + 18 subarrays and each group into two. Each "half feed" containing 8 or 9 subarrays is deployed somewhat independently from the others. Additionally, this deployment may be accomplished at an orbit height which is accessible by the STS, thus potentially EVA servicable. Since the feed deployment mechanism represents only 2.1% of the total system weight redundancy may be considered without excessive increase of overall system weight.

The second group of problems are related to thermal instability. The total thermal energy influx to the feed varies drastically during operational

conditions. Figure 5.13 shows projected cross sections of the feed for the 0 to 90° Sun angle range. The varying amount of intercepted solar flux causes three effects:

1. Deformation of the feed structure relative to its nominal position,

2. Deformation of the microwave radiating circuit relative to its ideal geometry,

Variation of the ambient temperature of the radiometers.

The deformation of the feed structure (tilt, wharping, translation) causes a movement of the beam centers relative to an arbitrary reference and relative to each other. Additionally, a beam shape deformation and sidelobe level deterioration may take place. Among these effects only the movement of beam centers relative to the arbitrary reference may be significant. For a given revisit position these pointing errors remain relatively constant and vary only slowly during the year. Thus most of the introduced errors can be taken into effect by an appropriate calibration procedure. Additionally, the feed support structure must be designed with thermal shield protected low temperature coefficient materials.

The deformation of the microwave radiating circuit and particularly the quality of contact between printed circuits and coaxial components could cause a variation of input impedances of individual subarrays, which in turn could cause a frequency dependent variation of subarray radiation pattern, internal loss, and transfer function. At the end, these variations manifest themselves to variations in the antenna noise temperature. The above effects can be minimized by the use of RF transparent, high quality multilayer thermal shields. These types of protections introduce a certain RF loss (noise temperature component) which decreases during the mission due to radiation damage. At the same time the effectiveness of the thermal shield decreases.
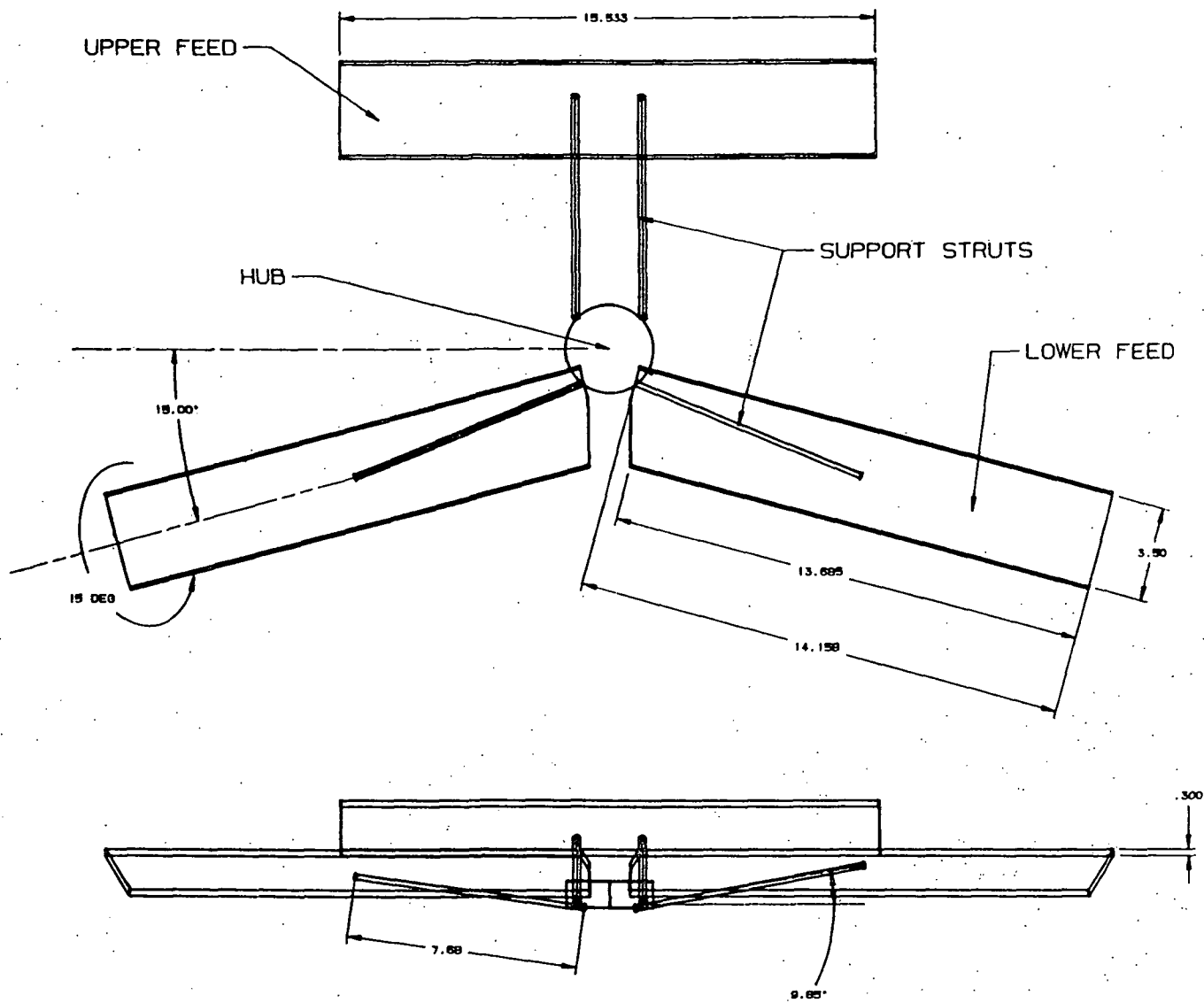
Figure 5.13(a) - Projected cross section of feeds for various Sun angles.

O DEG

I5 DEG

3O DEG

45 DEG

75 DEG

9O DEG
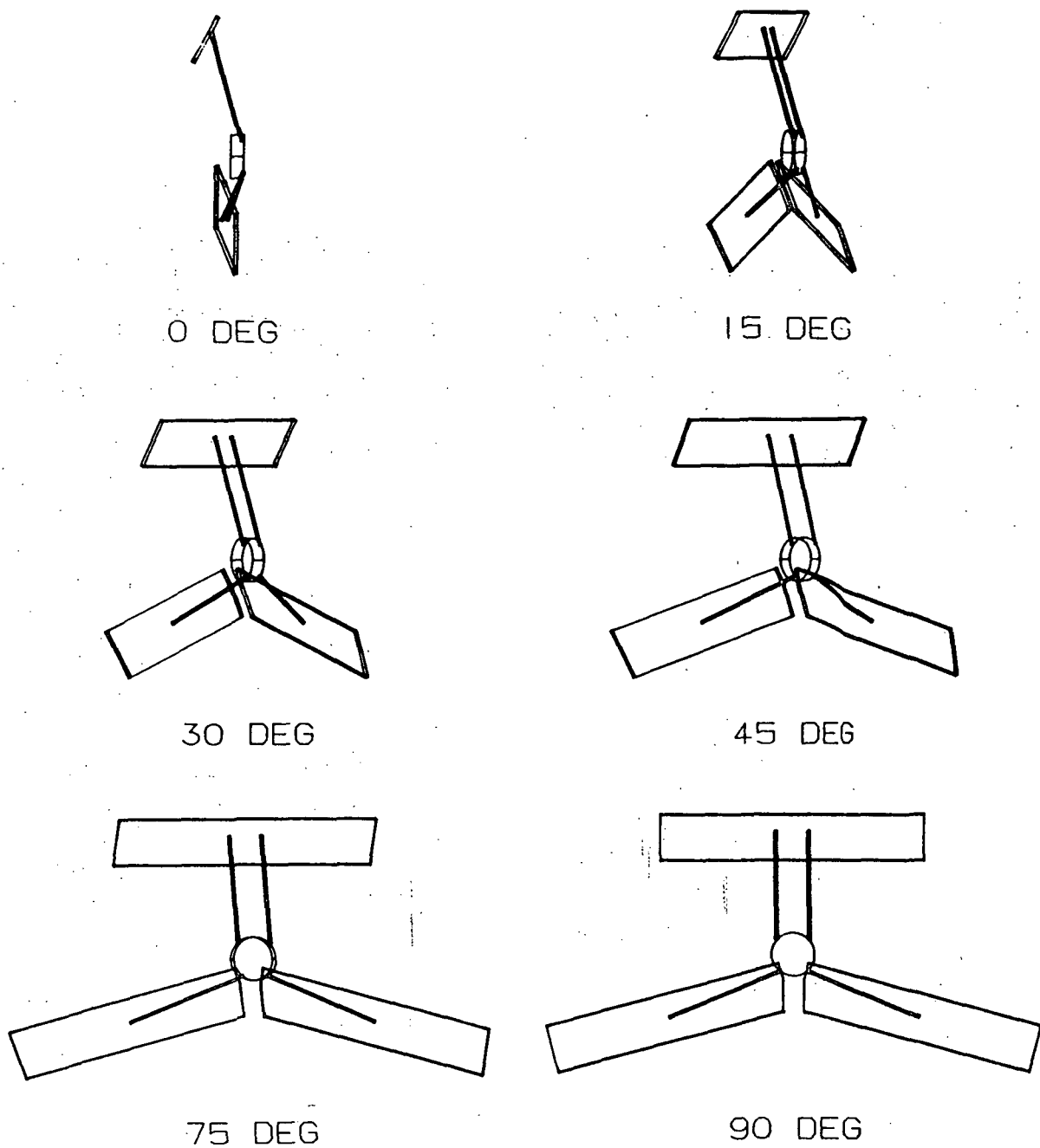
Figure 5.13(b) - Projected cross section of feeds for various Sun angles.

190

Thus the radiating element side of the shield must be designed for maximum tolerable loss at the beginning of mission and minimum thermal protection at the end of mission.

The effect of variation of ambient temperature on the performance of radiometer can be minimized by passive temperature control (heat sink, heat pipe) and/or by heaters. In Table 5.1 a considerable part of the radiometer weight is associated with the use of heat sinks, which are mounted on the Earth facing side of the radiometer boxes. A further increase in the mass of the heat sink may be desirable. This will not affect significantly the over-all weight of the system, but it may increase the feed package thickness, thus it becomes unimplementable from packaging point of view. Consequently, the use of active heat control can be a desirable option.

6. TECHNOLOGY DEVELOPMENT REQUIREMENTS

Since the beginning of NASA Langley Research Center's Large Space Structure Development Program, considerable progress was made in the area of the optics. To study the optics first was logical, because this part of the system is physically larger, it is usable for a number of missions with different feeds and without its design the feed design cannot be started.

However, as Table 5.1 indicates the weight of the optics for a typical radiometer mission represents only 25.8% of the total payload weight. On that basis it can be suspected that a larger complexity and cost is associated to the remaining (feed related) part of the system. Consequently, if the development of an overall soil moisture measuring radiometer system is contemplated serious research and development on the feed related items must now begin.

The technology development need of this area are summarized in Table 6.1.

The following comments can be added to Table 6.1.

Radio frequency

a. An adequately accurate software to simulate the radiation characteristics of printed circuit type subarrays with element numbers up to about 50 must be developed. Some less accurate form of such software exist. However, existing software does not consider accurately the element pattern of various patch shapes, their frequency dependency and neglects mutual coupling. Additionally, no capability for arbitrary element locations is available. Software extension must include coupling between thermally introduced deformations and changes in the radiation pattern.

b. In order to predict the input reflection coefficient, power division, loss and noise temperature characteristics of subarrays up to 50 elements a scattering matrix software program must be developed. This program must cover

TABLE 6.1

Technology development needs related to the feed of the

soil moisture measuring radiometer

1. Radio frequency
    Feed pattern software
    Feed circuit scattering matrix software
    Secondary pattern software
    Feed array implementation
    Radiometer
    Reconfigurable feed
    Radiometer system tests
2. Structure
    Panel structure
    Support structure
    Deployment structure
3. Kinematics
    Flattening
    Positioning
    Orientation
4. Thermal
    Shield
    Sink
    Active
5. Control
    Deployment
    Fine positioning
6. Monitor
    Location
    Temperature
    Aging

---

the applicable power division trees for suspended stripline components, like straight sections, bends, couplers, loads, connectors. Output data shall include return loss, transmission line loss, noise temperature, and complex power division as a function of frequency.

c. Secondary pattern software shall be further developed to accept results from the primary pattern software program. Such a program must be applicable for secondary pattern synthesis in the hoop column antenna optics environment. Related minimize based synthesis programs are available for shaped beam communication satellite antennas. However, existing programs

cannot take the presently required large element numbers and they are slow for the presently required large directivities. Additionally, no software exists for the synthesis of maximum beam efficiency. While existing beam shape synthetizing minimax programs in principle operate similarly to the present requirement the new software must include significant modification, extentions and even change of principles if better calculation efficiency is attempted.

d. According to Figure 4.32, eleven different types of feed arrays are needed for the radiometer. The simplest contains 18, the most complex 41 radiating elements. The feed technology development may start with the 18 element array and eventually include the maximum element number. Specific aims of these development shall be control of radiation performance, minimization of loss and weight, minimum frequency variation and temperature sensitivity.

e. Reconfigurable subarray in the 18 to 41 element range shall be developed. Reconfigurability is for compensation of reflector surface inaccuracies in the changing environment. Two classes of this type of arrays may be recognized: Phase only and phase-amplitude variant arrays. Required technology is printed 0–90° and 0–360° phase shifters either at RF or IF frequencies. In the later case a low noise down converter is employed at each radiating element with a common LO and reconfiguration is accomplished after preamplification.

f. A radiometer shall be developed which considers the r-f, mechanical and thermal interface requirements presented by the feed design.

g. An integrated feed radiometer package test shall be implemented which includes ground based radiation tests, environmental tests, airborne tests and STS experiments. Accuracy of prediction, thermal, and material stability are the main issues for these tests.

Structure

a. The basic panel structure represents different shapes and sizes than employed on previous space based arrays, like SAR. New strucurally optimum and thermally acceptable panel structures must be developed.

b. Support structures to hol the feed arrays during stos and deployed conditions must be developed. These structures must handle the applicable loads and required accuracies.

c. Structures as part of the deployment system must be designed and verified.

Kinematics

Detailed study of the kinematics for the feed deployment is necessary in order to select the optimum system for the deployment of required type of feed arrays. Generally, the deployment system must accomplish these functions: flattening, positioning and orientation of the feed. All these are part of the initial deployment. Additionally, the orientation function may be utilized to improve system performance during operational conditions. For instance a fine feed positioning capability may be used to slightly relocate the foot print without reorienting the complete antenna system.

Thermal

a. Thermal shields which are RF transparent at the operational frequency with adequate solar flux reflectivity shall be developed. (This is a refinement of existing design.)

b. Use of heat sink and heat pipes for the present environment shall be studied and optimumdesign developed.

c. Use of active temperature control shall be documented.

Control

Control systems shall be developed to handle the stability requirements of the radiometer during deployment and during operation. This shall include orientation maneuvers, orbit height change maneuvers and retrieval procedures. Additionally, control methods are required for fine positioning of the overall radiometer or some of its specific beam clusters.

Monitor

a. The most important special monitor function is the determination of the pointing status of the inidvidual beams of the radiometer. This may be accomplished by r-f or optical position determination of individual subarrays or feed panels and measurement of some reference point locations of the sub-aperture reflectors.

b. A temperature monitoring system must be developed in such a manner that system calibration can be updated as a function of specific temperature readouts at appropriatly selected locations.

c. The antenna is composed from a number of different materials. Many of them may display variations in the space environment. Consequently it is important to introduce some monitoring function whichcan detect effects of these variations.

7. CONCLUSIONS

The use of the hoop column antenna for soil moisture measuring radiometer applications have been investigated at the conceptual level.

The study indicates, that the major mission requirement of a nominal 10 km spatial resolution, 3 days revisit time and near complete coverage of the temperate zones of the Earth can be accomplished with a 118 m diameter antenna. Thelimitations associated to the blockage caused by the column and the feeds can be greatly reduced by the use of 2, 3, or 4 subapertures. While there are no drastic differences between these subaperture selections, preliminary studies indicate that the three subaperture configurations represent a reasonable overall compromise. Such a system allows the use of 52 beams, each shaped by subarrays containing 18 to 41 radiating elements. The resultant optics-feed payload can be packaged into a single STS flight weighting approximately 8470 lb and subsequently placed into a 678 km to 787 km high orbit.

The study indicates that 74.2% of the total payload weight is in the feed-radiometer package, thus this part of the system may represent the complexity center. The implementation of the studied radiometer will require technology development effort in this area. The major development requirements are identified in the study.

Standard Bibliographic Page

1. Report No. NASA CR-178154	2. Government Accession No.	3. Recipient's Catalog No.
4. Title and Subtitle **A Design Study for the Use of a Multiple Aperture Deployable Antenna for Soil Moisture Remote Sensing Satellite Applications**		5. Report Date August 1986
		6. Performing Organization Code
7. Author(s) Peter Foldes		8. Performing Organization Report No.
9. Performing Organization Name and Address Foldes Incorporated 1131 Radnor Hill Road Wayne, PA 19087		10. Work Unit No.
		11. Contract or Grant No. NAS1-17209
12. Sponsoring Agency Name and Address National Aeronautics and Space Administration Washington, D.C. 20546		13. Type of Report and Period Covered Contractor Report
		14. Sponsoring Agency Code 506-44-21-03

15. Supplementary Notes
Langley Technical Monitor: Thomas G. Campbell
Final Report

16. Abstract

This report describes a study using a multiple aperture reflector antenna system for a multiple beam radiometer soil moisture remote sensing satellite. For this study a multiple beam-pushbroom approach is used for wide swath coverage; and a large aperture is used for achieving high spatial resolution. An objective of this study was to determine the optimum multiple aperture configuration which could be properly packaged and deployed by the Space Transportation System (STS) and would provide nearly optimum swath and resolution characteristics.

The structural concept considered is the Hoop Column antenna system which can provide multiple offset-fed reflectors within a symmetrical, cable stiffened structure. The study results indicate that a triple aperture system having 3 55-meter reflectors contained in the symmetrical space frame will provide 52 beams at L-Band. The resulting spatial resolution would vary from 8.44 km to 10.87 km depending upon the specific beam in the multiple beam system. A structural concept is described which is shuttle compatible.

17. Key Words (Suggested by Authors(s)) Radiometer, Multiple Beam Antennas Soil Moisture Satellite Pushbroom Radiometer Large Deployable Antenna Parabolic Reflector Hoop/Column		18. Distribution Statement Unclassified - Unlimited Subject Category 33	
19. Security Classif.(of this report) Unclassified	20. Security Classif.(of this page) Unclassified	21. No. of Pages 208	22. Price A10

NASA Langley Form 63 (June 1985)